2016-12-01

Investigation of Dynamic Biological Systems Using Direct Injection and Liquid Chromatography Mass Spectrometry

Adam Clayton Swensen
Brigham Young University

Investigation of Dynamic Biological Systems Using Direct Injection and Liquid Chromatography Mass Spectrometry

Adam Clayton Swensen

A dissertation submitted to the faculty of
Brigham Young University
in partial fulfillment of the requirements for the degree of

Doctor of Philosophy

John C. Price, Chair
Richard K. Watt
Steven W. Graves
Joshua L. Andersen
Chad R. Hancock

Department of Chemistry and Biochemistry

Brigham Young University

2016

ABSTRACT

Investigation of Dynamic Biological Systems Using Direct Injection
and Liquid Chromatography Mass Spectrometry

Adam Clayton Swensen
Department of Chemistry and Biochemistry, BYU
Doctor of Philosophy

In biological systems, small changes can have significant impacts. It is, therefore, very important to be able to identify these changes in order to understand what is occurring in the organism. In many cases, this is not an easy task. Mass spectrometry has proven to be a very useful tool in elucidating biological changes even at a very small scale. Several different mass spectrometry based techniques have been developed to discover and investigate complex biological changes. Some of these techniques, such as proteomics, have been through years of development and have advanced to the point that anyone can complete complex analyses of global protein identification and measurement with relative ease. Other techniques are still developing and still have some ground to cover in terms of experimental outcome and ease of execution. Herein we show improvements we have made in high-throughput high-resolution mass spectrometry based techniques to identify and quantify small molecules that are involved in significant biological changes. To begin, we show that our improved high-resolution mass spectrometry based lipidomics techniques are capable of identifying small changes in diseased states that are associated with inflammation, mitochondrial shape and function, and cancer. With our techniques we have been able to extract, identify, and quantify several thousand unique lipid species from complex samples with confidence. Our initial studies looked at global lipidome profiles of differing tissue types from human and mouse biopsies. This was then adapted to compare the global lipidomes of diseased states against healthy states in asthmatic lung tissue, cigarette smoke treated cells, high fat high sugar (HFHS) stressed animals (with and without additional treatment), and in signaling lipids associated with cell death resistance and growth signaling in pancreatic cancer. As a result of our success with lipidomic method improvement we then adapted our techniques and knowledge for use in elucidating small molecule signaling peptides and oxidation changes in proteins. We were able to show that our improved liquid chromatography mass spectrometry based small molecule assays are capable of identifying and quantifying small peptides and protein modifications that would otherwise be undetectable using traditional techniques. This work resulted in the development of a scalable method to detect and quantify the small iron-regulatory hormone known as hepcidin from a variety of samples such as blood, urine, and cell-culture media. We were also instrumental in evaluating and revising a new ultra-high pressure liquid chromatography (UHPLC) system that allows for better separation of analytes from complex mixtures for identification and quantification. Through these advances we hope to aid researchers and clinicians to enable them to use mass spectrometry to further our knowledge about the small but significant changes that regulate complex biological systems.

Keywords: mass spectrometry, proteomics, lipidomics, metabolomics, cancer research, liquid chromatography, sphingosine kinase, hepcidin, ceramide

ACKNOWLEDGEMENTS

If I had been asked two years prior to starting my graduate studies if I was considering an advanced degree, I would have flatly answered “NO.” Growing up it was never in my plans to get a PhD. I knew that my Dad had always desired an advanced degree but that desire had not carried on to me. After he passed away at a young age due to cancer my world came to a stop and everything changed. My aspirations and goals in life changed and I found myself applying to the PhD program at BYU. I hoped to put myself into a better position to help my family and to add to my Dad’s legacy by fulfilling through me a dream that he always had.

Of course, this journey would not have been possible without loving support from so many people. First and foremost, I have to thank my wife, Elise, for her patience, tolerance, guidance, and loving support. Without her support, this never would have happened. She is a wonderful wife, mother, and woman. Although she doesn’t realize how much she has helped now, I also want to thank my daughter, Piper. She has changed the way I look at life and gave me the determination to endure. She has brought out deeper emotions in me than I ever knew I had. As we prepare for the arrival of her younger sister she makes me realize what a great blessing and responsibility it is to be a parent. Even though my wife will probably roll her eyes at this, I also have to thank my dog, Daxter. He came to us at a time in our lives when we really needed him. He has shown great patience and love toward us and has been a tremendous support to me. Even though I don’t think I’ll ever be able to express to him how grateful I am for him I hope we’ll be together after this life.

I also want to thank my Mom for being such a great example to me. Her enthusiasm and loving support was tremendously helpful during this process. As was the loving support I received from my brother, Alex, and sister, Amberlee. Thank you!

I also want to thank my advisors Dr. John T. Prince and Dr. John C. Price. This journey hasn't been easy for them either. Having started graduate school only four months after my Dad's passing it wasn't easy for me adjust and cope with the grief that so often filled my life. Their patient support for me as I worked on my intellectual and emotional development made this possible. So I really need to thank them for not giving up on me and helping me make it to this point. I want to thank my committee members for their generous support especially during the difficult time when the Prince Lab dissolved. Without their help and guidance, the transition to the J.C. Price Lab would have been much harder and my projects would be less impactful.

Among the most notable people I want to thank, I want to thank Cata for her support and attentive ear. She is an amazing person. Andy for his example and words of encouragement. I also want to thank members of the Prince Lab, James, Tamil, Ryan, Huan for teaching me so much. I want to thank the J.C. Price Lab members as well, Brad, Richard, Monique and many others for their support of me especially as I made my awkward transfer into their lab. There are too many people to list to whom I owe thanks.

Finally, I want to thank our Heavenly Father. Without his guidance and patience with me I never would have gone to graduate school or been able to finish. My greatest scientific breakthroughs only came as a result of his guidance and as answers to my prayers. It was His hand that made this work possible.

TABLE OF CONTENTS

TABLE OF FIGURES

Chapter 1: Introduction

Chapter 2: Mitochondrial fission mediates ceramide-induced metabolic disruption in skeletal muscle

Chapter 2: Cigarette smoke increases cardiomyocyte ceramide accumulation and inhibits mitochondrial respiration

Chapter 2: Ceramides mediate cigarette smoke-induced metabolic disruption in mice

Chapter 2: Cardiomyocyte mitochondrial respiration is reduced by receptor for advanced glycation end-product signaling in a ceramide-dependent manner

Chapter 3: Introduction

Chapter 3: Lipidomic profiling identifies modified sphingosine kinase 1 regulation, and cell-fate signaling in pancreatic cancer

TABLE OF TABLES

Chapter 1: Introduction

Chapter 3: Lipidomic profiling identifies modified sphingosine kinase 1 regulation and cell-fate signaling in pancreatic cancer: Supplemental Information

CHAPTER 1:

Introduction to Mass Spectrometry Based Global –Omics Techniques and the Development of Novel Detection and Quantification Assays

Introduction:

Even very small changes in a cell can result in significant consequences. These consequences could only affect the cell itself, or affect the tissue in which it resides, or even affect the organism as a whole. For example, a relatively small change in the activity of lipid signaling enzyme can trigger a cell to grow, metastasize, resist cell death, and eventually become cancer; or another change could elicit the exact opposite response and make it so that the cell becomes sensitive to cell death signaling and can be removed from the organism before problems arise. Knowing what causes these changes and what exactly these changes are is paramount to understanding the underlying biological process. Ever since ancient Greek philosophers began their systematic study of anatomy and biology it has been the goal of scientists to discover what it is that makes things live and how they are regulated.

Many techniques have been employed to study complex biological systems. Some of these techniques have been around for hundreds of years. Most of these techniques relied on large scale observations of the entire organism. While these studies were helpful most did not address or even comprehend the complex chemical nature of the changes that resulted in their observations. The advent of mass spectrometry and the ability to detect, identify, and measure very small molecules from complex biological systems has made it possible for scientists to now

truly understand the underlying mechanisms that regulate life processes at a scale that was not even imagined a century ago.

Mass spectrometry is extremely useful and versatile. We can use mass spectrometry to study single molecules from simple chemical reactions or use it to study millions of complex molecules from complex matrices. For studying complex biological systems several techniques have been developed to look at molecules involved in complex biological systems. It is now possible to extract proteins from cells and tissues and identify thousands of unique proteins and their quantification. This technique is known as proteomics. The root of the word proteomics refers to what is being observed the "prote-", proteins, and the neo-suffix "-omics" which comes from the Greek –ωμα denoting a totality. We are observing the totality of the proteins from a sample. From proteomics we can determine expression differences or regulatory differences between proteins or even how they interact within the cell. Proteins are actually some of the largest molecules found within cell. Smaller molecules can also be extracted and identified on a global scale. These studies are most often known as metabolomics or the totality of metabolites in a sample. One of the sub-categories of this technique involves the isolation and identification of lipids from complex biological samples. This technique is known as lipidomics.

My initial research delved into the study of lipidomics and the isolation, identification, and quantification of lipids. The field of lipidomics really has not been around for very long. It is a complex process to extract lipids (in a non-biased way) from biological samples. It is an even harder process to separate and give identities to these lipids species especially since their characteristic fragmentation patterns in mass spectrometry are not as easily predicted as they are with proteins. In this work I will demonstrate the processes I developed and improved for the complete non-biased extraction of global lipidomes (the collection of all lipids in a cell or

organism) their identification and quantification. My research first identified dozens of existing extraction techniques which I evaluated and compared to determine the best approaches to avoid biases in extraction. From there I developed techniques that could be employed with the mass spectrometer that minimize concentration bias in the ionization and detection of lipids through high-resolution direct injection mass spectrometry. These techniques involved the use of ionizing adducts doped into the complex mixtures and the use of intra-source separations. I was also participated in the development of new software that greatly enhanced the throughput, speed, versatility, and efficiency of our new processes. Using this toolkit of techniques, I was able to answer many biological questions that were the result of lipid regulation. I identified lipids that were crucial in the mechanism of mitochondrial fission, crucial in metabolic disruptions, crucial to receptor signaling molecules, and to the regulation of cancer growth and death. Herein I demonstrate some of the great advances we made in progressing the field of lipidomics.

During the course of my research, we found that our techniques were not only useful for isolating small lipid molecules but they were useful in isolating other small molecules as well, including peptide hormones. Small peptide hormones can be difficult to detect and quantify from complex mixtures but they have many of the same chemical characteristics as lipids. Cysteine-rich peptides for example contain a strongly electronegative thiol group that prevents the peptide from ionizing well using traditional electrospray mass spectrometry techniques. Using our knowledge gained from lipid isolations and their ionization properties we were able to isolate a cysteine-rich key iron-regulatory hormone, hepcidin-25, from complex matrices. Then through chemical covalent modifications we were able to overcome much of the ionization resistant character of the molecule and allow it to be detected on common mass spectrometers even in

very low concentrations. This technique made it possible to detect small changes that occurred in hepcidin-25 regulation in animal models of chronic inflammation.

One of the key instrumental components required to detect small concentration changes in proteins and peptides is a high pressure liquid chromatography (HPLC) system. Chromatography allows for the separation of compounds in a mixture based on their chemical characteristic and their affinity to the column material. In order for a chromatography column to operate at its highest potential and achieve the greatest separations it needs to operate with low volumes at very high pressure. This is especially true for small, low abundance, hard to ionize molecules. Herein we also demonstrate our involvement with the development of an ultra-high-pressure liquid chromatography system that can allow for full baseline chromatographic separations of similar molecules for identification by mass spectrometry.

The highly efficient chromatographic separations of similar molecules can then afford to us the ability to identify and quantify small chemical changes that occur to proteins either within or without a biological context. Herein we show the ability to distinguish specific oxidation differences in a protein shell, ferritin, due to the action of a previously unknown iron reducing chemical, ophen.

Mass spectrometry has really opened the door to complex global analyses of biological systems. Through mass spectrometry based techniques we are able to pinpoint the exact biological mechanism that is resulting in the macroscopic changes we observe. We demonstrated the ability to identify thousands of lipids from a single sample and use that to find an active oncogenic pathway as well as discovering the lipid contribution to several diseased states. We developed a technique to identify and quantify a key compound involved in iron regulation. Additionally, we helped develop and evaluate powerful new HPLC system for sample

separations. Our techniques are always improving and in time and through the contribution of thousands of scientists these techniques hold the potential to provide fast, simple, robust assays that can be used to evaluate biological systems and treat disease.

In Depth Introduction to Lipidomics and Technique Development:

Lipids function in diverse cellular roles including: maintenance of cellular structure and electrochemical gradients, subcellular partitioning, energy storage, first and second messenger cell signaling, protein trafficking and membrane anchoring. These important small molecules are often discounted and understudied. Compared to the information available for nucleic acids and proteins, there exists a void of information regarding lipid global composition, quantitation, and regulation. Until recently the most common experiments involving lipids only targeted single lipid categories and/or species for study, but this gives an incomplete picture of the global dynamic state of the cell. A more comprehensive picture of the dynamic lipidome allows for greater in-depth study of global categorical and single lipid species regulation. Lipid species can be identified and tracked as cellular conditions change to give an indication of underlying regulatory processes such as metabolic disorders and disregulation of energy storage homeostasis. Key to the analysis of the global lipidome is the ability to elucidate hundreds, and at times thousands, of high-confidence lipid identities across all lipid categories allowing for accurate study of the dynamic state of the lipidome and the important roles that lipids play in the cell.

As one of the newest of the emerging "omics" fields, lipidomics has already produced very insightful and useful data that have increased our knowledge of the cell. The causative effect of insulin resistance[1, 2], metabolic syndrome[3], cardiovascular disease[4], and some cancers have been discovered through studying lipids.[5] Correlations with many other varied diseases

including Alzheimer's disease[6], atherosclerosis[7], and obesity[8] have been described using a lipidomics approach. One of the most promising areas of lipidomics research in diseases today is the elucidation of compositional lipidome changes as a result of cancer. As cancerous cells develop and mature, they undergo a morphological plasticity change in their cellular membranes[9]. Cancerous cells show other changes that include self-regulated growth, resistance to inhibitory and apoptotic signals, angiogenesis, immortality, and metastasis. Collectively, these have become known as the "Hallmarks of Cancer".[9, 10] The role of lipid metabolism and the use of lipidomics are proving to be crucial to our ability to understand some of these hallmark characteristics of cancer. The observable cellular morphological changes can often be associated to the cellular membrane whose composition is more than fifty percent by mass composed of lipids.[11] The morphological changes that are observed in subcellular compartments of a cancer cell have also been correlated with compositional changes in the lipid membrane.[3] These help illuminate our understanding of observable theories such as the Warburg effect[12]. Compositional changes in membrane lipids in a cancer cell are required to bestow some of the characteristics observed in cancerous tissue or in other diseases. For example, Chenais et al. and colleagues have demonstrated that breast cancer proliferation will only occur when coupled to membrane lipid compositional changes.[13] Legembre et al. demonstrated that lipid raft micro-domains play a crucial role in Fas-mediated apoptosis[14] which is suppressed in cancer cells. There are many more lipid related discoveries waiting to be made.

Previous experimentation has shown that cancer cells isolated from similar tissues show many related hallmark characteristics and behaviors.[9, 10] We propose there are many similarities in the cellular lipid compositions among many cancerous cell types. For example, when cancer metabolism shifts to favor glycolysis under anaerobic conditions, the NADH molecular reserves

must be recycled. Lipogenesis is one of the cellular pathways in which the cell oxidizes and recycles the NADPH molecular reserves without the use of the electron transport chain and oxidative phosphorylation. In effect, cells in a state of metabolic disregulation exhibit lipogenesis patterns that have universal similarities. We developed and outlined an approach to elucidate lipid species that are related to the effects of cancer stress on lipid metabolism in many cancerous cell types. There are several oncogenic pathways that could present similar behaviors in lipid metabolism and *de novo* synthesis that could present a general compartmentalized sub-lipidome fingerprint common to many if not all cancerous cell types.

The effects of diet can also have a great impact on the ability of cancer to grow. Intake of high levels of saturated fats have been positively correlated with prostate[15], ovarian[16], breast[17], colon[18], and other cancers. In the human pancreatic cancer cell line Capan1 it has been shown that cancer cells deprived of serum lipids cannot sustain proliferative growth.[19] Other unusual dietary effects are seen in cancer as well. Like all cells, fast-growing cancer cells must produce a phospholipid bilayer for their membrane. Dietary sources alone are not enough to fuel the demand for membrane lipid species and cancerous cells must produce these lipids through *de novo* anabolic pathways. It is estimated that nearly 95% of the lipids required for cell proliferation in tumor cells are made *de novo*. Human cells are only capable of making certain fatty acid chain lengths through lipogenesis and certain lipid species are favored under the stressful conditions of a cancer cell. This leads to a heavily biased lipid membrane composition favored toward those even-number chain length fatty acid containing *de novo* synthesized lipids. Our techniques are capable of elucidating the lipid species created *de novo* and detect their global signature within the cellular lipidome.

Disease	Lipid	Sample
Obesity	Lysophosphatidylcholines, Ether phospholipids	Monozygotic Twin Study[20]
	Phosphatidylcholine, Phosphatidic acid, Ceramide, Sphingomyelin, Phosphatidylethanolamine	Monozygotic Twin Study[21]
	Ceramide, Triacylglycerol	Mouse liver[22]
Hypertension	Ether lipids, Cholesterol	Blood plasma[23]
Diabetes	Cardiolipin	Mice myocardial sample [24]
	Triacylglycerol	Murine myocardium [25]
Alzheimer	Sulfatide	Human Brain [26]
Transient Cerebral ischemia (stroke)	Phosphatidylcholine, Phosphatidylinositol, Phosphatidylserine, Sphingomyelin, Cardiolipin	Gerbils Brain [27]
Breast cancer	Phosphatidylcholine	Clinical breast cancer tissues[28]
Chronic glomerulonephritis	Phosphatidylinositol, Phosphatidylserine,	Blood plasma[29]
Cystic fibrosis	Lysophosphatidylcholine, Phosphatidylcholine,	Blood plasma[30]
Fabry disease	Lactosylceramide, Ceramide, Glucosylceramide, Sphingomyelin	Urine samples[31]
Mitochondrial dysfunction	Cardiolipin	Mouse heart[32]
Epithelial barrier dysfunction	n-3 Polyunsatyrated Fatty acids	Epithelial cell[33]
Gaucher disease	Ceramide-monohexoside	pericardial fluid[34]
Hepatic steatosis	Phosphatidylcholine, Cholesteryl ester, Triacylglycerol	Mice liver[35]
Neuro-degeneration	Sulfatide	Mice brain[36]
Ovarian cancer	Lysophosphatidicacid, Lysophosphatidylinositol, Sphingosylphosphorylcholine. Lysophosphorylcholine	Ascitic fluid[37]
Asthma	Phosphatidylcholine , Phosphatidylglycerol	Sputum, bronchoalveolar lavage fluid [38, 39]

Heart failure	Tetralinoleoylcardiolipin	Rat and explanted human heart [40]
Mitochondrial dysfunction and disease	Cardiolipin	Many studies with mouse, rat, human samples For review [41]
Rheumatoid arthritis	Phosphatidylcholine, lysophosphatidylcholine	Human plasma [42]
Barth syndrome	Monolysocardiolipin, Cardiolipin	Dried bloodspots[43, 44]

Table 1: Lipid Associated Diseases. Fluctuations in lipid homeostasis have been associated with many diseases and their progression. This table helps demonstrate the important role that lipids play in cellular health and maintenance and the diversity of diseases that are assiociated with disregulation of lipids.

Lipids have been proven to be excellent biomarkers for a variety of diseases (Table 1.1). Previous experimentation in the field of lipidomics has already identified significant lipid species changes that are associated with ovarian[45] and prostate[46] cancers. Experimentation has also shown that many cells, especially those under cellular stress or undergoing prolific growth, are known to shed lipid molecules into blood serum.[47]

Lipidomics provides a detailed fingerprint of the unique composition of lipids in a cell. We have been able to differentiate tissues solely by fingerprinting the cells unique lipid compositions. The lipid composition of a muscle cell varies greatly from the composition of a brain cell and also varies greatly from the composition of a liver cell. Conversely, differences in lipid composition of the same type of tissue from individual to individual shows little variance. Indeed it is much harder to distinguish lipidome fingerprints of liver tissue samples from two individuals than it is to distinguish the differences between liver and lung tissues in the same

individual. Some of these same lipidome fingerprinting characteristics can also be observed with cancerous tissues. Based on our preliminary results, the lipidome profile of a rapidly growing pancreatic cancer cell is very distinct from the lipidome profile of a healthy pancreatic cell. Using a lipidomics approach to obtain the unambiguous identification of cancerous tissue could prove to be invaluable for physicians treating cancer patients. Similar techniques have already seen limited intraoperative clinical use by measuring lipid smoke vapors and identifying lipid profile changes on the fly that can differentiate cancerous and healthy tissues.[48]

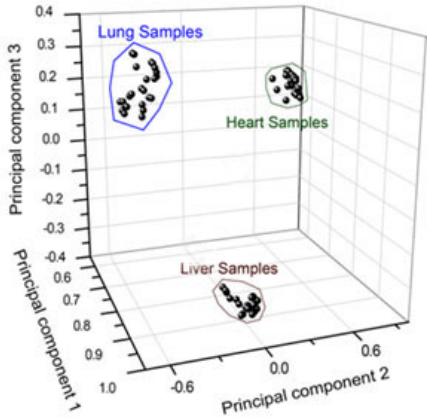

Figure 1: Principle component analysis of lipidomics data The shotgun lipidomics data of lipid extracts of lung, heart, liver samples from mice. The results were subjected to PCA analysis. The analysis contains 3 sets of biological, sample and technical replicates each.

The Importance of Complete Lipid Extraction

In order to obtain a complete and accurate snapshot of the complete global lipidome it is vital that all of the lipids are successfully extracted from the cells or tissue that are being analyzed. This doesn't just apply to the lipids in the cellular membrane but also to the organelles

and cellular compartments and the lipids that can be found not associated with bilayers or membranes. There are many varied extraction techniques for isolating and concentrating lipids from samples. While these methods do extract and concentrate lipids, is there a bias in the lipid categories and classes that are removed? In order to answer this question, we set out to test 30 popular methods for extracting lipids from simple and complex matrices. Some of the methods claimed to extract complete lipid profiles while other techniques specialized in certain lipid categories and classes.

Extraction Techniques		
Method Name	Extraction Chemicals	Reference
Folch Method	Chloroform/Methanol	(Folch et al., J Biol Chem 1957, 226, 497)*[49]
Bligh and Dyer Method	Chloroform/Methanol/Isopropanol	(Can J Biochem Physiol 1959, 37, 911)*[50]
	NaCl added	(Hajra, lipids, 1974, 9, 502)[51]
	Acetic Acid added	(Weerheim AM et al., Anal Biochem 2002, 302, 191)[52]
Two Step Bligh and Dyer Method	Chloroform/Methanol/Isopropanol	From bacteria with focus on fatty acids (Lewis T et al., J Microbiol Meth 2000, 43, 107)[53]
	Chloroform/Methanol/Isopropanol	Miniaturized method (Burja AM et al., J Agric Food Chem 2007, 55, 4795)[54]
Cequier-Sanchez Method	Dichloromethane/methanol	(Cequier-Sanchez et al., J Agric Food Chem 2008, 56, 4297)[55, 56]

	Hexane/isopropanol	(Anal Biochem 1978, 90, 420)[57]
		(Eder K et al. Clin Chim Acta 1993, 219, 93)[58]
		For Sphingolipids (Markham JE et al., J Biol Chem 2006, 281, 22684)[59]
		Total Lipids from Algae (Ryckebosch E et al., JAOCS 2012, 89, 189)[60]
MTBE	MTBE/Methanol/Water	(Matyash V et al., J Lipid Res 2010, 49, 1137)[61]
		Blood Lipids (Ichihara K et al., Lipids 2011, 46, 297)[62]
Hexane only	Hexane	(Baümler ER et al., JAOCS 2010, 87, 1489)[63]
Dry-column method	$NaSO_4$ (an)/Celite diatomaceous earth/dichloromethane/methanol	(Marmer WN et al. Lipids 1981, 16, 365)[64]
		(Elmer-Frohlich K et al., JAOCS 1992, 69, 243)[65, 66]
Patented Multi-Column "matrix solid-phase dispersion"	C-18 bonded silica column	(Lewis T et al., J Microbiol Meth 2000, 43, 107)[53]
Extraction of lipids from unicellular organisms	NaCl/chloroform/methanol/water	(Axelsson, M et al., PLOS One, 2014, v.9(2), e89643)[67]

Extraction of highly polar lipids	Chloroform/methanol/water	(Dreyfus et al., Anal Biochem 1977, 249, 67-78)[68]
	Chloroform/methanol/water/butanol	(Bodennec J et al., J Lipid Res 2003, 44, 218) Recovery after Folch method[69]
Total Plasma lipids	KH_2PO_4/Chloroform/methanol Triton X-114 detergent (Use proteins later)	(Ferraz TPL et al., J Biochem Biophys Meth 2004, 58, 187)[70]
Lipid extraction from serum, plasma, plant seeds	EDTA/butanol/di-isopropyl ether	(Cham BE et al., J Lipid Res 1976, 17, 176)[71]
	TCA/Acetone added	To remove lipids from protein samples. (Wang R et al., J Biological Chemistry 2004, 279, 46835)[72]
Plasma fatty acids and acylglycerols	Isopropanol/heptane/H_2SO_4/Silica gel	(Dole, V.P. et al., J Clin Invest 1956, 37, 350)[73]
	Chloroform/methanol/HCl	(Honeyman et al., Biochem J 1983, 212, 489)[74]
	Add proteinaceous disk	(Lloyd et al., Br J Haematol 1972, 23, 571-585)[75]
Extraction of lipids from plant material	Chloroform/butanol/methanol/ Heptane/NaCl	(Kumari P et al., Anal Biochem 2011, 415, 134)[76] Comparison paper.
		(Zheng G et al., JAOCS 2012, 89, 561) Comparison paper.

Mineralized samples	EDTA/HCl after other methods	(Wu L et al., J Biol Chem 2002, 277, 5126)[77]
Skin Surface	Lipid free absorbent paper/medical tape/diethyl ether	(Michael-Jubeli R et al., J Lipid Res 2011, 52, 143)[78]

Table 2: Lipid Extraction Techniques. A list of popular lipid extraction techniques used for total and specialized lipid extractions from various tissues. Many techniques do to the nature of the extraction or the solvents used introduce a bias to the categories and classes of lipids that are extracted. In order to get a complete unbiased global snapshot of lipid composition these biases must be eliminated. We used many of the techniques listed in this table to establish our own extraction technique with the least perceived bias we could establish.

In order to evaluate the effectiveness of each extraction technique we prepared a representative mixture in lipid standards of known concentration and formed an emulsion from which we attempted extraction of the lipids. This proved useful to evaluate some of the methods but is not representative of normal extraction conditions. Most samples we use for global lipidomics contain several thousand lipid species across all eight lipid categories. In order to test extractions in complex samples we prepared several mouse tissue types including brain, lung, liver, fat, and heart. We added a cocktail of lipid standards of known concentration. These lipids contained odd-chain fatty acids, deuterium labels, or unnatural moieties in order to minimize overlap with exogenous lipid types. We performed lipid extractions on the tissues using the techniques listed in Table 1.2. Lipid identification and quantitation was completed using a direct inject IonMax ESI with a flow rate of 8 microliters per minute. Collection of high-resolution spectra (100,000 resolution) was completed using a Thermo Scientific LTQ Orbitrap XL tandem

mass spectrometer. Spectra were collected in positive and negative modes (intra-source separation) with representative fragmentation spectra collected for identification and verification purposes. Only identifications with less than 3 ppm deviations were considered for this study. Post-run alignment was completed by realigning the spectra to match the known internal standards that were identified from each run.

We found that the extraction techniques that were published for total lipid extractions still have some categorical biases. Most methods rely on the hydrophobic lipid interaction and thereby miss some of the more hydrophilic lipid species. The opposite is true for the hydrophilic extraction techniques that do not successfully extract the lipid species with hydrophobic character. This was determined through comparison of the different extraction quantitation results. Since there is not a comprehensive complete database for all lipid types with concentration data for each tissue type we needed to find another method to determine what total concentrations we should expect in representative samples. We used a "boot-strapping" method by which we would add lipid identifications and quantitation to a database for each method that yielded a high detected concentration for each lipid category. Then we were able to compare each method individually to the "boot-strapped" total to see which technique was the closest. We determined that the Bligh and Dyer and two-step Bligh and Dyer techniques yielded the closest percentage match to the "boot-strapped" database total. We therefore chose this method and made only minor modifications to this technique for our future global lipidome extractions used for future study.

Lipidomic Analysis Software, a Complex Problem:

Without additional computational help it would take years to evaluate a single complex global lipidomic sample. One complex lipidomic sample that we analyzed in our lab had

~200,000 unique peaks ranging from ~50 m/z up to ~2,700 m/z. Lipids often contain one or more neutromer peak (inclusion of a naturally occurring heavy isotope in the lipid structure). However, the most difficult problem resulted when two different lipids had the same chemical composition but differing structures. We can overcome some of these problems with the inclusion of adduct species that preferentially bind to certain functional groups or through fragmentation of the lipid to ascertain identity through fragmentation patterning. To put this simply, it is a complex exhausting process that requires some automation in order to make the analysis feasible.

To address this complex analysis problem, we developed a suite of lipidomic analysis software that takes advantage of the high-resolution capabilities of the LTQ Orbitrap mass spectrometer. This software is under the MSpire family of Ruby based mass spectrometry software and is available freely through GitHub under the name MSpire-Lipidomics. When scans are completed at a resolution of 100,000 or greater we see separation of peaks based on mass defect and high-confidence identification of chemical formula. Work in our lab and in other labs has shown that identifications made at a resolution of 100,000 or greater and with error less than 3 ppm categorical assignments of lipid identities can be made with greater than 95% accuracy in complex samples. We aid the confidence of these assignments by making a cocktail of lipid standards with at least one artificial (odd-chain lipid when possible) standard for each of the eight lipid categories. We have also developed a number of confidence filters that we apply after the initial analysis in order to decrease the number of false positive identifications. Using our specialized and adapted extraction techniques and our suite of software tools with confidence filters it has become common for us to identify and quantify several thousand lipid species from a single sample. This data can then be used to look at specific targets within the lipidome or to

allow comparison of global characteristic changes that occurred in the entire lipidome. This data can also be searched repeatedly for new information without need to find or develop new specialized extractions and analyses for each experiment.

Conclusion:

The wealth of knowledge that can be gained through global and targeted lipidomic studies is tremendous. We can learn so much about metabolism, signaling, and disease by studying and identifying lipids. Lipids are not the simple bi-layer only molecules they were once thought to be. Lipids have many functions that are only now being fully appreciated. But in order for lipidomics to continue to grow and develop it is vital that confident identifications be made and that quantitation data be accurate. This is not a simple task and unfortunately is not as simple as other established fields such as genomics and proteomics. At this point in time the software tools are not as robust in the lipidomics field because of the complex nature of the samples and their varying characteristics and the complexity of the analysis. Hopefully in the future we will have better tools and more robust software as to allow us to tap into this vital wealth of knowledge we can gain by understanding the complex world of lipids.

Works Cited:

1. Hotamisligil, G. S.; Peraldi, P.; Budavari, A.; Ellis, R.; White, M. F.; Spiegelman, B. M., IRS-1-mediated inhibition of insulin receptor tyrosine kinase activity in TNF-alpha- and obesity-induced insulin resistance. *Science* **1996,** *271* (5249), 665-8.
2. Chavez, J. A.; Summers, S. A., A ceramide-centric view of insulin resistance. *Cell metabolism* **2012,** *15* (5), 585-94.

3. Kiebish, M. A.; Han, X.; Cheng, H.; Chuang, J. H.; Seyfried, T. N., Cardiolipin and electron transport chain abnormalities in mouse brain tumor mitochondria: lipidomic evidence supporting the Warburg theory of cancer. *Journal of lipid research* **2008,** *49* (12), 2545-56.

4. Watson, A. D., Thematic review series: systems biology approaches to metabolic and cardiovascular disorders. Lipidomics: a global approach to lipid analysis in biological systems. *Journal of lipid research* **2006,** *47* (10), 2101-11.

5. Swinnen, J. V.; Verhoeven, G., Androgens and the control of lipid metabolism in human prostate cancer cells. *The Journal of steroid biochemistry and molecular biology* **1998,** *65* (1-6), 191-8.

6. Wood, P. L., Lipidomics of Alzheimer's disease: current status. *Alzheimer's research & therapy* **2012,** *4* (1), 5.

7. Ekroos, K.; Janis, M.; Tarasov, K.; Hurme, R.; Laaksonen, R., Lipidomics: a tool for studies of atherosclerosis. *Current atherosclerosis reports* **2010,** *12* (4), 273-81.

8. Donovan, E. L.; Pettine, S. M.; Hickey, M. S.; Hamilton, K. L.; Miller, B. F., Lipidomic analysis of human plasma reveals ether-linked lipids that are elevated in morbidly obese humans compared to lean. *Diabetology & metabolic syndrome* **2013,** *5* (1), 24.

9. Hanahan, D.; Weinberg, R. A., Hallmarks of cancer: the next generation. *Cell* **2011,** *144* (5), 646-74.

10. Hanahan, D.; Weinberg, R. A., The hallmarks of cancer. *Cell* **2000,** *100* (1), 57-70.

11. Alberts, B., *Molecular biology of the cell*. 5th ed.; Garland Science: New York, 2008.

12. Warburg, O.; Wind, F.; Negelein, E., The Metabolism of Tumors in the Body. *J Gen Physiol* **1927,** *8* (6), 519-30.

13. Chenais, B.; Blanckaert, V., The janus face of lipids in human breast cancer: how polyunsaturated Fatty acids affect tumor cell hallmarks. *International journal of breast cancer* **2012,** *2012*, 712536.

14. Legembre, P.; Daburon, S.; Moreau, P.; Moreau, J. F.; Taupin, J. L., Modulation of Fas-mediated apoptosis by lipid rafts in T lymphocytes. *J Immunol* **2006,** *176* (2), 716-20.

15. Huang, M.; Narita, S.; Numakura, K.; Tsuruta, H.; Saito, M.; Inoue, T.; Horikawa, Y.; Tsuchiya, N.; Habuchi, T., A high-fat diet enhances proliferation of prostate cancer cells and activates MCP-1/CCR2 signaling. *The Prostate* **2012,** *72* (16), 1779-88.

16. Blank, M. M.; Wentzensen, N.; Murphy, M. A.; Hollenbeck, A.; Park, Y., Dietary fat intake and risk of ovarian cancer in the NIH-AARP Diet and Health Study. *British journal of cancer* **2012,** *106* (3), 596-602.

17. Rockenbach, G.; Di Pietro, P. F.; Ambrosi, C.; Boaventura, B. C.; Vieira, F. G.; Crippa, C. G.; Da Silva, E. L.; Fausto, M. A., Dietary intake and oxidative stress in breast cancer: before and after treatments. *Nutricion hospitalaria* **2011,** *26* (4), 737-44.

18. Perse, M.; Injac, R.; Strukelj, B.; Cerar, A., High fat mixed lipid diet modifies protective effects of exercise on 1,2 dimethylhydrazine induced colon cancer in rats. *Technology in cancer research & treatment* **2012,** *11* (3), 289-99.

19. Clerc, P.; Bensaadi, N.; Pradel, P.; Estival, A.; Clemente, F.; Vaysse, N., Lipid-dependent proliferation of pancreatic cancer cell lines. *Cancer research* **1991,** *51* (14), 3633-8.

20. Pietilainen, K. H.; Sysi-Aho, M.; Rissanen, A.; Seppanen-Laakso, T.; Yki-Jarvinen, H.; Kaprio, J.; Oresic, M., Acquired obesity is associated with changes in the serum lipidomic profile independent of genetic effects--a monozygotic twin study. *PLoS One* **2007,** *2* (2), e218.

21. Pietilainen, K. H.; Rog, T.; Seppanen-Laakso, T.; Virtue, S.; Gopalacharyulu, P.; Tang, J.; Rodriguez-Cuenca, S.; Maciejewski, A.; Naukkarinen, J.; Ruskeepaa, A. L.; Niemela, P. S.; Yetukuri, L.; Tan, C. Y.; Velagapudi, V.; Castillo, S.; Nygren, H.; Hyotylainen, T.; Rissanen, A.; Kaprio, J.; Yki-Jarvinen, H.; Vattulainen, I.; Vidal-Puig, A.; Oresic, M., Association of lipidome remodeling in the adipocyte membrane with acquired obesity in humans. *PLoS Biol* **2011,** *9* (6), e1000623.

22. Yetukuri, L.; Katajamaa, M.; Medina-Gomez, G.; Seppanen-Laakso, T.; Vidal-Puig, A.; Oresic, M., Bioinformatics strategies for lipidomics analysis: characterization of obesity related hepatic steatosis. *BMC Syst Biol* **2007,** *1*, 12.

23. Graessler, J.; Schwudke, D.; Schwarz, P. E.; Herzog, R.; Shevchenko, A.; Bornstein, S. R., Top-down lipidomics reveals ether lipid deficiency in blood plasma of hypertensive patients. *PLoS One* **2009,** *4* (7), e6261.

24. Han, X.; Yang, J.; Yang, K.; Zhao, Z.; Abendschein, D. R.; Gross, R. W., Alterations in myocardial cardiolipin content and composition occur at the very earliest stages of diabetes: a shotgun lipidomics study. *Biochemistry* **2007,** *46* (21), 6417-28.

25. Gross, R. W.; Han, X., Shotgun lipidomics of neutral lipids as an enabling technology for elucidation of lipid-related diseases. *Am J Physiol Endocrinol Metab* **2009,** *297* (2), E297-303.

26. Han, X.; D, M. H.; McKeel, D. W., Jr.; Kelley, J.; Morris, J. C., Substantial sulfatide deficiency and ceramide elevation in very early Alzheimer's disease: potential role in disease pathogenesis. *J Neurochem* **2002,** *82* (4), 809-18.

27. Katajamaa, M.; Miettinen, J.; Oresic, M., MZmine: toolbox for processing and visualization of mass spectrometry based molecular profile data. *Bioinformatics* **2006,** *22* (5), 634-6.

28. Hilvo, M.; Denkert, C.; Lehtinen, L.; Muller, B.; Brockmoller, S.; Seppanen-Laakso, T.; Budczies, J.; Bucher, E.; Yetukuri, L.; Castillo, S.; Berg, E.; Nygren, H.; Sysi-Aho, M.; Griffin, J. L.; Fiehn, O.; Loibl, S.; Richter-Ehrenstein, C.; Radke, C.; Hyotylainen, T.; Kallioniemi, O.; Iljin, K.; Oresic, M., Novel theranostic opportunities offered by characterization of altered membrane lipid metabolism in breast cancer progression. *Cancer research* **2011,** *71* (9), 3236-45.

29. Jia, L.; Wang, C.; Zhao, S.; Lu, X.; Xu, G., Metabolomic identification of potential phospholipid biomarkers for chronic glomerulonephritis by using high performance liquid chromatography-mass spectrometry. *J Chromatogr B Analyt Technol Biomed Life Sci* **2007,** *860* (1), 134-40.

30. Guerrera, I. C.; Astarita, G.; Jais, J. P.; Sands, D.; Nowakowska, A.; Colas, J.; Sermet-Gaudelus, I.; Schuerenberg, M.; Piomelli, D.; Edelman, A.; Ollero, M., A novel lipidomic strategy reveals plasma phospholipid signatures associated with respiratory disease severity in cystic fibrosis patients. *PLoS One* **2009,** *4* (11), e7735.

31. Fuller, M.; Sharp, P. C.; Rozaklis, T.; Whitfield, P. D.; Blacklock, D.; Hopwood, J. J.; Meikle, P. J., Urinary lipid profiling for the identification of fabry hemizygotes and heterozygotes. *Clin Chem* **2005,** *51* (4), 688-94.

32. Han, X.; Yang, J.; Cheng, H.; Yang, K.; Abendschein, D. R.; Gross, R. W., Shotgun lipidomics identifies cardiolipin depletion in diabetic myocardium linking altered

substrate utilization with mitochondrial dysfunction. *Biochemistry* **2005,** *44* (50), 16684-94.

33. Benton, H. P.; Wong, D. M.; Trauger, S. A.; Siuzdak, G., XCMS2: processing tandem mass spectrometry data for metabolite identification and structural characterization. *Analytical chemistry* **2008,** *80* (16), 6382-9.

34. Fujiwaki, T.; Yamaguchi, S.; Sukegawa, K.; Taketomi, T., Application of delayed extraction matrix-assisted laser desorption ionization time-of-flight mass spectrometry for analysis of sphingolipids in cultured skin fibroblasts from sphingolipidosis patients. *Brain Dev* **2002,** *24* (3), 170-3.

35. van Ginneken, V.; Verhey, E.; Poelmann, R.; Ramakers, R.; van Dijk, K. W.; Ham, L.; Voshol, P.; Havekes, L.; Van Eck, M.; van der Greef, J., Metabolomics (liver and blood profiling) in a mouse model in response to fasting: a study of hepatic steatosis. *Biochim Biophys Acta* **2007,** *1771* (10), 1263-70.

36. Kiebish, M. A.; Young, D. M.; Lehman, J. J.; Han, X., Chronic caloric restriction attenuates a loss of sulfatide content in PGC-1alpha-/- mouse cortex: a potential lipidomic role of PGC-1alpha in neurodegeneration. *J Lipid Res* **2012,** *53* (2), 273-81.

37. Xiao, Y. J.; Schwartz, B.; Washington, M.; Kennedy, A.; Webster, K.; Belinson, J.; Xu, Y., Electrospray ionization mass spectrometry analysis of lysophospholipids in human ascitic fluids: comparison of the lysophospholipid contents in malignant vs nonmalignant ascitic fluids. *Anal Biochem* **2001,** *290* (2), 302-13.

38. Wright, S. M.; Hockey, P. M.; Enhorning, G.; Strong, P.; Reid, K. B.; Holgate, S. T.; Djukanovic, R.; Postle, A. D., Altered airway surfactant phospholipid composition and reduced lung function in asthma. *J Appl Physiol* **2000,** *89* (4), 1283-92.

39. Heeley, E. L.; Hohlfeld, J. M.; Krug, N.; Postle, A. D., Phospholipid molecular species of bronchoalveolar lavage fluid after local allergen challenge in asthma. *Am J Physiol Lung Cell Mol Physiol* **2000,** *278* (2), L305-11.

40. Horai, H.; Arita, M.; Kanaya, S.; Nihei, Y.; Ikeda, T.; Suwa, K.; Ojima, Y.; Tanaka, K.; Tanaka, S.; Aoshima, K.; Oda, Y.; Kakazu, Y.; Kusano, M.; Tohge, T.; Matsuda, F.; Sawada, Y.; Hirai, M. Y.; Nakanishi, H.; Ikeda, K.; Akimoto, N.; Maoka, T.; Takahashi, H.; Ara, T.; Sakurai, N.; Suzuki, H.; Shibata, D.; Neumann, S.; Iida, T.; Funatsu, K.; Matsuura, F.; Soga, T.; Taguchi, R.; Saito, K.; Nishioka, T., MassBank: a public repository for sharing mass spectral data for life sciences. *J Mass Spectrom* **2010,** *45* (7), 703-14.

41. Mora, J. F.; Van Berkel, G. J.; Enke, C. G.; Cole, R. B.; Martinez-Sanchez, M.; Fenn, J. B., Electrochemical processes in electrospray ionization mass spectrometry. *J Mass Spectrom* **2000,** *35* (8), 939-52.

42. Fuchs, B.; Schiller, J.; Wagner, U.; Hantzschel, H.; Arnold, K., The phosphatidylcholine/lysophosphatidylcholine ratio in human plasma is an indicator of the severity of rheumatoid arthritis: investigations by 31P NMR and MALDI-TOF MS. *Clin Biochem* **2005,** *38* (10), 925-33.

43. Kulik, W.; van Lenthe, H.; Stet, F. S.; Houtkooper, R. H.; Kemp, H.; Stone, J. E.; Steward, C. G.; Wanders, R. J.; Vaz, F. M., Bloodspot assay using HPLC-tandem mass spectrometry for detection of Barth syndrome. *Clin Chem* **2008,** *54* (2), 371-8.

44. Valianpour, F.; Mitsakos, V.; Schlemmer, D.; Towbin, J. A.; Taylor, J. M.; Ekert, P. G.; Thorburn, D. R.; Munnich, A.; Wanders, R. J.; Barth, P. G.; Vaz, F. M.,

Monolysocardiolipins accumulate in Barth syndrome but do not lead to enhanced apoptosis. *J Lipid Res* **2005,** *46* (6), 1182-95.

45. Liu, Y.; Chen, Y.; Momin, A.; Shaner, R.; Wang, E.; Bowen, N. J.; Matyunina, L. V.; Walker, L. D.; McDonald, J. F.; Sullards, M. C.; Merrill, A. H., Jr., Elevation of sulfatides in ovarian cancer: an integrated transcriptomic and lipidomic analysis including tissue-imaging mass spectrometry. *Molecular cancer* **2010,** *9*, 186.

46. Zhou, X.; Mao, J.; Ai, J.; Deng, Y.; Roth, M. R.; Pound, C.; Henegar, J.; Welti, R.; Bigler, S. A., Identification of plasma lipid biomarkers for prostate cancer by lipidomics and bioinformatics. *PLoS One* **2012,** *7* (11), e48889.

47. Erickson, K. A.; Smith, M. E.; Anthonymuthu, T. S.; Evanson, M. J.; Brassfield, E. S.; Hodson, A. E.; Bressler, M. A.; Tucker, B. J.; Thatcher, M. O.; Prince, J. T.; Hancock, C. R.; Bikman, B. T., AICAR inhibits ceramide biosynthesis in skeletal muscle. *Diabetol Metab Syndr* **2012,** *4* (1), 45.

48. Balog, J.; Sasi-Szabo, L.; Kinross, J.; Lewis, M. R.; Muirhead, L. J.; Veselkov, K.; Mirnezami, R.; Dezso, B.; Damjanovich, L.; Darzi, A.; Nicholson, J. K.; Takats, Z., Intraoperative Tissue Identification Using Rapid Evaporative Ionization Mass Spectrometry. *Science translational medicine* **2013,** *5* (194).

49. Folch, J.; Lees, M.; Sloane Stanley, G. H., A simple method for the isolation and purification of total lipides from animal tissues. *The Journal of biological chemistry* **1957,** *226* (1), 497-509.

50. Bligh, E. G.; Dyer, W. J., A rapid method of total lipid extraction and purification. *Canadian journal of biochemistry and physiology* **1959,** *37* (8), 911-7.

51. Hajra, A. K., On extraction of acyl and alkyl dihydroxyacetone phosphate from incubation mixtures. *Lipids* **1974,** *9* (8), 502-5.

52. Weerheim, A. M.; Kolb, A. M.; Sturk, A.; Nieuwland, R., Phospholipid composition of cell-derived microparticles determined by one-dimensional high-performance thin-layer chromatography. *Analytical biochemistry* **2002,** *302* (2), 191-8.

53. Lewis, T.; Nichols, P. D.; McMeekin, T. A., Evaluation of extraction methods for recovery of fatty acids from lipid-producing microheterotrophs. *Journal of microbiological methods* **2000,** *43* (2), 107-16.

54. Burja, A. M.; Armenta, R. E.; Radianingtyas, H.; Barrow, C. J., Evaluation of fatty acid extraction methods for Thraustochytrium sp. ONC-T18. *Journal of agricultural and food chemistry* **2007,** *55* (12), 4795-801.

55. Hara, A.; Radin, N. S., Lipid extraction of tissues with a low-toxicity solvent. *Analytical biochemistry* **1978,** *90* (1), 420-6.

56. Cequier-Sanchez, E.; Rodriguez, C.; Ravelo, A. G.; Zarate, R., Dichloromethane as a solvent for lipid extraction and assessment of lipid classes and fatty acids from samples of different natures. *Journal of agricultural and food chemistry* **2008,** *56* (12), 4297-303.

57. Harshman, S.; Conlin, J. G., A simplified procedure for isolating plasma membranes from cultured mouse fibroblast cells: 3T3 and SV-3T3. *Analytical biochemistry* **1978,** *90* (1), 98-106.

58. Eder, K.; Reichlmayr-Lais, A. M.; Kirchgessner, M., Studies on the extraction of phospholipids from erythrocyte membranes in the rat. *Clinica chimica acta; international journal of clinical chemistry* **1993,** *219* (1-2), 93-104.

59. Markham, J. E.; Li, J.; Cahoon, E. B.; Jaworski, J. G., Separation and identification of major plant sphingolipid classes from leaves. *The Journal of biological chemistry* **2006,** *281* (32), 22684-94.

60. Ryckebosch, E.; Muylaert, K.; Eeckhout, M.; Ruyssen, T.; Foubert, I., Influence of drying and storage on lipid and carotenoid stability of the microalga Phaeodactylum tricornutum. *Journal of agricultural and food chemistry* **2011,** *59* (20), 11063-9.

61. Matyash, V.; Liebisch, G.; Kurzchalia, T. V.; Shevchenko, A.; Schwudke, D., Lipid extraction by methyl-tert-butyl ether for high-throughput lipidomics. *Journal of lipid research* **2008,** *49* (5), 1137-46.

62. Ichihara, K.; Yoneda, K.; Takahashi, A.; Hoshino, N.; Matsuda, M., Improved methods for the fatty acid analysis of blood lipid classes. *Lipids* **2011,** *46* (3), 297-306.

63. Dejoye Tanzi, C.; Abert Vian, M.; Chemat, F., New procedure for extraction of algal lipids from wet biomass: a green clean and scalable process. *Bioresource technology* **2013,** *134*, 271-5.

64. Johnson, S.; Knight, R.; Marmer, D. J.; Steele, R. W., Immune deficiency in fetal alcohol syndrome. *Pediatric research* **1981,** *15* (6), 908-11.

65. Zheng, G., Purification of Extracted Fatty Acids from the Microalgae Spirulina. *JAOCS* **2012,** *89* (1), 561-566.

66. Elmer-Frohlich, K. L., Paul A., Faster and Easier Methods for Quantitative Lipid Extraction and Fractionation from Miniature Samples of Animal Tissues. *JAOCS* **1992,** *69* (3), 243-245.

67. Axelsson, M.; Gentili, F., A single-step method for rapid extraction of total lipids from green microalgae. *PloS one* **2014,** *9* (2), e89643.

68. Dreyfus, H.; Aunis, D.; Harth, S.; Mandel, P., Gangliosides and phospholipids of the membranes from bovine adrenal medullary chromaffin granules. *Biochimica et biophysica acta* **1977,** *489* (1), 89-97.

69. Bodennec, J.; Pelled, D.; Futerman, A. H., Aminopropyl solid phase extraction and 2 D TLC of neutral glycosphingolipids and neutral lysoglycosphingolipids. *Journal of lipid research* **2003,** *44* (1), 218-26.

70. Ferraz, T. P.; Fiuza, M. C.; Dos Santos, M. L.; Pontes De Carvalho, L.; Soares, N. M., Comparison of six methods for the extraction of lipids from serum in terms of effectiveness and protein preservation. *Journal of biochemical and biophysical methods* **2004,** *58* (3), 187-93.

71. Cham, B. E.; Knowles, B. R., A solvent system for delipidation of plasma or serum without protein precipitation. *Journal of lipid research* **1976,** *17* (2), 176-81.

72. Brasaemle, D. L.; Dolios, G.; Shapiro, L.; Wang, R., Proteomic analysis of proteins associated with lipid droplets of basal and lipolytically stimulated 3T3-L1 adipocytes. *The Journal of biological chemistry* **2004,** *279* (45), 46835-42.

73. Dole, V. P., Fractionation of plasma nonesterified fatty acids. *Proceedings of the Society for Experimental Biology and Medicine. Society for Experimental Biology and Medicine* **1956,** *93* (3), 532-3.

74. Honeyman, T. W.; Strohsnitter, W.; Scheid, C. R.; Schimmel, R. J., Phosphatidic acid and phosphatidylinositol labelling in adipose tissue. Relationship to the metabolic effects of insulin and insulin-like agents. *The Biochemical journal* **1983,** *212* (2), 489-98.

75. Lloyd, J. V.; Nishizawa, E. E.; Haldar, J.; Mustard, J. F., Changes in 32 p-labelling of platelet phospholipids in response to ADP. *British journal of haematology* **1972,** *23* (5), 571-85.

76. Kumari, P.; Reddy, C. R.; Jha, B., Comparative evaluation and selection of a method for lipid and fatty acid extraction from macroalgae. *Analytical biochemistry* **2011,** *415* (2), 134-44.

77. Wu, L. N.; Genge, B. R.; Kang, M. W.; Arsenault, A. L.; Wuthier, R. E., Changes in phospholipid extractability and composition accompany mineralization of chicken growth plate cartilage matrix vesicles. *The Journal of biological chemistry* **2002,** *277* (7), 5126-33.

78. Michael-Jubeli, R.; Tfayli, A.; Bleton, J.; Baillet-Guffroy, A., Chemometric approach for investigating the skin surface lipids (SSLs) composition: influence of geographical localization. *European journal of dermatology : EJD* **2011,** *21 Suppl 2*, 63-71.

CHAPTER 2:

Global Lipidomics of Diseased States

Introduction:

Once I had established a methodical, reliable, and reproducible model for extracting lipid species from complex biological matrices with an accompanying high-throughput high-confidence lipid identification software suite for use with high-resolution mass spectrometry data it was time to use this knowledge to answer important scientific questions. These techniques were used to gather data for our own research and also to help other research groups that were trying to answer questions about lipid identifications and quantitation.

The first work that was attempted with these new techniques was a tissue-by-tissue global lipidomics database for a mouse model. One of our collaborators provided us with mice from a control group of one of their experiments. Mice were dissected in order to collect skin, adipose, liver, kidney, stomach, pancreas, intestines, heart, lung, bone marrow, and brain. Samples were treated with our extraction technique and then high-resolution mass spectrometry data was collected in both positive and negative ion modes with intra-source separation with ammonium acetate. Over 1500 high-confidence lipid identities were generated for each tissue type. Each tissue type identification and quantification data point was analyzed using a principle component analysis. Tissue type identifications could be clearly separated in a three-dimensional PCA plot. Interestingly we found that the lipid identifications had greater variation between tissue types than the difference that was observed between samples of the same tissues between different individuals of the control group. Also through this experiment we were able to establish expected

lipid concentrations within tissues because we utilized a cocktail of lipid standards of known concentration. This database proved to be helpful for experience and also for comparison with our future experiments.

Our developed lipidomic techniques would then be used most significantly in collaborative efforts where I was heavily involved in experimental direction and design and helped several lab groups and individuals identify and quantify biologically significant lipids from complex matrices. Lipids were collected from cell tissue culture, from extracted muscle fibers, and from whole animal organs. These collaborative efforts resulted in the publication of four lipidomics dependent papers which follow.

Mitochondrial fission mediates ceramide-induced metabolic disruption in skeletal muscle

Summarizing my Contribution: I was approached by the primary author and her advisor due to my experience with global lipidomics. The hypothesis at the time was that ceramide accumulations inside the cell and especially in mitochondria were leading to mitochondrial fission thereby causing metabolic disruption. These accumulations were due to metabolic stress of a high-fat high-sugar (HFHS) diet that the mice were given. I contributed in the development of the experiment and helped develop a model to induce ceramide accumulations by adding short chain ceramides (C2-ceramide). These short chain ceramides are cell membrane permeable and could be added to cell through simple fluid addition. Through my work with global lipidomics we were able to confirm that the short-chain ceramides were involved in trans-esterification reactions resulting in fatty-acid swapping to form longer chain length functional ceramides. I completed all of the lipid identifications and quantitation using high-resolution mass spectrometry based lipidomics. I also contributed to the writing process, formatting, and editing of this manuscript.

Melissa E. Smith, Trevor S. Tippetts, Eric S. Brassfield, Braden J. Tucker, Adelaide Ockey, Adam Clayton Swensen, Tamil S. Anthonymuthu, Trevor D. Washburn, Daniel A. Kane, John T. Prince, Benjamin T. Bikman

Biochemical Journal Dec 15, 2013, 456 (3) 427-439; DOI: 10.1042/BJ20130807

Abstract

Ceramide is a sphingolipid that serves as an important second messenger in an increasing number of stress-induced pathways. Ceramide has long been known to affect the mitochondria, altering both morphology and physiology. We sought to assess the impact of ceramide on skeletal muscle mitochondrial structure and function. A primary observation was the rapid and dramatic division of mitochondria in ceramide-treated cells. This effect is likely to be a result of increased Drp1 (dynamin-related protein 1) action, as ceramide increased Drp1 expression and Drp1 inhibition prevented ceramide-induced mitochondrial fission. Further, we found that ceramide treatment reduced mitochondrial O2 consumption (i.e. respiration) in cultured myotubes and permeabilized red gastrocnemius muscle fibre bundles. Ceramide treatment also increased H2O2 levels and reduced Akt/PKB (protein kinase B) phosphorylation in myotubes. However, inhibition of mitochondrial fission via Drp1 knockdown completely protected the myotubes and fibre bundles from ceramide-induced metabolic disruption, including maintained mitochondrial respiration, reduced H2O2 levels and unaffected insulin signalling. These data suggest that the forced and sustained mitochondrial fission that results from ceramide accrual may alter metabolic function in skeletal muscle, which is a prominent site not only of energy demand (via the mitochondria), but also of ceramide accrual with weight gain.

Introduction

The current worldwide trends of increasing prevalence of obesity and Type 2 diabetes suggest the complexity of the problem and the need for intensive research to discover effective therapeutic interventions. The perfect metabolic storm of dietary excess, poor nutrient quality and reduced physical activity combine to increase the risk of developing insulin resistance, which is not only the foundation of Type 2 diabetes, but is also a contributing cause and consequence of obesity [1,2]. These causal factors (i.e. poor diet and sedentary living) lead to two

distinct theories regarding the aetiology of obesity-induced metabolic disruption, namely altered mitochondrial function and ceramide accumulation.

Despite being commonly represented as small segmented structures, mitochondria are highly dynamic organelles undergoing continuous fission and fusion. Indeed, the word mitochondrion itself reveals the typical state of the mitochondrion (mitos means thread) as reticular rather than segmented. Increasingly, evidence suggests that mitochondrial structure determines mitochondrial function [3], including substrate metabolism [4,5] and mitochondrial bioenergetics [6]. Given that obesity and Type 2 diabetes have been considered a malady of maladaptive mitochondria, it is not surprising that interventions to stimulate mitochondrial fission or fusion elicit disparate effects on metabolic function, such as mitochondrial respiration [6] and insulin signaling [5]. A consensus suggests mitochondrial fusion as beneficial in maintaining insulin sensitivity and resisting fat gain with dietary challenge [4,5].

In addition to altered mitochondrial function, the second factor that may explain obesity-induced metabolic disruption is the accumulation of the sphingolipid ceramide. Ceramide is known to accumulate in insulin-sensitive [7], as well as high-metabolic-rate, organs [7–10], eliciting a potentially powerful impact on whole-body metabolic function. Ceramide is known to induce insulin resistance via decayed Akt/PKB (protein kinase B) phosphorylation, as well as to increase the generation of mitochondria-derived ROS (reactive oxygen species) [11,12], which are increased with mitochondrial fission [13].

With these two distinct theories in mind (i.e. altered mitochondrial function and ceramide accrual), we sought to test the unifying hypothesis that ceramide forces mitochondrial fission, which is a critical mediator of ceramide-induced metabolic disruption. In support of this hypothesis, we observed that exogenous and endogenous ceramide levels increased

mitochondrial fission in cultured cells via Drp1 (dynamin-related protein 1). Increased fission was associated with reduced mitochondrial respiration, likely at complex II, and increased production of ROS. Moreover, we found that mitochondrial fission is important in ceramide-induced insulin resistance, as cells co-treated with a Drp1 inhibitor maintained insulin signalling despite the presence of ceramide. Lastly, mice fed a HFHS (high-fat high-sugar) diet experienced glucose and insulin intolerance relative to SD (standard diet)-fed mice and HFHS-fed mice supplemented with myriocin to inhibit serine palmitoyltransferase, the rate-limiting enzyme in ceramide biosynthesis. Moreover, the myriocin-treated HFHS-fed mice did not gain excess weight. Additionally, mitochondrial respiration was partially blunted in the RG (red gastrocnemius) muscle of the HFHS-fed mice, but not of those receiving myriocin. In the end, the present study suggests the potential efficacy of therapies that reduce excess ceramide accrual and/or prevent ceramide-induced mitochondrial fission in the treatment of obesity and insulin resistance.

Materials and Methods

Animals

Male C57Bl/6 mice were separated at 8 weeks into one of four treatment groups for 12 weeks: (i) SD (Harlan Teklad 8604), (ii) HFHS diet [Harlan Taklad 2018+15% (w/v) sucrose water], (iii) SD with myriocin (SD+Myr) and (iv) HFHS diet with myriocin (HFHS+Myr). For myriocin supplementation, myriocin was supplied in drinking water at 2.5 μg/ml, which, with average drinking patterns, equates to approximately 0.3 mg/kg of body weight per day [14]. Following the treatment period, mice underwent intraperitoneal glucose (Sigma–Aldrich; G7021) and insulin (Actrapid; Novo Nordisk) tolerance tests. For both tests, mice were fasted for 6 h and received an injection of either glucose (1 g/kg of body weight) or insulin (0.75 unit/kg of body

weight). Blood glucose was determined at the times indicated in the Figures using the Bayer Contour glucose meter. Studies were conducted in accordance with the principles and procedures outlined in the National Institutes of Health Guide for the Care and Use of Laboratory Animals and were approved by the IACUC (Institutional Animal Care and Use Committee) at Brigham Young University.

Cell culture

C2C12 murine myoblast cells were maintained in DMEM (Dulbecco's modified Eagle's medium) plus 10% FBS (Invitrogen). For differentiation into myotubes, C2C12 myoblasts were grown to confluency and the medium was replaced with DMEM plus 10% horse serum (Invitrogen). Myotubes were used for experiments on day 4 of differentiation. For fatty acid treatment, palmitic acid (Sigma–Aldrich; catalogue number P5585) was dissolved in EtOH (ethanol) and diluted to the desired concentration in DMEM containing 2% (w/v) BSA (Sigma–Aldrich; A9576) and added to the cell culture at 0.5 mM, which is a physiological post-prandial fatty acid concentration [15]. For ceramide treatment, C2 (C2-ceramide; N-acetyl-D-sphingosine; Sigma–Aldrich; A7191) was diluted in EtOH in a 10 mM stock solution. For Mdivi-1 (mitochondrial division inhibitor 1) treatment, Mdivi-1 (Sigma–Aldrich; M0199) was diluted in DMSO in a 50 mM stock solution. For sptlc2 (serine palmitoyltransferase, long chain base subunit 2; also known as SPT2) knock down, procedures were followed according to the manufacturer's instructions (Santa Cruz Biotechnology; sc-77377).

Lipid analysis

For isolation of lipids, pellets were re-suspended in 900 µl of ice-cold chloroform/methanol (1:2), incubated for 15 min on ice, then briefly vortex-mixed. Separation of

aqueous and organic phases required addition of 400 µl of ice-cold water and 300 µl of ice-cold chloroform. The organic phase was collected into a fresh vial, and lipids were dried in a vacuum centrifuge (Eppendorf Concentrator Plus). Lipids were characterized and quantified using a shotgun lipidomics technique on a Thermo Scientific LTQ Orbitrap XL mass spectrometer. Evaporated lipid samples were re-suspended in a 2:1 chloroform/methanol Folch solution (200 µl). The re-suspended lipids were then combined with a modified 2:1:1.25 chloroform/methanol/propan-2-ol Bligh and Dyer solution (800 µl) with 15 mM ammonium acetate acting as an ionizing adduct. A 1.74 µM phosphatidylethanolamine internal standard (1 µl) was spiked into each sample for mass calibration and characterization data alignment. Samples were analysed using a 2.5 min mass-window-scanning method in positive-ion mode at a resolution of 60000 [fwhm (full width at half maximum) at 400 m/z] for all primary MS1 scans. MS2 (tandem MS) fragmentation data were also collected and manually verified for each mass window to give additional confidence to the correct identification of abundant lipid species. Three technical replicate mass spectrometer runs were performed on each sample. Samples were injected at 10 µl/min using a direct-inject ESI soft-ionization spray head from a Hamilton GASTIGHT glass syringe. The spray voltage and capillary temperature were maintained at 5.0 kV and 275°C respectively. Each technical replicate was run in random order to reduce systematic bias. Data were analysed using in-house-developed peak summarization, recalibration and lipid identification software using lipid database information from the Lipid MAPS (LIPID Metabolites and Pathways Strategy) Lipidomics Gateway database [16]. To ensure high-confidence identifications, an intensity threshold estimated to be 5% above the instrumental static signal was implemented. Lipid identities were only assigned when significantly observable peaks were identified in at least two of the three technical replicate runs. Non-zero lipid quantities were

averaged from the replicate runs. The lipid species identified across different ionization states or with adducts were totalled together. Quantification was completed by normalizing total ion counts to the relative abundance of the internal standard that was spiked into each sample.

Mitochondrial morphology

C2C12 myoblasts were grown to confluence in chamber slides (NUNC Lab-Tek II Chambered Coverglass System; 155382) and differentiate at day 4. The mitochondrial dye MitoTracker Red CMXRos (Molecular Probes; M7512), dissolved in anhydrous DMSO, was added to cultured myotubes at a concentration of 250 nM. The cells were incubated for 30 min at 37°C in the dark and then visualized using a confocal microscope (Olympus IX81). For muscle mitochondrial imaging, the RG muscle was extracted and fixated in 0.1 M sodium cacodylate and 3% gluteraldehyde at pH 7.3 for 3 h. The tissues were washed in 0.1 M sodium cacodylate (six times for 10 min) and then washed in ddH2O (double-distilled water; six times for 10 min). Post-fixation occurred in 1% OsO4 (0.1 M for 2h at 22°C). The samples were then soaked overnight in 0.5% uranyl acetate at 4°C. The tissues were dehydrated in a graded series of acetone (10 min steps of 10%, 30%, 50%, 70%, 95% and 100% three times) then embedded in Spurrs® resin. Ultrathin sections (90 nm thick) were cut with a microtome and diamond blade then stained with 0.4% lead citrate. The samples were then imaged with transmission electron microscopy.

Quantitative real-time PCR

Total RNA was extracted and purified from tissues using TRIzol® (Invitrogen) according to the manufacturer's recommendations. cDNA was synthesized from mRNA via reverse transcription–PCR using a commercial cDNA synthesis kit with oligo(dT) primers (iScript Select

cDNA Synthesis; Bio-Rad Laboratories). Quantitative real-time PCR was performed with Evagreen Ssofast (Bio-Rad Laboratories) using a Bio-Rad Laboratories CFX Connect Real-Time PCR Detection system. Primer sequences were 5′-ACAGGATGCAGAAGGAGATTAC-3′ and 5′-CACAGAGTACTTGCGCTCAGGA-3′ as the forward and reverse primers respectively for actin, 5′-ACTTGACCTCCCTACTGGC-3′ and 5′-TCCTCTATCCCGTTGACACC-3′ as the forward and reverse primers respectively for Drp1, and 5′-AAGTCCGGGAAGCTGAAAGT-3′ and 5′-TCTCGGTTATGGAACCAACC-3′ as the forward and reverse primers respectively for Mfn2 (mitofusin 2). β-Actin reactions were performed side by side with every sample analysed. Changes in the mRNA level of each gene for each treatment were normalized to that of the β-actin control mRNA according to Pfaffl [17].

Protein analysis

Tissue and cell extracts lysed and protein content was determined using a BCA protein assay (Pierce) and the sample volumes were adjusted so that precisely 50 μg of protein was loaded into each lane. After the addition of sample buffer, samples were resolved by SDS/PAGE (10% gel), transferred on to nitrocellulose membranes and immunoblotted using methods described previously [18]. After incubation with primary antibody, blots were incubated with an HRP (horseradish peroxidase)-conjugated secondary antibody. HRP activity was assessed with ECL solution (Thermo Scientific) and exposed to film. The primary antibodies used were: anti-SPT2 (Abcam; ab23696), anti-phospho-Akt (Cell Signaling Technology; 4058S), anti-Akt/PKB (Sigma–Aldrich; 217005), the OxPhos Complex Kit (Invitrogen; 457999) and anti-actin (Cell Signaling Technology; 8457S). The secondary antibodies used were: anti-(mouse IgG) (Cell Signaling Technology; 7076S) and anti-(rabbit IgG) (Cell Signaling Technology; 7074S).

Cell and muscle fibre bundle permeabilization

For the cells, C2C12 myotubes were detached in culture dishes with 0.05% trypsin/EDTA (Sigma) and growth medium was added to the culture. Contents were transferred into a tube and centrifuged for 10 min at 1500 g at room temperature (25°C). After removal of the supernatant, cells were resuspended in mitochondrial respiration buffer 05 [MiR05; 0.5 mM EGTA, 10 mM KH2PO4, 3 mM MgCl2·6H2O, 60 mM K-lactobionate, 20 mM Hepes, 110 mM sucrose and 1 mg/ml fatty-acid-free BSA (pH 7.1)] plus 1 mg/ml digitonin and gently rocked at room temperature for 5 min before centrifugation at 10 min at 1500 g for 5 min. After discarding the supernatant, cells were then suspended in 2.2 ml of warm MiR05 and transferred into chambers in a O2K respirometer (Oroboros Instruments). Following the respiration protocol (outlined below), cells were removed from the chambers and used for further analysis, including protein quantification. For skeletal muscle use, the RG muscle was quickly removed from mice following cervical dislocation and immediately placed in ice-cold buffer X [60 mM K-Mes, 35 mM KCl, 7.23 mM K2-EGTA, 2.77 mM CaK2-EGTA, 20 mM imidazole, 20 mM tuarine, 5.7 mM ATP, 15 mM PCr (phosphocreatine) and 6.56 mM MgCl2·6H2O (pH 7.1)] and trimmed of connective tissue. Small fibre bundles were prepared and gently separated along their longitudinal axis under a surgical scope (Olympus, ST) to a size of around 1 mg. Bundles were then transferred into a tube with chilled buffer X and 50 µg/ml saponin, rocked at 4°C for 30 min, and then washed in buffer Z [105 mM K-Mes, 30 mM KCl, 10 mM KH2PO4, 5 mM MgCl2·6H2O and 0.5 mg/ml BSA (pH 7.1)] at 4°C for at least 15 min.

Mitochondrial respiration

High-resolution O2 consumption was determined at 37°C in permeabilized cells (MiR05) and fibre bundles (buffer Z) using the Oroboros Instruments O2K oxygraph. Before the addition of the samples into the respiration chambers, a baseline respiration rate was determined. After

addition of the sample, the chambers were hyperoxygenated to ~350 nmol/ml. Following this, respiration was determined according to two SUIT (substrate-uncoupler-inhibitor titration) protocols [5]. For SUIT1, to determine the general electron transport system function, electron flow through complex I was supported by GM (glutamate+malate; 10 and 2 mM respectively) to determine O2 consumption from proton leak (GML). Following stabilization, ADP (2.5 mM) was added to determine oxidative phosphorylation capacity (GMP). The integrity of the outer mitochondrial membrane was then tested by adding cytochrome c (10 μM; GMcP). Succinate was added (GMSP) for complex I+II electron flow into the Q-junction. To determine the full ETS (electron-transport system) capacity over oxidative phosphorylation, the chemical uncoupler FCCP (carbonyl cyanide p-trifluoromethoxyphenylhydrazone) was added (0.05 μM, followed by 0.025 μM steps until maximal O2 flux was reached). Complex II-supported ETS was then measured by inhibiting complex I with Rot (rotenone; 0.5 μM). Lastly, residual O2 consumption was measured by adding antimycin A (2.5 μM) to block complex III action, effectively stopping any electron flow. This provides a rate of respiration that is used as a baseline and all presented values are controlled for by using this baseline. SUIT2 was used to determine complex II-specific respiration. This SUIT involved succinate (10 mM) with the addition of Rot (0.5 μM), for complex II-mediated leak respiration [S(Rot)L], and then ADP (2.5 mM), for complex II-mediated oxidative phosphorylation. Lastly, maximal ETS was determined by the addition of FCCP as above. Similarly, residual O2 consumption was determined by antimycin A (2.5 μM) addition and all values were controlled for using this value.

H2O2 emission

H2O2 emission was measured using an Amplex Red Hydrogen Peroxide/Peroxidase Assay kit (Molecular Probes; A22188). A reaction mixture containing 50 μM Amplex Red and

0.1 unit/ml HRP in KRPG (Krebs-Ringer phosphate glucose) buffer was prepared (145 mM NaCl, 5.7 mM sodium phosphate, 4.86 mM KCl, 0.54 mM CaCl2, 1.22 mM MgSO4 and 5.5 mM glucose). The reaction mixture was pre-warmed in a 96-well plate with 100 µl of mixture per well. A 20 µl aliquot of cells suspended in KRPG buffer (~1.5×104 cells) were added to each well. Samples were incubated for 1 h. Fluorescence was measured with a microplate reader (Molecular Devices; Gemini EM).

Statistics

Data are presented as means±S.E.M. Data were compared by ANOVA with Tukey's post-hoc analysis (Graphpad Prism). Significance was set at $P<0.05$.

Results

Ceramide increases mitochondrial fission via Drp1

Drp-1 is a mitochondrial fission protein that induces outer membrane 'pinching' in the division of tubular mitochondria. Drp1 mRNA expression was significantly increased in C2C12 myotubes within 4 h of C2 (20 µM) treatment, and peaked after 8 h with a 3-fold increase compared with the baseline (Figure 1B). Further, C2 treatment (20 µM) caused mitochondrial fission in mouse C2C12 myotubes after 16 h of treatment (Figure 1A). However, pre-treatment with Mdivi-1, an inhibitor of Drp1 [19], prevented mitochondrial fission (Figure 1A). Functionally, C2-induced mitochondrial fission led to significantly reduced complex II-supported respiration (GMSP), as determined by O2 consumption in permeabilized C2C12 myotubes in the presence of glutamate, malate, succinate and ADP (Figure 1C). This was completely prevented by the co-treatment of Mdivi-1 in cell culture (Figure 1C).

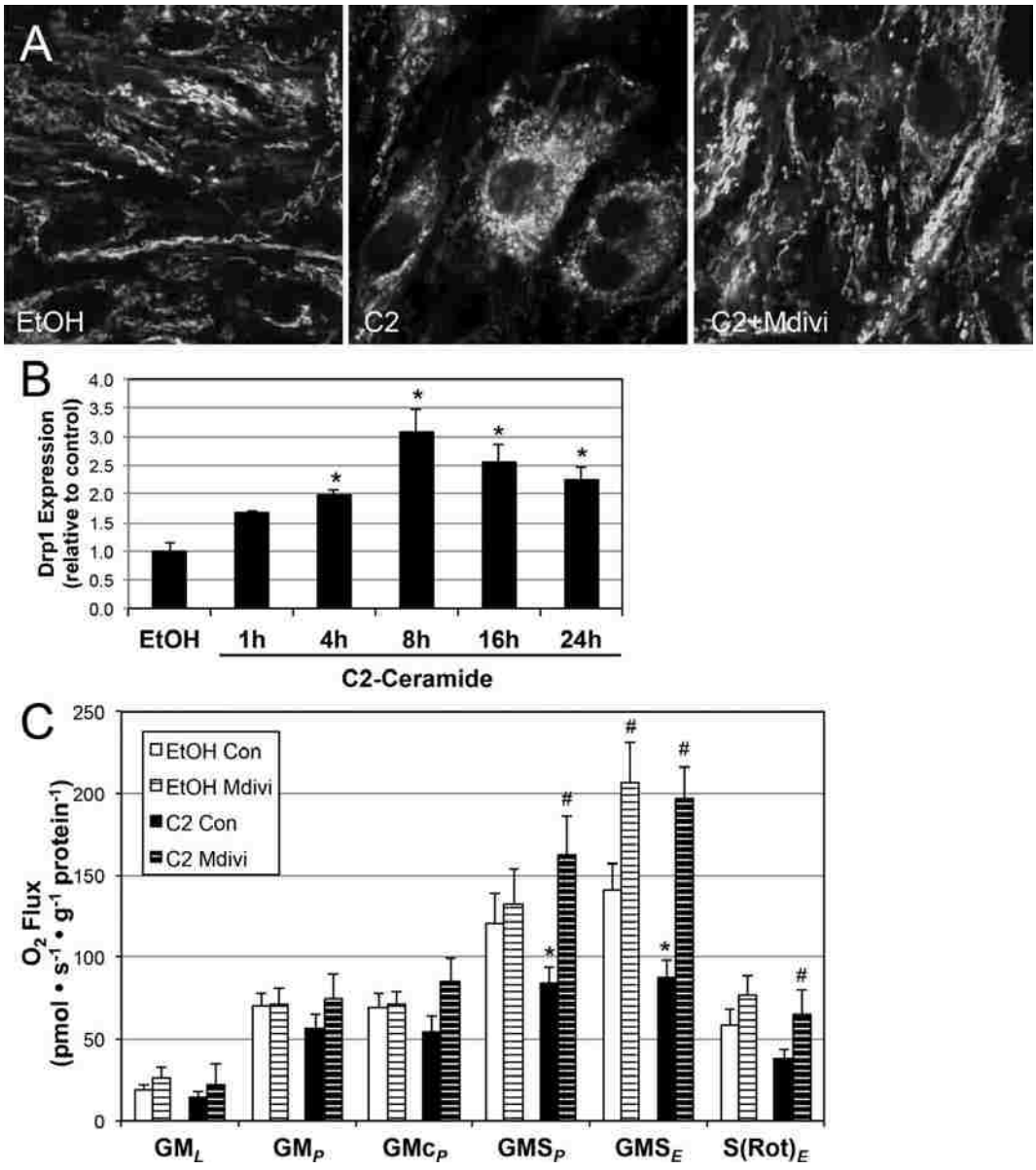

Figure 1: Ceramide induces mitochondrial fission and reduces mitochondrial respiration

(A) C2C12 myotubes were treated with vehicle (EtOH), C2 (40 μM) or C2 and Mdivi-1 (150 μM) for 16 h. MitoTracker Red was then added to visualize mitochondria via confocal microscopy (n=5). (B) Following treatment with C2 (40 μM) for the indicated time points, Drp1 gene expression was quantified via quantitative real-time PCR (n=5). (C) Myotubes were treated with C2 (40 μM) or vehicle (EtOH) in the presence or absence of Mdivi-1 (150 μM) for 16 h.

Following treatment, the rate of O2 consumption was determined using SUIT1 (see the Materials and methods section for details) (n=3). *P<0.05 for C2 compared with EtOH; #P<0.05 for Mdivi compared with the control (Con).

To further confirm the effect of ceramide on mitochondrial fission, we explored the role of endogenously produced ceramides in response to fatty acid treatment. Accordingly, the sptlc2 gene was knocked down via siRNA (Santa Cruz Biotechnology) to prevent ceramide biosynthesis. Complete loss of the SPT2 protein was found at 120 h (Figure 2A) and subsequent experiments occurred at this time. The functionality of knock down was confirmed by the observed prevention of increased ceramide accrual with PA (palmitate) treatment (Figure 2B). Similar to ceramide treatments, PA resulted in mitochondrial fission (Figure 2C). Drp1 gene expression was elevated approximately 3-fold in the PA-treated cells, but not in SPT2-knockdown cells (Figure 2D), suggestive of the importance of ceramide in Drp1 expression. Moreover, mitochondria in cells lacking SPT2 were more fused than control cells receiving PA (Figure 2C). Although not as dramatic as in C2-treated cells, PA treatment also blunted respiration from complex-II-supported oxidative phosphorylation (GMSP; Figure 2E).

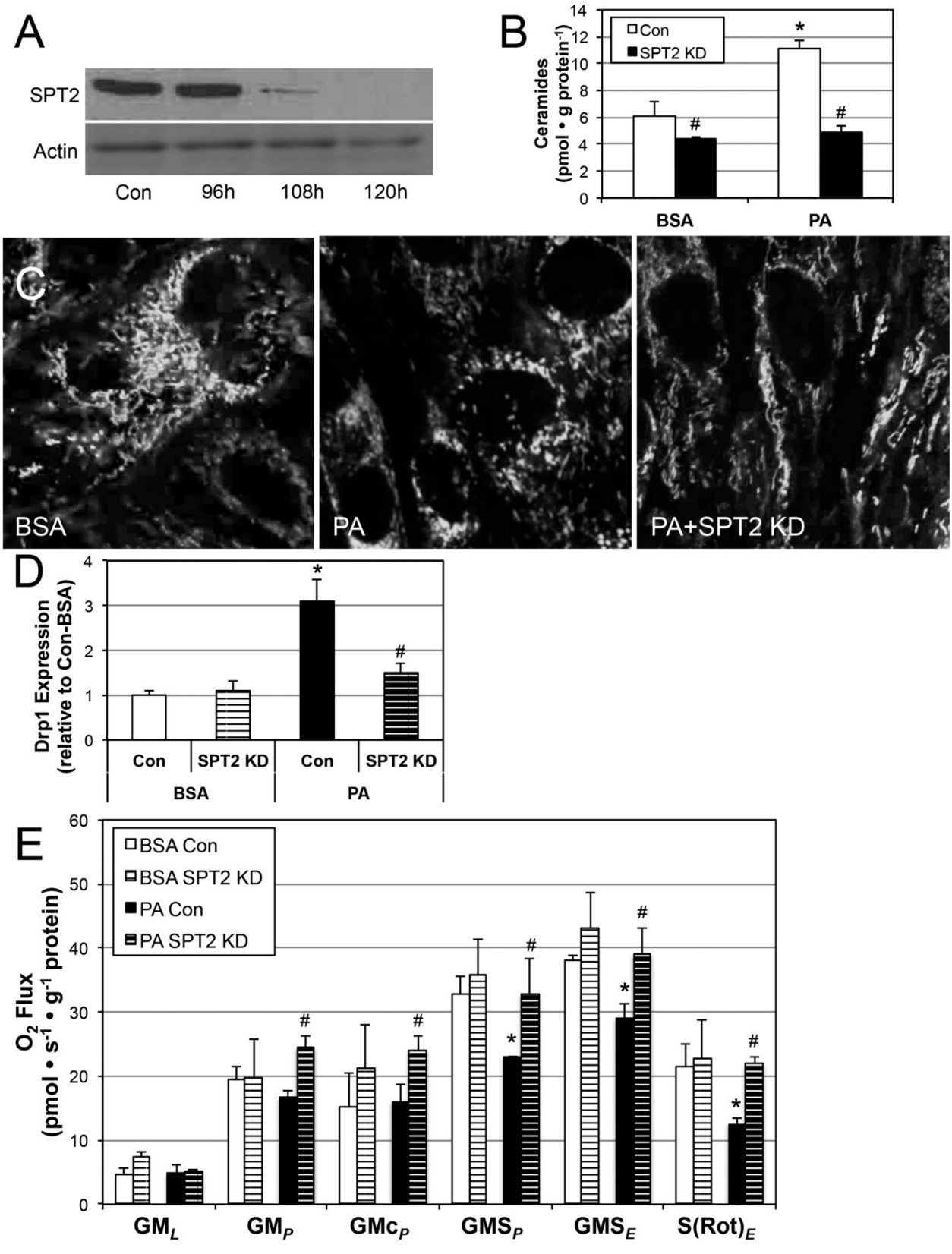

Figure 2: PA mimics the effects of ceramide on mitochondrial structure and function

(A) SPT2 was knocked down using Sptlc2 siRNA in C2C12 myotubes (n=3). (B) The functional effect of the SPT2 knockdown was confirmed by treating control (Con) and SPT2-knockdown (KD) myotubes (n=5). (C) C2C12 myotubes were treated with BSA and BSA-conjugated PA (0.5 mM) for 16 h and the mitochondrial network was visualized with MitoTracker Red via confocal microscopy and compared with PA-treated SPT2-knockdown cells (n=5). (D) Following treatment with PA, Drp1 gene expression was quantified from control and SPT2-knockdown cells via quantitative real-time PCR (n=5). (E) Control and SPT2-knockdown myotubes were treated with BSA alone (BSA) or BSA-conjugated PA (PA) for 16 h. Following treatment, the rate of O2 consumption was determined with SUIT1 (see the Materials and methods section for details) (n=3). *P<0.05 for PA compared with BSA; #P<0.05 for SPT2-knockdown compared with control cells.

Ceramide inhibits complex II-supported mitochondrial respiration

Given our observations of a preferentially greater inhibition of complex II-supported mitochondrial respiration with ceramide treatment, we sought to elucidate this effect more directly. Accordingly, C2C12 myotubes were treated overnight with C2 or vehicle (EtOH). Although no significant difference was observed with succinate and Rot alone to determine leak respiration [S(Rot)L], the addition of ADP to induce oxidative phosphorylation elicited a robust increase in respiration in vehicle-treated cells that was less evident in ceramide-treated cells (Figure 3A). The same discrepancy was observed with the addition of the uncoupler FCCP, which collapses the chemiosmotic gradient via proton transport. This change in complex II-supported respiration occurred independent of a change in the amount of complex II (Figure 3B, CII – Fp subunit).

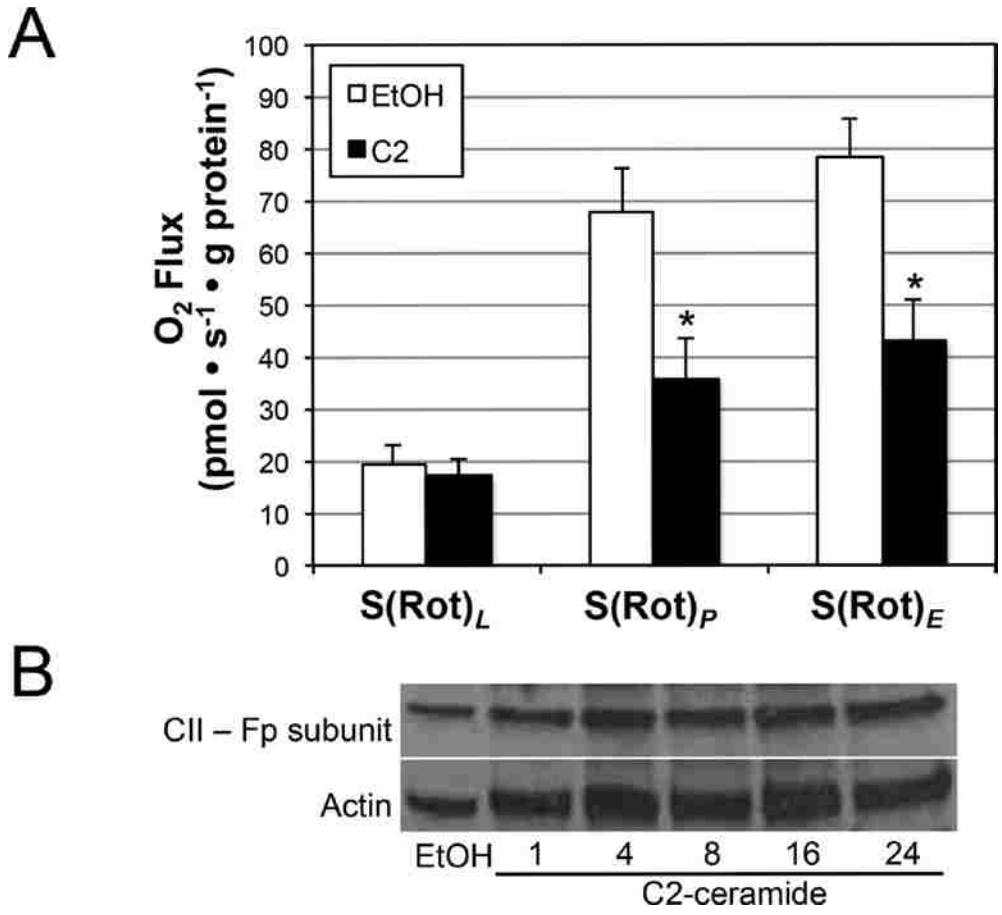

Figure 3: Complex II-mediated mitochondrial respiration is adversely affected by ceramide treatment

(A) Vehicle- (EtOH) and C2- (40 μM) treated cells were permeabilized and O2 consumption was determined with SUIT2 (see the Materials and methods section for details) (n=6). *P<0.05 for C2 compared with EtOH. (B) Complex II (CII) Fp subunit levels were determined in C2-treated cells over various time points as an assessment of complex II presence in the cells (n=2).

Inhibition of mitochondrial fission prevents reduced mitochondrial respiration with ceramide ex vivo

Next, we sought to replicate our findings in whole muscle. Accordingly, the RG muscle was dissected from C57Bl6 mice and permeabilized. After permeabilization, fibre bundles were washed and placed in oxygraph sample chambers (O2K, Oroboros Instruments) filled with 2 ml of buffer Z and vehicle (EtOH) or C16-ceramide (20 μM). Further analyses included the addition of Mdivi-1 to inhibit Drp1-mediated mitochondrial fission. Upon placement in the chambers, fibre bundles were incubated in the buffer at 37°C for 10 min. Following this, respiration was determined according to the indicated SUIT protocol [5]. We observed a significant increase in leak respiration (GML) in those fibres treated with Mdivi-1, although this difference did not linger with the addition of ADP (Figure 4). We are not the first to note increased proton-leak-dependent respiration with increased mitochondrial fusion [20]. In contrast with Mdivi-1 treatment, ceramide-treated muscle fibre bundles exhibited a significantly blunted respiration with complex I- and II-supported respiration. No effect was observed when fibre bundles were treated with C2 or C6-ceramide (results not shown).

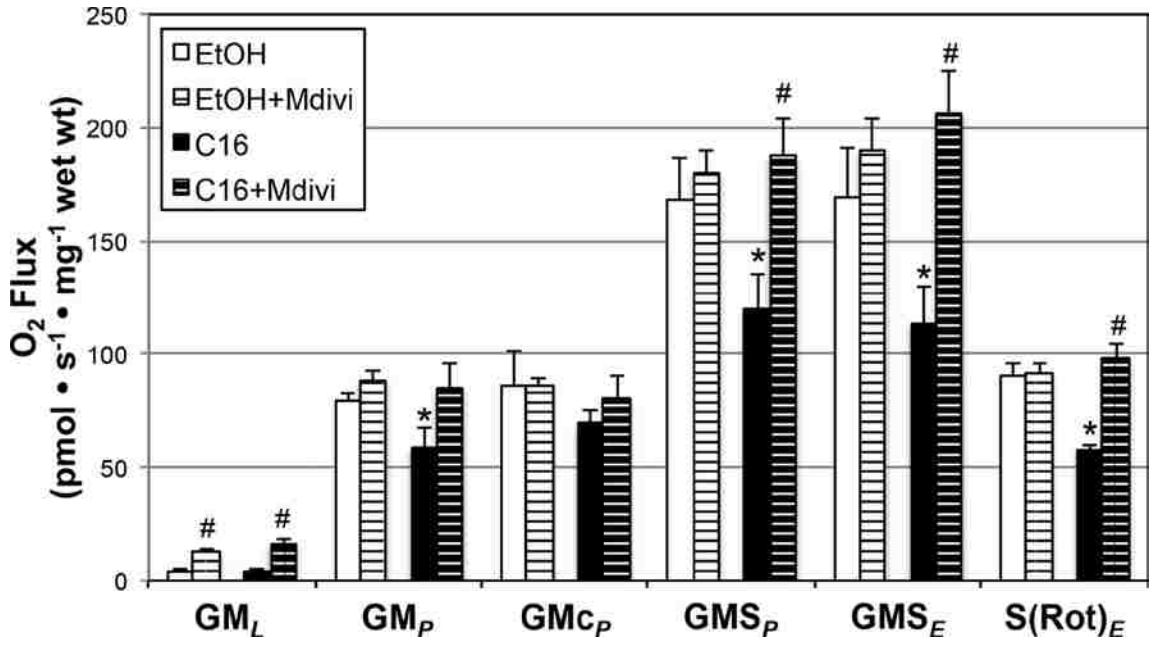

Figure 4: Mitochondrial fission is a requisite for ceramide-induced decayed mitochondrial respiration

O2 consumption was determined in permeabilized RG muscle treated with vehicle (EtOH), vehicle with Mdivi-1 (EtOH+Mdivi) to inhibit Drp1, C16-ceramide (C16) alone or with Mdivi-1 (C16+Mdivi) using SUIT 1 (see the Materials and methods section for details) (n=5). *P<0.05 for C16 compared with EtOH; #P<0.05 for Mdivi compared with the control (Con).

Mitochondrial fission is necessary for ceramide-induced ROS generation and insulin resistance in muscle

Mouse myotubes were treated with C2 or PA in the presence or absence of Mdivi-1 for 12 h. Following treatment, cells were washed with PBS and exposed to Amplex Red to quantify H2O2 production. Although C2 alone elicited an increase in fluorescence with Amplex Red treatment, this effect was mitigated by inhibition of mitochondrial fission by Mdivi-1 co-

treatment (Figure 5A). Considering the evidence suggesting redox-sensitive phosphorylation events in the regulation of the insulin signalling pathway [21], we explored the effect of blocking mitochondrial fission, with its subsequent reduction in H2O2 formation, on muscle insulin signalling. Inhibition of mitochondrial fission with Mdivi-1 protected Akt/PKB phosphorylation with insulin stimulation in C2-treated myotubes (Figure 5B).

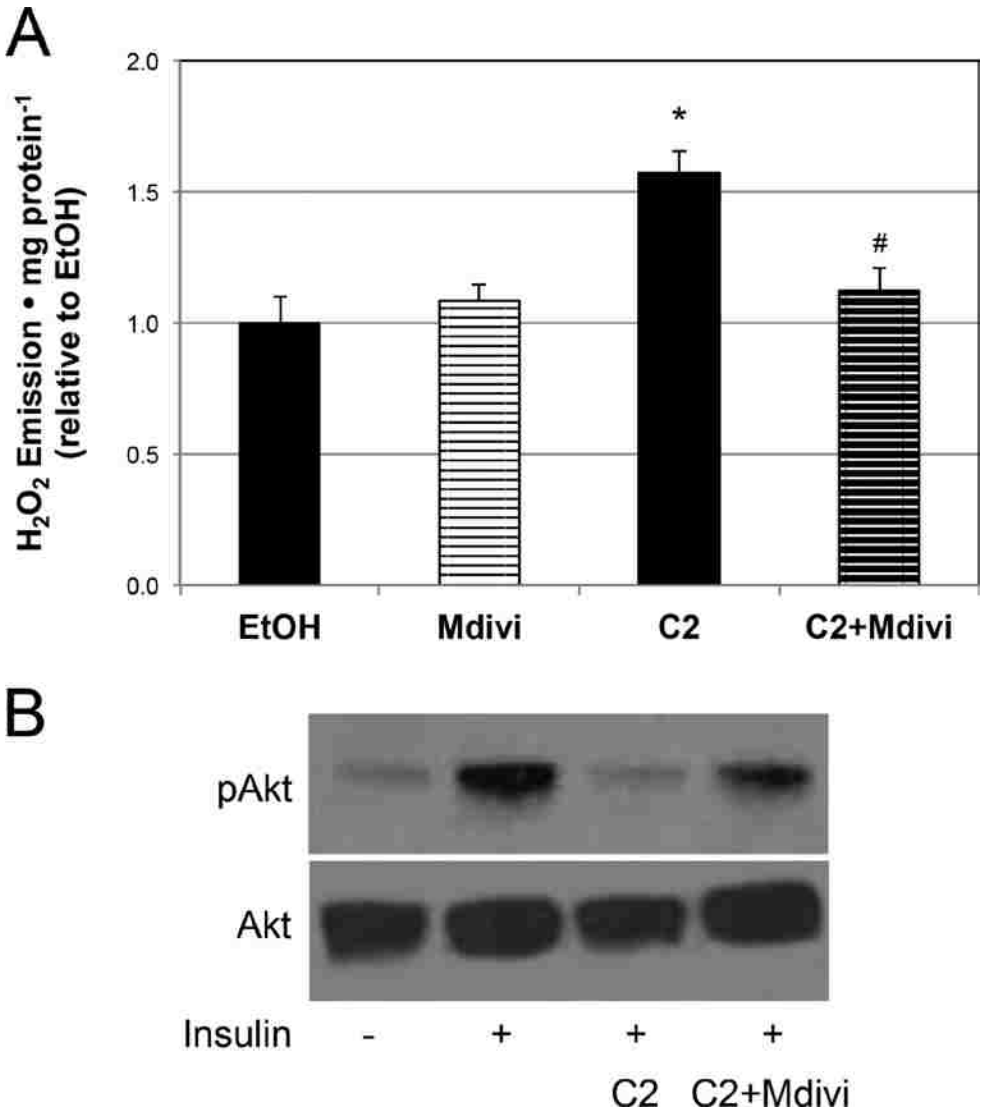

Figure 5: Mitochondrial fission inhibition prevents ceramide-induced H2O2 generation and insulin signaling

(A) C2C12 myotubes were treated with vehicle (EtOH), Mdivi-1 (Mdivi), C2 and C2 with Mdivi-1 (C2+Mdivi) followed by incubation with Amplex Red (n=5). (B) Following a 16 h treatment with C2 without (C2) or with (C2+Mdivi) Mdivi-1, cells were treated with 100 nM insulin for 10 min (n=3). Inhibition of mitochondrial fission prevented both C2-induced H2O2 and the loss of insulin signalling. *P<0.05 for C2 compared with EtOH; #P<0.05 for C2+Mdivi compared with C2.

ROS generation is not necessary for mitochondrial fission or altered mitochondrial respiration with PA and ceramide treatments

To address whether ROS are necessary for the mitochondria-specific effects of both ceramide and PA, we replicated earlier experiments with the addition of the glutathione precursor NAC (N-acetylcysteine), an effective reducing agent known to neutralize H2O2 [22,23]. We found that C2-treated cells that were pre-treated with NAC appeared to experience a similar degree of mitochondrial fission as the C2 treatment alone (Figure 6A). Functionally, NAC pre-treatment likewise failed to prevent reduced mitochondrial respiration in ceramide- and PA-treated myotubes (Figures 6B and 6C respectively).

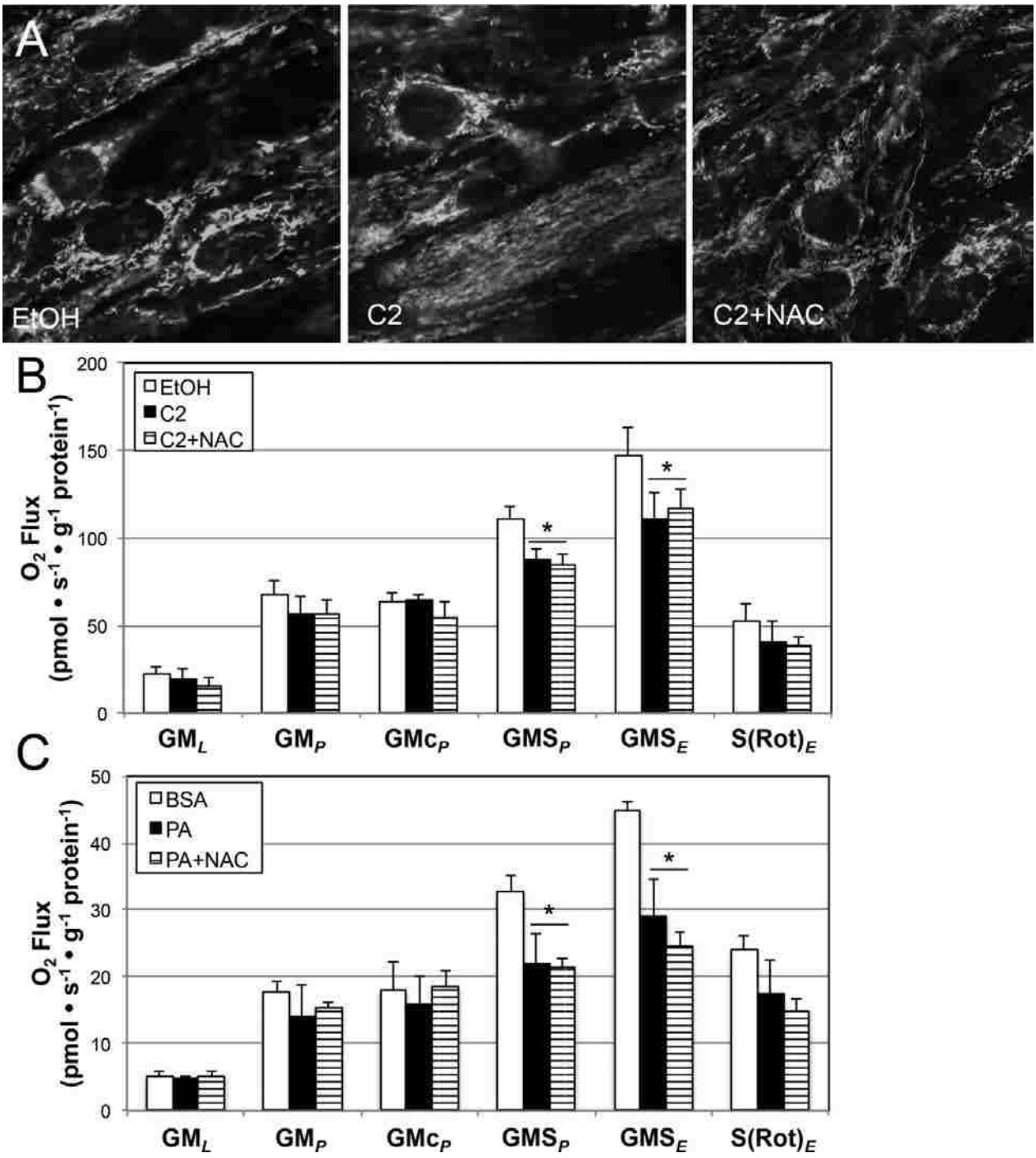

Figure 6: NAC does not prevent ceramide-induced mitochondrial alterations

(A) C2C12 cells were treated with vehicle (EtOH), C2 (40 μM) and C2 with NAC (5 mM; C2+Mdivi) followed by incubation with Amplex Red (n=2). (B) Myotubes were treated with vehicle (EtOH) or C2 (40 μM) in the presence or absence of NAC (5 mM) for 16 h (n=3). (C)

Myotubes were treated with vehicle (BSA) or PA (0.5 mM) in the presence or absence of NAC (5 mM) for 16 h (n=3). Following both treatments in (B) and (C) the rate of O2 consumption was determined with SUIT1 (see the Materials and methods section for details). *P<0.05 for C2 and PA compared with EtOH and BSA.

Inhibition of ceramide biosynthesis prevents metabolic disruption with dietary challenge

Male 8-week-old C57Bl6 mice were separated into one of four treatment groups for 12 weeks: (i) SD, (iii) HFHS diet, (iii) SD with myriocin (SD+Myr) and (iv) HFHS diet with myriocin (HFHS+Myr). No differences in food or water consumption were noted between the SD and SD+Myr groups and the HFHS and HFHS+Myr groups, although both the HFHS and HFHS+Myr groups consumed more water than the SD groups (results not shown). Marked differences in body weight were noted early in the dietary intervention, which lingered until the conclusion of the study period. Specifically, the HFHS group, but not the HFHS+Myr group, gained significantly greater body weight over the course of the study (Figure 7A). Further, the HFHS group experienced a significant reduction in glucose and insulin tolerance, but the HFHS+Myr group did not have a reduced response (Figures 7B and 7C respectively).

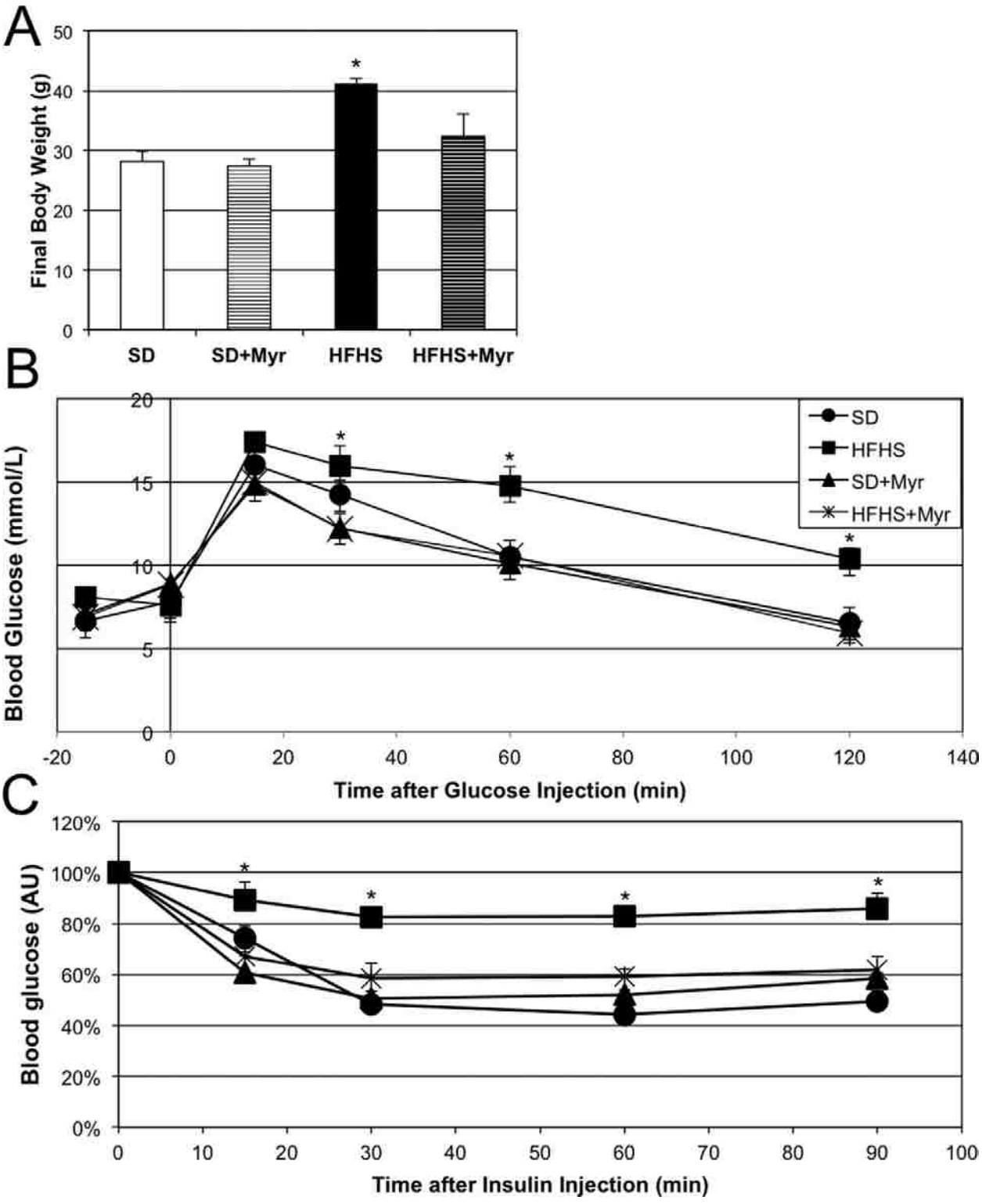

Figure 7: Ceramide inhibition prevents diet-induced weight gain and improves insulin sensitivity

(A) Following a 12 week dietary intervention, mice fed a HFHS diet weighed significantly more than mice fed a SD without (SD) or with (SD+Myr) myriocin. Mice fed a HFHS diet with myriocin supplementation (HFHS+Myr) did not gain excess weight. Following the treatment period, intraperitoneal glucose [(B) 1g/kg of body weight] and insulin [(C) 0.75 unit/kg of body weight] tolerance tests were conducted. In every case, myriocin improved the metabolic profile (n=6). *P<0.05 for the HFHS diet compared with the HFHS diet and myriocin.

Owing to insufficient samples of RG muscle, full statistical analyses were not performed for ceramides and Drp1 expression in the RG. Thus, to determine the effect of intervention in a similarly highly oxidative mitochondria-rich tissue, the soleus muscle was used as a surrogate for a complimentary analysis. Both muscles are commonly used in analyses of muscle mitochondrial capacity [24]. Ceramide levels were significantly elevated in the soleus of the HFHS group compared with the SD groups, but not in the HFHS+Myr group (Figure 8B). As mentioned above, statistical analysis of RG ceramide levels (Figure 8A) was not possible, although a trend appears to suggest a difference exists. Analysis of Drp1 expression in the soleus muscle revealed a robust increase in Drp1 expression with the HFHS diet over the other groups (Figure 9B), suggesting a role for Drp1 in mediating diet-induced mitochondrial fission. A lack of tissue for RG muscle analysis prevented statistical analysis, although the given data suggested a similar trend in the RG as noted in the soleus muscle (Figure 9A). Analysis of mitochondrial O2 consumption in permeabilized muscle (RG) fibre bundles revealed a selective reduction in respiration in the HFHS group (Figure 9C). Specifically, both myriocin-treated groups had slightly higher leak respiration in the presence of GM alone (GML). This trend of myriocin to increase respiration continued to various degrees throughout the protocol, but was most apparent

in the HFHS group. Moreover, respiration was blunted with both complex I- and II-mediated oxidative phosphorylation, although the difference was once again amplified with complex II-supported respiration. A portion of each RG muscle was prepared for electron microscopy to determine mitochondrial morphology with the various interventions (Figure 10). Little difference in size of both the subsarcolemmal (Figure 10, left-hand panels) and intramyofibrillar (Figure 10, right-hand panels) mitochondrial populations was noted between the SD-fed animals (Figure 10A) and those with myriocin supplementation (Figure 10B). In contrast, the HFHS diet appeared to result in markedly smaller and more segmented mitochondria than the SD groups (Figure 10C). However, long-term treatment of HFHS-fed animals with myriocin prevented this (Figure 10D). In particular, the subsarcolemmal mitochondria in the RG from the HFHS+Myr group appeared larger than those from any other group.

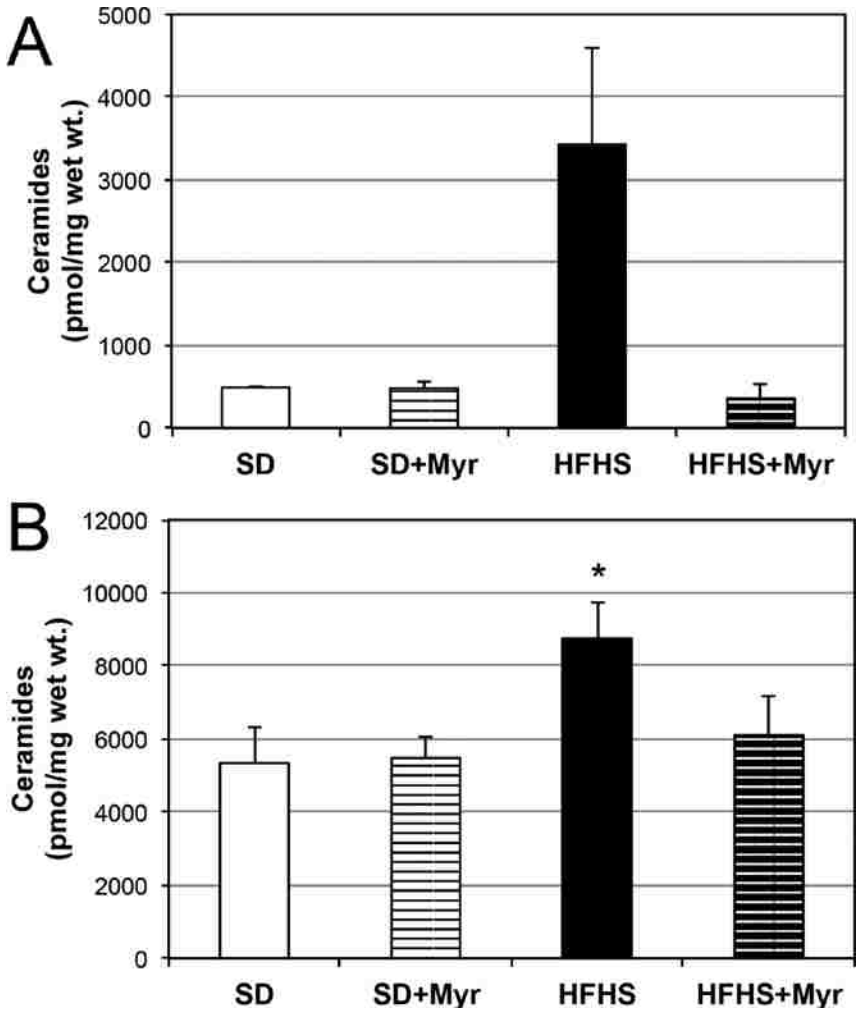

Figure 8: Skeletal muscle ceramide levels with treatments

Ceramides were measured in the RG (A) and soleus (B) muscles. Owing to a shortage of samples, statistical analysis was not possible for the RG muscle (n=2–3). As a surrogate for RG muscle, levels of ceramide were analysed in the soleus muscle, which is a similarly highly oxidative muscle fibre type. Ceramide levels were significantly elevated in the soleus muscle after the HFHS compared with the SD treatment (n=6). Although the reduction in ceramides was not significant with the addition of myriocin (Myr) in the HFHS group, the trend is suggestive of an effect. *$P<0.05$ for the HFHS compared with the SD.

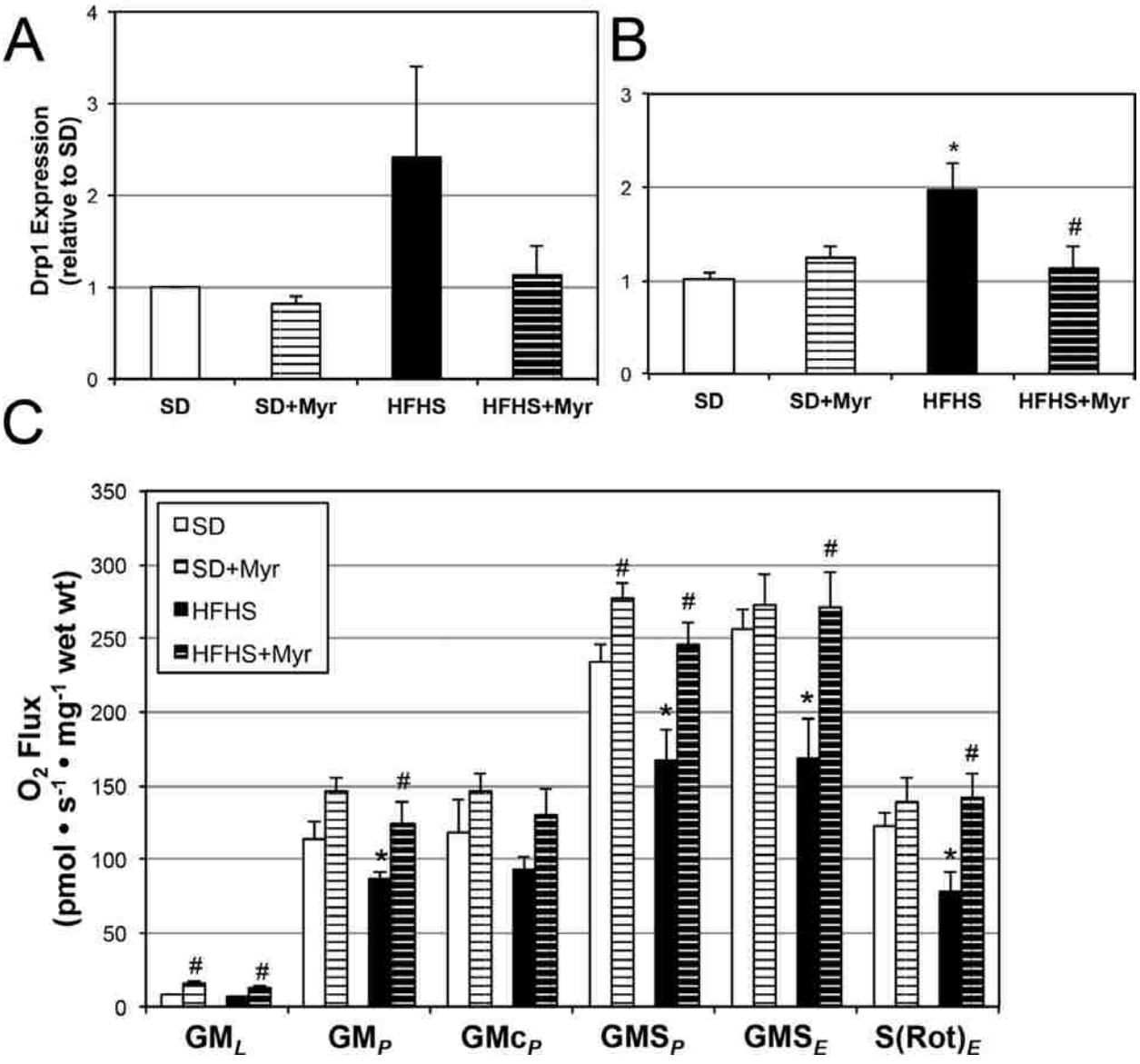

Figure 9: Ceramide inhibition protects diet-induced alterations in mitochondrial function

Drp1 expression was determined in the RG (A) and soleus (B) muscles from mice following a 12 week dietary intervention. Owing to insufficient samples of RG muscles (n=2–3), the soleus muscle was used as a surrogate (n=6). Mice fed a HFHS diet expressed significantly higher levels of Drp1 in the soleus muscle than all other groups. (C) O2 consumption was determined in permeabilized RG muscles from the four dietary interventions using SUIT1 (see the Materials

and methods section for details) (n=6). *P<0.05 for the HFHS diet compared with the SD. #P<0.05 for HFHS diet and myriocin compared with the HFHS diet alone.

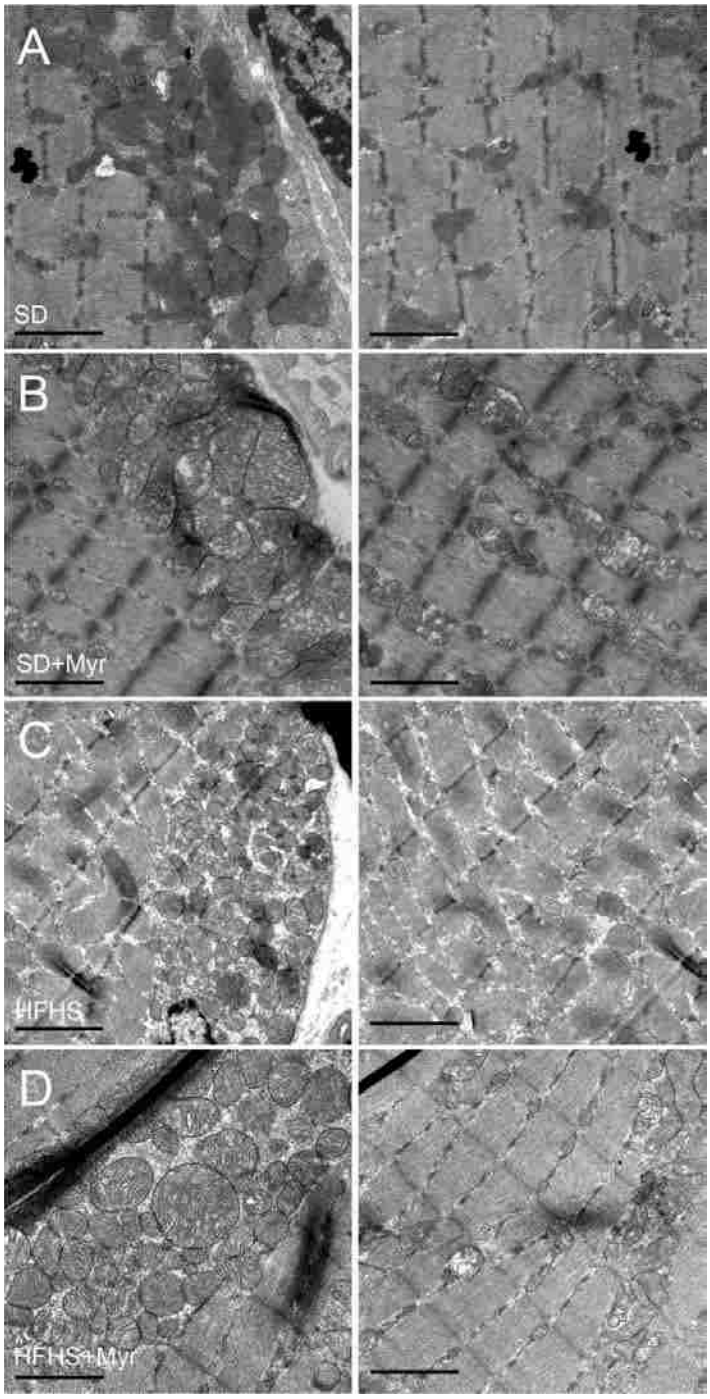

Figure 10: Ceramide inhibition prevents diet-induced alterations in mitochondrial morphology

Visualization of subsarcolemmal (left-hand panels) and intramyofibrillar (right-hand panels) RG muscle mitochondrial fractions suggest that myriocin supplementation increased mitochondrial size [(B) compared with (A) and (D) compared with (C)] (n=3). In particular, the HFHS intervention appeared to result in markedly smaller mitochondria (C), but not with myriocin supplementation (D). Scale bars, 1 μm.

Discussion

The basic conclusion of the present study is that division of the cellular mitochondrial network in muscle cells mediates the reduced mitochondrial respiration and loss of insulin signalling that accompanies ceramide accumulation. Given the widespread finding of skeletal muscle ceramide accumulation with weight gain [8,25–27], this conclusion invites a novel perspective in understanding the observations that defective mitochondrial fusion may cause, exacerbate, or is certainly related to, obesity and insulin resistance [4,5,20,28,29].

The metabolic ramifications of the physical structure of mitochondria have appropriately received more attention in recent years and may assist in understanding metabolic disruption with obesity. Indeed, mitochondrial morphology may be relevant in the altered fuel handling evident in the muscle of obese and diabetic humans. The observation by Kelley et al. [30,31] of a 'metabolic inflexibility' in obese and diabetic subjects stemmed from the inability of these subjects to oxidize glucose when provided with a glucose load. Interestingly, these same groups of subjects have been found to carry reduced proteins that drive mitochondrial fusion, namely Mfn2 [20,28,32]. A lack or overexpression of Mfn2 decreases or increases glucose oxidation respectively [33]. Thus the observed metabolic inflexibility with obesity/diabetes may in reality

stem from a shift towards mitochondrial fission and reduced mitochondrial fusion. Although our report focuses on Drp1, which we consistently found elevated in response to ceramide, we have also explored the effect of ceramide on Mfn2. Whereas the HFHS diet had no effect on soleus muscle Mfn2 expression, myriocin supplementation had a dramatic effect. Mfn2 expression was increased significantly in both the SD+Myr and HFHS+Myr groups (Supplementary Figure S1 at http://www.biochemj.org/bj/456/bj4560427add.htm). It is tempting to speculate that ceramide accumulation in skeletal muscle would force mitochondrial fission, which would subsequently result in reduced mitochondrial capacity and function, as well as insulin resistance, ultimately exacerbating weight gain.

Myriocin is usually administered every 24–48 h by intraperitoneal injection. Given the efficacy of oral myriocin supplementation, the findings of the present study reveal a novel and effective delivery method for myriocin. Regardless of the delivery, ceramide inhibition with myriocin has consistently led to an improved metabolic profile and resistance to metabolic insults, such as diet-induced obesity. Indeed, we observed a similar resistance to the deleterious effects of dietary challenge on glucose and insulin tolerance as that noted by the Lopaschuk and co-workers [34]. Moreover, it is tempting to speculate that the reduced whole-body O2 consumption in the HFD (high-fat diet) group, but not in the myriocin-treated HFD group, in their study [34] is partly a result of the more dramatic and disparate O2 consumption rates we observed in permeabilized ceramide-depleted and -replete muscle cells and fibre bundles (Figures 1, 2, 4 and 8). We also noted a lack of body weight gain with myriocin supplementation in spite of an HFHS diet intervention (Figure 8A). These results support similar findings of an obesity-resistant effect of myriocin [35] and other inhibitors of ceramide biosynthesis [36], be they pharmacological [37] or genetic [38].

The results from the present study support those by Jheng et al. [5] that recently explored the effect of lipid overload and dietary challenge on mitochondrial fission and function. Although they did not elucidate the role of ceramides, Jheng *et al*. [5] found that PA, but not unsaturated oleate, increased mitochondrial fission. Interestingly, they found that addition of oleate to PA-treated cells prevented the mitochondrial fission evident with PA alone. Given our previous observation that oleate prevents PA-induced ceramide accrual [8], the findings by Jheng *et al*. [5] support ceramide's role as an activator of mitochondrial fission. Further, Jheng *et al*. [5] observed that Drp1 expression was increased with PA treatment and was an essential mediator of PA-induced mitochcondrial fission. Critically, although we similarly found an increase in Drp1 expression with PA treatment, inhibition of ceramide synthesis blunted the effect (Figure 2D).

These studies suggest a paradigm wherein ceramide leads to altered mitochondrial dynamics, with subsequent changes in mitochondrial function, including altered respiration and ROS generation. However, oxidative stress from ROS is among the numerous cellular insults known to induce ceramide biosynthesis [36], which invites the theory that ROS are both a cause and consequence of the observed mitochondrial dysfunction. To address the possibility that ROS mediate, and thus precede, ceramide-induced changes in mitochondrial function, multiple experiments with ceramide treatment were replicated with the addition of NAC, a glutathione precursor known to reduce levels of H2O2 [22,23,39]. Pre-treatment with NAC failed to protect cells from ceramide-induced mitochondrial fission (Figure 6A) as well as reduced mitochondrial respiration with both C2 and PA treatment (Figures 6B and 6C). Altogether, these findings suggest that ROS do not mediate the mitochondria-specific effects of ceramide accumulation.

The site of ceramide biosynthesis in the cells may be relevant in the ability of ceramide to induce mitochondrial fission. Interestingly, the two organelles involved in mitochondrial fission, namely the mitochondria and the ER (endoplasmic reticulum), are two prominent sources of intracellular ceramide [11,40,41]. Physical coupling between the ER and mitochondria is necessary for mitochondrial fission, which may explain the somewhat disparate findings that have studied ceramide and mitochondrial function. Previous work that has explored the specific effect of ceramide on mitochondrial respiration has been performed largely, perhaps exclusively, in isolated mitochondria [36,42–44]. Our observation of a ceramide-induced reduction in mitochondrial respiration in intact cells and muscle fibers is the first we know of. The different sources and state of the mitochondria (i.e. isolated heart mitochondria compared with mitochondria in permeabilized skeletal muscle cells and fibers) may explain differences in the effects of ceramide on specific aspects of mitochondrial O2 consumption. In particular, we consistently found a decay in complex II-mediated respiration, whereas Gudz *et al*. [43] found complex III to be highly affected by ceramide accrual, although complex II involvement in respiration was not determined in that study. Di Paolo et al. [42], in contrast, found a complex II-specific inhibition of ceramide with state 3 (ADP supported) respiration, which corroborates the findings of the present study (Figure 3). It is important to note that given the necessity of physical interaction between the ER and mitochondria for mitochondrial fusion and fission, isolated mitochondria seem to be a less ideal model with which to explore the role of mitochondrial structure in altering mitochondrial respiration. Indeed, we have found that treating isolated heart mitochondria with Mdivi-1 is not effective at preventing a loss of respiration with ceramide (T.S. Tippetts and B.T. Bikman, unpublished work). Given that ceramide reduces respiration in isolated mitochondria [42,43], and presumably in the absence of any known fusion–fission events, these observations

introduce the possibility of a fission-independent mechanism. However, we believe our consistent findings in whole cells and muscle fibres that fission is required for ceramide-induced loss of mitochondrial respiration represents the likely physiological event, where changes in mitochondrial structure can occur very rapidly. Indeed, significant mitochondrial fission can occur in minutes in response to PA [5]. Perhaps related to this, we found that waiting 5–10 min was necessary to observe a reduction in respiration in muscle fibre bundles treated with C16-ceramide (Figure 4), which is sufficient time for ceramide to cause mitochondrial fission (Supplementary Figure S2 at http://www.biochemj.org/bj/456/bj4560427add.htm).

To confirm the specificity of ceramide to modify mitochondrial structure and function, we regularly used dihydroceramide as a negative control. Dihydroceramide (C2, C6 and C16 in permeabilized muscle fibres and C2 in permeabilized C2C12 myotubes) had no effect on altering mitochondrial respiration, a finding supported by others [42,43]. Nevertheless, dihydroceramides, the immediate precursor to ceramides, may regulate respiration. Siddique *et al*. [45] recently found that cells deficient in Des1 (dihydroceramide desaturase 1), which lack the enzyme that introduces the distinguishing double bond in the sphingolipid backbone, accumulate dihydrosphingolipids, including dihydroceramides, exhibit reduced mitochondrial respiration [45]. A critical difference may be the experimental protocols used in the various studies. Whereas the present study and others [42,43], which found no effect of dihydroceramides, used exogenous (and mostly non-biological, e.g. C2 and C6) dihydroceramides, the results by Siddique et al. [45] were observed under conditions of endogenously altered dihydrosphingolipid levels where a variety of dihydroceramides are increased, including C18, C24 and C24:1.

Ceramide has long been known to inhibit insulin signaling via a two-pronged attack on Akt/PKB action, inhibiting Akt/PKB translocation to the cell membrane as well as activating a protein phosphatase that prevents sufficient Akt/PKB phosphorylation[46,47]. The observation in the present study, and others[5], of the insulin-sensitizing effect of inhibited mitochondrial fission may lend credence to the theory that redox-sensitive alterations in phosphorylation of proteins relevant in insulin signal transduction may mediate insulin resistance[21].

Inhibition of ceramide-induced mitochondrial division may have diverse clinical applications, from acutely protecting against ischaemia/reperfusion injury[48] to chronically treating insulin resistance[5]. Ultimately, however, an erroneous assumption from these results would be that mitochondrial fusion is better for the cell than mitochondrial fission. In reality, maintaining freedom for both fusion and fission is a fundamental factor to ensure adequate bioenergetic utility of the mitochondria. The results of the present study suggest that ceramide may prevent the healthy dynamic cycling of mitochondria, essentially forcing sustained fission. Given the relevance of mitochondrial morphology to obesity and insulin resistance/diabetes[29], these findings add to the mounting obvious applications and benefits of pharmaceutical therapies aimed at preventing excess ceramide biosynthesis. Nonetheless, and importantly, on-going efforts should explore the most effective combination of physical activity and, especially, improved nutritional intervention to prevent excess ceramide accumulation and alleviate subsequent metabolic disruption.

Author Contributions

Melissa Smith, Trevor Tippetts, Eric Brassfield and Benjamin Bikman performed all of the cell culture experiments. Melissa Smith, Trevor Tippetts, Eric Brassfield, Adelaide Ockey and Benjamin Bikman performed all of the animal experiments. Trevor Tippetts, Eric Brassfield,

Daniel Kane and Benjamin Bikman assessed mitochondrial respiration, with H2O2 analysis performed by Melissa Smith and Braden Tucker. Melissa Smith and Trevor Washburn performed the confocal imaging experiments, and Trevor Tippetts and Eric Brassfield performed the electron microscopy. Melissa Smith, Adam Swensen, Tamil Anthonymuthu, John Prince and Benjamin Bikman isolated and analyzed the lipids. Melissa Smith, Benjamin Bikman, and Adam Swensen planned all of the experiments and wrote the paper.

Funding

This work was supported by Brigham Young University via a Graduate Research Fellowship (to M.E.S), an Undergraduate ORCA (Office of Research and Creative Activities) grant (to B.J.T.) and a Gerontology Research Award (to B.T.B.).

Abbreviations:

C2, C2-ceramide; DMEM, Dulbecco's modified Eagle's medium; Drp1, dynamin-related protein 1; ER, endoplasmic reticulum; EtOH, ethanol; ETS, electron-transport system; FCCP, carbonyl cyanide p-trifluoromethoxyphenylhydrazone; GM, glutamate+malate; HFD, high-fat diet; HFHS, high-fat high-sugar; HRP, horseradish peroxidase; KRPG, Krebs–Ringer phosphate glucose; Mdivi-1, mitochondrial division inhibitor 1; Mfn2, mitofusin 2; NAC, N-acetylcysteine; PA, palmitate; PKB, protein kinase B; RG, red gastrocnemius; ROS, reactive oxygen species; Rot, rotenone; SD, standard diet; sptlc2/SPT2, serine palmitoyltransferase, long chain base subunit 2; SUIT, substrate-uncoupler-inhibitor-titration

Works Cited:

1. Kimokoti R. W., Gona P., Zhu L., Newby P. K., Millen B. E., Brown L. S., D'Agostino R. B., Fung T. T. (**2012**) Dietary patterns of women are associated with incident abdominal obesity but not metabolic syndrome. *J. Nutr*. 142:1720–1727.
2. Hotamisligil G. S., Peraldi P., Budavari A., Ellis R., White M. F., Spiegelman B. M. (**1996**) IRS-1-mediated inhibition of insulin receptor tyrosine kinase activity in TNF-α- and obesity-induced insulin resistance. *Science* 271:665–668.
3. Liesa M., Palacin M., Zorzano A. (**2009**) Mitochondrial dynamics in mammalian health and disease. *Physiol. Rev*. 89:799–845.
4. Sebastian D., Hernandez-Alvarez M. I., Segales J., Sorianello E., Munoz J. P., Sala D., Waget A., Liesa M., Paz J. C., Gopalacharyulu P., et al. (**2012**) Mitofusin 2 (Mfn2) links mitochondrial and endoplasmic reticulum function with insulin signaling and is essential for normal glucose homeostasis. *Proc. Natl. Acad. U.S.A.* 109:5523–5528.
5. Jheng H. F., Tsai P. J., Guo S. M., Kuo L. H., Chang C. S., Su I. J., Chang C. R., Tsai Y. S. (**2012**) Mitochondrial fission contributes to mitochondrial dysfunction and insulin resistance in skeletal muscle. *Mol. Cell. Biol*. 32:309–319.
6. Westermann B. (**2012**) Bioenergetic role of mitochondrial fusion and fission. *Biochim. Biophys. Acta* 1817:1833–1838.
7. Holland W. L., Bikman B. T., Wang L. P., Yuguang G., Sargent K. M., Bulchand S., Knotts T. A., Shui G., Clegg D. J., Wenk M. R., et al. (**2011**) Lipid-induced insulin resistance mediated by the proinflammatory receptor TLR4 requires saturated fatty acid-induced ceramide biosynthesis in mice. *J. Clin. Invest*. 121:1858–1870.

8. Bikman B. T., Guan Y., Shui G., Siddique M. M., Holland W. L., Kim J. Y., Fabrias G., Wenk M. R., Summers S. A. (**2012**) Fenretinide prevents lipid-induced insulin resistance by blocking ceramide biosynthesis. *J. Biol. Chem*. 287:17426–17437.

9. Lightle S. A., Oakley J. I., Nikolova-Karakashian M. N. (**2000**) Activation of sphingolipid turnover and chronic generation of ceramide and sphingosine in liver during aging. *Mech. Ageing Dev*. 120:111–125.

10. Giusto N. M., Roque M. E., Ilincheta de Boschero M. G. (**1992**) Effects of aging on the content, composition and synthesis of sphingomyelin in the central nervous system. *Lipids* 27:835–839.

11. Summers S. A. (**2006**) Ceramides in insulin resistance and lipotoxicity. Prog. *Lipid Res*. 45:42–72.

12. Kim W. H., Choi C. H., Kang S. K., Kwon C. H., Kim Y. K. (**2005**) Ceramide induces non-apoptotic cell death in human glioma cells. *Neurochem. Res*. 30:969–979.

13. Youle R. J., Karbowski M. (**2005**) Mitochondrial fission in apoptosis. *Nat. Rev. Mol. Cell Biol.* 6:657–663.

14. del Rio M. L., Pabst O., Ramirez P., Penuelas-Rivas G., Forster R., Rodriguez-Barbosa J. I. (**2007**) The thymus is required for the ability of FTY720 to prolong skin allograft survival across different histocompatibility MHC barriers. *Transplant. Int*. 20:895–903.

15. Fraser D. A., Thoen J., Rustan A. C., Forre O., Kjeldsen-Kragh J. (**1999**) Changes in plasma free fatty acid concentrations in rheumatoid arthritis patients during fasting and their effects upon T-lymphocyte proliferation. *Rheumatology* 38:948–952.

16. Fahy E., Subramaniam S., Murphy R. C., Nishijima M., Raetz C. R., Shimizu T., Spener F., van Meer G., Wakelam M. J., Dennis E. A. (**2009**) Update of the LIPID MAPS comprehensive classification system for lipids. *J. Lipid Res*. 50:S9–S14.

17. Pfaffl M. W. (**2001**) A new mathematical model for relative quantification in real-time RT-PCR. *Nucleic Acids Res*. 29:e45.

18. Bikman B. T., Zheng D., Reed M. A., Hickner R. C., Houmard J. A., Dohm G. L. (**2010**) Lipid-induced insulin resistance is prevented in lean and obese myotubes by AICAR treatment. *Am. J. Physiol.: Regul., Integr. Comp. Physiol*. 298:R1692–R1699.

19. Cassidy-Stone A., Chipuk J. E., Ingerman E., Song C., Yoo C., Kuwana T., Kurth M. J., Shaw J. T., Hinshaw J. E., Green D. R., Nunnari J. (**2008**) Chemical inhibition of the mitochondrial division dynamin reveals its role in Bax/Bak-dependent mitochondrial outer membrane permeabilization. Dev. *Cell* 14:193–204.

20. Bach D., Pich S., Soriano F. X., Vega N., Baumgartner B., Oriola J., Daugaard J. R., Lloberas J., Camps M., Zierath J. R., et al. (**2003**) Mitofusin-2 determines mitochondrial network architecture and mitochondrial metabolism. A novel regulatory mechanism altered in obesity. *J. Biol. Chem*. 278:17190–17197.

21. Fisher-Wellman K. H., Neufer P. D. (**2012**) Linking mitochondrial bioenergetics to insulin resistance via redox biology. *Trends Endocrinol. Metab*. 23:142–153.

22. Ozer M. K., Parlakpinar H., Cigremis Y., Ucar M., Vardi N., Acet A. (**2005**) Ischemia-reperfusion leads to depletion of glutathione content and augmentation of malondialdehyde production in the rat heart from overproduction of oxidants: can caffeic acid phenethyl ester (CAPE) protect the heart? *Mol. Cell. Biochem*. 273:169–175.

23. Du C., Gao Z., Venkatesha V. A., Kalen A. L., Chaudhuri L., Spitz D. R., Cullen J. J., Oberley L. W., Goswami P. C. (**2009**) Mitochondrial ROS and radiation induced transformation in mouse embryonic fibroblasts. *Cancer Biol. Ther*. 8:1962–1971.

24. Baldwin K. M., Klinkerfuss G. H., Terjung R. L., Mole P. A., Holloszy J. O. (**1972**) Respiratory capacity of white, red, and intermediate muscle: adaptative response to exercise. *Am. J. Physiol*. 222:373–378.

25. Adams J. M. 2nd., Pratipanawatr T., Berria R., Wang E., DeFronzo R. A., Sullards M. C., Mandarino L. J. (**2004**) Ceramide content is increased in skeletal muscle from obese insulin-resistant humans. *Diabetes* 53:25–31.

26. Amati F., Dube J. J., Alvarez-Carnero E., Edreira M. M., Chomentowski P., Coen P. M., Switzer G. E., Bickel P. E., Stefanovic-Racic M., Toledo F. G., Goodpaster B. H. (**2011**) Skeletal muscle triglycerides, diacylglycerols, and ceramides in insulin resistance: another paradox in endurance-trained athletes? *Diabetes* 60:2588–2597.

27. Bikman B. T. (**2012**) A role for sphingolipids in the pathophysiology of obesity-induced inflammation. *Cell. Mol. Life Sci*. 69:2135–2146.

28. Hernandez-Alvarez M. I., Thabit H., Burns N., Shah S., Brema I., Hatunic M., Finucane F., Liesa M., Chiellini C., Naon D., et al. (**2010**) Subjects with early-onset type 2 diabetes show defective activation of the skeletal muscle PGC-1α/Mitofusin-2 regulatory pathway in response to physical activity. *Diabetes Care* 33:645–651.

29. Zorzano A., Liesa M., Palacin M. (**2009**) Role of mitochondrial dynamics proteins in the pathophysiology of obesity and type 2 diabetes. *Int. J. Biochem. Cell Biol*. 41:1846–1854.

30. Kelley D. E., Goodpaster B., Wing R. R., Simoneau J. A. (**1999**) Skeletal muscle fatty acid metabolism in association with insulin resistance, obesity, and weight loss. *Am. J. Physiol*. 277:E1130–E1141.

31. Kelley D. E., Mandarino L. J. (**2000**) Fuel selection in human skeletal muscle in insulin resistance: a reexamination. *Diabetes* 49:677–683.Abstract

32. Bach D., Naon D., Pich S., Soriano F. X., Vega N., Rieusset J., Laville M., Guillet C., Boirie Y., Wallberg-Henriksson H., et al. (**2005**) Expression of Mfn2, the Charcot–Marie–Tooth neuropathy type 2A gene, in human skeletal muscle: effects of type 2 diabetes, obesity, weight loss, and the regulatory role of tumor necrosis factor α and interleukin-6. *Diabetes* 54:2685–2693.

33. Pich S., Bach D., Briones P., Liesa M., Camps M., Testar X., Palacin M., Zorzano A. (**2005**) The Charcot–Marie–Tooth type 2A gene product, Mfn2, up-regulates fuel oxidation through expression of OXPHOS system. *Hum. Mol. Genet*. 14:1405–1415.

34. Ussher J. R., Koves T. R., Cadete V. J., Zhang L., Jaswal J. S., Swyrd S. J., Lopaschuk D. G., Proctor S. D., Keung W., Muoio D. M., Lopaschuk G. D. (**2010**) Inhibition of de novo ceramide synthesis reverses diet-induced insulin resistance and enhances whole-body oxygen consumption. *Diabetes* 59:2453–2464.

35. Yang G., Badeanlou L., Bielawski J., Roberts A. J., Hannun Y. A., Samad F. (**2009**) Central role of ceramide biosynthesis in body weight regulation, energy metabolism, and the metabolic syndrome. *Am. J. Physiol.: Endocrinol. Metab*. 297:E211–E224.

36. Bikman B. T., Summers S. A. (**2011**) Ceramides as modulators of cellular and whole-body metabolism. *J. Clin. Invest*. 121:4222–4230.

37. Preitner F., Mody N., Graham T. E., Peroni O. D., Kahn B. B. (**2009**) Long-term Fenretinide treatment prevents high-fat diet-induced obesity, insulin resistance, and hepatic steatosis. *Am. J. Physiol.: Endocrinol. Metab*. 297:E1420–E1429.

38. Tsukumo D. M., Carvalho-Filho M. A., Carvalheira J. B., Prada P. O., Hirabara S. M., Schenka A. A., Araujo E. P., Vassallo J., Curi R., Velloso L. A., Saad M. J. (**2007**) Loss-of-function mutation in Toll-like receptor 4 prevents diet-induced obesity and insulin resistance. *Diabetes* 56:1986–1998.

39. Redpath C. J., Bou Khalil M., Drozdzal G., Radisic M., McBride H. M. (**2013**) Mitochondrial hyperfusion during oxidative stress is coupled to a dysregulation in calcium handling within a C2C12 cell model. *PLoS ONE* 8:e69165.

40. Bionda C., Portoukalian J., Schmitt D., Rodriguez-Lafrasse C., Ardail D. (**2004**) Subcellular compartmentalization of ceramide metabolism: MAM (mitochondriaassociated membrane) and/or mitochondria? *Biochem. J*. 382:527–533.

41. Shimeno H., Soeda S., Sakamoto M., Kouchi T., Kowakame T., Kihara T. (**1998**) Partial purification and characterization of sphingosine N-acyltransferase (ceramide synthase) from bovine liver mitochondrion-rich fraction. *Lipids* 33:601–605.

42. Di Paola M., Cocco T., Lorusso M. (**2000**) Ceramide interaction with the respiratory chain of heart mitochondria. *Biochemistry* 39:6660–6668.

43. Gudz T. I., Tserng K. Y., Hoppel C. L. (**1997**) Direct inhibition of mitochondrial respiratory chain complex III by cell-permeable ceramide. *J. Biol. Chem*. 272:24154–24158.

44. Yu J., Novgorodov S. A., Chudakova D., Zhu H., Bielawska A., Bielawski J., Obeid L. M., Kindy M. S., Gudz T. I. (**2007**) JNK3 signaling pathway activates ceramide synthase leading to mitochondrial dysfunction. *J. Biol. Chem*. 282:25940–25949.

45. Siddique M. M., Li Y., Wang L., Ching J., Mal M., Ilkayeva O., Wu Y. J., Bay B. H., Summers S. A. (**2013**) Ablation of dihydroceramide desaturase 1, a therapeutic target for the treatment of metabolic diseases, simultaneously stimulates anabolic and catabolic signaling. *Mol. Cell. Biol*. 33:2353–2369.

46. Salinas M., Lopez-Valdaliso R., Martin D., Alvarez A., Cuadrado A. (**2000**) Inhibition of PKB/Akt1 by C2-ceramide involves activation of ceramide-activated protein phosphatase in PC12 cells. *Mol. Cell. Neurosci*. 15:156–169.

47. Stratford S., DeWald D. B., Summers S. A. (**2001**) Ceramide dissociates 3′-phosphoinositide production from pleckstrin homology domain translocation. *Biochem. J*. 354:359–368.

48. Novgorodov S. A., Gudz T. I. (**2009**) Ceramide and mitochondria in ischemia/reperfusion. *J. Cardiovasc. Pharmacol*. 53:198–208.

Cigarette smoke increases cardiomyocyte ceramide accumulation and inhibits mitochondrial respiration

Summarizing my Contribution: I was involved in the development of this experiment in all of the aspects that involved ceramide identification and quantitation. The hypothesis that we developed was that inflammatory stress on heart and lung cells caused by exposure to cigarette smoke was leading to an accumulation of the lipid species ceramide. These ceramides then play a significant role in modifying the morphology and function of mitochondria. We observed that ceramide concentrations did indeed correlate with reduced mitochondrial capacity and function in a ceramide dependent fashion. I helped determine treatment conditions for lipid accumulations. I helped develop and teach delicate specialized sphingolipid specific lipid extractions. I also conducted all high-resolution mass spectrometry based lipidomic identifications and quantitation. I generated and helped put together all of the figures that involved ceramide quantitation for the differing treatment states. I was involved in the writing, formatting, and editing of this manuscript.

Trevor S Tippetts, Duane R Winden, Adam Clayton Swensen, Michael B Nelson, Mikayla O Thatcher, Rex R Saito, Tyler B Condie, Kurtis J Simmons, Allan M Judd, Paul R Reynolds and Benjamin T BikmanEmail author

BMC Cardiovascular DisordersBMC series open, inclusive and trusted201414:165

DOI: 10.1186/1471-2261-14-165

Received: 6 October 2014Accepted: 17 November 2014Published: 22 November 2014

Abstract

Background

Cigarette smoking is a common and lethal worldwide habit, with considerable mortality stemming from its deleterious effects on heart function. While current theories posit altered blood lipids and fibrinogen metabolism as likely mediators, none have explored the role of the sphingolipid ceramide in exacerbating heart function with smoke exposure. Ceramide production is a consequence of cigarette smoke in the lung, and considering ceramide's harmful effects on mitochondrial function, we sought to elucidate the role of ceramide in mediating smoke-induced altered heart mitochondrial respiration.

Methods

Lung cells (A549) were exposed to cigarette smoke extract (CSE) and heart cells (H9C2) were exposed to the lung-cell conditioned medium. Adult male mice were exposed sidestream cigarette smoke for 8 wk with dietary intervention and ceramide inhibition. Ceramides and heart cell or myocardial mitochondrial respiration were determined.

Results

Lung cell cultures revealed a robust response to cigarette smoke extract in both production and secretion of ceramides. Heart cells incubated with lung-cell conditioned medium revealed a pronounced inhibition of myocardial mitochondrial respiration, though this effect was mitigated with ceramide inhibition via myriocin. In vivo, heart ceramides increased roughly 600% in adult mice with long-term sidestream cigarette smoke exposure. This resulted in a significant ceramide-dependent reduction in left myocardial mitochondrial respiration, as heart mitochondria from the mice exposed to both smoke and myriocin injections respired normally.

Conclusions

These results suggest ceramide to be an important mediator of altered myocardial mitochondrial function with cigarette smoke exposure. Thus, anti-ceramide therapies might be considered in the future to protect heart mitochondrial function with smoke exposure.

Introduction

Cigarette smoke exposure is the leading cause of preventable deaths worldwide[1] and is among the top ten contributors to the worldwide health burden[2]. Despite concerted social efforts to reduce smoking prevalence, current trends suggest the number of smokers will increase worldwide[3,4]. Moreover, cigarette smoke is a common inhaled toxin—almost half of the U.S. population is regularly exposed to cigarette smoke[5,6] and approximately 20% of young children live with someone who smokes in the home[7]. Much of smoking's health burden stems from the increased risk of chronic diseases like cancer, emphysema, and cardiovascular disease[8,9], including cardiomyopathy—a deterioration of heart muscle.

Cardiomyocytes are highly oxidative cells with a tremendous reliance on mitochondrial capacity [10], and altered mitochondrial function can lead to heart failure[11,12,13], a common consequence of cardiomyopathy. Considering the importance of healthy mitochondrial function in cardiomyocyte homeostasis, a valuable area of study is to elucidate the factors that mediate altered heart mitochondrial physiology and its effects with cigarette smoke exposure. Previous studies have observed that cigarette smoke exposure inhibits mitochondrial respiratory function in blood cells[14] and myocardium[15], but a mediating mechanism has yet to be identified.

Cigarette smoke has long been known to robustly activate inflammatory pathways in the lung[16], which increases ceramide biosynthesis[17,18]. Importantly, ceramides are known to disrupt

mitochondrial structure and function[19,20], possibly increasing risk of cardiomyopathy[21]. Thus, the purpose of these studies was to determine whether the sphingolipid ceramide mediates cardiomyocyte mitochondrial disruption with cigarette smoke exposure. Considering the lung's apposition with the environment, the lung is a logical site of external pathogen-induced stress, a product of which is ceramide biosynthesis[17]. Moreover, given the heart's location relative to pulmonary blood flow, the heart is a reasonable site of lung-derived ceramide uptake.

Materials and Methods

Cell culture

Cigarette smoke extract (CSE) was generated as previously described with slight modifications[22]. Briefly, one 2RF4 research cigarette (University of Kentucky, Lexington, KY) was continuously smoked by connecting the filtered end of the cigarette to a vacuum pump, pulling the particles into 5 ml of DMEM/F12 and the resulting medium was defined as 100% CSE. The total particulate matter content of 2RF4 cigarettes is 11.7 mg/cigarette, tar is 9.7 mg/cigarette, and nicotine is 0.85 mg/cigarette. Dilutions were made using DMEM/F12 + 10% FBS. Human type II–like pulmonary adenocarcinoma cells (A-549; passage 10-15) were maintained in DMEM/F12 supplemented with 10% FBS (Invitrogen) and antibiotics. Cells were split into 6-well dishes and grown to 80% confluence. H9C2 cardiomyocytes were maintained in DMEM +10% FBS. For differentiation into myotubes, cells were grown to confluency and the medium was replaced with DMEM +10% horse serum (Invitrogen, Grand Island, NY). Myotubes were used for experiments on day 3 of differentiation. A-549 cultures were exposed to media supplemented with 10% CSE or media alone for 4 h, after which the medium was transferred to differentiated H9C2 cardiomyocytes (termed "conditioned medium") for 12 h. Where indicated, cells were treated with myriocin (10 μM, Sigma, M1177), a known and widely

used inhibitor of ceramide biosynthesis. Muscle cells were harvested for RNA, protein, and lipid isolation following treatments. Cell survival during treatments was confirmed by trypan blue exclusion.

Animals

Male C57Bl6 mice were housed in a conventional animal house and maintained on a 12-hour light–dark cycle. Two animal studies were conducted. In the first study, animals received standard diet chow (Harlan Teklad 8604) and water ad libitum. At 12 wk of age, animals were randomly divided into room air and cigarette smoke (CS)-exposed groups. Mice were placed in soft restraints and connected to the exposure tower of a nose-only exposure system (InExpose System, Scireq, Canada). Animals were nasally exposed to sidestream CS generated by research cigarettes where a computer-controlled puff was generated every minute, leading to 10 min of CS exposure followed by 10 min of fresh air, repeated once. The CS-exposed group inhaled CS from two cigarettes per day for one week, at which point the dosage was increased to two cigarettes twice daily. Control animals were similarly handled and restrained in fresh air for the same duration. For the second study, 12-wk-old mice were separated into one of eight treatment groups for eight weeks. Each of the following groups were duplicated to have one group receive vehicle or myriocin injections (0.3 mg/kg) every other day for a total of eight groups: 1) control – standard diet chow, no smoke; 2) cigarette smoke exposure (two cigarettes, twice daily) with standard diet chow; 3) high-fat, high-sugar diet (Harlan Teklad 45F30S); 4) high-fat, high-sugar diet with cigarette smoke exposure. Tissues were harvested at the conclusion of the study period. Studies were conducted in accordance with the principles and procedures outlined in the National Institutes of Health Guide for the Care and Use of Laboratory Animals and were

approved by the Institutional Animal Care and Use Committee (IACUC) at Brigham Young University.

Lipid analysis

For isolation of lipids, cell pellets or tissue were suspended in 900 µl ice-cold chloroform/methanol (1:2) and incubated for 15 minutes on ice, then briefly vortexed. Separation of aqueous and organic phases required addition of 400 µl of ice-cold water and 300 µl of ice-cold chloroform. The organic phase was collected into a fresh vial, and lipids were dried in a vacuum centrifuge (Eppendorf Concentrator Plus). Lipids were characterized and quantified using a shotgun lipidomics technique on a Thermo Scientific LTQ Orbitrap XL mass spectrometer. Evaporated lipid samples were re-suspended in a 2:1 chloroform: methanol Folch solution (200 µL). The re-suspended lipids were then combined with a modified 2:1:1.25 chloroform: methanol: isopropanol Bligh and Dyer solution (800 µL) with 15 mM ammonium acetate acting as an ionizing adduct. A 1.74 µM phosphatidylethanolamine, 1 µM C-17 ceramide, 1 µM tripalmitin internal standard cocktail (1 µL) was spiked into each sample for mass calibration and characterization data alignment. Samples were analyzed using a 2.5-minute mass-window scanning method in positive-ion mode at a resolution of 100,000 (FWHM at 400 m/z) for all primary MS1 scans. MS2 fragmentation data was also collected (PQD at relative intensity of 35) and manually verified for each mass window to give additional confidence to the correct identification of abundant lipid species. Three technical replicate mass spectrometer runs were performed on each sample. Samples were injected at 8 µL/min using a direct-inject electrospray ionization (ESI) soft-ionization spray head from a Hamilton GASTIGHT glass syringe. A nitrogen sheath gas spray flow rate of 8 (arb. Units) was used for all runs. The spray voltage and capillary temperature were maintained at 5.0 KV and 275°C respectively. Each technical

replicate was run in random order to reduce systematic bias. Data were analyzed using in-house developed peak summarization, recalibration, and lipid identification software using lipid database information from the LIPID Metabolites and Pathways Strategy (Lipid MAPS) Lipidomics Gateway database[23]. To ensure high-confidence identifications, an intensity threshold estimated to be 5% above instrumental static signal was implemented. Lipid identities were only assigned when significantly observable peaks were identified in at least two of the three technical replicate runs. Non-zero lipid quantities were averaged from the replicate runs. The lipid species identified across different ionization states or with adducts were totaled together. Quantification was completed by normalizing total ion counts to the relative abundance of the internal standard that was spiked into each sample.

Cell and myocardium permeabilization

For cells, H9C2 cardiomyocytes were detached in culture dishes with 0.05% trypsin-EDTA (Sigma) and growth medium was added to the culture. Contents were transferred to a tube and centrifuged for 10 min at 1000 × g at RT. After removal of supernatant, cells were lifted in MiR05 [0.5 mM EGTA, 3 mM MgCl2, 60 mM K-lactobionate, 20 mM taurine, 10 mM KH2PO4, 20 mM HEPES, 110 mM sucrose, and g/l BSA (Sigma; A3803) adjusted to pH 7.1] plus 1 mg/ml digitonin and gently rocked at RT for 5 min before centrifugation at 1000 × g for 5 min. After discarding supernatant, cells were then suspended in 2.2 ml warm MiR05 and transferred to chambers in the O2K (Oroboros Instruments, Innsbruck, Austria). Following respiration protocol (outlined below), cells were removed from the chambers and used for further analysis, including protein quantification. For myocardial mitochondrial respiration, left ventricle was quickly removed from euthanized mice and immediately placed in ice-cold buffer X (60 mM K-MES, 35 mM KCl, 7.23 mM K2EGTA, 2.77 mM CaK2EGTA, 20 mM imidazole, 20 mM

tuarine, 5.7 mM ATP, 15 mM PCr, 6.56 mM MgCl2-6H2O, pH 7.1) and trimmed of connective tissue. Small fiber bundles were prepared and gently separated along their longitudinal axis under a surgical scope (Olympus, ST) to 1-2 mg. Bundles were then transferred to a tube with chilled buffer X and 50 µg/ml saponin and rocked at 4°C for 30 min, then washed in buffer Z (105 mM K-MES, 30 mM KCl, 10 mM KH2PO4, 5 mM MgCl2-6H2O, 0.5 mg/ml BSA, pH 7.1) at 4°C for at least 15 min. Samples were then blotted dry and weighed.

Mitochondrial isolation

To isolate mitochondria from left ventricle myocardium, the whole heart was placed in isolation buffer (300 mM sucrose, 10 mM Na-HEPES, 0.2 mM EDTA, pH 7.2) and the left ventricle isolated. After finely mincing the sample, trypsin (Sigma T9935) was added for two minutes before adding trypsin inhibitor (Sigma T9003). The sample was then transferred to a conical tube and allowed to settle. After removal of supernatant, samples were resuspended in isolation buffer with BSA (Sigma A3803) and homogenized with Teflon pestle before centrifugation (600 × g for 10 min at 4°C). Supernatant was then transferred to a new tube and centrifuged (8000 × g for 15 min at 4°C), then washed by gently adding isolation buffer and rotating the tube. A portion of this suspension is used for protein quantification. The pellet was then resuspended with isolation buffer + BSA.

Mitochondrial respiration protocol

High-resolution O2 consumption was determined at 37°C in permeabilized cells and fiber bundles using the Oroboros O2K Oxygraph with MiR05 respiration buffer. Before addition of sample into respiration chambers, a baseline respiration rate was determined. After addition of sample, the chambers were hyperoxygenated to ~350 nmol/ml. Following this, respiration was

determined by all or parts of the following substrate-uncoupler-inhibitor-titration (SUIT) protocol[24]: electron flow through complex I was supported by glutamate + malate (10 and 2 mM, respectively) to determine basal oxygen consumption (GM B). Following stabilization, ADP (2.5 mM) was added to determine oxidative phosphorylation capacity (GM P). Succinate was added (GMS P) for complex I + II electron flow into the Q-junction. To determine full electron transport system (F) capacity over oxidative phosphorylation, the chemical uncoupler carbonyl cyanide 4-(trifluoromethoxy) phenylhydrazone (FCCP) was added (0.05 μM, followed by 0.025 μM steps until maximal O2 flux was reached). Complex II-supported ETS was then measured by inhibiting complex I with rotenone (Rot; 0.5 μM). Mitochondrial membrane integrity was tested in all experiments by adding cytochrome c (10 μM; GMc P). Lastly, residual oxygen consumption was measured by adding antimycin A (2.5 μM) to block complex III action, effectively stopping any electron flow, which provides a baseline rate of respiration. Where indicated, C2-ceramide (Sigma A7191; 20 μM) was added to respiration chambers.

Statistics

Data are presented as the mean ± SEM. Data were compared by ANOVA with Tukey's post-hoc analysis (Graphpad Prism; La Jolla, CA). Significance was set at $p < 0.05$.

Results

Ceramide inhibits cardiomyocyte mitochondrial respiration

To determine the effects of ceramide on cardiac mitochondrial respiration, we utilized two models. First, mitochondria were isolated from left ventricle myocardium. During the course of the respiration protocol in the isolated mitochondria, C2-ceramide was added to one oxygraph chamber. The addition of ceramide (+C2) elicited a rapid and significant reduction in

mitochondrial respiration that was sustained through maximal respiration with FCCP (Figure 1A; see Methods for protocol details). A second model was the use of permeabilized intact left ventricle myocardium. One sample was incubated with C2-ceramide throughout the length of the protocol, which elicited a sustained reduction in mitochondrial respiration throughout the entire protocol (Figure 1B).

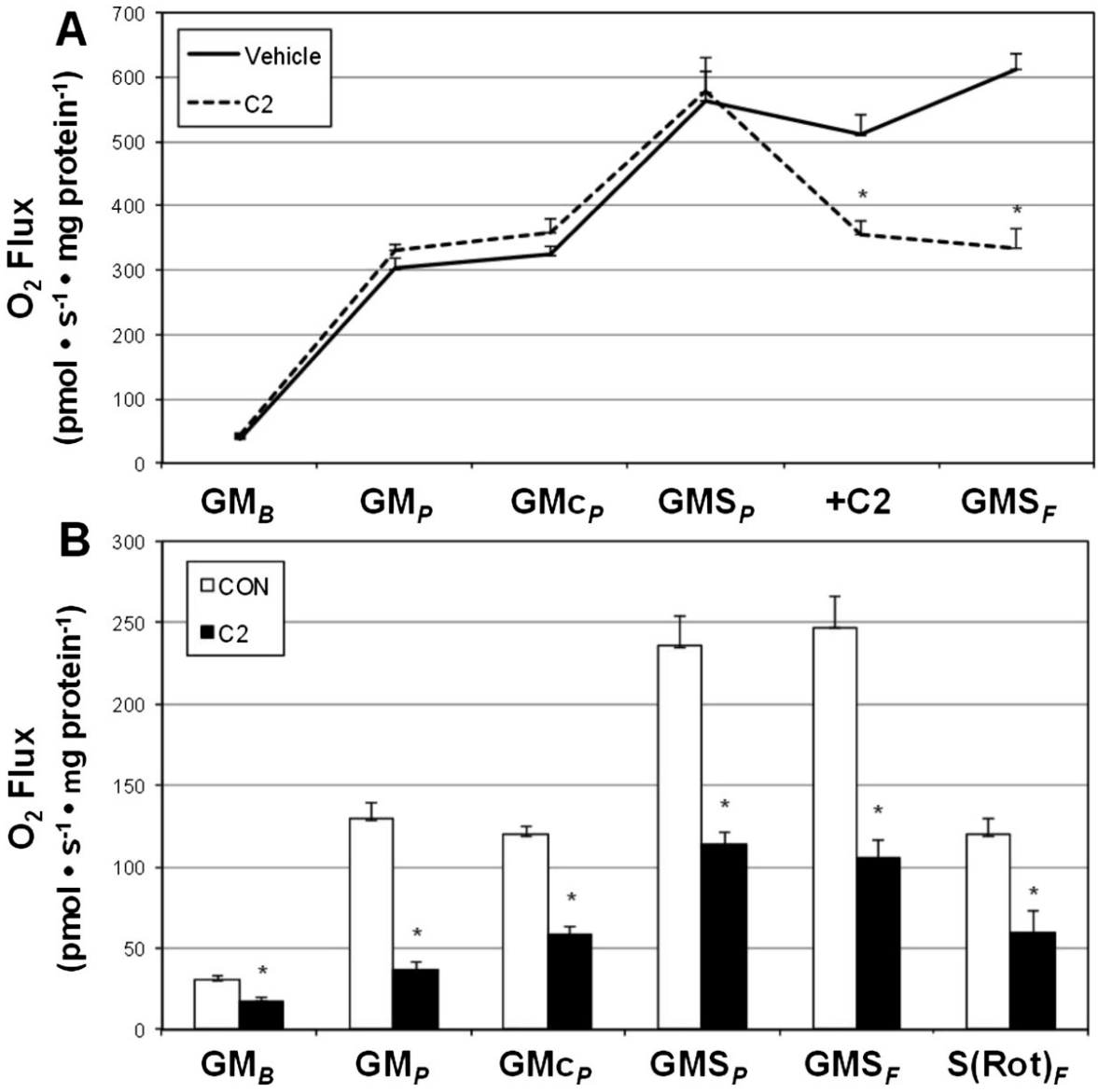

Figure 1: Ceramide inhibits left ventricle mitochondrial respiration.

A: Respiration rates of mitochondria isolated from left ventricle myocardium with addition of C2-ceramide during respiration protocol (20 μM; n = 4). B: Mitochondrial respiration from permeabilized left ventricle myocardium (30 min) with continuous incubation with C2-ceramide (20 μM; n = 8). See Methods for more details on respiration protocol. *P <0.05.

Cigarette smoke extract increases lung cell ceramide production and secretion

The deleterious effect of cigarette smoking on heart function is undeniable, but the mechanism communicating the pulmonary insult to the heart is not clear. As proof of concept that the lung is capable of producing and secreting ceramides with smoke exposure, we treated A549 alveolar type 2 cells with cigarette smoke extract (CSE). Relative to PBS treatment, ceramides increased over 60% in CSE-treated lung cells, though this effect was mitigated with myriocin co-treatment (Figure 2A). Further, CSE treatment elicited an almost three-fold increase in ceramide secretion into medium compared with PBS treatment (Figure 2B). We also observed an upward trend (P = 0.069) in circulating ceramides from whole blood following 5 d of sidestream smoke exposure in adult mice (Figure 2C).

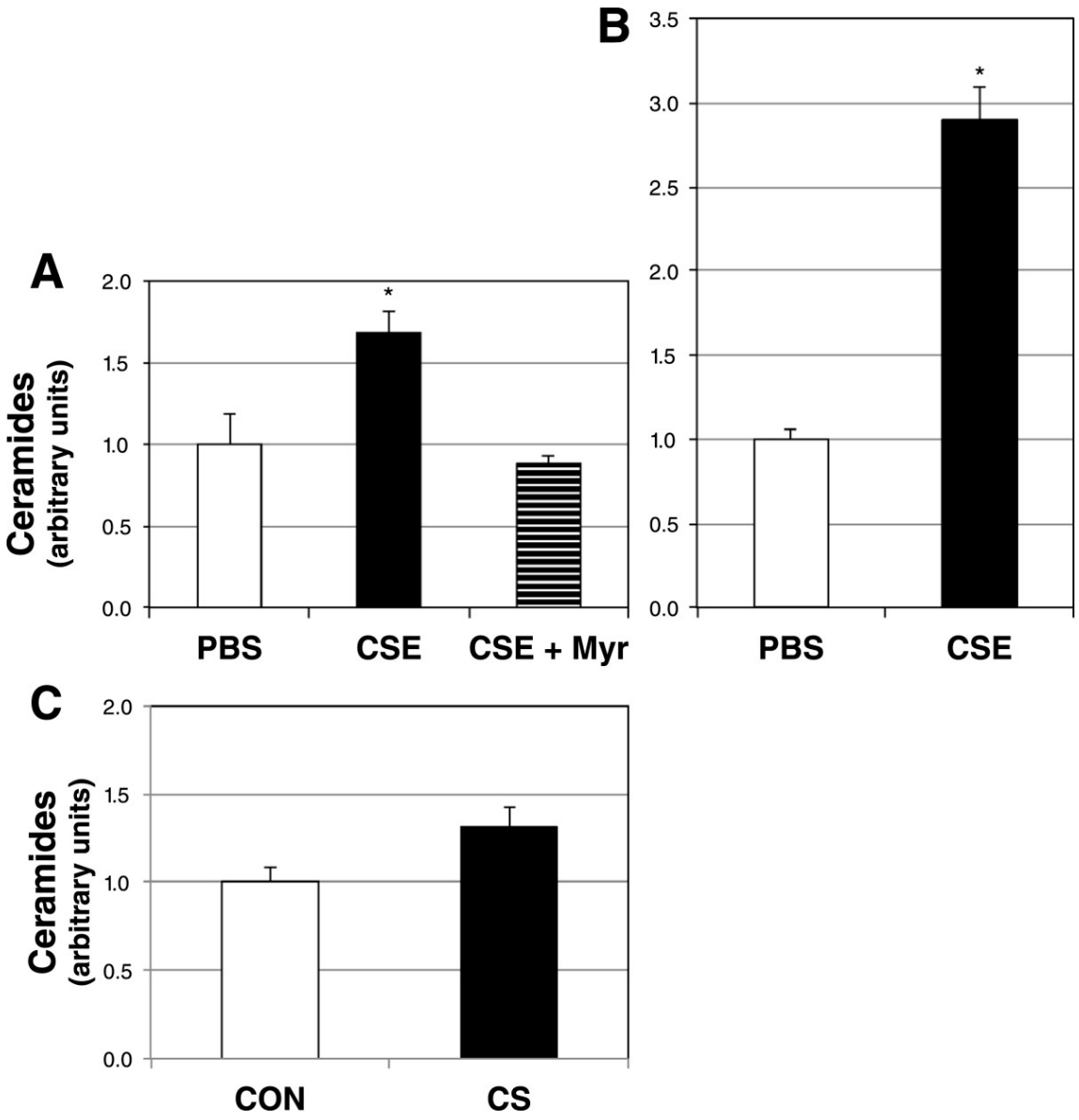

Figure 2: Lung cells make and secrete ceramide in response to cigarette smoke extract.

A: Ceramide levels in A549 cells treated with PBS- or 10% cigarette smoke extract-containing medium without (CSE) or CSE with myriocin (CSE + Myr), a ceramide inhibitor, for 12 h (n = 6). B: Ceramides in culture medium of A549 cells following a 12-h treatment with PBS or CSE (n = 6). C. Ceramides were determined from whole blood of adult mice following 5 d of

room air (CON) or sidestream cigarette smoke (CS) ($P = 0.069$; $n = 5$). *$P < 0.05$ for CSE vs. PBS.

Ceramide is necessary for smoke extract-induced altered cardiomyocyte mitochondrial disruption

To determine the effects of lung cell-secreted ceramides on heart cell function, we utilized a conditioned medium in vitro model. Briefly, following incubation with PBS- or CSE-containing medium, with or without myriocin co-treatment, the conditioned medium from lung cells was transferred to H9C2 cardiomyotubes for 12 h. Following the incubation with conditioned medium, we determined cardiomyotube ceramide accrual and mitochondrial respiration. Ceramides were significantly increased in cardiomyotubes treated with conditioned medium from CSE-treated lung cells (Figure 3A). However, when lung cells received treatment with myriocin in addition to CSE, the conditioned medium had no effect on heart cell ceramides (Figure 3A). Mitochondrial respiration in the heart cells followed a similar trend as ceramides. Namely, respiration in heart cells receiving CSE conditioned medium was negatively affected, but not when myriocin was included in the lung cell culture medium (Figure 3B).

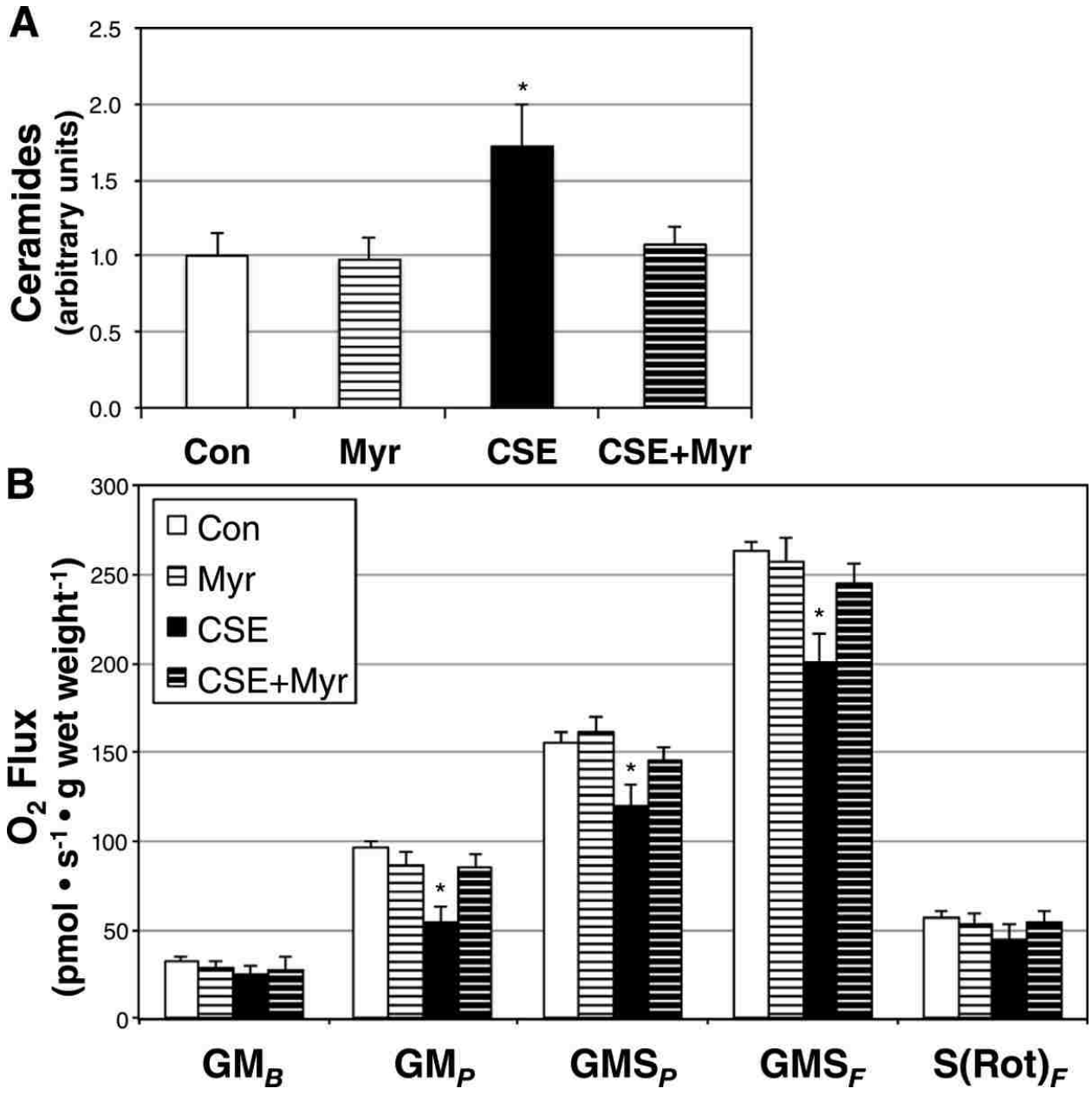

Figure 3: Ceramide is necessary for decreased mitochondrial respiration in myocardial cells following treatment with conditioned medium from CSE-treated lung cells.

A: Ceramide levels in H9C2 cardiomyocytes treated with conditioned medium from A549 alveolar type 2 cells following incubation with normal growth medium (Con), Con with myriocin (Myr), cigarette smoke extract (CSE), and CSE with Myr (CSE + Myr) (n = 4). B: Mitochondrial

respiration from H9C2 cardiomyocytes following treatment in identical conditions (n = 5). See Methods for more details on respiration protocol. *P <0.05 for CSE vs. Con.

Ceramide inhibition prevents reduced myocardial mitochondrial respiration with cigarette smoke

To more accurately determine the role of ceramides in mediating smoke-induced decayed heart mitochondrial respiration, we exposed animals to CS for 1 wk while receiving injections of PBS (vehicle) or myriocin every other day. Left ventricle ceramides increased four fold with CS compared with room air-exposed mice (Figure 4A) with vehicle injections, though myriocin prevented this effect. Moreover, respiration was protected from CS in myriocin-injected animals (Figure 4B).

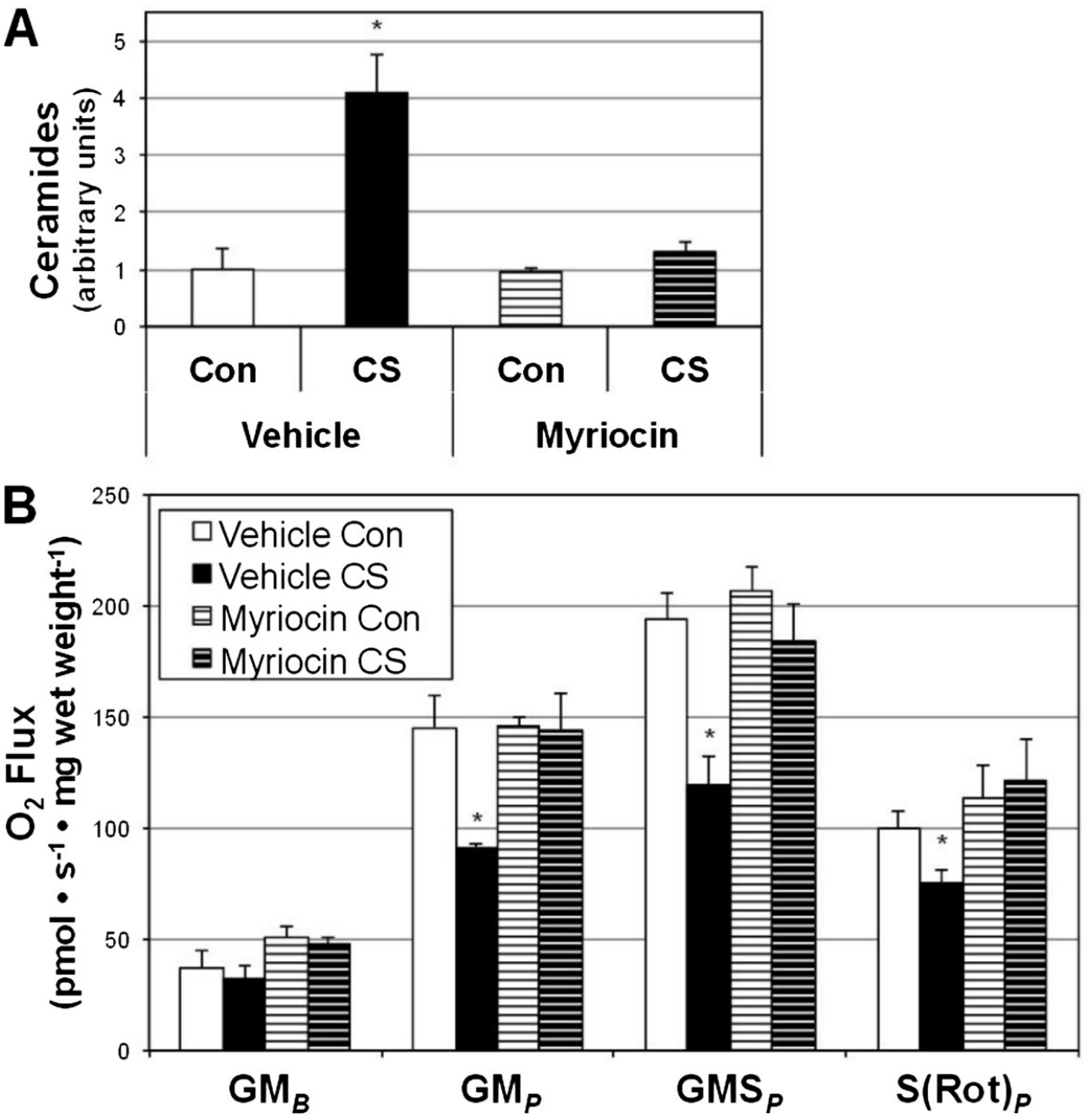

Figure 4: Myriocin prevents left ventricle ceramide accrual and mitochondrial dysfunction with cigarette smoke.

Mice were exposed to room air (Con) or cigarette smoke (CS) for 1 wk while receiving PBS (vehicle) or myriocin injections every other day. A: Ceramides were measured from left ventricle

following treatment period (n = 6). B: Mitochondrial respiration was reduced with CS treatment in vehicle-injected animals (n = 6). *P <0.05 for CS vs all other treatments.

Given the evidence suggesting the role of diet in increasing heart complications[25] and ceramide accrual[26], we provided a high-fat, high-sugar (Western diet; WD) to animals in conjunction with smoke (or room air) exposure over the course of an 8-wk study. Similar to before, animals received vehicle (PBS) or myriocin injections every other day. In addition to observing a roughly 6-fold increase in heart ceramides with smoke exposure, we found an equally great increase in heart ceramides in animals receiving WD diet and smoke (Figure 5A). However, ceramide inhibition was only partially successful in the WD + CS group. In general, ceramide accrual was associated with reduced myocardial mitochondrial respiration (Figure 5B).

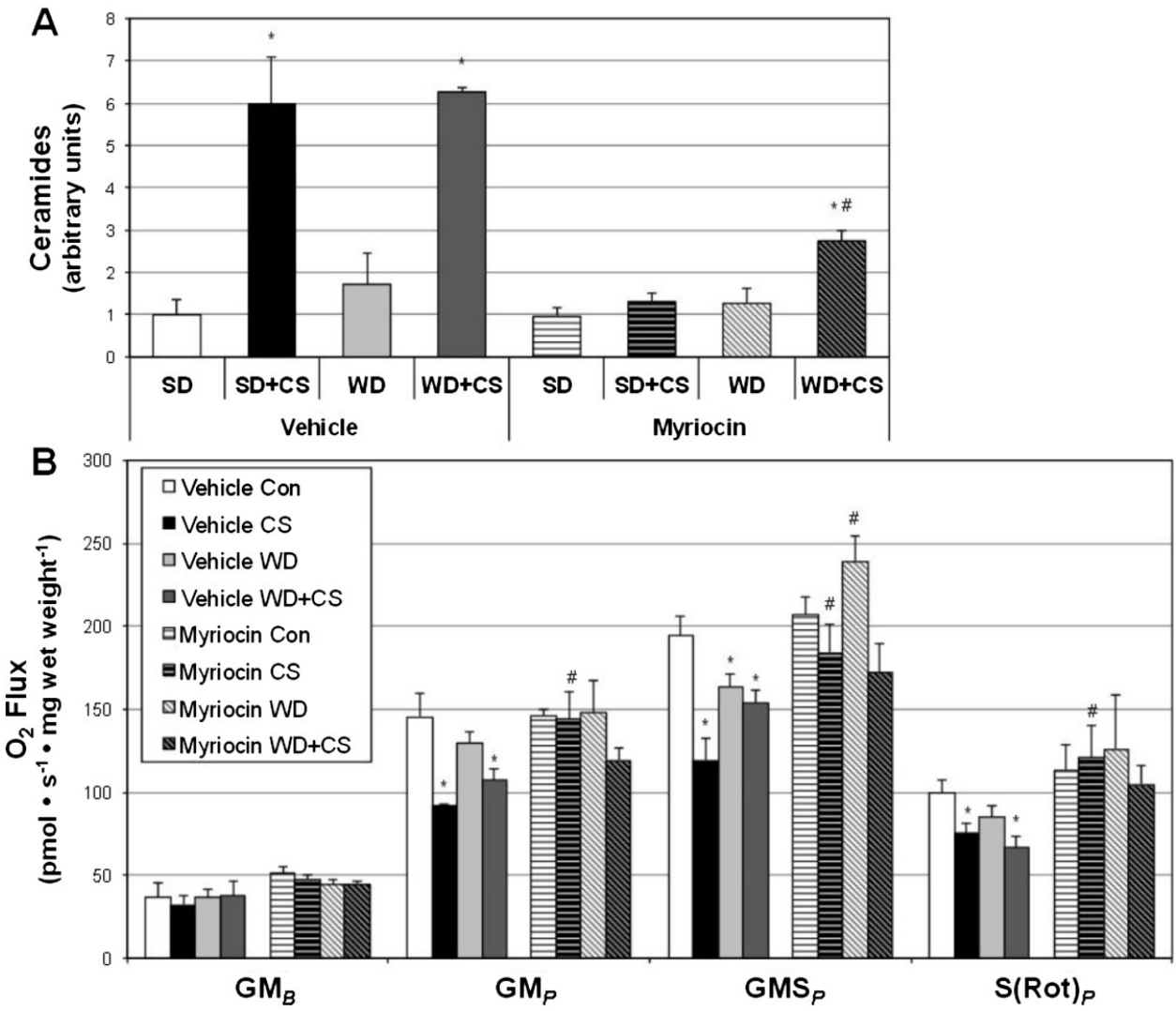

Figure 5 Western diet exerts a minimal effect on heart ceramides in smoke-exposed mice.

Mice were exposed to room air (Con) or cigarette smoke (CS) for 8 wk while receiving PBS (vehicle) or myriocin injections every other day. Mice also received either a standard diet (SD) or Western diet (WD). A: Ceramides were measured from left ventricle following treatment period (n = 4). B: Mitochondrial respiration was determined from permeabilized left ventricle myocardium (n = 8). *P <0.05 for treatment vs. Vehicle SD. #P <0.05 for WD + CS myriocin vs. WD + CS vehicle.

Discussion

Previous research demonstrated that smoke exposure contributes to cardiomyopathy[27,28], which can be a consequence of altered mitochondrial function[21], and we have recently shown that sidestream smoke alters mitochondrial function in skeletal muscle[29]. Considering current worldwide smoking trends[3,4], cardiomyopathy and other cardiovascular burdens mediated by cigarette smoke are likely to increase. To date, the main instigators thought to mediate the heart-specific effects of smoking are altered blood lipids and changes in fibrinogen metabolism[30,31], though the actual impact of these mechanisms is unknown[30]. While ceramides are known to mediate cellular disruption in the lung with smoking[32], its impact on cardiomyocyte function with smoking has not been adequately explored. Thus, the purpose of this project was to determine the role of tobacco smoke-induced ceramides in disrupting cardiomyocyte mitochondrial function. Our major discoveries were that lung cells secrete ceramide with sidestream smoke exposure and that ceramide accumulates in heart tissue and alters mitochondrial function.

To our knowledge, the first study to explore the effects of ceramide on mitochondrial respiration was published by the Hoppel laboratory, where they observed a rapid and robust inhibition of respiration in isolated heart mitochondria upon ceramide treatment[20], and subsequent work corroborates these findings[33]. We confirm those observations by Gudz *et al*.[20] in isolated heart mitochondria and report similar findings in permeabilized left ventricle. Additionally, we have previously shown that ceramides substantially inhibit complex II action and that the general adverse effect of ceramides on mitochondrial respiration is dependent on ceramide-induced mitochondrial fission[24]. Similarly, our findings of ceramide accrual in the lung with smoking corroborate those from other laboratories[34,35,36], but while previous work focused

on ceramide generation via sphingomyelinase, our effective use of myriocin suggests the importance of de novo ceramide synthesis in sidestream smoke-induced ceramide accumulation. However, while myriocin injections were sufficient to completely block ceramide accrual with smoking or diet separately, it was insufficient to prevent an increase in ceramides with combined smoking and diet. This may be a result of insufficient myriocin action in the midst of an overpowering stimulus (diet and smoke combined), or that sphingomyelinase may be particularly relevant in our combined treatment.

Importantly, we not only find increased ceramide production in lung cells with smoke exposure, but also ceramide release, providing proof of concept that the lung may be at least a source of systemic ceramide accrual with smoke exposure. This is supported by our finding of an upward trend in circulating ceramides with smoke exposure. Nonetheless, ongoing experiments are testing the hypothesis that secreted ceramide by smoke-exposed pulmonary tissues travel and accumulate in cardiac muscle. Related to this, our conclusions that ceramide is the relevant component within the cultured medium upon transfer of medium from lung cells to cardiomyocytes is based on our use of myriocin. However, due to the harmful cocktail of molecules within the CSE, it is possible that a non-ceramide variable exists.

The level of ceramide accumulation we observe in the heart with smoking is substantial. We have previously quantified ceramide in various tissues (i.e., skeletal muscle, liver, brain) with dietary intervention[17,24,37] and rarely observed greater than a roughly twofold increase in ceramides; similar changes have been observed in the heart[26]. However, cigarette smoking appears to be a more robust inducer of systemic ceramide accumulation compared with diet. We found a roughly four-fold increase in heart ceramides after only 1 wk of smoke exposure (Figure 4) that increased to a six-fold change with an 8-wk exposure (Figure 4A). Interestingly,

supplementing the smoking regimen with a dietary component (Western diet, Harlan Teklad 45F30S) had no additive effect on heart ceramides (Figure 5A).

Conclusions

In conjunction with our recent findings of altered skeletal muscle function with cigarette smoke exposure[29], the results of these studies implicate ceramide as an important mediator of myriad systemic metabolic effects. In particular, we find evidence that ceramides are a mediator of sidestream smoke-induced altered heart mitochondrial function. While interventions to promote smoking cessation should continue, the increase in worldwide smoking and cardiovascular complications highlights the need for immediate therapies. Our findings suggest that ceramide inhibition may be a novel and potentially valuable therapeutic modality to protect heart function for those who are unwilling or unable to vacate smoke environments.

Declarations

Author Contributions

TST, MBN, MOT, RRS, TBC, KJS conducted cell culture studies. TST, DRW, MBN, MOT, RRS, TBC, KJS performed animal studies. TST, ACS, MOT isolated and quantified ceramides. TST, BTB performed mitochondrial assays. PRR provided technical expertise with sidestream cigarette smoke studies. AMJ, BTB conceived of the study. BTB and ACS prepared the manuscript. All authors read, edited, and approved the final manuscript.

Works Cited:

1. WHO urges more countries to require large, graphic health warnings on tobacco packaging: the WHO report on the global tobacco epidemic, 2011 examines anti-tobacco mass-media campaigns. *Cent Eur J Public Health*. **2011**, 19: 133-151.
2. Deitel M: Overweight and obesity worldwide now estimated to involve 1.7 billion people. *Obes Surg*. **2003**, 13: 329-330. 10.1381/096089203765887598.
3. Ng M, Freeman MK, Fleming TD, Robinson M, Dwyer-Lindgren L, Thomson B, Wollum A, Sanman E, Wulf S, Lopez AD, Murray CJL, Gakidou E: Smoking prevalence and cigarette consumption in 187 countries, 1980-2012. *JAMA*. **2014**, 311: 183-192. 10.1001/jama.2013.284692.
4. Results from the 2010 National Survey on Drug Use and Health: Summary of National Findings. Substance Abuse and Mental Health Services Administration. 2011
5. Pirkle JL, Flegal KM, Bernert JT, Brody DJ, Etzel RA, Maurer KR: Exposure of the US population to environmental tobacco smoke: the Third National Health and Nutrition Examination Survey, 1988 to 1991. *JAMA*. **1996**, 275: 1233-1240. 10.1001/jama.1996.03530400021033.
6. Pirkle JL, Bernert JT, Caudill SP, Sosnoff CS, Pechacek TF: Trends in the exposure of nonsmokers in the U.S. population to secondhand smoke: 1988–2002. *Environ Health Perspect*. **2006**, 114: 853-858. 10.1289/ehp.8850.
7. Vital signs: nonsmokers' exposure to secondhand smoke - United States, 1999-2008. *MMWR Morb Mortal Wkly Rep*. **2010**, 59: 1141-1146.
8. Smoking-attributable mortality, years of potential life lost, and productivity losses--United States, 2000-2004. *MMWR Morb Mortal Wkly Rep*. **2008**, 57: 1226-1228.

9. Lakier JB: Smoking and cardiovascular disease. *Am J Med*. **1992**, 93: 8S-12S. 10.1016/0002-9343(92)90620-Q.

10. Lopaschuk GD, Jaswal JS: Energy metabolic phenotype of the cardiomyocyte during development, differentiation, and postnatal maturation. *J Cardiovasc Pharmacol*. **2010**, 56: 130-140. 10.1097/FJC.0b013e3181e74a14.

11. Winter SC, Buist NR: Cardiomyopathy in childhood, mitochondrial dysfunction, and the role of L-carnitine. *Am Heart J*. **2000**, 139: S63-69. 10.1067/mhj.2000.103935.

12. Holmgren D, Wahlander H, Eriksson BO, Oldfors A, Holme E, Tulinius M: Cardiomyopathy in children with mitochondrial disease; clinical course and cardiological findings. *Eur Heart J*. **2003**, 24: 280-288.

13. Lesnefsky EJ, Moghaddas S, Tandler B, Kerner J, Hoppel CL: Mitochondrial dysfunction in cardiac disease: ischemia–reperfusion, aging, and heart failure. *J Mol Cell Cardiol*. **2001**, 33: 1065-1089. 10.1006/jmcc.2001.1378.

14. Miro O, Alonso JR, Jarreta D, Casademont J, Urbano-Marquez A, Cardellach F: Smoking disturbs mitochondrial respiratory chain function and enhances lipid peroxidation on human circulating lymphocytes. *Carcinogenesis*. **1999**, 20: 1331-1336. 10.1093/carcin/20.7.1331.

15. Knight-Lozano CA, Young CG, Burow DL, Hu ZY, Uyeminami D, Pinkerton KE, Ischiropoulos H, Ballinger SW: Cigarette smoke exposure and hypercholesterolemia increase mitochondrial damage in cardiovascular tissues. *Circulation*. **2002**, 105: 849-854. 10.1161/hc0702.103977.

16. Reynolds PR, Schmitt RE, Kasteler SD, Sturrock A, Sanders K, Bierhaus A, Nawroth PP, Paine R, Hoidal JR: Receptors for advanced glycation end-products targeting protect

against hyperoxia-induced lung injury in mice. *Am J Respir Cell Mol Biol*. **2010**, 42: 545-551. 10.1165/rcmb.2008-0265OC.

17. Holland WL, Bikman BT, Wang LP, Yuguang G, Sargent KM, Bulchand S, Knotts TA, Shui G, Clegg DJ, Wenk MR, Pagliassotti MJ, Scherer PE, Summers SA: Lipid-induced insulin resistance mediated by the proinflammatory receptor TLR4 requires saturated fatty acid-induced ceramide biosynthesis in mice. *J Clin Invest*. **2011**, 121: 1858-1870. 10.1172/JCI43378.

18. Bikman BT: A role for sphingolipids in the pathophysiology of obesity-induced inflammation. *CMLS*. **2012**, 69: 2135-2146. 10.1007/s00018-012-0917-5.

19. Bikman BT, Summers SA: Ceramides as modulators of cellular and whole-body metabolism. *J Clin Invest*. **2011**, 121: 4222-4230. 10.1172/JCI57144.

20. Gudz TI, Tserng KY, Hoppel CL: Direct inhibition of mitochondrial respiratory chain complex III by cell-permeable ceramide. *J Biol Chem*. **1997**, 272: 24154-24158. 10.1074/jbc.272.39.24154.

21. Marin-Garcia J, Goldenthal MJ, Pierpont ME, Ananthakrishnan R: Impaired mitochondrial function in idiopathic dilated cardiomyopathy: biochemical and molecular analysis. *J Card Fail*. **1995**, 1: 285-291. 10.1016/1071-9164(95)90003-9.

22. Reynolds PR, Cosio MG, Hoidal JR: Cigarette smoke-induced Egr-1 upregulates proinflammatory cytokines in pulmonary epithelial cells. *Am J Respir Cell Mol Biol*. **2006**, 35: 314-319. 10.1165/rcmb.2005-0428OC.

23. Fahy E, Subramaniam S, Murphy RC, Nishijima M, Raetz CR, Shimizu T, Spener F, van Meer G, Wakelam MJ, Dennis EA: Update of the LIPID MAPS comprehensive classification system for lipids. *J Lipid Res*. **2009**, 50 (Suppl): S9-14.

24. Smith ME, Tippetts TS, Brassfield ES, Tucker BJ, Ockey A, Swensen AC, Anthonymuthu TS, Washburn TD, Kane DA, Prince JT, Bikman BT: Mitochondrial fission mediates ceramide-induced metabolic disruption in skeletal muscle. *Biochem J.* **2013**, 456: 427-439. 10.1042/BJ20130807.

25. Wilson CR, Tran MK, Salazar KL, Young ME, Taegtmeyer H: Western diet, but not high fat diet, causes derangements of fatty acid metabolism and contractile dysfunction in the heart of Wistar rats. *Biochem J*. **2007**, 406: 457-467. 10.1042/BJ20070392.

26. Baranowski M, Blachnio A, Zabielski P, Gorski J: PPARalpha agonist induces the accumulation of ceramide in the heart of rats fed high-fat diet. *J Physiol Pharmacol*. **2007**, 58: 57-72.

27. Gvozdjakova A, Bada V, Sany L, Kucharska J, Kruty F, Bozek P, Trstansky L, Gvozdjak J: Smoke cardiomyopathy: disturbance of oxidative processes in myocardial mitochondria. *Cardiovasc Res*. **1984**, 18: 229-232. 10.1093/cvr/18.4.229.

28. Lough J: Cardiomyopathy produced by cigarette smoke. Ultrastructural observations in guinea pigs. *Arch Pathol Lab Med*. **1978**, 102: 377-380.

29. Thatcher MO, Tippetts TS, Nelson MB, Swensen AC, Winden DR, Hansen ME, Anderson MC, Johnson IE, Porter JP, Prince JT, Reynolds PR, Bikman BT: Ceramides mediate cigarette smoke-induced metabolic disruption in mice. *Am J Physiol Endocrinol Metab*. **2014**

30. Cullen P, Schulte H, Assmann G: Smoking, lipoproteins and coronary heart disease risk. Data from the Munster Heart Study (PROCAM). *Eur Heart J*. **1998**, 19: 1632-1641. 10.1053/euhj.1998.1086.

31. Newby DE, Wright RA, Labinjoh C, Ludlam CA, Fox KA, Boon NA, Webb DJ: Endothelial dysfunction, impaired endogenous fibrinolysis, and cigarette smoking: a mechanism for arterial thrombosis and myocardial infarction. *Circulation*. **1999**, 99: 1411-1415. 10.1161/01.CIR.99.11.1411.

32. Petrache I, Natarajan V, Zhen L, Medler TR, Richter AT, Cho C, Hubbard WC, Berdyshev EV, Tuder RM: Ceramide upregulation causes pulmonary cell apoptosis and emphysema-like disease in mice. *Nat Med*. **2005**, 11: 491-498. 10.1038/nm1238.

33. Novgorodov SA, Gudz TI: Ceramide and mitochondria in ischemia/reperfusion. *J Cardiovasc Pharmacol*. **2009**, 53: 198-208. 10.1097/FJC.0b013e31819b52d5.

34. Schweitzer KS, Hatoum H, Brown MB, Gupta M, Justice MJ, Beteck B, Van Demark M, Gu Y, Presson RG, Hubbard WC, Petrache I: Mechanisms of lung endothelial barrier disruption induced by cigarette smoke: role of oxidative stress and ceramides. *Am J Physiol Lung Cell Mol Physiol*. **2011**, 301: L836-846. 10.1152/ajplung.00385.2010.

35. Filosto S, Castillo S, Danielson A, Franzi L, Khan E, Kenyon N, Last J, Pinkerton K, Tuder R, Goldkorn T: Neutral sphingomyelinase 2: a novel target in cigarette smoke-induced apoptosis and lung injury. *Am J Respir Cell Mol Biol*. **2011**, 44: 350-360. 10.1165/rcmb.2009-0422OC.

36. Levy M, Khan E, Careaga M, Goldkorn T: Neutral sphingomyelinase 2 is activated by cigarette smoke to augment ceramide-induced apoptosis in lung cell death. *Am J Physiol Lung Cell Mol Physiol*. **2009**, 297: L125-133. 10.1152/ajplung.00031.2009.

37. Bikman BT, Guan Y, Shui G, Siddique MM, Holland WL, Kim JY, Fabrias G, Wenk MR, Summers SA: Fenretinide prevents lipid-induced insulin resistance by blocking

ceramide biosynthesis. *J Biol Chem*. **2012**, 287: 17426-17437.

10.1074/jbc.M112.359950.

Ceramides mediate cigarette smoke-induced metabolic disruption in mice

Summarizing my Contribution: I was involved in the development of this experiment in all of the aspects that involved ceramide identification and quantitation. I helped determine treatment conditions for lipid accumulations. Our hypothesis for this paper was that cigarette smoke exposure to lung cells was leading to inflammation induced production of ceramide lipids. The subsequent accumulation of ceramide class lipids leads to lipid shedding and transport into the blood stream of the treated individual. These shed lipids then work their way through the circulatory system of the effected individual and accumulate in sensitive tissues such as the heart. Using my lipidomic techniques I was able to track theses accumulations throughout the body and tissues. The locations that had the greatest metabolic disruptions were also the locations with greatest accumulations of ceramide. I helped develop and teach careful specialized sphingolipid specific lipid extractions. I completed the extractions of lipids from cell pellets and developed the internal standards that were spiked into each sample to aid in mass alignment in the identification phase of the mass spectrometry based lipidomics I also conducted all high-resolution mass spectrometry based lipidomic identifications and quantitation. I generated and helped put together all of the figures that involved ceramide quantitation for the differing treatment states. I was involved in the writing, formatting, and editing of this manuscript.

Mikayla O. Thatcher, Trevor S. Tippetts, Michael B. Nelson, Adam Clayton Swensen, Duane R. Winden, Melissa E. Hansen, Madeline C. Anderson, Ian E. Johnson, James P. Porter, Paul R. Reynolds, Benjamin T. Bikman

American Journal of Physiology - Endocrinology and Metabolism Published 15 November 2014
Vol. 307 no. 10, E919-E927 DOI: 10.1152/ajpendo.00258.2014

Abstract

Cigarette smoke exposure increases lung ceramide biosynthesis and alters metabolic function. We hypothesized that ceramides are released from the lung during cigarette smoke exposure and result in elevated skeletal muscle ceramide levels, resulting in insulin resistance and altered mitochondrial respiration. Employing cell and animal models, we explored the effect of cigarette smoke on muscle cell insulin signaling and mitochondrial respiration. Muscle cells were treated with conditioned medium from cigarette smoke extract (CSE)-exposed lung cells, followed by analysis of ceramides and assessment of insulin signaling and mitochondrial function. Mice were exposed to daily cigarette smoke and a high-fat, high-sugar (HFHS) diet with myriocin injections to inhibit ceramide synthesis. Comparisons were conducted between these mice and control animals on standard diets in the absence of smoke exposure and myriocin injections. Muscle cells treated with CSE-exposed conditioned medium were completely unresponsive to insulin stimulation, and mitochondrial respiration was severely blunted. These effects were mitigated when lung cells were treated with the ceramide inhibitor myriocin prior to and during CSE exposure. In mice, daily cigarette smoke exposure and HFHS diet resulted in insulin resistance, which correlated with elevated ceramides. Although myriocin injection was protective against insulin resistance with either smoke or HFHS, it was insufficient to prevent insulin resistance with combined CS and HFHS. However, myriocin injection restored muscle mitochondrial respiration in all treatments. Ceramide inhibition prevents metabolic disruption in muscle cells with smoke exposure and may explain whole body insulin resistance and mitochondrial dysfunction in vivo.

Obesity and cigarette smoking are two of the largest causes of preventable deaths worldwide, increasing the risk of multiple illnesses such as heart disease, stroke, airway infections, and diabetes[31,52]. The incidences of smoking and obesity mirror each other in nations across the globe; where one risk factor is increasing, the other follows[31,52]. This correlation has elicited speculation of a causative association between toxin exposure, such as cigarette smoke, and metabolic disruption[6,11,42], which adds another layer of complexity to the already convoluted search for a treatment for obesity and its comorbidities. Although cigarette smoke contains chemicals that reportedly increase energy expenditure and promote weight loss[29], smoke exposure is associated with increased visceral adipose accumulation[46,48] that increases with greater smoking frequency[46].

Two lines of evidence may support the theory that cigarette smoke causes metabolic disruption leading to fat gain. First, cigarette smoke exposure is known to disturb mitochondrial function and biogenesis[3,37], which may compromise the cell's ability to use fat for fuel. Second, insulin resistance and hyperinsulinemia are common features attending regular smoking[4,15,20,43,44], and insulin is a potent inducer of adipocyte expansion and fat gain[30,36,50]. How smoke exposure causes both of these deleterious metabolic consequences is unclear. Of the myriad mediators that may disrupt healthy metabolic function in response to cigarette smoke exposure, the particular effects of the sphingolipid ceramide on cellular insulin sensitivity and mitochondrial function elucidate a novel mechanism and potential therapeutic target[9].

The lung produces ceramides in response to cigarette smoke exposure[24,35], which may explain the altered metabolic function evident with smoking[7,18]. Ceramide is a well-established mediator of both insulin resistance[12,49] and compromised mitochondrial function[25,47]. Based on these observations, the purpose of our study was to test the hypothesis that cigarette smoke

exposure leads to ceramide accumulation in systemic tissues, particularly skeletal muscle, and mediates insulin resistance and altered mitochondrial function. Additionally, by using a rodent smoke exposure model, these studies provide evidence that long-term cigarette smoke exacerbates weight gain.

Materials and Methods

Cell culture.

Cigarette smoke extract (CSE) was generated as previously described, with slight modifications[45]. Briefly, one 2RF4 research cigarette (University of Kentucky, Lexington, KY) was continuously smoked by connecting the filtered end of the cigarette to a vacuum pump, pulling the particles into 5 ml of DMEM-F12, and the resulting medium was defined as 100% CSE and diluted with culture medium to 10%. The total particulate matter content of 2RF4 cigarettes is 11.7 mg/cigarette, tar is 9.7 mg/cigarette, and nicotine is 0.85 mg/cigarette. Human type II-like pulmonary adenocarcinoma cells (A-549) were maintained in DMEM-F12 supplemented with 10% FBS (Invitrogen, Grand Island, NY) and antibiotics. Cells were split into six-well dishes and grown to 80% confluence. C2C12 muscle cells were maintained in DMEM + 10% FBS. For differentiation into myotubes, myoblasts were grown to confluence, and the medium was replaced with DMEM + 10% horse serum (Invitrogen). Myotubes were used for experiments on day 4 of differentiation. A-549 cultures were exposed to serum-free medium supplemented with 10% CSE or medium alone for 4 h, after which the medium was transferred to differentiated C2C12 myotubes (termed “conditioned medium”) for 12 h. Where indicated, cells were treated with myriocin (10 μM; Sigma, M1177). Muscle cells were harvested for RNA, protein, and lipid isolation following treatments.

Animals.

Male C57Bl/6 mice were housed in a conventional animal house and maintained on a 12:12-h light-dark cycle. Two animal studies were conducted. In the first study, animals received standard diet chow (Harlan-Teklad 8604) and water ad libitum. At 12–14 wk of age, animals were randomly divided into room air- and cigarette smoke (CS)-exposed groups. Mice were placed in soft restraints and connected to the exposure tower of a nose-only exposure system (InExpose System; Scireq, Canada). Animals were nasally exposed to mainstream CS generated by research cigarettes where a computer-controlled puff was generated every minute, leading to 10 s of CS exposure followed by 50 s of fresh air. The CS-exposed group inhaled CS from two consecutive cigarettes per day for 3 wk, at which point the dosage was increased to two cigarettes twice daily. Control animals were similarly handled and restrained in fresh air for the same duration. After the 6-wk course, mice underwent intraperitoneal glucose (G7021; Sigma-Aldrich, St. Louis, MO) and insulin (Actrapid; Novo Nordisk, Plainsboro, NJ) tolerance tests. For both tests, mice were fasted for 6 h and received an injection of either glucose (1 g/kg body wt) or insulin (0.75 U/kg body wt). Blood glucose was determined at the times indicated in the figures, using the Bayer Contour glucose meter. For the second study, 12-wk-old mice were separated into one of several treatment groups for 8 wk. Each of the following groups was duplicated to have one group receive vehicle or myriocin injections (0.3 mg/kg) every other day for a total of eight groups: 1) control: standard diet chow, no smoke; 2) cigarette smoke (CS) exposure (two cigarettes, twice daily) with standard diet chow; 3) high-fat, high-sugar (HFHS) diet (Harlan-Teklad 45F30S); 4) HFHS diet with CS exposure. Tissues were harvested at the conclusion of the study period and following a 6-h fast. Insulin resistance was assessed using fasting blood glucose and insulin (MP Biomedicals; Insulin RIA kit, 07260102) to compute a

homeostatic model assessment (HOMA-IR) score, as previously described (8). Studies were conducted in accordance with the principles and procedures outlined in the National Institutes of Health Guide for the Care and Use of Laboratory Animals and were approved by the Institutional Animal Care and Use Committee (IACUC) at Brigham Young University.

Lipid analysis.

Lipids were extracted and quantified as described previously[47]. Briefly, lipids were isolated with chloroform-methanol (1:2), and after addition of water, the organic phase was collected and dried. After resuspension, lipids were quantified using a shotgun lipidomics technique on a Thermo Scientific LTQ Orbitrap XL mass spectrometer.

Protein quantification and quantitative real-time PCR.

Protein and message were quantified as described previously[21,47]. Primers were used as listed previously[21]. β-Actin reactions were performed side by side with every sample analyzed. The following antibodies were used: β-actin (Cell Signaling, no. 4967), Akt (no. 9272), p-Akt-Ser473 (no. 9271), GSK3β (no. 9315), p-GSK3β-Ser9 (no. 9323), SPT2 (Santa Cruz Biotechnology, no. sc-27500), anti-oxphos complex (Invitrogen, no. 457999).

Changes in the mRNA level of each gene following treatments were normalized to the β-actin control mRNA according to Pfaffl (39).

Cell and muscle fiber bundle permeabilization.

Cells and tissue were prepared for the mitochondrial respiration assay as described previously (47). Following the respiration protocol (outlined below), samples were removed from the chambers and used for further analysis, including protein quantification.

Mitochondrial respiration protocol.

High-resolution O2 consumption was determined at 37°C in permeabilized cells and fiber bundles, using the Oroboros O2K Oxygraph (Innsbruck, Austria) with MiR05 respiration buffer as described previously[38,47]. Respiration was determined by all or parts of the following substrate-uncoupler-inhibitor-titration (SUIT) protocol[32]: electron flow through complex I was supported by glutamate + malate (10 and 2 mM, respectively) to determine O2 consumption from proton leak (GML). Following stabilization, ADP (2.5 mM) was added to determine oxidative phosphorylation capacity (GMP). Where indicated, outer mitochondrial membrane integrity was tested by adding cytochrome c (10 μM, GMcP). Succinate was added (GMSP) for complex I+II electron flow into the Q-junction. To determine full electron transport system (ETS) capacity over oxidative phosphorylation in cells, the chemical uncoupler carbonyl cyanide 4-(trifluoromethoxy) phenylhydrazone (FCCP) was added (0.05 μM followed by 0.025 μM steps until maximal O2 flux was reached). Complex II-supported ETS was then measured by inhibiting complex I with rotenone (Rot; 0.5 μM). Last, residual O2 consumption was measured by adding antimycin A (2.5 μM) to block complex III action, effectively stopping any electron flow. This value provides a rate of respiration that is used as a baseline.

Glycogen assay.

Glycogen was measured from cells where indicated, according to the manufacturer's instructions (BioVision, Milpitas, CA).

Statistics.

Data are presented as mean ± SE. Data were compared by ANOVA with Tukey's post hoc analysis (Graphpad Prism, La Jolla, CA). Significance was set at $P < 0.05$.

Results

A549 cells produce and secrete ceramide in response to CS extract.

Compared to PBS-treated cells, ceramide was significantly elevated in alveolar type 2 A549 cells following treatment with cigarette smoke extract (CSE) for 4 h (Fig. 1A). However, this effect was prevented when CSE treatment was supplemented with myriocin (CSE+Myr; Fig. 1A). Myriocin inhibits the initial and rate-limiting step in de novo ceramide biosynthesis, serine palmityoltransferase (SPT) by preventing condensation of palmitoyl-CoA and serine. The relevance of SPT was further determined by measuring the gene expression of SPT2. CSE treatment elicited an over twofold increase in SPT2 gene expression and protein (Fig. 1, B and C), providing evidence of the role of the de novo pathway in CSE-induced ceramide biosynthesis. In addition to ceramide production, we sought to determine the ability of A549 cells to secrete ceramide. Accordingly, lipids were isolated and ceramides measured following 8-h treatment with PBS and CSE medium (± myriocin; Fig. 2). Medium from CSE-treated cells contained ~60% more ceramide than PBS-treated cells.

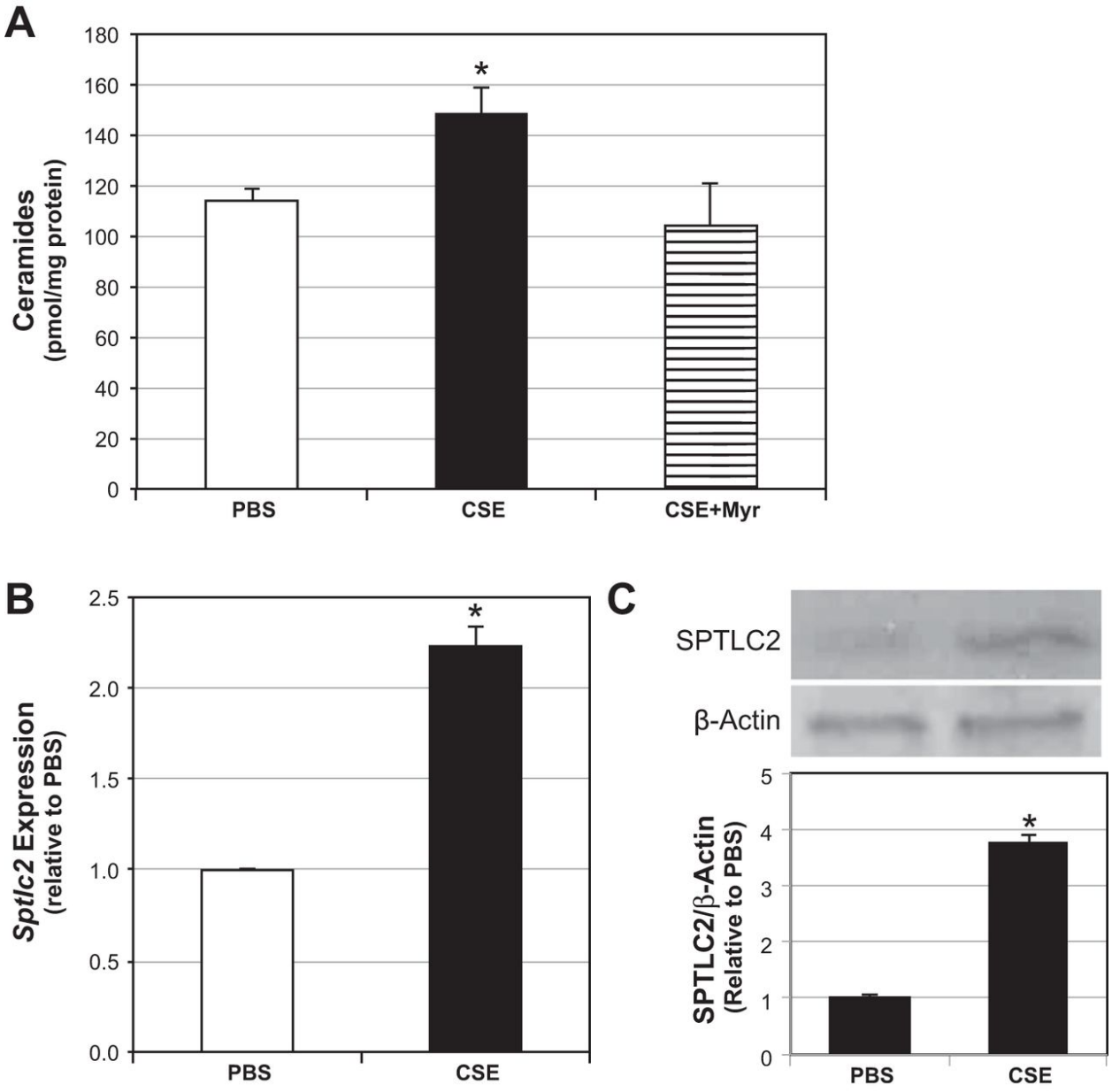

Figure 1: Cigarette smoke extract (CSE) increases ceramide biosynthesis.

Alveolar type 2 cells (A549) were treated with PBS or CSE without (CSE) or with myriocin (CSE+Myr; 10 μM) suspended in growth medium. Following treatment period, ceramides (A; n = 6) and serine palmityoltransferase 2 (Sptlc2) gene (B; n = 6), and protein (C; n = 3) levels were measured. *$P < 0.05$ for CSE vs. other treatments.

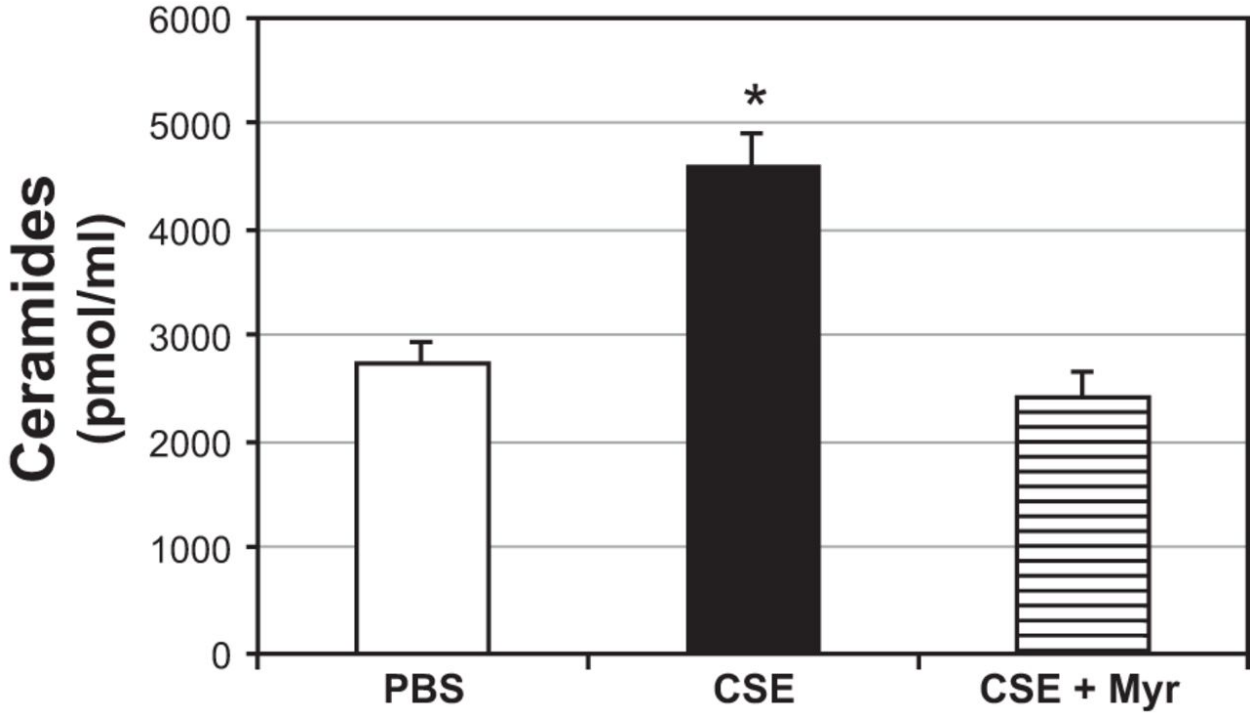

Figure 2: A549 cells secrete ceramide.

A549 cells were treated with PBS or CSE without (CSE) or with myriocin (CSE+Myr; 10 μM) suspended in growth medium. Following 8 h, treatment medium was replaced with fresh growth medium for 16 h, after which lipids were isolated from the medium and analyzed for ceramides. *$P < 0.05$ for CSE vs. other treatments; $n = 5$.

Muscle cells treated with lung cell conditioned medium have higher ceramide levels.

To determine the effect of lung cell-secreted ceramides on muscle cell ceramide metabolism, conditioned medium from PBS- and CSE-treated cells (± myriocin) was harvested from A549 cells and placed on C2C12 myotubes for 12 h, as outlined in Fig. 3A. Myotubes treated with conditioned medium from CSE-treated cells (SCM) had significantly higher levels

of ceramide than both myotubes treated with PBS-conditioned medium (CCM) and addition of myriocin to CSE treatment (SCM+Myr; Fig. 3B).

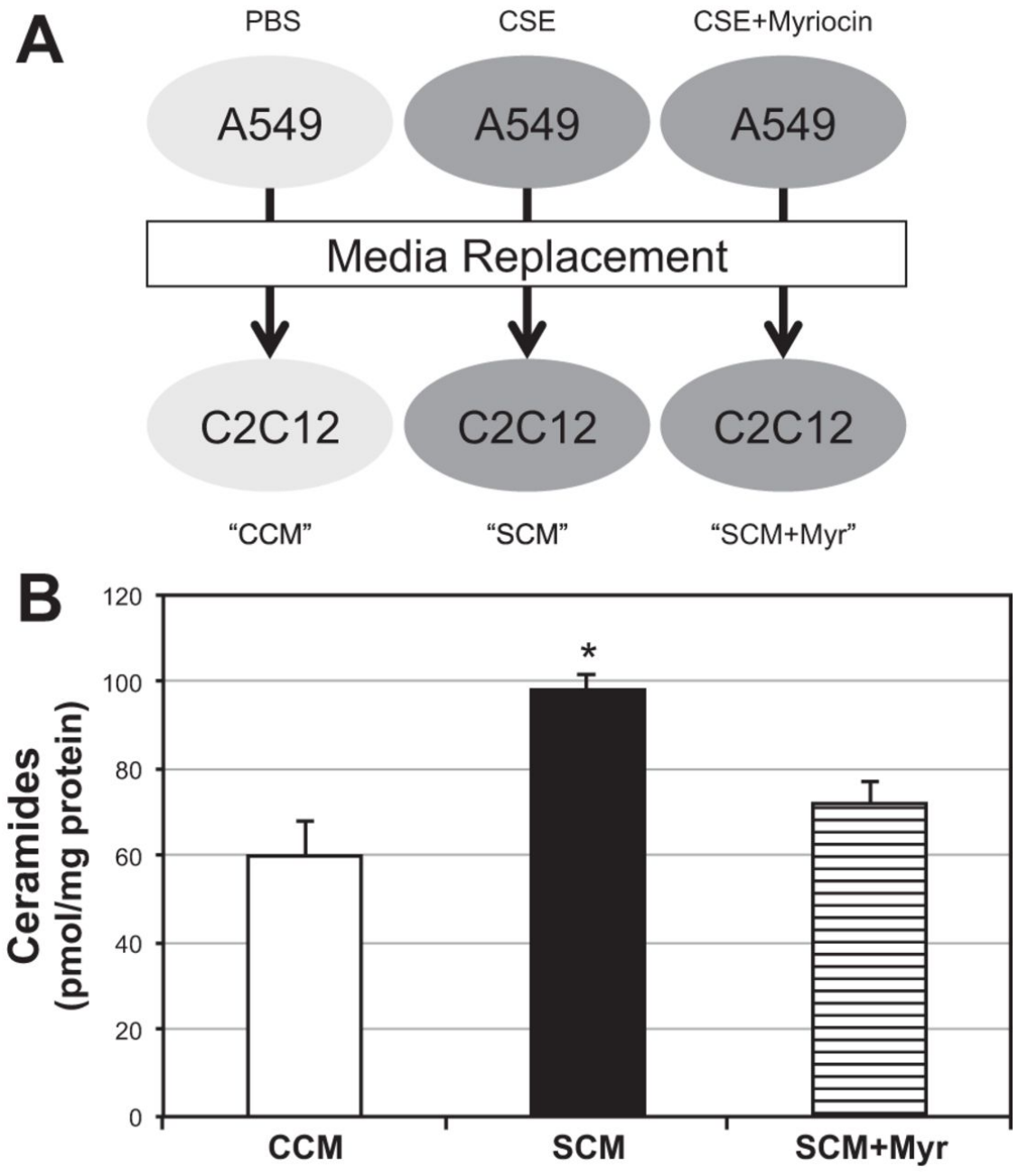

Figure 3: Smoke-treated lung cell conditioned medium increases muscle cell ceramide biosynthesis.

Skeletal muscle cells (C2C12) were treated with conditioned medium from A549 cells. A: schema indicating culture medium handling. B: muscle cells treated with conditioned medium from A549 cells following incubation with control (CCM), cigarette smoke extract medium (SCM), and SCM with myriocin (SCM+Myr; 10 μM). *$P < 0.05$ for CSE vs. other treatments; n = 5.

Muscle cells experience metabolic disruption following SCM treatment.

Two important aspects of metabolic disruption that may mediate obesity-related morbidities and/or exacerbate weight gain are the reduction of muscle insulin sensitivity and altered mitochondrial respiration. Similarly, to the above, C2C12 myotubes were treated with conditioned medium from A549 cells previously treated with normal medium, CSE, or CSE+Myr. Following 12-h serum-free conditioned medium treatment, myotubes were stimulated with insulin for 10 min. As an indicator of insulin signaling, Akt and GSK3β phosphorylation was determined. Whereas CCM myotubes experienced a marked increase in both Akt and GSK3β phosphorylation in response to insulin, myotubes treated with SCM failed to respond to insulin (Fig. 4A). However, when myotubes were treated with SCM+Myr, insulin responsiveness was restored (Fig. 4A). These results were strengthened by determining glycogen accrual with similar treatments (Fig. 4B).

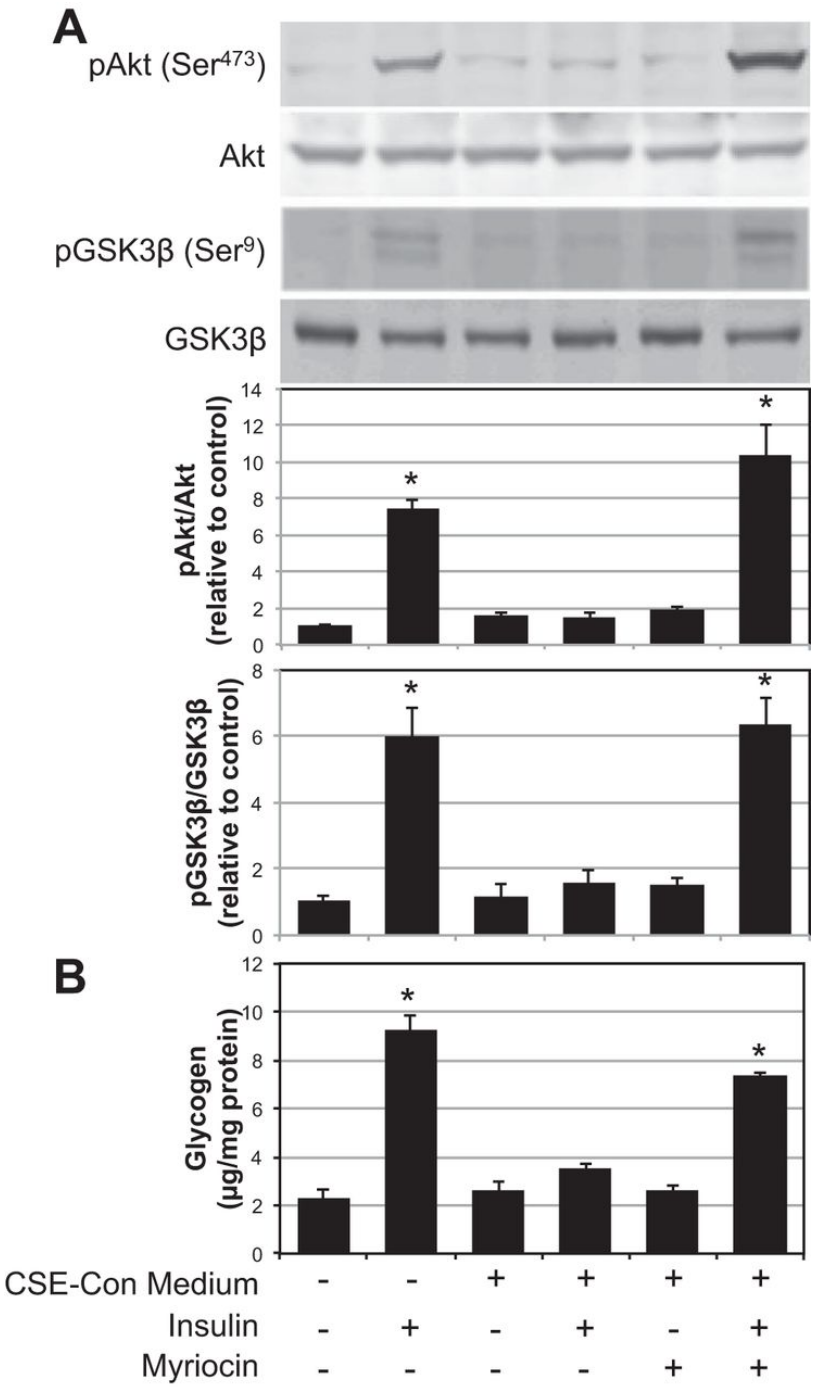

Figure 4: Inhibition of ceramide biosynthesis prevents lung cell conditioned medium-induced loss of muscle cell insulin signaling.

Skeletal muscle cells (C2C12) were treated with conditioned medium from PBS- and CSE-treated A549 cells. C2C12 myotubes were treated with serum-free conditioned medium from

CSE-treated A549 cells ± myriocin (10 μM) to block ceramide biosynthesis. At the end of the treatment period, cells were treated with insulin (100 nM, 10 min) before being lysed for immunoblotting (A; n = 4) and glycogen analysis (B; n = 6). *P < 0.05 for treatment vs. control.

To determine mitochondrial respiration, following similar treatments indicated above, myotubes were permeabilized to undergo a substrate-uncoupler-inhibitor titration protocol (protocol details provided in materials and methods). No difference in rates of mitochondrial O2 was observed between treatment conditions with addition of glutamate and malate (Leak state; Fig. 5A). However, addition of ADP to measure respiration with complex I-mediated oxidative phosphorylation (GMP) revealed a marked contrast, where O2 consumption failed to increase in myotubes treated with SCM. Similar results were found with addition of succinate to introduce complex II-mediated respiration GMSP, as well as FCCP addition to measure uncoupled respiration (GMSE). Addition of rotenone (complex I inhibitor) resulted in a general reduction and equalization of respiration rates regardless of treatment [S(Rot)E]. Addition of myriocin to CSE treatment completely protected mitochondrial respiration (SCM+Myr), and rates were comparable to control (CCM) throughout the assay. All together, these findings suggest a severely compromised ability of muscle cell mitochondria to respire in the midst of the high-ceramide state caused by CS. The smoke-induced decrease in mitochondrial respiration may at least partly result from the slight yet significant ceramide-dependent reduction in complex III and IV protein evident in SCM-treated cells (Fig. 5B).

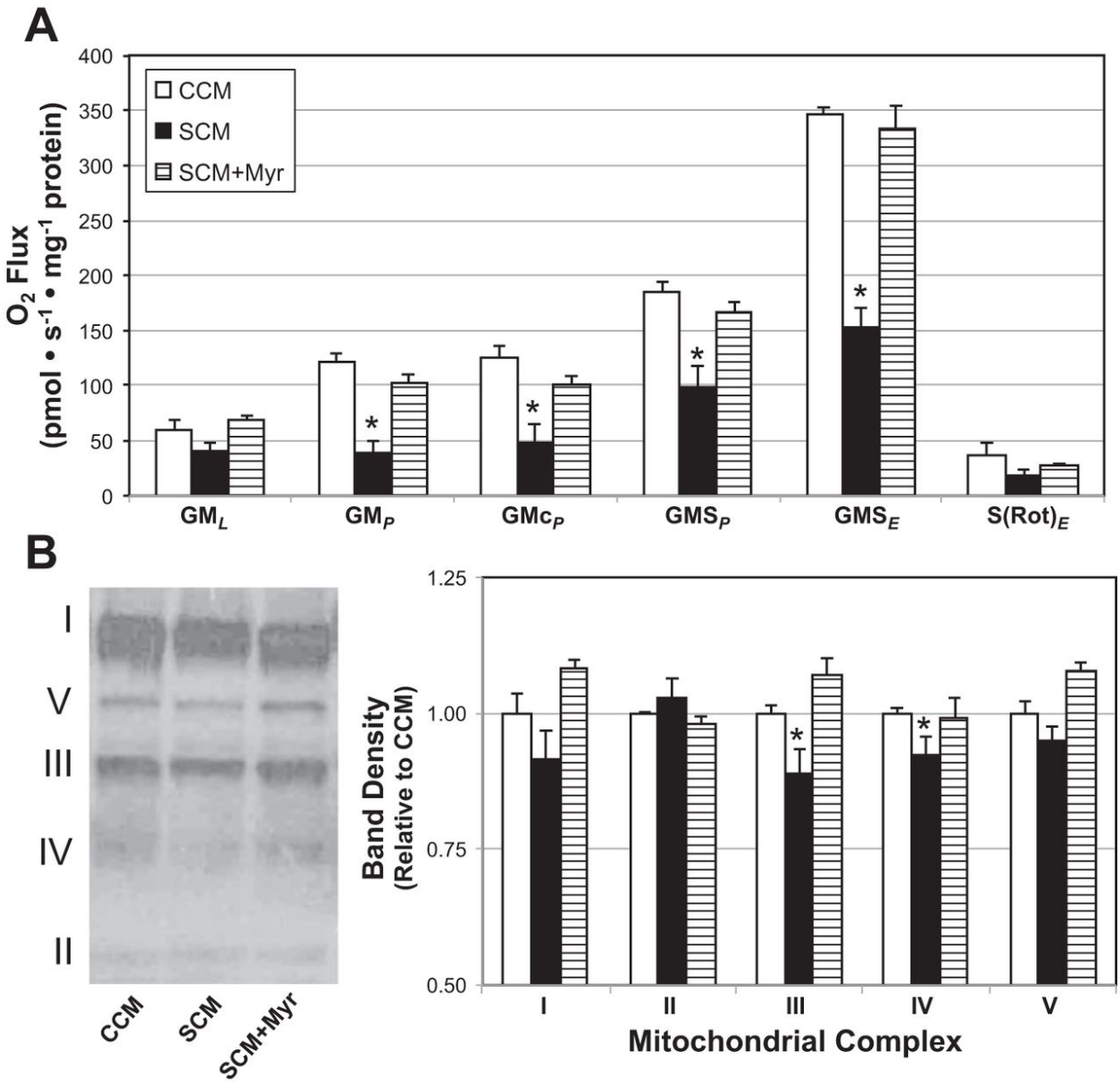

Figure 5: Inhibition of ceramide biosynthesis protects muscle cell mitochondrial respiration.

Skeletal muscle cells (C2C12) were treated with conditioned medium from A549 cells. A: myotubes were treated PBS- and CSE-A549-conditioned medium ± myriocin (CCM, SCM, SCM+Myr, respectively). Following treatment, muscle cell mitochondrial O2 consumption was determined according to the protocol outlined in materials and methods (n = 6). GML, glutamate

(10 mM) + malate (2 mM); GMP, +ADP (2.5 mM); GMcP, +cytochrome c (10 μM); GMSP, +succinate (10 mM); GMSE, +FCCP (0.05 μM+); S(Rot)E, +rotenone (0.5 μM); and +antimycin A (2.5 μM) as baseline. B: Western blot and quantification were performed on sample lysates to determine levels of mitochondrial complexes (n = 3). *P < 0.05 for SCM vs. other treatments.

CS exposure causes metabolic disruption in mice.

In an effort to determine whether CS causes insulin resistance, adult male mice were exposed to CS daily for 6 wk. Treatment period was determined by the length of time necessary to observe differences in glucose tolerance and insulin sensitivity. We found that smoke-exposed mice became less glucose tolerant (Fig. 6A) and less insulin sensitive (Fig. 6B) than control mice. Furthermore, the insulin resistance was attended by altered ceramides; smoke-exposed mice had significantly elevated ceramides in multiple tissues, including lung (Fig. 6D), blood (Fig. 6E), and skeletal muscle (Fig. 6G), but not in liver (Fig. 6D). A portion of the gastrocnemius was permeabilized to assess mitochondrial respiration (Fig. 6C). We found that ADP-supported complex I-mediated respiration (GMP) was significantly blunted in smoked animals. This difference was further exaggerated with succinate addition (GMSP) to introduce complex II but was absent with uncoupling by the addition of FCCP (GMSE), suggesting that maximal, but not submaximal, mitochondrial respiration rate in the muscle is unaffected by CS exposure.

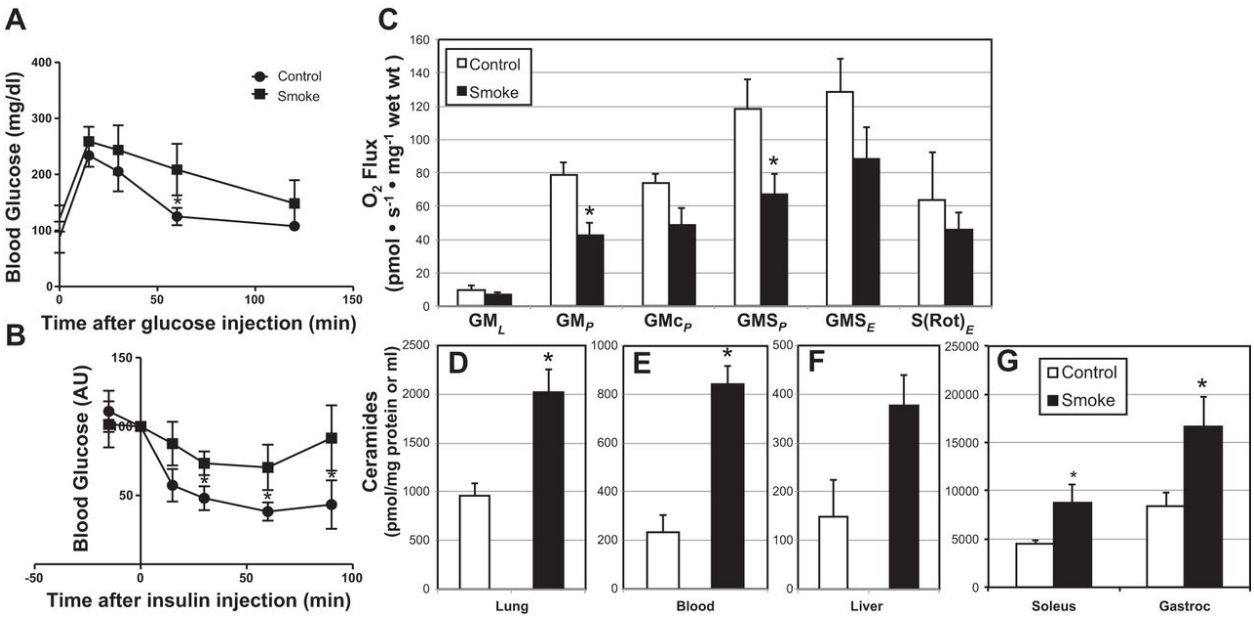

Figure 6: Cigarette smoke (CS) increases tissue ceramides and causes insulin resistance and reduced mitochondrial respiration.

Adult male C57Bl/6 mice were exposed to restraint (Control) or sidestream CS (Smoke) daily for 6 wk. Glucose (A; 1 g/kg body wt ip) and insulin (B; 0.75 U/kg body wt ip) tolerance tests were performed and mitochondrial respiration analyzed in red gastrocnemius according to the protocol outlined in materials and methods (C). Ceramides were determined in lung (D; $P < 0.05$, $n = 4$), blood (E; $P < 0.05$, $n = 4$), liver (F; $P = 0.07$, $n = 4$), and soleus ($P < 0.05$, $n = 8$) and gastrocnemius ($P < 0.05$, $n = 7$) (G). *$P < 0.05$ for smoke vs. control.

Ceramide inhibition prevents smoke-induced metabolic disruption, but not with combined CS and HFHS diet.

The previous animal experiment provided proof of concept that CS exposure causes insulin resistance. To elucidate the role of ceramides in smoke-induced metabolic disruption,

mice received vehicle or myriocin injections every other day to inhibit ceramide biosynthesis. Additionally, mice received a longer smoking regimen with the addition of a dietary intervention. Namely, animals received standard diet (SD) chow or the HFHS diet. The rationale for the dietary intervention was to more closely mimic current real world conditions, considering that smokers tend to engage in less healthy eating habits than nonsmokers (28). Interestingly, CS exposure (SD+CS) alone increased body weight (Fig. 7A), despite no apparent difference in eating habits (Sup. Fig. 1). The HFHS diet also resulted in significantly higher body weight compared with animals fed SD, although the HFHS+CS combination resulted in the highest weight gain among all groups (Fig. 7A). However, myriocin injection prevented CS-induced weight gain and mitigated HFHS-induced weight gain but was insufficient to prevent weight gain with combined HFHS+CS (Fig. 7A). Ceramides increased in soleus with all interventions (Fig. 7B). Myriocin injection prevented significant ceramide gains with all treatments. At the conclusion of the study, fasting blood glucose and insulin levels were used to determine HOMA-IR score following the 8-wk treatment period (Fig. 7C). HOMA-IR scores suggested pronounced insulin resistance with smoke (SD+CS) and dietary intervention (HFHS, HFHS+CS), but this was significantly mitigated with myriocin treatment. Last, red gastrocnemius fibers were separated and permeabilized to determine mitochondrial respiration (Fig. 8). With vehicle injections, CS exposure, regardless of diet, blunted mitochondrial respiration throughout the protocol, although inhibition with HFHS diet alone became apparent only after addition of succinate (GMSP). Myriocin injections failed to prevent reduced respiration with the various treatments, but it offered some protection, considering that respiration was generally higher with myriocin than the comparable vehicle-treated conditions.

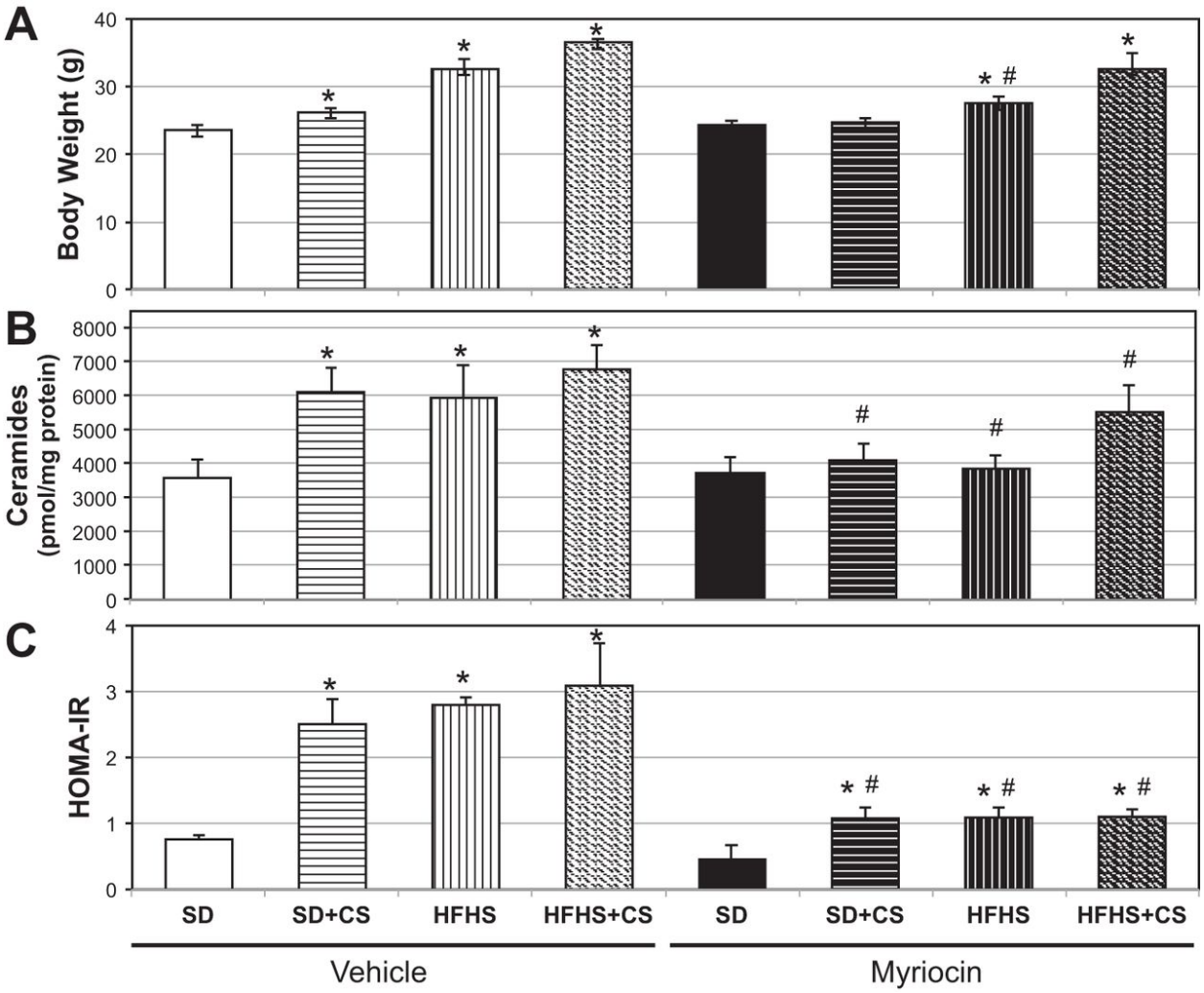

Figure 7: Effects of myriocin on metabolic parameters with smoking and diet.

Twelve-week-old mice were placed on 1 of 4 treatments [SD, standard diet; SD+CS, +daily CS exposure; high-fat, high-sugar (HFHS) diet; and HFHS+CS] while receiving vehicle or myriocin (0.3 mg/kg ip) injections every other day. Body weight (A), soleus ceramides (B), and fasting blood glucose and insulin (C) were measured at the conclusion of the study period. *P < 0.05 for treatment vs. SD within each group; #P < 0.05 for comparable treatment between myriocin vs. vehicle; n = 6–12.

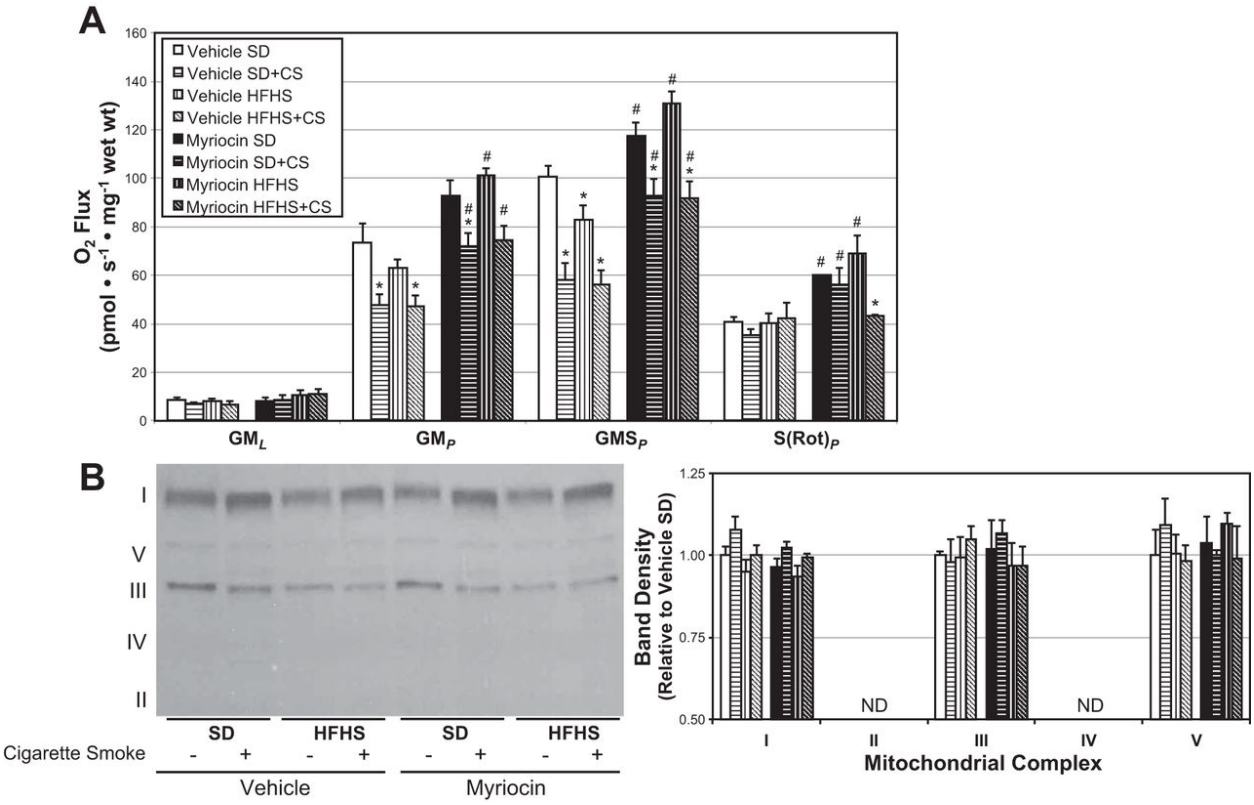

Figure 8: Ceramide inhibition protects skeletal muscle mitochondrial respiration.

Red gastrocnemius fibers were separated and permeabilized from mice following one of four treatments (SD: standard diet; SD+CS: + daily cigarette smoke exposure; HFHS: high-fat, high-sugar diet; HFHS+CS) while receiving vehicle or myriocin (0.3 mg/kg) I.P. injections every other day. Following treatment, muscle cell mitochondrial oxygen consumption was determined according to the protocol outlined in the Methods section (A; n = 6). GML, glutamate (10 mM) + malate (2 mM); GMP, +ADP (2.5 mM); GMcP, +cytochrome c (10 μM); GMSP, +succinate (10 mM); GMSE, +FCCP (0.05 μM+); S(Rot)E, +rotenone (0.5 μM); and +antimycin A (2.5 μM) as baseline. Western blot was performed on sample lysates to determine levels of mitochondrial complexes (B; n = 4). *p < 0.05 for treatment vs. SD within each group; #P < 0.05 for comparable treatment between myriocin vs. vehicle.

Discussion

Dr. Gerald Reaven was the first to identify a relationship between smoking and insulin resistance over 20 years ago[22], and his initial findings have been corroborated by multiple studies since then[4,10,19]. Although previous findings may reveal a mechanism (i.e., insulin resistance) whereby smoking results in systemic diseases[17,27], the ensuing decades have failed to implicate a mediating molecular process linking smoking and insulin resistance. In addition to insulin resistance, smoking compromises mitochondrial function[5,34,37]. The purpose of this report was to determine the role of the sphingolipid ceramide as a mediator of CS-induced metabolic disruption, i.e., insulin resistance and reduced mitochondrial function.

Our first step was to determine whether lung cells, specifically alveolar type 2 cells or bronchial epithelial cells (data not shown), produce and secrete ceramide in response to CSE. We observed that both cells secrete ceramides with smoke exposure, but the response is greater in alveolar type 2 cells. Previous studies exploring the source of blood ceramides have revealed a prominent role for the liver in producing and packaging ceramides into lipoproteins for transport from the liver throughout the body[16]. However, ceramides are able to cross the cell membrane without lipoproteins[16], which is our predicted mechanism for ceramides exiting lung cells. However, once in the blood, ceramides are likely transported via albumin or, more likely, lipoproteins[51]. Upon confirming ceramide secretion from lung cells, we utilized a cell culture system of treating myotubes with conditioned medium from alveolar type 2 cells that were treated with CSE with or without myriocin to inhibit ceramide synthesis. Our findings of a protective effect on insulin signaling and mitochondrial respiration with myriocin-treated lung cells suggest that ceramides are necessary for smoke-induced metabolic disruption in vitro. Results from our animal studies are noteworthy, considering that chronic smoking caused insulin

resistance. Importantly, the dose and method of cigarette smoke exposure we used has been previously shown to yield similar levels of blood carboxyhemoglobin seen in human smokers[53]. To determine the role of ceramides in insulin signaling and mitochondrial function in vivo, we performed a second and similar smoking regimen that prolonged the smoke exposure (from 6 to 8 wk), and included a HFHS diet with regular myriocin injections. The rationale for the HFHS diet was to more closely mimic real world conditions, considering smokers tend to engage in less healthy eating habits than nonsmokers[28]. In general, the combination of CS and HFHS diet tended to exacerbate the effects of smoke alone, including body weight, ceramides, and HOMA-IR. Ceramide inhibition with myriocin treatment tended to mitigate these negative effects. Together, our findings build upon the initial observations of smoking and disturbed metabolic function[13,22,44] and allow, for the first time, a definitive implication of ceramides as a mediator of CS-induced metabolic disruption.

Similarly, to insulin resistance, CS elicits a host of negative effects on mitochondria, including inhibition of respiration (34, 37) and increased ROS generation[5]. It is tempting to speculate these effects may be a result of altered mitochondrial dynamics, which is affected by smoke exposure[23]. We have recently shown that mitochondrial fission is necessary for ceramide-induced changes in mitochondrial function, including varied respiration and ROS production[47].

CS is a common environmental toxin, with half of the US population being regularly exposed[40, 41] and ~20% of young children living with someone who smokes in the home[2]. Every day, almost 4,000 young adults smoke their first cigarette and 1,000 become habitual smokers[1]. We intentionally utilized sidestream (i.e., second-hand) smoke in this study, given that it affects both smokers and bystanders. Our findings, in conjunction with numerous observational studies[4,15,20,43,44] linking smoking with insulin resistance are relevant to current metabolic

syndrome and obesity concerns, given that insulin resistance is the crux of the pathologies that constitute the metabolic syndrome[26]. Previous animal studies have indicated weight loss in smoke-exposed mice[14], although the treatment length was considerably shorter than that used in this study (4 days vs. 8 wk). However, whether smoking exerts an anti- or pro-obesogenic effect in humans is unclear. Smoking is traditionally considered to prevent fat gain, but these observations are exclusively cross-sectional[15]. In contrast, prospective studies following large cohorts reveal that initiation of smoking promotes greater fat gain compared with nonsmokers[48] and heavy smoking increases the fat gain[33]. Given insulin's potent actions in increasing fat mass[30,36,50], the hyperinsulinemia that accompanies insulin resistance may be an important regulator of smoke-induced fat gain. Importantly, while cross-sectional studies suggest that smokers may indeed weigh less (e.g., lower BMI), they also tend to have a higher waist-to-hip ratio[15], suggesting increased visceral fat, which is an additional feature of the metabolic syndrome. Our data suggest that ceramide is an important mediator of the metabolic disruption and weight gain that accompanies chronic smoke exposure.

This study presents the perspective that smoking disrupts healthy metabolic function and, via ceramide accrual, increases risk of weight gain, especially when smoking is combined with a typical Western diet. Future efforts are currently focused on exploring the role of ceramide in other smoke-related pathologies, including the considerable smoke-induced cardiovascular burden. These findings reveal a new metabolic concern for smokers who struggle to quit, but we consider the concern even greater for those exposed to cigarette smoke as bystanders, particularly at early ages. In the end, the results suggest a potential use for anti-ceramide therapies in preventing at least some of the metabolic consequences of smoke exposure.

Disclosures

No conflicts of interest, financial or otherwise, are declared by the author(s).

Author Contributions

Author contributions: M.O.T., T.S.T., M.B.N., A.C.S., D.R.W., M.E.H., M.C.A., I.E.J., and B.T.B. performed experiments; M.O.T., A.C.S., and B.T.B. analyzed data; M.O.T., T.S.T., M.B.N., D.R.W., M.E.H., J.P.P., P.R.R., A.C.S., and B.T.B. interpreted results of experiments; M.O.T. and B.T.B. prepared figures; M.O.T. and B.T.B. drafted manuscript; M.O.T., A.C.S., P.R.R., and B.T.B. edited and revised manuscript; M.O.T., T.S.T., M.B.N., A.C.S., D.R.W., M.C.A., I.E.J., J.P.P., P.R.R., and B.T.B. approved final version of manuscript; D.R.W., J.P.P., P.R.R., and B.T.B. conceived and designed experiments.

Works Cited:

1. Anonymous. Results from the 2010 National Survey on Drug Use and Health: Summary of National Findings. Washington, DC: *Substance Abuse and Mental Health Services Administration*, **2011**.

2. Anonymous. Vital signs: nonsmokers' exposure to secondhand smoke—United States, **1999–2008**. *Morbid Mortal Weekly Report* 59: 1141–1146, 2010.

3. Agarwal AR, Yin F, Cadenas E. Short-term cigarette smoke exposure leads to metabolic alterations in lung alveolar cells. *Am J Respir Cell Mol Biol*, **2014**.

4. Attvall S, Fowelin J, Lager I, Von Schenck H, Smith U. Smoking induces insulin resistance–a potential link with the insulin resistance syndrome. *J Int Med* 233: 327–332, **1993**.

5. Barreiro E, del Puerto-Nevado L, Puig-Vilanova E, Perez-Rial S, Sanchez F, Martinez-Galan L, Rivera S, Gea J, Gonzalez-Mangado N, Peces-Barba G. Cigarette smoke-induced oxidative stress in skeletal muscles of mice. *Respir Physiol Neurobiol* 182: 9–17, **2012**.

6. Bergman BC, Perreault L, Hunerdosse D, Kerege A, Playdon M, Samek AM, Eckel RH. Novel and reversible mechanisms of smoking-induced insulin resistance in humans. *Diabetes* 61: 3156–3166, **2012**.

7. Bikman BT. A role for sphingolipids in the pathophysiology of obesity-induced inflammation. *Cell Mol Life Sci* 69: 2135–2146, **2012**.

8. Bikman BT, Guan Y, Shui G, Siddique MM, Holland WL, Kim JY, Fabrias G, Wenk MR, Summers SA. Fenretinide prevents lipid-induced insulin resistance by blocking ceramide biosynthesis. *J Biol Chem* 287: 17426–17437, **2012**.

9. Bikman BT, Summers SA. Ceramides as modulators of cellular and whole-body metabolism. *J Clin Invest* 121: 4222–4230, **2011**.

10. Borissova AM, Tankova T, Kirilov G, Dakovska L, Krivoshiev S. The effect of smoking on peripheral insulin sensitivity and plasma endothelin level. *Diabetes Metab* 30: 147–152, **2004**.

11. Bray GA, Champagne CM. Beyond energy balance: there is more to obesity than kilocalories. *J Am Diet Assoc* 105: S17–23, **2005**.

12. Chavez JA, Knotts TA, Wang LP, Li G, Dobrowsky RT, Florant GL, Summers SA. A role for ceramide, but not diacylglycerol, in the antagonism of insulin signal transduction by saturated fatty acids. *J Biol Chem* 278: 10297–10303, **2003**.

13. Chen CC, Li TC, Chang PC, Liu CS, Lin WY, Wu MT, Li CI, Lai MM, Lin CC. Association among cigarette smoking, metabolic syndrome, and its individual components: the metabolic syndrome study in Taiwan. *Metab Clin Exper* 57: 544–548, **2008**.

14. Chen H, Vlahos R, Bozinovski S, Jones J, Anderson GP, Morris MJ. Effect of short-term cigarette smoke exposure on body weight, appetite and brain neuropeptide Y in mice. *Neuropsychopharmacology* 30: 713–719, **2005**.

15. Chiolero A, Faeh D, Paccaud F, Cornuz J. Consequences of smoking for body weight, body fat distribution, and insulin resistance. *Am J Clin Nutr* 87: 801–809, **2008**.

16. Contreras FX, Villar AV, Alonso A, Kolesnick RN, Goni FM. Sphingomyelinase activity causes transbilayer lipid translocation in model and cell membranes. *J Biol Chem* 278: 37169–37174, **2003**.

17. DeFronzo RA, Ferrannini Insulin resistance E. A multifaceted syndrome responsible for NIDDM, obesity, hypertension, dyslipidemia, and atherosclerotic cardiovascular disease. *Diabetes Care* 14: 173–194, **1991**.

18. Du J, Wang Y, Hunter R, Wei Y, Blumenthal R, Falke C, Khairova R, Zhou R, Yuan P, Machado-Vieira R, McEwen BS, Manji HK. Dynamic regulation of mitochondrial function by glucocorticoids. *Proc Natl Acad Sci* USA 106: 3543–3548, **2009**.

19. Ebersbach-Silva P, Alves T, Fonseca AT, Oliveira MA, Machado UF, Seraphim PM. Cigarette smoke exposure severely reduces peripheral insulin sensitivity without changing GLUT4 expression in oxidative muscle of Wistar rats. Arquiv Brasil *Endocrinol Metabol* 57: 19–26, **2013**.

20. Eliasson B, Mero N, Taskinen MR, Smith U. The insulin resistance syndrome and postprandial lipid intolerance in smokers. *Atherosclerosis* 129: 79–88, **1997**.

21. Erickson KA, Smith ME, Anthonymuthu TS, Evanson MJ, Brassfield ES, Hodson AE, Bressler MA, Tucker BJ, Thatcher MO, Prince JT, Hancock CR, Bikman BT. AICAR inhibits ceramide biosynthesis in skeletal muscle. *Diabetol Metab Syndrome* 4: 45, **2012**.

22. Facchini FS, Hollenbeck CB, Jeppesen J, Chen YD, Reaven GM. Insulin resistance and cigarette smoking. *Lancet* 339: 1128–1130, **1992**.

23. Gannon AM, Stampfli MR, Foster WG. Cigarette smoke exposure elicits increased autophagy and dysregulation of mitochondrial dynamics in murine granulosa cells. *Biol Reprod* 88: 63, **2013**.

24. Goldkorn T, Filosto S. Lung injury and cancer: Mechanistic insights into ceramide and EGFR signaling under cigarette smoke. *Am J Respir Cell Mol Biol* 43: 259–268, **2010**.

25. Gudz TI, Tserng KY, Hoppel CL. Direct inhibition of mitochondrial respiratory chain complex III by cell-permeable ceramide. *J Biol Chem* 272: 24154–24158, **1997**.

26. Haffner SM, Valdez RA, Hazuda HP, Mitchell BD, Morales PA, Stern MP. Prospective analysis of the insulin-resistance syndrome (syndrome X). *Diabetes* 41: 715–722, **1992**.

27. Hamabe A, Uto H, Imamura Y, Kusano K, Mawatari S, Kumagai K, Kure T, Tamai T, Moriuchi A, Sakiyama T, Oketani M, Ido A, Tsubouchi H. Impact of cigarette smoking on onset of nonalcoholic fatty liver disease over a 10-year period. *J Gastroenterol* 46: 769–778, ***2011***.

28. Hebert JR, Kabat GC. Differences in dietary intake associated with smoking status. *Eur J Clin Nutr* 44: 185–193, **1990**.

29. Hofstetter A, Schutz Y, Jequier E, Wahren J. Increased 24-hour energy expenditure in cigarette smokers. *New Engl J Med* 314: 79–82, **1986**.

30. Hustvedt BE, Lovo A. Correlation between hyperinsulinemia and hyperphagia in rats with ventromedial hypothalamic lesions. *Acta Physiol Scand* 84: 29–33, **1972**.

31. Jha P. Avoidable global cancer deaths and total deaths from smoking. *Nat Rev Cancer* 9: 655–664, **2009**.

32. Jheng HF, Tsai PJ, Guo SM, Kuo LH, Chang CS, Su IJ, Chang CR, Tsai YS. Mitochondrial fission contributes to mitochondrial dysfunction and insulin resistance in skeletal muscle. *Mol Cell Biol* 32: 309–319, **2012**.

33. John U, Hanke M, Rumpf HJ, Thyrian JR. Smoking status, cigarettes per day, and their relationship to overweight and obesity among former and current smokers in a national adult general population sample. *Int J Obes (Lond)* 29: 1289–1294, **2005**.

34. Knight-Lozano CA, Young CG, Burow DL, Hu ZY, Uyeminami D, Pinkerton KE, Ischiropoulos H, Ballinger SW. Cigarette smoke exposure and hypercholesterolemia

increase mitochondrial damage in cardiovascular tissues. *Circulation* 105: 849–854, **2002**.

35. Levy M, Khan E, Careaga M, Goldkorn T. Neutral sphingomyelinase 2 is activated by cigarette smoke to augment ceramide-induced apoptosis in lung cell death. *Am J Physiol Lung Cell Mol Physiol* 297: L125–L133, **2009**.

36. Makimattila S, Nikkila K, Yki-Jarvinen H. Causes of weight gain during insulin therapy with and without metformin in patients with Type II diabetes mellitus. *Diabetologia* 42: 406–412, **1999**.

37. Miro O, Alonso JR, Jarreta D, Casademont J, Urbano-Marquez A, Cardellach F. Smoking disturbs mitochondrial respiratory chain function and enhances lipid peroxidation on human circulating lymphocytes. *Carcinogenesis* 20: 1331–1336, **1999**.

38. Pesta D, Gnaiger E. High-resolution respirometry: OXPHOS protocols for human cells and permeabilized fibers from small biopsies of human muscle. *Methods Mol Biol* 810: 25–58, **2012**.

39. Pfaffl MW. A new mathematical model for relative quantification in real-time RT-PCR. *Nucleic Acids Res* 29: e45, **2001**.

40. Pirkle JL, Bernert JT, Caudill SP, Sosnoff CS, Pechacek TF. Trends in the exposure of nonsmokers in the U.S. population to secondhand smoke: 1988–2002. *Environ Health Persp* 114: 853–858, **2006**.

41. Pirkle JL, Flegal KM, Bernert JT, Brody DJ, Etzel RA, Maurer KR. Exposure of the US population to environmental tobacco smoke: the Third National Health and Nutrition Examination Survey, 1988 to 1991. *JAMA* 275: 1233–1240, **1996**.

42. Rajagopalan S, Brook RD. Air pollution and type 2 diabetes: mechanistic insights. *Diabetes* 61: 3037–3045, **2012**.

43. Reaven G, Tsao PS. Insulin resistance and compensatory hyperinsulinemia: the key player between cigarette smoking and cardiovascular disease? *J Am Coll Cardiol* 41: 1044–1047, **2003**.

44. Reaven GM, Chen YD. Insulin resistance and cigarette smoking. *Lancet* 340: 377, **1992**.

45. Reynolds PR, Cosio MG, Hoidal JR. Cigarette smoke-induced Egr-1 upregulates proinflammatory cytokines in pulmonary epithelial cells. *American J Respir Cell Mol Biol* 35: 314–319, **2006**.

46. Shimokata H, Muller DC, Andres R. Studies in the distribution of body fat. III. Effects of cigarette smoking. *JAMA* 261: 1169–1173, **1989**.

47. Smith ME, Tippetts TS, Brassfield ES, Tucker BJ, Ockey A, Swensen AC, Anthonymuthu TS, Washburn TD, Kane DA, Prince JT, Bikman BT. Mitochondrial fission mediates ceramide-induced metabolic disruption in skeletal muscle. *Biochem J* 456: 427–439, **2013**.

48. Speizer FE. Getting some breathing room–persuading patients to stop smoking. *Western J Med* 157: 585–586, **1992**.

49. Summers SA. Ceramides in insulin resistance and lipotoxicity. *Prog Lipid Res* 45: 42–72, **2006**.

50. Velasquez-Mieyer PA, Cowan PA, Arheart KL, Buffington CK, Spencer KA, Connelly BE, Cowan GW, Lustig RH. Suppression of insulin secretion is associated with weight loss and altered macronutrient intake and preference in a subset of obese adults. *Int J Obes Rel Metab Dis* 27: 219–226, **2003**.

51. Watt MJ, Barnett AC, Bruce CR, Schenk S, Horowitz JF, Hoy AJ. Regulation of plasma ceramide levels with fatty acid oversupply: evidence that the liver detects and secretes de novo synthesised ceramide. *Diabetologia* 55: 2741–2746, **2012**.

52. World Health Organization. Obesity and Overweight. http://wwwwhoint/mediacentre/factsheets/fs311/en/FactSheet311, **2012**.

53. Wright JL, Cosio M, Churg A. Animal models of chronic obstructive pulmonary disease. *Am J Physiol Lung Cell Mol Physiol* 295: L1–L15, **2008**.

Cardiomyocyte mitochondrial respiration is reduced by receptor for advanced glycation end-product signaling in a ceramide-dependent manner

Summarizing my Contribution: I was involved in the development of this experiment in all of the aspects that involved ceramide identification and quantitation. In this paper we treated cardiomyocytes *in vitro* with advanced glycation end products (AGEs). When cells were treated with an inhibitor of ceramide biosynthesis, myriocin, many of the detrimental side effects of AGE treatment were ameliorated. We therefore set forth to measure the specific effect that ceramide accumulations were having on the cells tested. In agreement with our hypothesis we were able to show that the detrimental effects of AGE treatment were best observed when ceramide concentrations were high. When ceramide biosynthesis was inhibited the negative effects of AGE treated were reduced thereby restoring mitochondrial function. I helped determine treatment conditions for lipid accumulations. I helped develop and teach careful specialized sphingolipid specific lipid extractions. I completed the extractions of lipids from cell pellets and developed the internal standards that were spiked into each sample to aid in mass alignment in the identification phase of the mass spectrometry based lipidomics I also conducted all high-resolution mass spectrometry based lipidomic identifications and quantitation. I generated and helped put together all of the figures that involved ceramide quantitation for the differing treatment states. I was involved in the writing, formatting, and editing of this manuscript.

Michael B. Nelson, Adam Clayton Swensen, Duane R. Winden, Jared S. Bodine, Benjamin T. Bikman, Paul R. Reynolds

American Journal of Physiology - Heart and Circulatory Physiology Published 1 July 2015 Vol. 309 no. 1, H63-H69 DOI: 10.1152/ajpheart.00043.2015

Abstract

Cigarette smoke exposure is associated with an increased risk of cardiovascular complications. The role of advanced glycation end products (AGEs) is already well established in numerous comorbidities, including cardiomyopathy. Given the role of AGEs and their receptor, RAGE, in activating inflammatory pathways, we sought to determine whether ceramides could be a mediator of RAGE-induced altered heart mitochondrial function. Using an in vitro model, we treated H9C2 cardiomyocytes with the AGE carboxy-methyllysine before mitochondrial respiration assessment. We discovered that mitochondrial respiration was significantly impaired in AGE-treated cells, but not when cotreated with myriocin, an inhibitor of de novo ceramide biosynthesis. Moreover, we exposed wild-type and RAGE knockout mice to secondhand cigarette smoke and found reduced mitochondrial respiration in the left ventricular myocardium from wild-type mice, but RAGE knockout mice were protected from this effect. Finally, conditional overexpression of RAGE in the lungs of transgenic mice elicited a robust increase in left ventricular ceramides in the absence of smoke exposure. Taken together, these findings suggest a RAGE-ceramide axis as an important contributor to AGE-mediated disrupted cardiomyocyte mitochondrial function.

Receptors for advanced glycation end-products (RAGEs) are important mediators of numerous chronic complications. Many of these conditions, including peripheral neuropathy[2], retinopathy[1,8], nephropathy[48], and cardiomyopathy[6,15], reduce quality of life[32] and often involve macrovascular and microvascular complications[7]. RAGE was originally characterized for its ability to bind advanced glycation end products (AGEs) and for its role as a prominent

feedforward receptor involved in inflammation[25]. AGEs are derived via the nonenzymatic combination of amino groups and reducing sugars[19], and hyperglycemia-mediated induction of protein glycosylation has been implicated in the production of systemic AGEs[13,46]. However, independent of blood glucose, cigarette smoke exposure increases AGE formation through Malliard chemical reactions involving smoke components and plasma proteins[20]. Whether through chronic hyperglycemia or secondhand cigarette smoke exposure, cellular responses provide abundant AGEs for RAGE signaling that causes enhanced expression of proinflammatory cytokines and deleterious inflammatory responses[17]. Two AGEs often found in increased abundance with diabetics and smokers are N(ε)-carboxy-methyllysine (CML)[34] and N(ε)-carboxy-ethyllysine[45].

In addition to RAGE, sphingolipids are another factor increasingly recognized to play a role in the progression of inflammatory disorders[3,16]. Ceramides, in particular, are a subset of sphingolipid that have been linked to cardiometabolic disruption[42], altered mitochondrial dynamics and function[4,36,39], increasing atheroma development[5], and mediating insulin resistance[41]. We have previously shown that ceramides are actively synthesized in the lung with cigarette smoke exposure[42].

Since activation of inflammatory signaling pathways has been shown to upregulate ceramide biosynthesis[3], it is plausible that RAGE-mediated inflammation can stimulate the synthesis and elaboration of ceramides. RAGE functions as other pattern recognition receptors, including Toll-like receptor (TLR)4, which increases ceramide biosynthesis upon activation[14]. This paradigm involving a connection between RAGE and ceramide, however, has yet to be fully investigated. Based on this intersection, we hypothesized that RAGE-AGE signaling would

increase cardiomyocyte ceramide accrual, thereby increasing ceramide-mediated cardiomyocyte mitochondrial dysfunction.

Materials and Methods

Cell culture.

Immortalized rat H9C2 cardiac myocytes were obtained from the America Type Cell Culture (Manassas, VA) and used at passages 9–12. CML-BSA was purchased from MBL (Woburn, MA), and myriocin was obtained from Sigma-Aldrich (St. Louis, MO). Cells were split into six-well plates and grown to confluency. Myriocin-treated cells were pretreated for 1 h with 1 μl of 10 mM myriocin. Cells were subsequently cotreated with either 30 μl CML-BSA/mL growth media or normal growth media for 24 h. All subsequent analysis took place after the exposure period.

Mice

Wild-type (WT) C57BL/6 mice are in house and were obtained from Jackson Laboratories (Bar Harbor, ME). RAGE knockout (KO) mice lacking membrane and soluble RAGE were generated on a C57BL/6 background. Conditional RAGE transgenic mice were also generated, which overexpress RAGE in the alveolar epithelium when fed doxycycline[28,37]. Doxycycline incorporation into murine diets caused the upregulation of RAGE in the lungs of transgenic mice from postnatal day 20 until the date of death at postnatal day 110[38]. Mice were kept on normal light-dark cycles and had free access to food and water. Housing and treatment of all mice were in accord with approved Institutional Animal Care and Use Committee protocols at Brigham Young University.

Smoke exposure.

For one study, WT and RAGE KO mice were randomly assigned to control and smoke-exposed groups and acutely treated using an in-house nose-only smoke exposure system (InExpose System, Scireq). Over the course of 1 wk, mice were restrained daily and connected to an exposure tower for 10 min, where they were nasally exposed to secondhand cigarette smoke from two cigarettes. Computer-generated puffs resulted in 10 s of secondhand exposure followed by 50 s of fresh air. After exposure, mice were then allowed to rest for 10 min before repeating the process two additional times until they had been exposed to a total of 6 cigarettes/day. The smoke challenge chosen in the present study was associated with a good tolerance of mice to the smoke sessions and an acceptable level of particulate density concentration according to literature[29,44]. Control animals were similarly handled and restrained but kept under a smoke-free environment. In a second chronic exposure study, WT mice were similarly assigned to control and smoke-exposed groups and exposed to secondhand smoke. The procedure, however, included exposure to 4 cigarettes/day for 8 wk. Studies were performed in accordance with principles outlined in the National Institutes of Health Guide for the Care and Use of Laboratory Animals.

Immunohistochemistry.

Heart tissue from control and cigarette smoke-exposed mice was fixed in 4% paraformaldehyde, processed, embedded in paraffin wax, sectioned, and stained according to standard immunohistochemical procedures[27,30]. The ceramide primary antibody used for immunohistochemical detection was obtained from Sigma-Aldrich (C8104-50TST, 1:500). Development in 3,3-diaminobenzidone revealed enhanced brown chromogen in tissues positive for ceramide expression.

Mass spectrometry.

In isolating lipids, pellets were suspended in ice-cold chloroform-methanol (1:2), incubated for 15 min on ice, and then briefly vortexed. Aqueous and organic phases were separated by the addition of ice-cold water and chloroform. The organic phase was collected in a fresh vial and dried via vacuum centrifugation (Eppendorf Concentrator Plus). Lipids were then characterized and quantified using shotgun lipidomics on a Thermo Scientific LTQ Orbitrap XL mass spectrometer, as previously described[12].

Mitochondrial respiration.

O2 consumption from H9C2 cardiomyocytes and cardiac muscle obtained from mice was determined using an O2K oxygraph (Oroboros Instruments). Cells [digitonin (1 mg/ml)] and tissue [saponin (50 μg/ml)] were then permeabilized. After permeabilization, samples were transferred to respiration chambers. Respiration was determined using a substrate-uncoupler-inhibitor titration protocol. Electron flow through complex 1 was assessed by supporting the system with glutamate (G; 10 mM) and malate (M; 2 mM). After stabilization, ADP was added to determine oxidative phosphorylation capacity (2.5 mM). Succinate (S; 10 mM) was then added to assess complex 1 + 2 electron flow. To determine full electron transport system capacity, the chemical uncoupler FCCP (E; 0.05 μM) was added. To assess complex 2 electron flow, complex 1 was then inhibited by including rotenone (0.5 μM).

Real-time PCR.

RNA from cells was isolated using TRIzol (Invitrogen, Grand Island, NY) and quantified via optical density measurement. Reverse transcription of RNA was performed using a Superscript III First-Strand Synthesis System to obtain cDNA for PCR. Primers for serine palmitoyltransferase (SPT)1, SPT2, and ceramide synthase (CerS)2 were obtained and diluted

according to the manufacturer's protocol. Bio-Rad iQ SYBR Green Supermix was used to perform real-time PCR along with previous cDNA, primers, and water. Values were assessed using the ΔΔCT method (where CT is threshold cycle), and comparisons were made with amplified actin. Control wells lacking template or reverse transcriptase were included to identify primer-dimer products and to exclude possible contaminants.

Immunoblot analysis.

Total protein from H9C2 cardiac myocytes and heart tissue was obtained after homogenization with RIPA buffer supplemented with protease inhibitors (Fisher Scientific, Waltham, MA). Protein was then quantified using a BCA Protein Assay Kit (Fisher Scientific), and 20 μg of the resulting lysate were blotted using a mouse polyclonal antibody (AF1179, R&D Systems, Pittsburg, PA) against RAGE (1:1,000), as previously described (45). Western blots were visualized and quantified using a LI-COR C-DiGit Blot Scanner (LI-Cor Biosciences). Quantification of RAGE was performed by densitometry, and normalization with actin provided comparisons between samples.

Statistics.

In vitro data presented are representative of experiments performed in triplicate and animal experiments involved at least 4 samples/group. Data are presented as means ± SE. Data were compared by ANOVA with Tukey's post hoc analysis (Graphpad Prism, La Jolla, CA). Significance was set at $P < 0.05$.

Results

AGEs reduced cardiomyocyte mitochondrial function in a ceramide-dependent manner.

CML is one of the most physiologically relevant AGEs in a diabetic context. To assess the effects of AGEs on cardiomyocytes, we treated H9C2s with growth media containing CML-BSA with and without myriocin, an inhibitor of SPT, the rate-limiting enzyme in de novo ceramide biosynthesis. Compared with control cells, gene expression levels of SPT1, SPT2, and CerS2 were significantly elevated in CML-treated cells (Fig. 1A). Similarly, compared with control conditions, cells exposed to CML-BSA showed a robust increase in ceramide production by mass spectometry but not when pretreated with myriocin (Fig. 1B, CML + myriocin). The increase in SPT and ceramides plausibly implicate RAGE as a factor contributing to de novo ceramide biosynthesis.

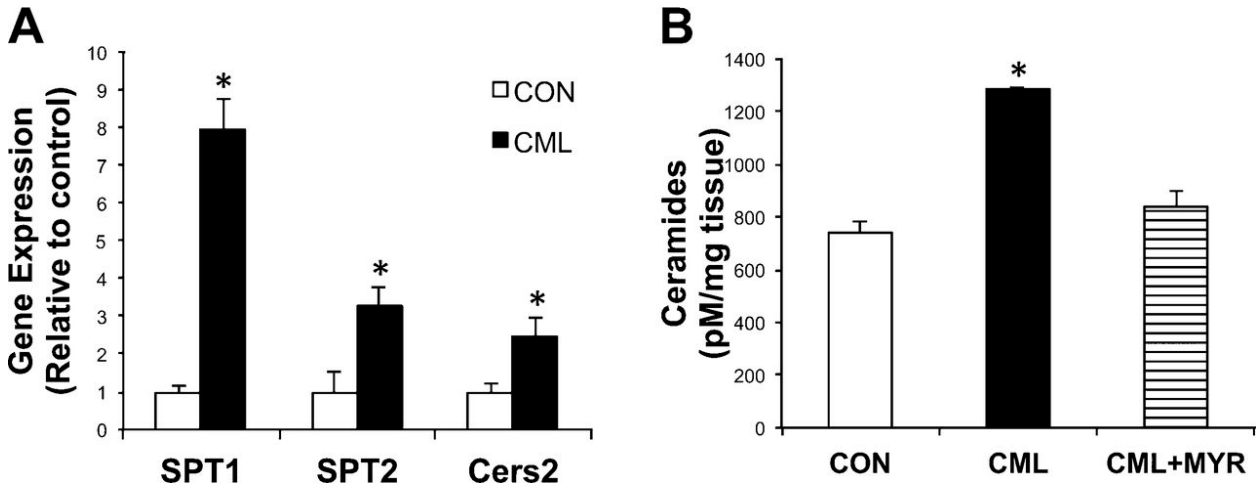

Figure 1: Receptor for advanced advanced glycation end product (RAGE) signaling increases do novo ceramide biosynthesis in cardiomyocytes.

Cardiac myocytes (H9C2) were treated for 24 h with either normal growth media [control (CON)] or growth media infused with carboxy-methyllysine (CML)-BSA (30 µl/ml growth media) with and without myriocin (Myr; 10 µM). After the treatment period, expression levels of serine palmitoyltransferase (SPT)1, SPT2, and ceramide synthase (CerS)2 were quantified (A; n = 3) in addition to ceramides (B; n = 3). *$P < 0.05$ for CML vs. other treatments.

To determine the effect of RAGE-mediated inflammation on heart cell function, we similarly exposed H9C2 cardiomyocytes to the same conditions described above and assessed mitochondrial respiration using a substrate-uncoupler-inhibitor titration protocol (see materials and methods). A significant reduction in respiration was elicited in cells treated with CML-BSA upon the addition of glutamate and malate [leak state (GML); Fig. 2A]. Pretreatment with myriocin, however, abolished the effects of CML-BSA and restored respiration to control levels. Similar results were also found upon stimulation of complex 1-mediated oxidative phosphorylation with ADP addition (GMP). The ddition of succinate to introduce complex II-mediated respiration (GMSP) revealed a slight departure from the trend; whereas CML-treated cells experienced a comparable increase in respiration as control cells, CML treatment appeared to blunt the normal response to succinate addition. We further observed reduced complex II function when analyzing the complex II control factor (GMSP less GMP; Fig. 2B). Similar to succinate addition, the addition of FCCP (respiration uncoupler; GMSE) failed to increase respiration with CML treatment to a level seen with control or myriocin treatment. Taken together, these findings suggest that respiration in cardiomyocytes is impaired by RAGE signaling and is mediated through increased ceramide accrual.

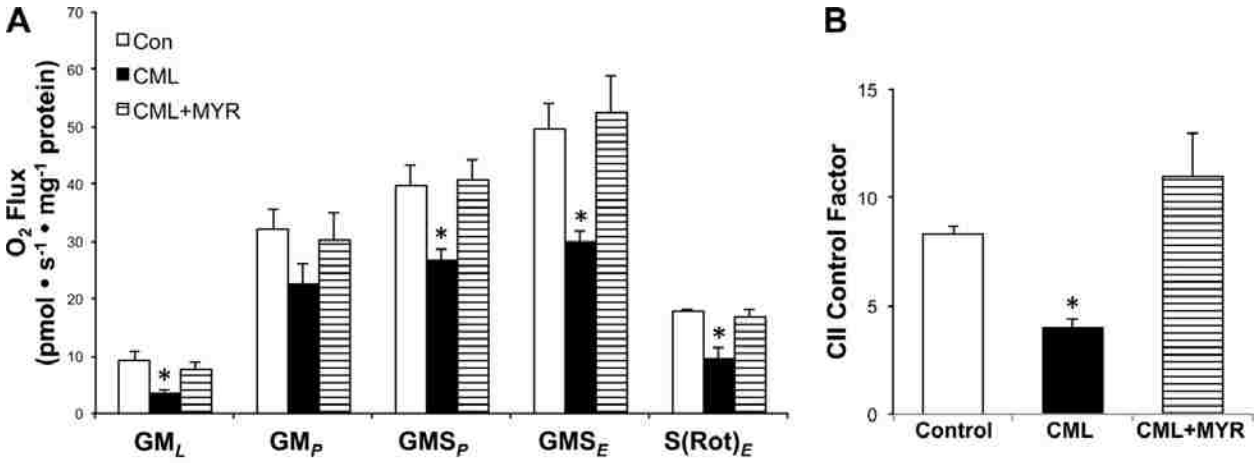

C

Abbreviation	Substrate	Condition
GM_L	Glutamate (10 mM) Malate (2 mM)	Leak (*L*)
GM_P	+ ADP (2.5 mM)	Phosphorylation (*P*)
GMS_P	+ Succinate (10 mM)	Phosphorylation (*P*)
GMS_E	+ FCCP (0.5 µM)	ETS Capacity (*E*)
$S(Rot)_E$	+ Rotenone (0.5 µM)	CII-supported ETS Capacity (*E*)

Figure 2: RAGE signaling reduces cardiomyocyte mitochondrial respiration through ceramide accrual.

Cardiac myocytes (H9C2, n = 3) were treated for 24 h with either normal growth media or growth media containing CML-BSA with and without Myr. After treatment, heart cell mitochondrial O2 consumption was assessed using a substrate-uncoupler-inhibitor titration protocol (A). Complex (C)II control factor was used to determine the specific effect on succinate addition on respiration (B). A description of the protocol is shown in C. ETS, electron transport chain. *P < 0.05 for CML vs. other treatments.

RAGE signaling contributed to cigarette smoke-induced ceramide accrual in cardiomyocytes.

Because AGEs and smoke impact ceramide levels in vitro, we next assessed whether similar effects occurred in vivo. Specifically, as RAGE expression is known to be elevated with inflammation and exposure to cigarette smoke[24,44], we sought to ascertain the expression profile of RAGE in cardiac tissue under both control conditions and after smoke exposure. To establish its expression in the heart, WT mice were restrained and exposed to either room air or secondhand cigarette smoke for 1 or 8 wk. After the treatment, we assessed RAGE protein expression in the left ventricular myocardium. Compared with control animals, RAGE expression was significantly elevated in animals after 1 wk (Fig. 3A) or 8 wk of secondhand cigarette smoke exposure (Fig. 3B). We next analyzed ceramide levels by mass spectrometry to assess whether ceramides are also elevated in cardiomyocytes after secondhand smoke exposure. WT mice exposed to acute cigarette smoke showed a significant increase in ceramides (Fig. 4A); however, this effect was diminished in RAGE KO mice after 1 wk of exposure. To qualitatively visualize these differences, we also performed immunohistochemistry on heart samples for ceramides. WT mice exposed to secondhand cigarette smoke expressed pronounced 3,3-diaminobenzidone-mediated staining for ceramides in heart tissue (Fig. 4B, arrow), but ceramides were qualitatively diminished in exposed RAGE KO mice (Fig. 4B).

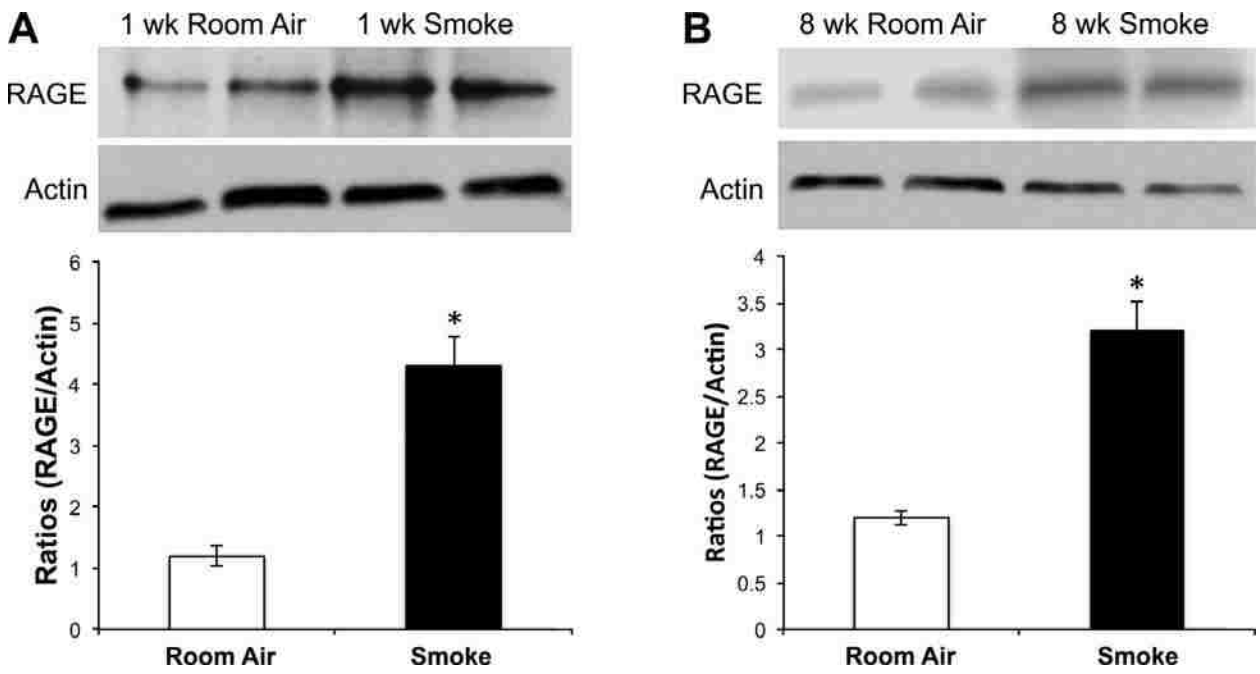

Figure 3: Cigarette smoke increases RAGE expression in the heart with secondhand cigarette smoke exposure.

Wild-type (WT) mice were restrained and exposed to either room air (n = 3) or secondhand cigarette smoke (n = 3, see materials and methods) for 1 (A) or 8 (B) wk. After the exposure period, Western blot analysis and quantification after normalization with actin were performed on heart tissue lysates to determine relative expression levels of RAGE. *P < 0.05 for smoke vs. room air.

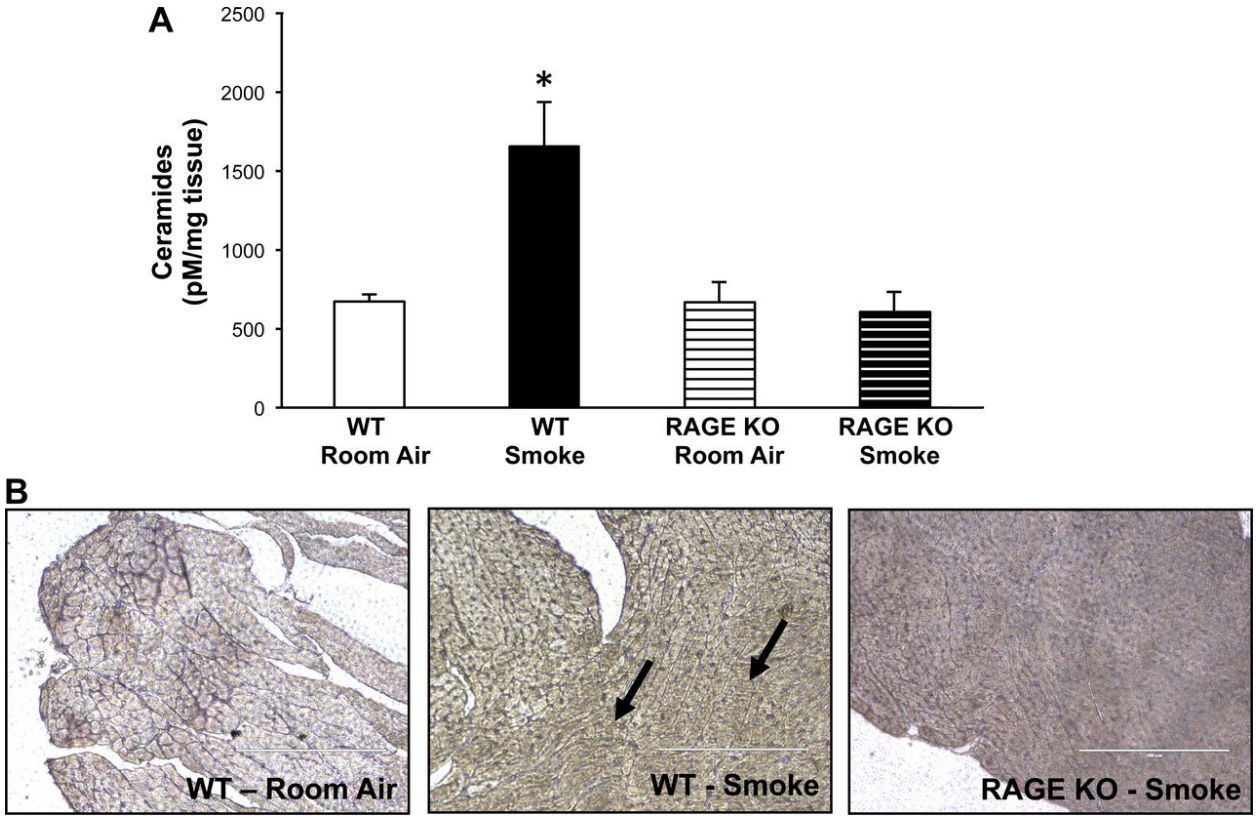

Figure 4: RAGE knockout (KO) prevents heart ceramide accrual with cigarette smoke.

WT and RAGE KO mice were restrained and exposed to either room air or acute secondhand cigarette smoke for 1 wk. After the exposure period, lipids were isolated from heart tissue and analyzed for ceramides (A). Immunohistochemical staining for ceramides was also performed to qualitatively determine any differences in heart tissue between WT and RAGE KO mice under the different exposure conditions (B). Ceramides were significantly increased in WT mice exposed to tobacco smoke (arrows) compared with exposed RAGE KO mice. Scale bars = 200 nm. *$P < 0.05$ for smoke vs. room air within each group.

RAGE signaling was necessary for cigarette smoke-mediated reductions in myocardial mitochondrial respiration.

After exposure to secondhand cigarette smoke, the left ventricular myocardium from WT and RAGE KO mice was permeabilized and assessed for mitochondrial respiration. WT mice showed altered mitochondrial respiration in response to acute cigarette smoke exposure (Fig. 5A). However, RAGE deletion was protective against secondhand smoke-induced respiration defects (Fig. 5A). As with cells, we observed reduced complex II function when analyzing the complex II control factor (GMSP less GMP; Fig. 5B).

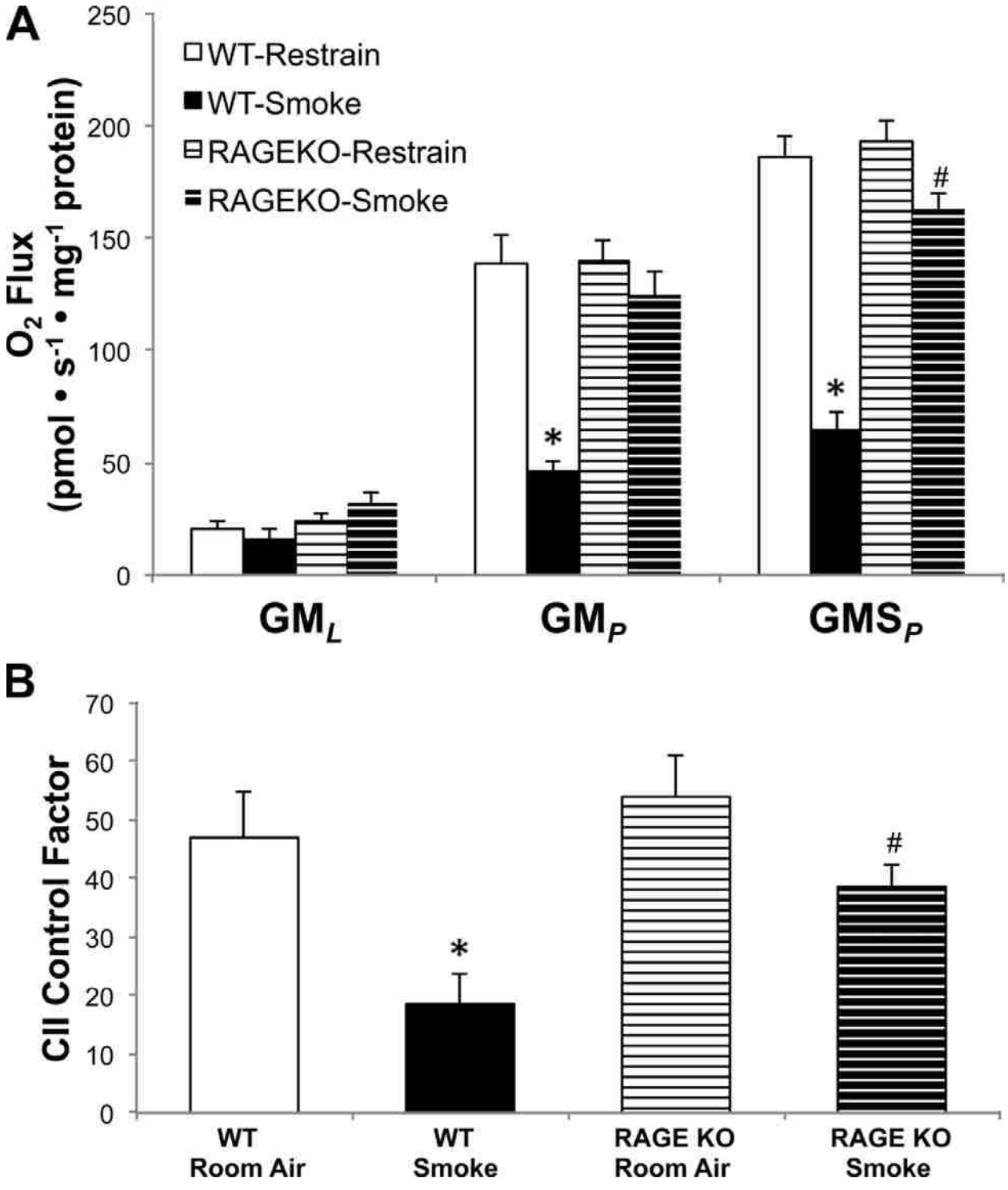

Figure 5: RAGE KO prevents cigarette smoke-induced reduced myocardial mitochondrial respiration.

WT and RAGE KO mice were restrained and exposed to either room air or acute secondhand cigarette smoke for 1 wk. After the exposure period, mitochondrial O2 consumption of cardiac myocytes was assessed (A). Complex II control factor was used to determine the specific effect on succinate addition on respiration (B). *$P < 0.05$ for smoke vs. other treatments; #$P < 0.05$ for smoke-exposed RAGE KO mice vs. room air-exposed RAGE KO mice.

Conditional pulmonary upregulation of RAGE increased biosynthesis of cardiomyocyte ceramides.

The experiments shown in Figs. 3–5 considered the biology of RAGE and ceramide in cardiomyocytes after controlled pulmonary exposure to secondhand smoke. To further assess the role of RAGE in promoting cardiac accumulation of ceramide, experiments were designed in the absence of smoke that compared control mice and conditional transgenic mice that genetically overexpress RAGE in the peripheral lung. Upregulation of RAGE in these mouse models has been validated by both immunoblot analysis and quantitative PCR (27, 29). Lipids were purified from heart tissue obtained from RAGE transgenic mice after 90 days of RAGE upregulation and age-matched nontransgenic control mice before subjection to mass spectrometry analysis. Compared with control mice, hearts from transgenic mice showed a significant increase in ceramides (Fig. 6), further supporting the notion that RAGE is a sufficient mediator of de novo ceramide biosynthesis in cardiac tissue.

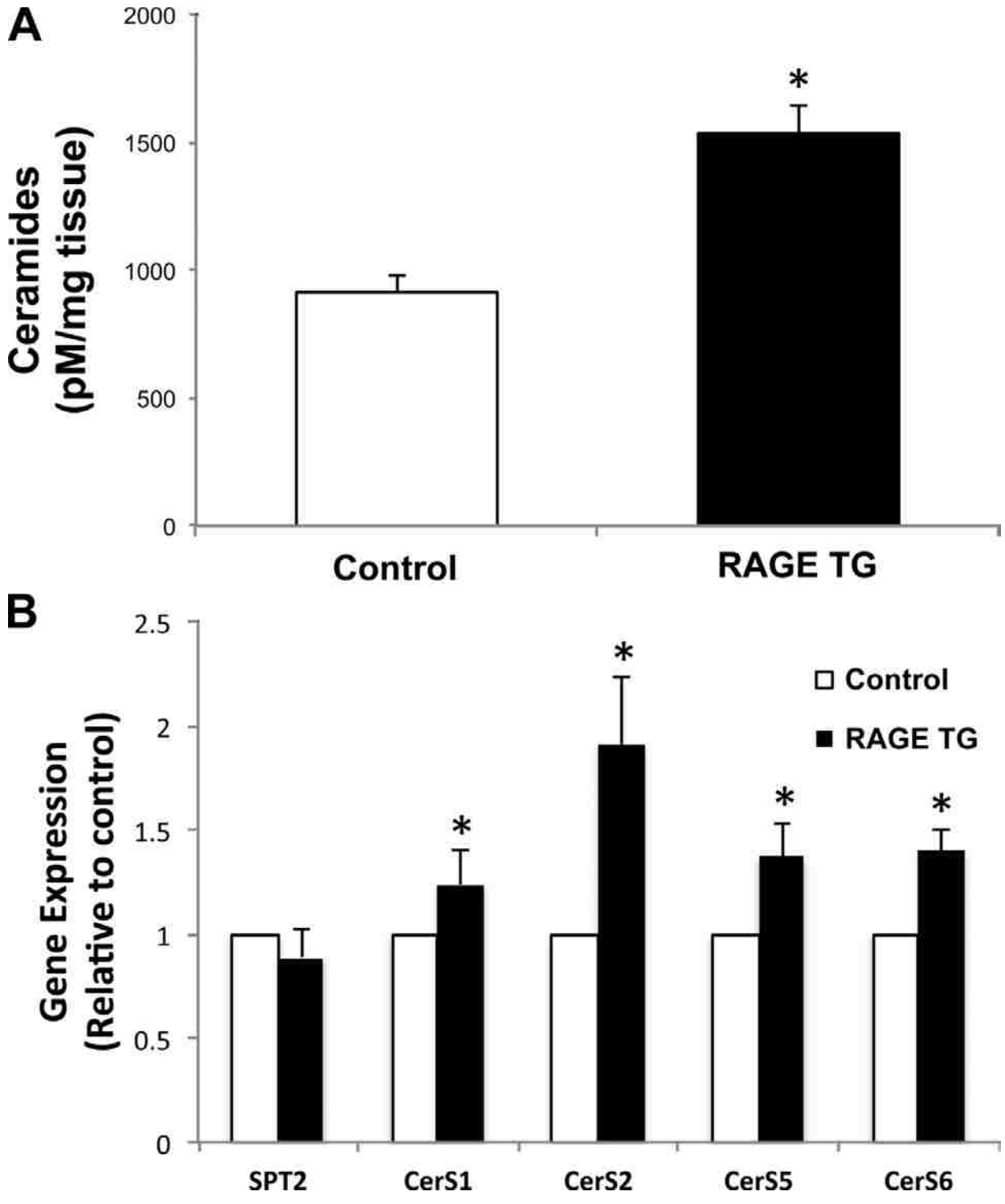

Figure 6: Conditional upregulation of pulmonary RAGE expression increases heart ceramides.

Nontransgenic control and RAGE transgenic (TG) mice, which overexpress RAGE, were euthanized and assessed for ceramide levels in cardiac tissue (A). Expression levels of SPT2, CerS1, CerS2, CerS5, and CerS6 were also quantified in hearts from control and RAGE TG mice (n = 3 mice/group) (B). *P < 0.05 for RAGE TG vs. control mice.

Discussion

This study assessed the effects of RAGE stimulation on cardiomyocyte ceramide accrual and mitochondrial function. Because AGEs are established factors in the progression of cardiovascular complications[15,21], our goal was to assess whether RAGE signaling leads to mitochondrial disruption in heart tissue and whether ceramide is an obligate mediator of these effects. Our results demonstrated that cardiomyocytes respond to AGE treatment with a robust increase in ceramide accrual. This increase may be due, at least in part, to increased expression of the initial and rate-limiting enzymes of ceramide biosynthesis (i.e., SPT) as well as CerS2. To our knowledge, our results are the first to establish a RAGE-ceramide axis within heart cells and tissue.

Under normal physiological circumstances, RAGE serves a protective role by generating a nonspecific inflammatory response to a host of heterogeneous compounds, but this process can become pathological with sustained activation and chronic inflammation[18]. Although the scope of our study was limited to the effects of RAGE and ceramides on cardiomyocyte mitochondrial function, both have been implicated in a host of diabetic and smoke-induced cardiovascular complications. However, AGEs inhaled by smokers may be chemically and functionally different compared with de novo AGE synthesis in uncontrolled diabetics. Ma *et al*.[15] revealed

that AGE-RAGE ablation prevents diabetes-induced altered cardiovascular function, including cardiomyopathy. Moreover, Park *et al*.[23] found that ceramide inhibition through SPT ablation is protective against dilated diabetes-induced cardiomyopathy. Thus, in light of our results of increased ceramides with RAGE activation in heart tissue, future work will seek to determine whether ceramides are necessary for altered heart function orchestrated by RAGE signaling. Importantly, mitochondrial dysfunction may play a critical role in the pathogenesis of cardiomyopathy[11]. This is relevant given our previous findings that ceramides directly disrupt mitochondrial physiology, reducing respiration and increasing oxidative stress[42], through a mitochondrial fission-dependent process[36]. We have previously found that ceramide accrual exhibited a widespread inhibition of mitochondrial respiration, but the effect appeared more selective to inhibiting complex II-mediated respiration. We note similar findings in this report: CML-treated cells did not experience the succinate-induced respiration increase evidenced in both control and myriocin-treated cells. Our demonstration that AGEs induce ceramide-dependent impairment in mitochondrial O2 flux may explain, at least in part, why diabetic hearts are characterized by contractile impairment from anomalous energy metabolism.

Our rationale for targeting RAGE as an activator of ceramide accrual in the heart stems from two observations: 1) as noted earlier, RAGE mediates cardiovascular complications[15]; and 2) RAGE shares common signaling intermediates in pathways known to activate ceramide biosynthesis, namely, TLR4. We reported in 2011 that TLR4 is required for lipid- and endotoxin-induced ceramide biosynthesis[14]. Interestingly, not only do TLR4 and RAGE share common downstream signaling (e.g., IL-1 receptor-associated kinase)[33], but also common ligand activators (e.g., high-mobility group protein B1)[10,35]. Our use of cigarette smoke exposure as an intervention to stimulate RAGE expression is based on our earlier reports of smoke exposure

eliciting a robust increase in lung RAGE expression[26,31], which is a necessary event in transducing inflammation. However, the increase in heart RAGE expression is novel and conveys the possible importance of RAGE modulation in heart complications. To our knowledge, while Denis *et al*.[9] were the first to find a ceramide-RAGE connection when they noted a roughly twofold increase in ceramides in cultured bovine pericytes with AGE exposure, our data may be the first to reveal this phenomenon in whole tissue. Moreover, our evidence of RAGE-mediated increased ceramides in animals exposed to cigarette smoke and in the lungs of RAGE transgenic mice speaks to the influence of lung RAGE signaling on heart ceramide accrual. Despite the clear implication of RAGE in ceramide accrual, important questions remain, such as to what extent RAGE signaling intermediates participate in ceramide biosynthesis and mitochondrial function and how pulmonary RAGE upregulation impacts ceramide accrual in heart tissue.

Given the considerable cardiovascular burden inherent to cigarette smoke exposure[40,43], our results provide a possible mechanism whereby smoke exposure leads to cardiovascular complications. Ceramide has been shown to mediate cardiomyopathy[22] and atherosclerosis[5] and inhibit nitric oxide-induced vasodilation[47]. Thus, our results may have broad implications for cardiovascular therapies.

In conclusion, our results demonstrate that RAGE signaling reduces heart mitochondrial respiration in a ceramide-dependent manner. Considering the dependence of the myocardium on normal mitochondrial function, these results provide evidence for the utility of anti-ceramide therapies in the treatment or prevention of multiple cardiovascular complications.

Grants

This work was supported by a grant from the Flight Attendant's Medical Research Institute (to P. R. Reynolds) and a BYU Mentoring Environment Grant (to P. R. Reynolds).

Disclosures

No conflicts of interest, financial or otherwise, are declared by the author(s).

Author Contributions

Author contributions: M.B.N., A.C.S., D.R.W., J.S.B., and B.T.B. performed experiments; M.B.N., A.C.S., B.T.B., and P.R.R. analyzed data; M.B.N., D.R.W., B.T.B., and P.R.R. interpreted results of experiments; M.B.N. and B.T.B. prepared figures; M.B.N., A.C.S., D.R.W., J.S.B., B.T.B., and P.R.R. edited and revised manuscript; M.B.N., A.C.S., D.R.W., J.S.B., B.T.B., and P.R.R. approved final version of manuscript; B.T.B. and P.R.R. conception and design of research; B.T.B. and P.R.R. drafted manuscript.

Acknowledgements

The authors acknowledge a team of undergraduate students at Brigham Young University including Tyson R. Jergensen, Jason R. Gassman, and Ryan J. Morris for assistance with histology and Dr. Juan Arroyo for assistance with immunoblot analysis. Furthermore, the authors express thanks to David B. Barton and Bryce C. Betteridge for assistance with the use of the animal smoke exposure machine.

Works Cited:

1. Abu El-Asrar AM, Nawaz MI, De Hertogh G, Alam K, Siddiquei MM, Van den Eynde K, Mousa A, Mohammad G, Geboes K, Opdenakker G. S100A4 is upregulated in

proliferative diabetic retinopathy and correlates with markers of angiogenesis and fibrogenesis. *Mol Vis* 20: 1209–1224, **2014**.

2. Bekircan-Kurt CE, Uceyler N, Sommer C. Cutaneous activation of rage in nonsystemic vasculitic and diabetic neuropathy. *Muscle Nerve* 50: 377–383, **2014**.

3. Bikman BT. A role for sphingolipids in the pathophysiology of obesity-induced inflammation. *Cell Mol Life Sci* 69: 2135–2146, **2012**.

4. Bikman BT, Summers SA. Ceramides as modulators of cellular and whole-body metabolism. *J Clin Invest* 121: 4222–4230, **2011**.

5. Bismuth J, Lin P, Yao Q, Chen C. Ceramide: a common pathway for atherosclerosis? *Atherosclerosis* 196: 497–504, **2008**.

6. Bodiga VL, Eda SR, Bodiga S. Advanced glycation end products: role in pathology of diabetic cardiomyopathy. *Heart Fail Rev* 19: 49–63, **2014**.

7. Chawla D, Bansal S, Banerjee BD, Madhu SV, Kalra OP, Tripathi AK. Role of advanced glycation end product (AGE)-induced receptor (RAGE) expression in diabetic vascular complications. *Microvasc Res* 95: 1–6, **2014**.

8. Chen M, Curtis TM, Stitt AW. Advanced glycation end products and diabetic retinopathy. *Curr Med Chem* 20: 3234–3240, **2013**.

9. Denis U, Lecomte M, Paget C, Ruggiero D, Wiernsperger N, Lagarde M. Advanced glycation end-products induce apoptosis of bovine retinal pericytes in culture: involvement of diacylglycerol/ceramide production and oxidative stress induction. Free *Radic Biol Med* 33: 236–247, **2002**.

10. Ding HS, Yang J, Chen P, Yang J, Bo SQ, Ding JW, Yu QQ. The HMGB1-TLR4 axis contributes to myocardial ischemia/reperfusion injury via regulation of cardiomyocyte apoptosis. *Gene* 527: 389–393, **2013**.

11. Duncan JG. Mitochondrial dysfunction in diabetic cardiomyopathy. *Biochim Biophys* Acta 1813: 1351–1359, **2011**.

12. Hansen ME, Tippetts TS, Anderson MC, Holub ZE, Moulton ER, Swensen AC, Prince JT, Bikman BT. Insulin increases ceramide synthesis in skeletal muscle. *J Diabetes Res 2014*: 765784, **2014**.

13. Hodgson K, Morris J, Bridson T, Govan B, Rush C, Ketheesan N. Immunological mechanisms contributing to the double burden of diabetes and intracellular bacterial infections. *Immunology* 144: 171–185, **2015**.

14. Holland WL, Bikman BT, Wang LP, Yuguang G, Sargent KM, Bulchand S, Knotts TA, Shui G, Clegg DJ, Wenk MR, Pagliassotti MJ, Scherer PE, Summers SA. Lipid-induced insulin resistance mediated by the proinflammatory receptor TLR4 requires saturated fatty acid-induced ceramide biosynthesis in mice. *J Clin Invest* 121: 1858–1870, **2011**.

15. Ma H, Li SY, Xu P, Babcock SA, Dolence EK, Brownlee M, Li J, Ren J. Advanced glycation endproduct (AGE) accumulation and AGE receptor (RAGE) up-regulation contribute to the onset of diabetic cardiomyopathy. *J Cell Mol Med* 13: 1751–1764, **2009**.

16. Maceyka M, Spiegel S. Sphingolipid metabolites in inflammatory disease. *Nature* 510: 58–67, **2014**.

17. Manigrasso MB, Juranek J, Ramasamy R, Schmidt AM. Unlocking the biology of RAGE in diabetic microvascular complications. *Trends Endocrinol Metab* 25: 15–22, **2014**.

18. Nedić O, Rattan SI, Grune T, Trougakos IP. Molecular effects of advanced glycation end products on cell signalling pathways, ageing and pathophysiology. *Free Radic Res* 47, Suppl 1: 28–38, **2013**.

19. Nicholl ID, Bucala R. Advanced glycation endproducts and cigarette smoking. *Cell Mol Biol (Noisy-le-grand)* 44: 1025–1033, **1998**.

20. Nicholl ID, Stitt AW, Moore JE, Ritchie AJ, Archer DB, Bucala R. Increased levels of advanced glycation endproducts in the lenses and blood vessels of cigarette smokers. *Mol Med* 4: 594–601, **1998**.

21. Nożyński J, Zakliczyński M, Konecka-Mrowka D, Zielinska T, Zakliczynska H, Nikiel B, Mlynarczyk-Liszka J, Mrowka A, Zembala-Nozynska E, Pijet M, Rdzanowska K, Lange D, Przybylski R, Zembala M. Advanced glycation end product accumulation in the cardiomyocytes of heart failure patients with and without diabetes. *Ann Transplant* 17: 53–61, **2012**.

22. Park TS, Hu Y, Noh HL, Drosatos K, Okajima K, Buchanan J, Tuinei J, Homma S, Jiang XC, Abel ED, Goldberg IJ. Ceramide is a cardiotoxin in lipotoxic cardiomyopathy. *J Lipid Res* 49: 2101–2112, **2008**.

23. Park TS, Rosebury W, Kindt EK, Kowala MC, Panek RL. Serine palmitoyltransferase inhibitor myriocin induces the regression of atherosclerotic plaques in hyperlipidemic ApoE-deficient mice. *Pharmacol Res* 58: 45–51, **2008**.

24. Ramasamy R, Schmidt AM. Receptor for advanced glycation end products (RAGE) and implications for the pathophysiology of heart failure. *Curr Heart Fail Rep* 9: 107–116, **2012**.

25. Reynolds PR, Kasteler SD, Cosio MG, Sturrock A, Hueckstead T, Hoidal JR. RAGE: developmental expression and positive feedback regulation by Egr-1 during cigarette smoke exposure in pulmonary epithelial cells. *Am J Physiol Lung Cell Mol Physiol* 294: L1094–L1101, **2008**.

26. Reynolds PR, Kasteler SD, Schmitt RE, Hoidal JR. Receptor for advanced glycation end-products signals through Ras during tobacco smoke-induced pulmonary inflammation. *Am J Respir Cell Mol Biol* 45: 411–418, **2011**.

27. Reynolds PR, Mucenski ML, Le Cras TD, Nichols WC, Whitsett JA. Midkine is regulated by hypoxia and causes pulmonary vascular remodeling. *J Biol Chem* 279: 37124–37132, **2004**.

28. Reynolds PR, Stogsdill JA, Stogsdill MP, Heimann NB. Up-regulation of receptors for advanced glycation end-products by alveolar epithelium influences cytodifferentiation and causes severe lung hypoplasia. *Am J Respir Cell Mol Biol* 45: 1195–1202, **2011**.

29. Rinaldi M, Maes K, De Vleeschauwer S, Thomas D, Verbeken EK, Decramer M, Janssens W, Gayan-Ramirez GN. Long-term nose-only cigarette smoke exposure induces emphysema and mild skeletal muscle dysfunction in mice. *Dis Model Mech* 5: 333–341, **2012**.

30. Robinson AB, Johnson KD, Bennion BG, Reynolds PR. RAGE signaling by alveolar macrophages influences tobacco smoke-induced inflammation. *Am J Physiol Lung Cell Mol Physiol* 302: L1192–L1199, **2012**.

31. Robinson AB, Stogsdill JA, Lewis JB, Wood TT, Reynolds PR. RAGE and tobacco smoke: insights into modeling chronic obstructive pulmonary disease. *Front Physiol* 3: 301, **2012**.

32. Rodriguez-Pascual C, Rodriguez-Justo S, García-Villar E, Narro-Vidal M, Torrente-Carballido M, Paredes-Galan E. Quality of life, characteristics and metabolic control in diabetic geriatric patients. *Maturitas* 69: 343–347, **2011**.

33. Sakaguchi M, Murata H, Yamamoto K, Ono T, Sakaguchi Y, Motoyama A, Hibino T, Kataoka K, Huh NH. TIRAP, an adaptor protein for TLR2/4, transduces a signal from RAGE phosphorylated upon ligand binding. *PLos One* 6: e23132, **2011**.

34. Schmitt S, Linder M, Ständker L, Hammes HP, Preissner KT. Identification of CML-modified proteins in hemofiltrate of diabetic patients by proteome analysis. *Exp Clin Endocrinol Diabetes* 116: 26–34, **2008**.

35. Sims GP, Rowe DC, Rietdijk ST, Herbst R, Coyle AJ. HMGB1 and RAGE in inflammation and cancer. *Annu Rev Immunol* 28: 367–388, **2010**.

36. Smith ME, Tippetts TS, Brassfield ES, Tucker BJ, Ockey A, Swensen AC, Anthonymuthu TS, Washburn TD, Kane DA, Prince JT, Bikman BT. Mitochondrial fission mediates ceramide-induced metabolic disruption in skeletal muscle. *Biochem J* 456: 427–439, **2013**.

37. Stogsdill JA, Stogsdill MP, Porter JL, Hancock JM, Robinson AB, Reynolds PR. Embryonic overexpression of receptors for advanced glycation end-products by alveolar epithelium induces an imbalance between proliferation and apoptosis. *Am J Respir Cell Mol Biol* 47: 60–66, **2012**.

38. Stogsdill MP, Stogsdill JA, Bodine BG, Fredrickson AC, Sefcik TL, Wood TT, Kasteler SD, Reynolds PR. Conditional overexpression of receptors for advanced glycation end-products in the adult murine lung causes airspace enlargement and induces inflammation. *Am J Respir Cell Mol Biol* 49: 128–134, **2013**.

39. Summers SA. Ceramides in insulin resistance and lipotoxicity. *Prog Lipid Res* 45: 42–72, **2006**.

40. Talukder MA, Johnson WM, Varadharaj S, Lian J, Kearns PN, El-Mahdy MA, Liu X, Zweier JL. Chronic cigarette smoking causes hypertension, increased oxidative stress, impaired NO bioavailability, endothelial dysfunction, and cardiac remodeling in mice. *Am J Physiol Heart Circ Physiol* 300: H388–H396, **2011**.

41. Thatcher MO, Tippetts TS, Nelson MB, Swensen AC, Winden DR, Hansen ME, Anderson MC, Johnson IE, Porter JP, Reynolds PR, Bikman BT. Ceramides mediate cigarette smoke-induced metabolic disruption in mice. *Am J Physiol Endocrinol Metab* 307: E919–E927, **2014**.

42. Tippetts TS, Winden DR, Swensen AC, Nelson MB, Thatcher MO, Saito RR, Condie TB, Simmons KJ, Judd AM, Reynolds PR, Bikman BT. Cigarette smoke increases cardiomyocyte ceramide accumulation and inhibits mitochondrial respiration. *BMC Cardiovasc Disord* 14: 165, **2014**.

43. Tonstad S, Svendsen M. Premature coronary heart disease, cigarette smoking, and the metabolic syndrome. *Am J Cardiol* 96: 1681–1685, **2005**.

44. Wood TT, Winden DR, Marlor DR, Wright AJ, Jones CM, Chavarria M, Rogers GD, Reynolds PR. Acute secondhand smoke-induced pulmonary inflammation is diminished in RAGE knockout mice. *Am J Physiol Lung Cell Mol Physiol* 307: L758–L764, **2014**.

45. Xue J, Rai V, Singer D, Chabierski S, Xie J, Reverdatto S, Burz DS, Schmidt AM, Hoffmann R, Shekhtman A. Advanced glycation end product recognition by the receptor for AGEs. *Structure* 19: 722–732, **2011**.

46. Xue J, Ray R, Singer D, Böhme D, Burz DS, Rai V, Hoffmann R, Shekhtman A. The receptor for advanced glycation end products (RAGE) specifically recognizes methylglyoxal-derived AGEs. *Biochemistry* 53: 3327–3335, **2014**.

47. Zhang QJ, Holland WL, Wilson L, Tanner JM, Kearns D, Cahoon JM, Pettey D, Losee J, Duncan B, Gale D, Kowalski CA, Deeter N, Nichols A, Deesing M, Arrant C, Ruan T, Boehme C, McCamey DR, Rou J, Ambal K, Narra KK, Summers SA, Abel ED, Symons JD. Ceramide mediates vascular dysfunction in diet-induced obesity by PP2A-mediated dephosphorylation of the eNOS-Akt complex. *Diabetes* 61: 1848–1859, **2012**.

48. Zhou X, Wang B, Zhu L, Hao S. A novel improved therapy strategy for diabetic nephropathy: targeting AGEs. *Organogenesis* 8: 18–21, **2012**.

CHAPTER 3:

The Discovery of an Oncogenic Enzyme in Pancreatic Cancer Involved in Cell-Fate Signaling

Introduction

Lipidomics of Pancreatic Cancer Pilot Study

Maintenance of cellular structure and electrochemical gradients, subcellular partitioning, energy storage, first and second messenger cell signaling, protein trafficking and membrane anchoring are all reliant on proper lipid concentrations and regulation. Using global lipid analyses, the causative effect of insulin resistance[1], metabolic syndrome[2], cardiovascular disease[3], and some cancers have been described.[4] Correlations between diseases and lipids have been made with many other varied diseases including Alzheimer's disease[5], atherosclerosis[6], and obesity.[7] Global analysis of lipids, known as lipidomics, is proving to be a powerful and indispensable method for studying the dynamic state of any cell.

One of the most promising areas of lipidomics research today is the elucidation of compositional lipidome changes as a result of cancer. We have shown through our own experimentation that the lipid composition of cancerous cells is dramatically different than their otherwise healthy counterparts. One of the differences we observe is the effect of metabolic deregulation on the global lipid composition. Anabolic synthesis of membrane and signaling lipids created as a result of oncogenic factors can be identified, detected, and tracked. One type of signaling lipid that we have detected is lysophosphatidic acid. Interacting with at least five known G-coupled protein receptors these signaling lipids are upstream activators of several known oncoproteins including Ras.[8]

Lipids are vital for cellular homeostasis and are often required for proper protein function. Weise et al. has shown that some oncoproteins such as K-Ras4B are not active until properly localized by lipid micro-domains.[9] Gault *et al*. has even shown that oncogenic K-Ras regulates sphingolipids in a sphingosine kinase 1 dependent manner.[10]

We collected and completed preliminary analysis of three pancreatic cell lines, hTERT-HPNE (a telomerase immortalized pancreas cell line), PSN1 (ductal pancreatic cancer), and PANC1 (ductal pancreatic cancer). We confirmed previous research based on lipidome profiling. More importantly we have been able to elucidate new knowledge about underlying cellular processes by analyzing lipidome changes. The abundant wealth of knowledge we can gain through lipidomics is tantalizing.

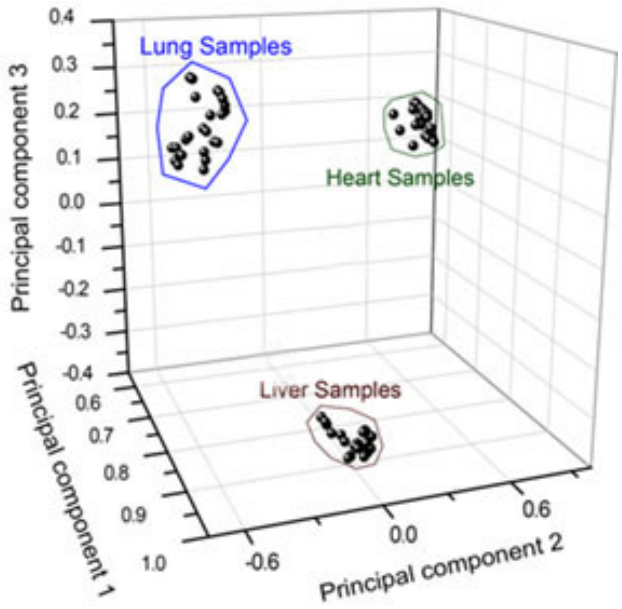

Figure 1: Principle component analysis of lipidomics data. The shotgun lipidomics data of lipid extracts of lung, heart, liver samples from mice. The results were subjected to PCA analysis. The analysis contains 3 sets of biological, sample and technical replicates each.

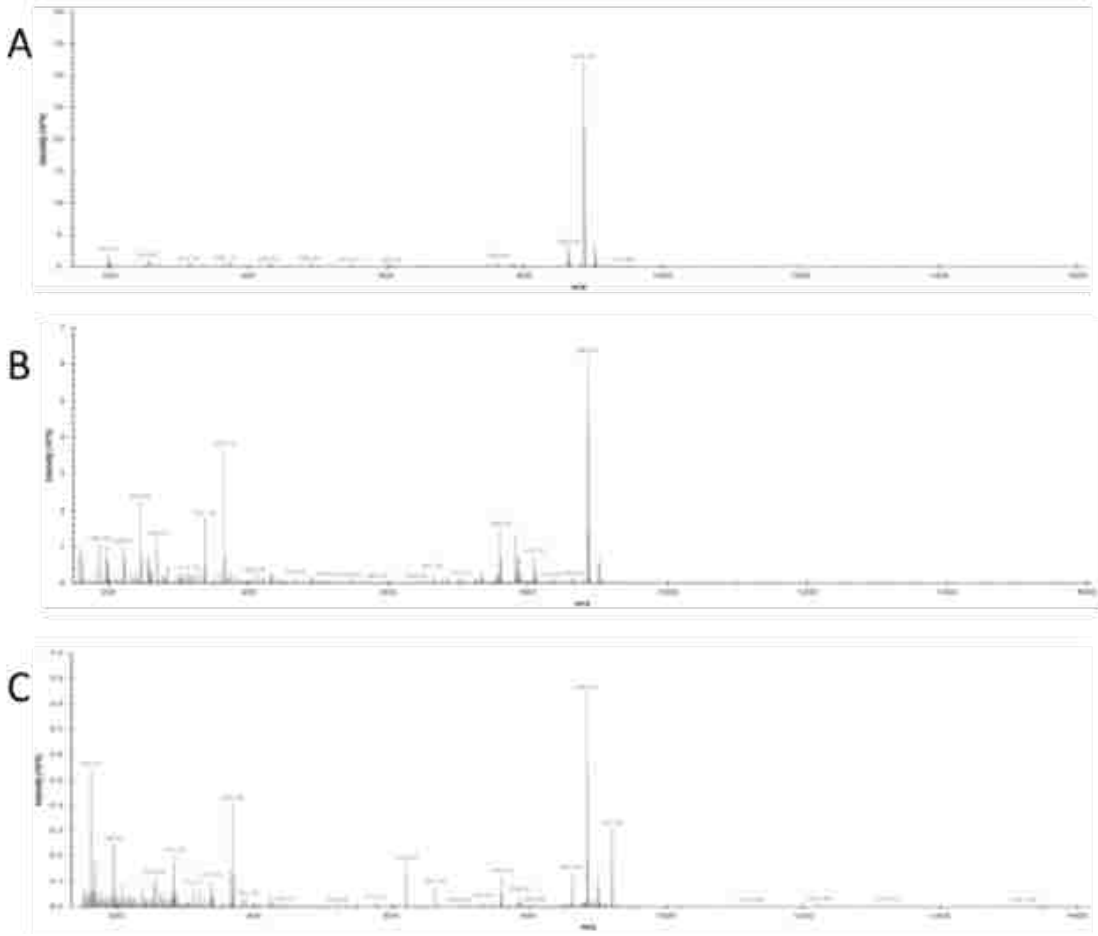

Figure 2: Primary MS[1] Mass Spectra of A) telomerase immortalized pancreas cells (hTERT-HPNE), B) pancreatic cancer cell line (PSN1), and C) pancreatic cancer cell line (PANC1). Spectra were collected using a Thermo Scientific LTQ Orbitrap XL mass spectrometer and a resolution of 100,000.

Lipid Composition Changes in Cancer

An estimated 5 x 10^6 lipid molecules are found per square μm of the cell membrane with a total of 10^9 total lipid molecules in the full membrane of a small cell. Approximately half of the mass of the outer cellular membrane is comprised of lipids.[11]

Being the major molecular species of membranes and of energy storage, cellular lipids play a crucial role for both physiological and cellular energy homeostasis. Perturbations in the lipid composition of a cell can be indication of disease and disregulation. As shown in Figure 1, we have demonstrated that samples from different tissues can be differentiated by using a lipidomics approach. We have also shown that the same approach can be used to differentiate cancerous tumor cells from healthy cells within the same tissue. Figure 2 illustrates some of the distinctive lipidome mass spectra fingerprints we have collected. Balog et al. has already demonstrated the usefulness of lipidome fingerprinting for the detection of cancer with the introduction and commercialization of the iKnife.[12] This technology cauterizes during surgical procedures and 'sniffs' the ionized smoke that arises from the cut by fingerprinting the ionized lipid cloud using mass spectrometry.

However, we are capable of taking this process one step farther by assigning specific lipid identifications to the peaks seen in the mass spectra. This doesn't only reveal a wealth of useful information that helps us distinguish cell types and tissues, it reveals information about the regulated state of the cell and can yield information about activated underlying metabolic and anabolic pathways. Figure 3 shows the categorical lipid compositions of the three pancreatic cell lines we have analyzed to date, as well as comparative lipid compositions of their fresh and used growth media. We gain a wealth of knowledge even from this simple categorical grouping. We observe that there is a drastic change in the most abundant lipid class found in healthy cells, phospholipids. This is indicative of global deregulated metabolism.[13] Additional lipid class compositions also show similar drastic metabolic changes (data not shown). We are confident we will be able to elucidate much more information about pancreatic cancer from the comprehensive databases we plan to create.

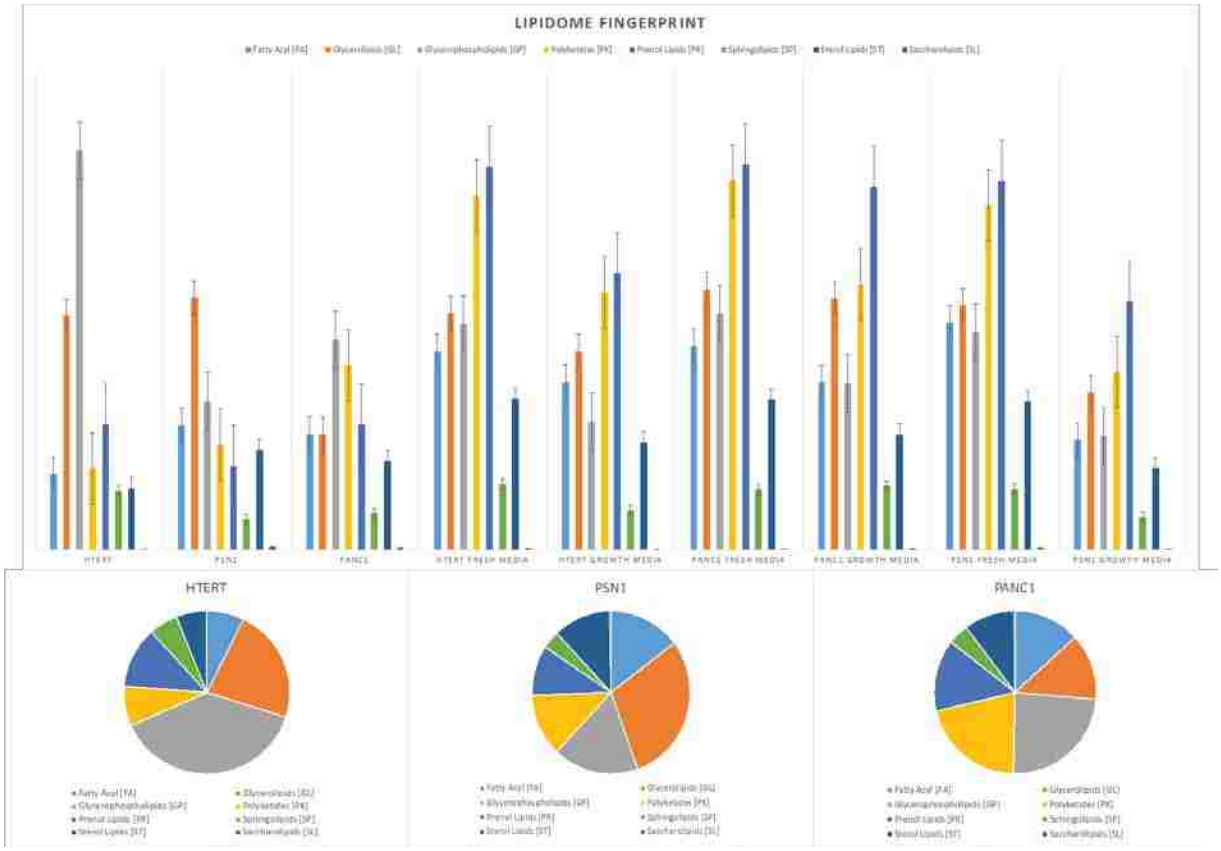

Figure 3: Categorical lipid compositions of hTERT-HPNE, PSN1, and PANC1. Data was averaged from sample duplicates that were run in technical triplicate, with and without additional ionizing adducts. Error bars indicate standard deviation.

Ras activation through Lysophosphatidic acids

Lipids can act as primary and secondary cellular messengers. Lysophosphatidic acids (LPAs) are a messenger lipid type that have only recently been discovered. Lin et al. and others have shown that LPAs act to regulate cell proliferation, growth, survival, migration, invasion, and promotion of angiogenesis.[8] LPAs act through at least five known G-protein coupled receptors that are capable of activating or deactivating many cellular processes. Acting through the Rho/ROCK/actomyosin and Ras/MEKK1 pathways, LPAs enhance cancer cell migration and accelerate focal adhesion formation.[14] Our data indicate that LPA levels in pancreatic cancer are grossly overexpressed. Figure 5 demonstrates some of the LPA species detected in our preliminary analysis. One species of LPA worth further investigation is PA(17:2(9Z,12Z)/0:0). No amount of this lipid was detected in hTERT-HPNE, but it was the most up-regulated signaling lipid species in both PSN1 and PANC1.

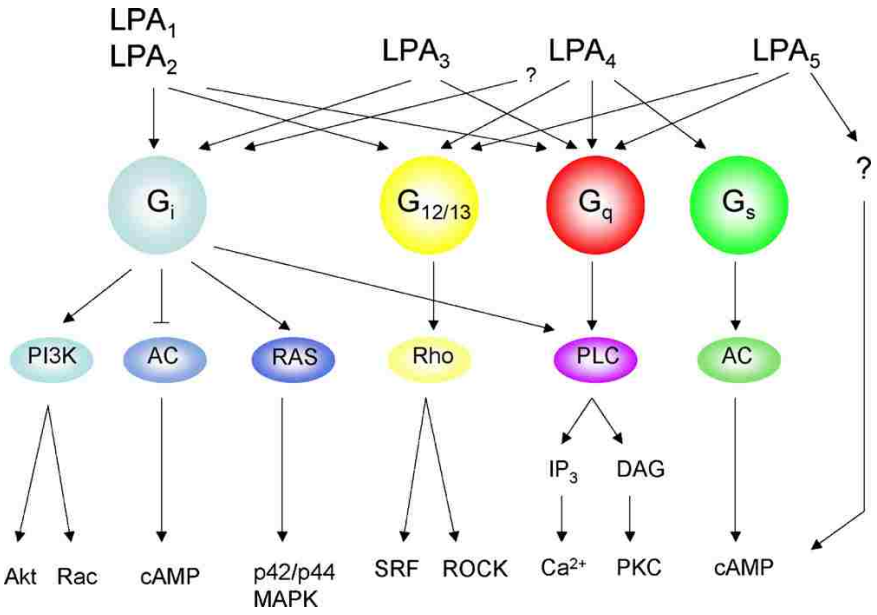

Figure 4: GPCR pathways activated by the signaling lipid species LPA class. Adopted from Lin *et al.*[8]

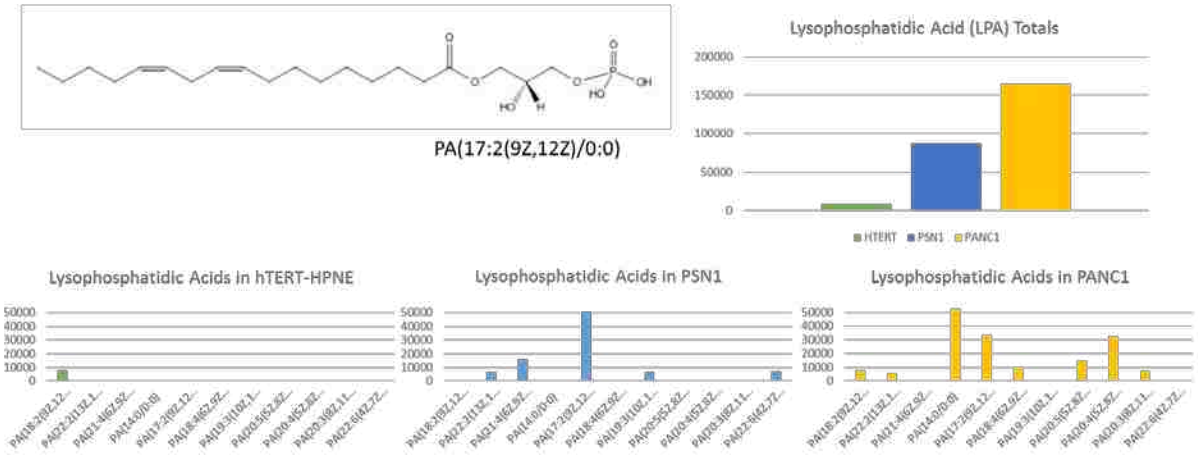

Figure 5: Lysophosphatidic Acids (LPAs) in Pancreatic Cancer. LPAs were found to be highly up-regulated in pancreatic cancer. Only one species of LPA was detected in hTERT-HPNE. Multiple species were detected in the cancerous pancreatic cells, including one species, PA(17:2(9Z,12Z)/0:0) that is observed up-regulated in both cancer cell types.

K-Ras Activation and Anchoring in Pancreatic Cancer

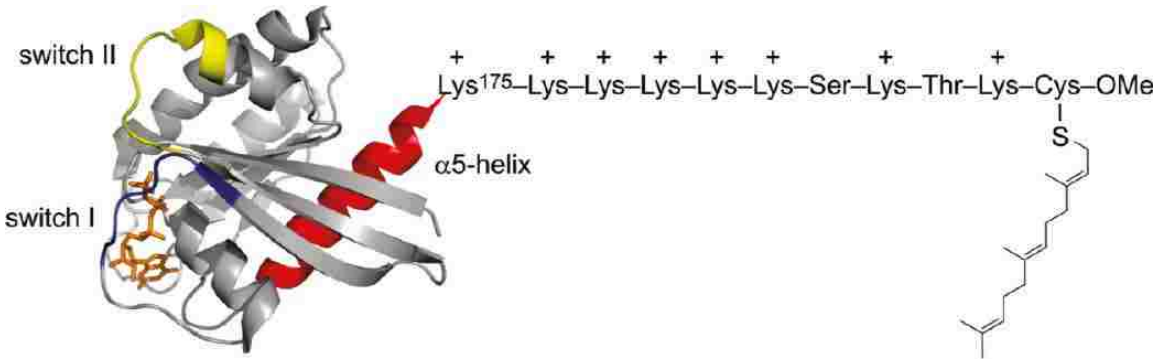

Figure 6: K-Ras4B contains a polybasic farnesylated lipid anchoring tail. It has been shown that K-Ras is only active when clustered properly on lipid micro-domains. Adopted from Weise *et al*.[10]

K-Ras is a GTPase and is a major oncoprotein found in pancreatic cancer. In order to function properly, K-Ras must be correctly localized to negatively-charged subcellular membranes. It only becomes functional and active when it forms nano-clusters in the presence of negatively charged acidic lipids found in membrane micro-domains.[9] K-Ras4B localizes itself with the use of a polybasic farnesylated C-terminal tail as illustrated in Figure 6. This tail is best stabilized by interacting with acidic lipid species such as phophoserines, cardiolipins, phosphoinositols, and phosphatidic acids. It has even been proposed that K-Ras activity is changed in the presence of polyphosphoinositols (PIPs), and that the surface interactions with the lipid membrane change the protein folding through interactions with the α5 helix. We have completed an analysis of some of the acidic lipid species found in the pancreatic cell lines. More experimentation is required to fully elucidate the effects of these acidic lipid micro-domains or to potentially determine how to interrupt the plasma membrane targeting of these membrane proteins.

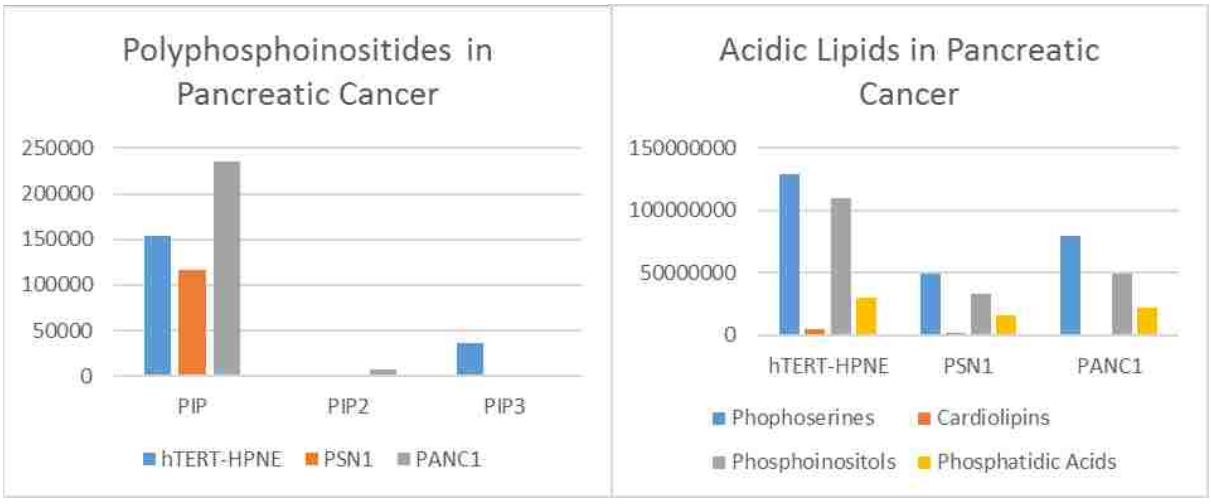

Figure 7: Polyphosphoinositide (PIP) and General Acidic Lipid Classes in Pancreatic Cancer. These lipid species have been shown to be important for the activity of oncoproteins such as K-Ras.[9]

Sphingosine Kinase (SphK1) Regulates Bioactive Sphingolipids

Gault *et al*. have shown that oncogenic K-Ras has the ability to regulate lipid member of a class of bioactive sphingolipids known as sphingosine-1-phosphate (S1P). It does this by regulating sphingosine kinase 1 (SK1). C-16 ceramide in particular is the target species that is converted to S1P by oncogenic K-Ras. We were able to show this exact character among the pancreatic cancer cell lines we studied. The cellular levels of S1P are observed to be highly up-regulated in pancreatic cancer when compared to the immortalized healthy pancreatic cells. The Gault *et al*. study was conducted in immortalized MEF cells. We were able to demonstrate similar behavior in human pancreatic cancer.

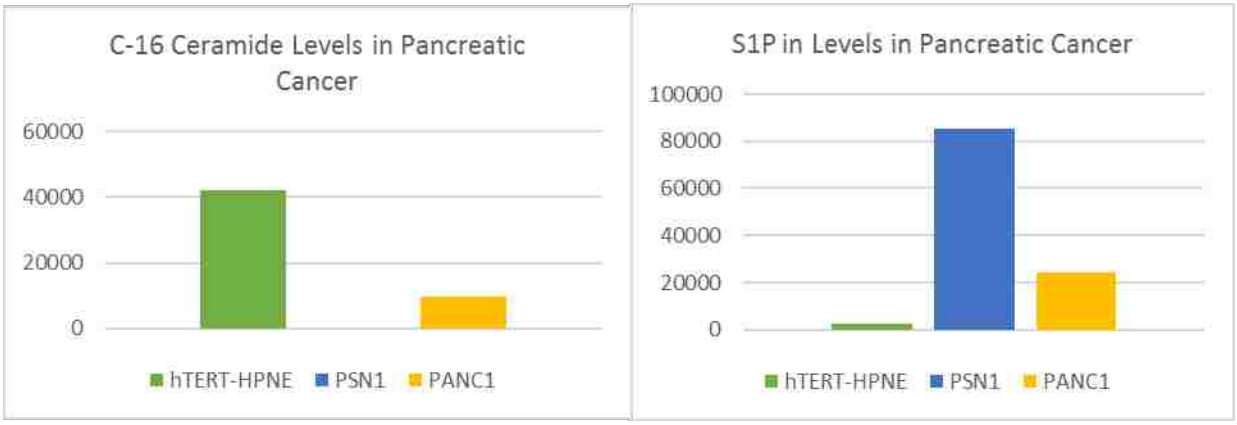

Figure 8: Sphingosine Kinase 1 like activity of K-Ras in Pancreatic Cancer. Sphingosine-1-phosphate levels rise as C-16 ceramide levels decrease in PSN1 and PANC1, suggesting that oncogenic K-Ras is potentially directly involved in the sphingolipid regulation through sphingosine kinase activity.

***In-vitro* Studies of Useful Pancreatic Cancer Metabolites**

Before plating and growing the cells for our study several aliquots of fresh growth media were collected and used in a comparative study against used growth media. These samples were analyzed using a lipidomic method. Through our experimentation we have discovered that each cancer cell type subsists on and excretes distinct lipid species. We could use this information to discover unique novel pancreatic cancer lipid biomarkers using a simple *in vitro* technique. Completing lipidomic analyses of growth media could also allow us to do future studies to discover specifically how diet affects the growth and lipid composition of pancreatic cancer. We have shown that this could potentially lead to new dietary treatment methods once we learn which lipids and metabolites most exacerbate cancer growth.

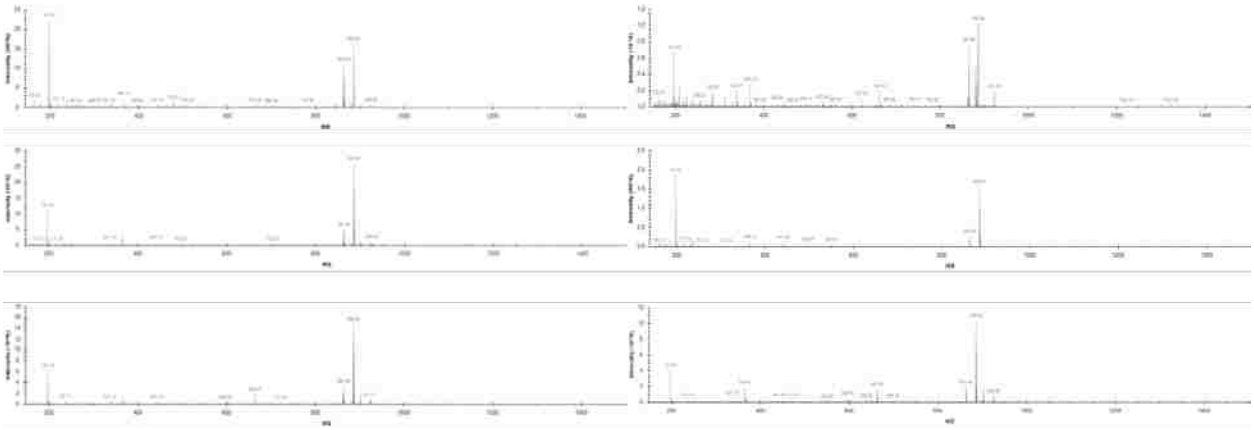

Figure 9: Metabolite Studies in Pancreatic Cancer. Fresh (left top: hTERT-HPNE, left middle: PSN1, left bottom: PANC1) and used (right top: hTERT-HPNE, right middle: PSN1, right bottom: PANC1) growth media from pancreatic cancer cells. Samples of fresh growth media were collected at the same time the cells grown. More growth media was collected before removing the cells from the plates. These samples will be analyzed to observe lipid composition changes affected by growth in the media.

Conclusion:

We have established that the use of lipidomics is indispensable in the study of cancer. We have demonstrated that cancerous cells can be differentiated from healthy cells based on their lipidome composition. This technique can greatly speed cancer detection and differentiation from health tissue. We have shown that the effects of oncoproteins found in pancreatic cancer can be observed using lipidomics, thereby indicating which oncongenes are active. We can can also quickly determine the phenotype of cancer on a patient by patient basis. Our work proves that lipidomics is a technique that can verify active oncogenes, help lipid biomarker discovery, We have greatly increased our knowledge about pancreatic cancer through the use of lipidomics.

Works Cited:

1. Hotamisligil, G. S.; Peraldi, P.; Budavari, A.; Ellis, R.; White, M. F.; Spiegelman, B. M., IRS-1-mediated inhibition of insulin receptor tyrosine kinase activity in TNF-alpha- and obesity-induced insulin resistance. *Science* **1996,** *271* (5249), 665-8.

2. Chavez, J. A.; Summers, S. A. A ceramide-centric view of insulin resistance. *Cell metabolism* **2012,** *15* (5), 585-94.

3. Kiebish, M. A.; Han, X.; Cheng, H.; Chuang, J. H.; Seyfried, T. N. Cardiolipin and electron transport chain abnormalities in mouse brain tumor mitochondria: lipidomic evidence supporting the Warburg theory of cancer. *Journal of lipid research* **2008,** *49* (12), 2545-56.

4. Watson, A. D. Thematic review series: systems biology approaches to metabolic and cardiovascular disorders. Lipidomics: a global approach to lipid analysis in biological systems. *Journal of lipid research* **2006,** *47* (10), 2101-11.

5. Swinnen, J. V.; Verhoeven, G. Androgens and the control of lipid metabolism in human prostate cancer cells. *The Journal of steroid biochemistry and molecular biology* **1998,** *65* (1-6), 191-8.

6. Wood, P. L. Lipidomics of Alzheimer's disease: current status. *Alzheimer's research & therapy* **2012,** *4* (1), 5.

7. Ekroos, K.; Janis, M.; Tarasov, K.; Hurme, R.; Laaksonen, R. Lipidomics: a tool for studies of atherosclerosis. *Current atherosclerosis reports* **2010,** *12* (4), 273-81.

8. Donovan, E. L.; Pettine, S. M.; Hickey, M. S.; Hamilton, K. L.; Miller, B. F. Lipidomic analysis of human plasma reveals ether-linked lipids that are elevated in morbidly obese humans compared to lean. *Diabetology & metabolic syndrome* **2013,** *5* (1), 24.

9. Lin, M. E.; Herr, D. R.; Chun, J. Lysophosphatidic acid (LPA) receptors: signaling properties and disease relevance. *Prostaglandins & other lipid mediators* **2010,** *91* (3-4), 130-8.

10. Weise, K.; Kapoor, S.; Denter, C.; Nikolaus, J.; Opitz, N.; Koch, S.; Triola, G.; Herrmann, A.; Waldmann, H.; Winter, R. Membrane-mediated induction and sorting of K-Ras microdomain signaling platforms. *Journal of the American Chemical Society* **2011,** *133* (4), 880-7.

11. Gault, C. R.; Eblen, S. T.; Neumann, C. A.; Hannun, Y. A.; Obeid, L. M. Oncogenic K-Ras regulates bioactive sphingolipids in a sphingosine kinase 1-dependent manner. *The Journal of biological chemistry* **2012,** *287* (38), 31794-803.

12. Alberts, B. *Molecular biology of the cell*. 4th ed.; *Garland Science: New York*, **2002**; p xxxiv, 1548 p.

13. Balog, J.; Sasi-Szabo, L.; Kinross, J.; Lewis, M. R.; Muirhead, L. J.; Veselkov, K.; Mirnezami, R.; Dezso, B.; Damjanovich, L.; Darzi, A.; Nicholson, J. K.; Takats, Z. Intraoperative tissue identification using rapid evaporative ionization mass spectrometry. *Science translational medicine* **2013,** *5* (194), 194ra93.

14. Santos, C. R.; Schulze, A. Lipid metabolism in cancer. *The FEBS journal* **2012,** *279* (15), 2610-23.

15. Ting, Y. L.; Sherr, D.; Degani, H. Variations in energy and phospholipid metabolism in normal and cancer human mammary epithelial cells. *Anticancer research* **1996,** *16* (3B), 1381-8.

16. Sawada, K.; Morishige, K.; Tahara, M.; Ikebuchi, Y.; Kawagishi, R.; Tasaka, K.; Murata, Y. Lysophosphatidic acid induces focal adhesion assembly through Rho/Rho-associated kinase pathway in human ovarian cancer cells. *Gynecologic oncology* **2002**, 87 (3), 252-9.

17. Bian, D.; Su, S.; Mahanivong, C.; Cheng, R. K.; Han, Q.; Pan, Z. K.; Sun, P.; Huang, S. Lysophosphatidic Acid Stimulates Ovarian Cancer Cell Migration via a Ras-MEK Kinase 1 Pathway. *Cancer research* **2004**, 64 (12), 4209-17.

Lipidomic profiling identifies modified sphingosine kinase 1 regulation, and cell-fate signaling in pancreatic cancer

Summarizing my Contribution: This project began as a collaboration with Dr. David Bearss' lab at BYU in the life science's department. Preliminary analysis of pancreatic cancer using genomic analysis, epigenomic analysis, and proteomic analysis did not yield any significant data for targeted drug treatment of the cancer. At the time I was beginning to have success with global lipidomic extractions, identifications, and quantitation using high-resolution mass spectrometry. For this reason, I was approached to see if I could find anything significant lipid differences in the pancreatic cancer cell lines. From this point on I managed the process and drove the direction of experimentation. Using data analysis tools we developed, I was able to discover several significant differences between healthy control cells and cancerous cells and ultimately chose the pathways that were deemed to be most significant in the cancer cells.

Adam C. Swensen, Tsz Yin Chan, Joshua L. Andersen, John T. Prince, John C. Price

Department of Chemistry and Biochemstry, Brigham Young University, Provo, Utah

Correspondence: JCPrice@chem.byu.edu

Submitted to Cancer Research 18 November 2016

Abstract

Many bioactive lipid species play key roles in cellular signaling. These lipid signals can evoke rapid and wide-ranging changes to cell metabolism and morphology. Here we show that a

mass spectrometry based lipidomic analysis of human ductal pancreatic cancer identified an imbalance in C16-ceramide and sphingosine-1-phosphate (S1P) molecules. This perturbation increases the growth rate, and protects these cells from the mitochondrial mediated apoptotic cell-signaling cascade. Regulation of sphingosine kinase 1 (SphK1) seems to be a major component of this alternate regulation of lipid signals. Importantly, we observed that different pancreatic cancer lines utilized unique alterations in SphK1 concentration and/or activation to alter regulation of sphingosine kinase activity, suggesting that SphK1 is an important regulatory node for the cancerous phenotype. Modified SphK1 activity resulted in pro-apoptotic signals changing into anti-apoptotic signals. This imbalance in the 'rheostat' between pro- and anti-apoptotic signals may, in part, explain the frequently aggressive and chemoresistent nature of pancreatic cancers.

Introduction

Lipids in the cell are separated into categories and classes based on their chemical structure. There is a large diversity of chemical structure and function among the lipids within these classes. The presence of different lipid classes in a membrane can be used to distinguish different structures in the cell (Figure 1A). Many lipids also act as messenger signals for cellular communication. These structural and signaling roles of the lipid classes can be coopted to support a cancerous phenotype. Signaling molecules like sphingolipids are of particular importance in supporting changes that lead to cancer[1-3].

Separation of the different species within each class can be difficult because biologically distinct lipids can share very similar chemical structures. Differentiation between structurally similar lipids is important, because they can have vastly different biological effects[4]. Cholesterol metabolism is a well-described example of lipid signaling and represents a good example of the

challenge[5], because widely divergent signals like cortisol and aldosterone vary only by the position of an oxygen and a proton in the structure.

Use of mass spectrometry has recently provided important insight into lipids as inducers of cancers[6], the importance of signaling lipid concentrations in response to drug treatment[7], and regulation of oncogenic proteins through lipid raft formation and anchoring[1, 8]. Mass spectrometry enables the simultaneous measurement of many lipid types (lipidomics), which has helped identify some of these roles, and reaffirmed that lipids are not just the passive structural molecules.

Here we used an unbiased lipidomics assay (Figure 1B) to compare concentrations of ~3000 lipid species between healthy and cancerous cells. Lipidomics methods are still in development and we found, similar to the work of Reis et al., that chemical extraction could bias the number of lipid species we observed[9]. In our experiments, using a modified form of Bligh and Dyer extraction, we could observe the maximum number of lipid species with a more balanced view of the major lipid classes. We also incorporated adduct formation, to maximize the ionization of the lipid species we extracted. Although we observed changes in many individual lipids, changes in sphingolipid concentrations were particularly interesting. We identified connected changes in two sphingolipids, which are major contributors to the cancerous phenotype in pancreatic cells. This is due to the strong role that sphingolipids play in cellular signaling and regulation. Cell fate can change based on the balance and regulation of key sphingolipid molecules[3].

Many sphingolipid species are second-messenger molecules that play a critical role in cellular homeostasis. Membrane sphingolipids are bioactive regulators of a diverse array of processes: cell growth, death, inflammation, adhesion, migration, angiogenesis, intracellular

trafficking, and senescence[2, 10, 11](Figure S2). Ceramide, a sub-class of sphingolipid, is a central molecule in sphingolipid metabolism, and important in anti-proliferative processes, such as senescence modulation, cell growth inhibition, endoplasmic reticulum stress responses, apoptosis induction[12, 13] and/or autophagy[14]. Ceramide is a required mediator of both extrinsic and intrinsic pathways of apoptosis[15]. It has been shown that endogenous ceramide generation is essential for apoptotic signaling in CD95- and TNFα-treated conditions[16]. Inhibition of the ceramide producing sphingomyelinase (SMase) effectively blocks cell death[17-19]. Elevated C16-ceramide levels increase mitochondrial outer membrane permeability, which mediates cytochrome c release[20]. Ceramide species are also direct regulators of many BCL-2 family proteins through multiple mechanisms[12, 21]. Without these vital second-messenger lipid molecules, the ability of the cell to undergo programmed cell death becomes severely impaired or in some cases disabled entirely[21, 22].

Competing sphingolipid signals. Interestingly, by removing the fatty acyl tail from ceramide the free sphingosine backbone can become another potent cellular signal. If the sphingosine is phosphorylated by the conserved lipid kinase, sphingosine kinase (SphK1), it creates sphingosine-1-phosphate (S1P) another important lipid secondary messenger which mediates motility, cell survival, and proliferation (Figure S3). In addition, S1P has an important paracrine signaling role because it potently stimulates angiogenesis[23]. Tests in human umbilical vein endothelial cells showed that adding S1P was sufficient to protect them from apoptosis, while inhibition of sphingosine kinase, which makes S1P, sensitized these cells to apoptosis[22]. Importantly, most sphingolipid metabolites (like ceramide and sphingosine) are predominantly located in membranes, while S1P can diffuse throughout the cell[24].

The effect of increased anti-apoptotic S1P is particularly important, because S1P is often created from ceramide[11]. This means that not only is there increased signaling for cellular motility and proliferation, but signals to arrest growth and initiate apoptosis through ceramide-linked pathways are reduced. Our lipidomics assay identified concurrent changes in C16-ceramide and S1P which point to SphK1 as a major contributor to lipid signaling imbalances and cell-fate signaling.

It is our hypothesis that this ceramide/S1P imbalance is present generally in pancreatic cancer cells and that it imparts some of the cell death resistant nature to the cancerous cells. We show that regulation of the sphingosine kinase enzyme is important to the accelerated growth rate and the resistance to apoptotic signaling in five different pancreatic cancer lines.

Materials and Methods

Experiments were collected using eight ductal adenocarcinoma pancreatic cancer cell lines including; PSN1, PANC1, BxPC3, and Capan1 (additional supplemental data available for HS766T, MiaPACA2, CfPAC1, and HPAC). The measured lipid concentrations in the cancerous cell lines were compared to the detected lipid concentrations in the telomerase immortalized healthy pancreatic cell line hTert-HPNE.

Cell culturing:

Cells were obtained from Dr. David Bearss at Tolero Pharmaceuticals and were not tested for mycoplasma contamination after arrival. Cells were cultured for ~ 6 months total in T-75 and T-25 cell culture flasks at 37^{o}C with 5.0% carbon dioxide in RPMI 1640 with L-glutamine and high glucose with amphotericin B (1 unit per mL) and penicillin/streptomycin (1x). Cells

were allowed to grow to 95% confluence before hard-splitting into new culture flasks. Assays were completed only after each cell line reached a consistent log phase growth rate to ensure consistent treatment.

Cells were harvested by incubating with 0.5% trypsin (Thermo), the soluble cells were then spun down at 2500 G. The pellet was rinsed in PBS and flash frozen in liquid N_2 and stored at -80°C until needed for the various assays.

Lipidomics assay development:

In order to achieve maximum breadth of lipid species identified and high reproducibility between samples we tested multiple sample preparation methods (supplemental Table 1). Cell pellets were re-suspended in 1.5 mL cell lysis buffer (0.1M Tris-HCl @ pH 7.6) and homogenized by circular cut tissue homogenizer (Omni) and vortex (30 seconds at 850 RPM). The homogenate was then transferred to glass vial (4.5 dram) where a two-phase extraction was completed to remove the lipid constituents. We found the modified Bligh and Dyer extraction method[25] to be the most reproducible method to achieve a large diversity of lipid classes. Sample collection and homogenization steps were performed under cold collection environments and under nitrogen to reduce oxidation. The final extraction mixture contained the 1.5 mL aqueous homogenate and then an additional 3 mL of chloroform/methanol/isopropanol (3:1:1.25, v/v/v). A larger extraction batch with the Bligh and Dyer was extracted over 24 hours with shaking gave the closest match a spiked standard. The organic lipid containing layer was then concentrated under reduced pressure at room temperature. The concentrated lipid extract was divided into two separate samples for comparison of adduct effects. The half sample analyzed without adduct was diluted with organic phase solution chloroform/methanol/isopropanol (3:1:1.25, v/v/v) with 0.1% formic acid (Thermo) at a 9-fold dilution by volume (9:1, solution: organic layer extraction) to a

total volume of 250 μL immediately prior to data collection. The half sample analyzed with adduct was diluted with the same organic phase solution with 0.1% formic acid and ammonium acetate (1.5 mM) to promote ionization of some of the neutral lipid species. The sample (with and without adduct) was run in both positive and negative instrument modes to increase specificity and variety of lipids through intra-source selection of differentially ionizable species. During sample dilution and immediately prior to data collection a 1 μL aliquot of 15 mM internal standard cocktail was added to aid in quantitation and mass alignment during the analysis phase. The internal cocktail contained at least 1 lipid from each category as classified by the LIPID MAPS database[26, 27]. When possible heavy isotope labeled or odd-chain length lipids were selected as standard to reduce biological overlap (see supplemental for recipe).

To reduce the influence of time-dependent fluctuation or cross contamination from run to run, the sample analysis schedule was randomized using a random number generator. In this way if the wash cycle between sample runs did not remove all the contaminants from the capillary line, the contaminated peak should not appear more than once in the technical replicates and is thereby removed by the data analysis filters. Sample (250 □L) was infused at 10 □L/min onto a Thermo LTQ-Orbitrap XL mass spectrometer using an IonMax ESI soft-ionization direct inject technique. During the infusion a high resolution (≥100,000) MS1 survey scan cycled through m/z "windows" (75-250 m/z, 250-400 m/z, 400-600 m/z, 600-800 m/z, and 800-1800 m/z). The top 5 most intense ions from each scan were selected for fragmentation, after an ion had been selected for fragmentation twice it was excluded from further MSMS selection.

The MSMS data was used to classify and identify individual ions (see below). The MS1 survey scan spectra summed across the entire acquisition period were used for quantification. All the data files were analyzed separately using in-house developed module for the MSPIRE

proteomics package[28] which compared the fragmentation pattern against expected fragments for the lipids within the LIPID MAPS[29] database. Data was filtered according to absolute mass accuracy (< 3 ppm), comparative peak inclusion (must appear in at least 2 of the 3 technical replicate runs), and possible modifications to adduct additions, in order to keep the most confident peak identifications. For quantitation data was normalized using the internal standards. The normalized summed spectral intensity for each sample was considered a single quantitative data point for an identified lipid. This process was run in biological triplicate, so each cell line or tissue type had at least 12 instrumental runs to compile and assess data statistics.

Verification of lipid identities:

The typical data acquisition measured approximately 2000 different ions. Initial lipid identifications were assigned for each ion based on the parent mass of ion in the primary survey scan. To increase accuracy, the m/z of each ion was corrected according to the standard curve of the internal standards (supplemental methods). The instrumental noise was determined as the baseline detection level across all spectra. Only those peaks that are estimated to be at least twice the level of the instrumental noise are included. Ions which differed from the theoretical mass by more than 3 ppm were removed from the data set. Next, putative lipid classifications from the LIPID MAPS[30] database are checked against the fragmentation data. Fragmentation data was not available for every putative lipid observed in the primary survey data, but it was used to test the identifications and test that the alignment is accurate (Figure S4). An identified lipid species was included in the high-confidence list only if it met criteria in two-thirds (8/12) of the sample spectra. Finally, manual evaluation of putative identities was conducted to evaluate the fragmentation chemistry. For example, if a peak is identified as a triacylglyceride, but only matches the spectra with an impossible modification, like neutral loss of ammonia, the peak is

eliminated or the next best match is evaluated. The curated list of high-confidence identifications was used to define the ions compared in the MS1 quantitation.

Western Blot Analysis:

Frozen cell pellets were lysed in RIPA lysis buffer supplemented with protease and phosphatase inhibitors (Pierce Thermo Scientific). Lysates were incubated at 4°C with gentle rotation for 15 min. Lysates were passed through 25G needle 10 times and centrifuged at 20,000 G for 10 min. Clear lysates were mixed in SDS sample buffer and 80ug of total protein were resolved on a 10% SDS-PAGE. Resolved proteins were transferred to Odyssey nitrocellulose membrane (Li-Cor) and blocked with 5% milk in TBS. Western blots incubated with primary antibody at 4ºC overnight and visualized using infrared fluorescent secondary antibodies and Li-Cor Odyssey system.

Flow cytometry cell death assays:

Cell death assays were completed by plating cells in T-75 flasks (~10,000 cells/cm^2) in log-phase growth and allowing a minimum of 6 hours for growth and adhesion before drug treatment. Growth media was replaced with fresh media prior to injection of drugs into culture flasks or plates. Cells were then treated for 12-24 hours with drugs. At the end of drug treatment, dead cells were removed and collected in a new plate. Cells were washed with 1x PBS and this was collected and combined into the new plate. Living adhered cells were removed from growth plates using 0.05% pH balanced trypsin at 37ºC and then transferred to the new plate. Under dark conditions on ice a 1 mg/100 mL solution of propidium iodide was mixed with light shaking into the cell mixture and allowed 15 minutes to stain. Cell counts were then collected on a red/blue

acoustically focused Applied Biosciences Attune flow cytometer at a scan rate of 200 µL/min using BL2-PI blue laser and BL1 blue laser. Data was analyzed with the Attune software.

Data analysis and statistical tests:

Normalization and lipid identification was conducted using in-house developed modules from MSPIRE module[28], MSPIRE-lipidomics written in the Ruby programming language. Statistical tests were conducted using Excel, and MatLab. Component plots were generated by assigning identities to MS identified peaks with their corresponding quantitation data using Perseus[31] and visualized with MatLab. The multi-dimensional data sets were reduced to 3 principle components and grouped for each cell sample that was completed.

Results:

Development of lipidomics based activity assay:

Lipidomics lags behind proteomics because of the relative difficulty of identifying specific lipids relative to protein sequences. We refined both sample preparation and data analysis methods to measure a large breadth of the lipidome. Several published extraction methods were evaluated to determine which method would best sample each of the major lipid classes and introduce the least amount of bias into our mass spectrometry analysis (supplemental Table 1). The evaluation of extraction methods was conducted using a spiked tissue homogenate containing eight lipid standards from seven lipid categories (recipe in supplemental). All methods had differential extraction efficiency with differences in the observed lipid categories and classes. Another complication is that mass spectrometry requires a charged molecule to make measurements. Many lipids do not have an intrinsic charge, but addition of ammonium acetate in the extraction protocol increased the coverage of lipids from all categories in both

positive and negative ion modes. Based on the initial lipid classifications we determined that a modification to Bligh and Dyer[25] extraction with addition of isopropanol and an ammonium acetate adduct resulted in the most reproducible, broad coverage of the major lipid categories (Figure 2, Supplemental Table 1). In order to verify reproducibility of the measurements, we completed data collection from all samples with a minimum technical triplicate. Total unique lipid identifications that met our criteria were compared for each of the extraction methods. We repeatedly identified a total of 3301 lipid species using the modified Bligh and Dyer, which dropped to 2264 species with other methods. The specificity of the identification varied based on the quality of the fragmentation data and the information available in the publically accessible databases[32, 33].

Sphingosine-1-phosphate and C16-cerimide levels are perturbed in pancreatic cancer cells.

For this study, we utilized a panel of ductal pancreatic cancer cells and compared them against an immortalized healthy line. A principle component analysis of the lipidome changes between cancerous and non-cancerous cells showed that among the ~3000 identified lipids, significant variations were observed in several lipid categories (Figure 2 A). Of particular interest, the pancreatic cancer cell lines all displayed severely depleted C16-ceramide levels with a corresponding increase in the levels of sphingosine-1-phosphate (S1P) relative to control (Figure 3). Levels of S1P in all pancreatic cancers were at least double that in the immortalized cell line. C16-ceramide and S1P are both potent cellular signals that form from a common sphingosine precursor (Figure S1). This suggests that the enzymes controlling sphingosine metabolism between C16-ceramide and S1P may be regulated differently in pancreatic cancer cells.

Sphingosine Kinase (SphK1) expression and activation is elevated in pancreatic cancer.

We tested whether the modified lipid profile observed in these cells was connected to SphK1 regulation. We observed that there was a measureable increase in the total SphK1 concentration for multiple cancer cell lines relative to an immortalized control cell line (Figure 4). The increase in SphK concentration was very similar to the trend for S1P and the inverse of the C16 ceramide (Figure 3). SphK1 is known to be activated by phosphorylation on serine 225. Western blot of phosphoserine 225, showed that all the cancerous lines had an increase in the amount of phosphorylation relative to the immortalized control (Figure 4B). Interestingly, CAPAN1 which did not have a measurable increase in SphK1 concentration (Figure 4A), had the highest levels of activating phosphorylation of all the cell lines. This suggests that individual cancer cell lines have used different mechanisms to increase SphK1 activity.

Inhibition of SphK slows growth and sensitizes cells to apoptotic signals.

We tested the effect of SphK1 inhibition (SKI-II) on multiple cell lines (Figures S5, S6). With flow cytometry, we used propidium iodide staining to count dead cells for plates treated for 12 hours with inhibitor versus control. The sensitivity to SKI-II as measured by EC50 (Figure 5C) was almost exactly inverse to the relative expression of SphK1 measured by western blot (Figure 4). When pancreatic cancer cells (PSN1, PANC1, CAPAN1, BxPC3) were treated with SKI-II at $1/10^{th}$ the EC50, the growth rates were greatly reduced. Growth rates were also reduced to a lesser extent in the already slower growing immortalized control, hTert-HPNE.

We tested how SKI-II changed the efficacy of inducers of apoptosis in these cells. Gemcitabine, a nucleoside mimetic commonly used to treat pancreatic cancer[34], induces apoptosis by inhibiting DNA polymerization to the next inbound nucleoside. The sensitivity to gemcitabine was independent of the SphK1 expression and/or phosphorylation and appeared to be more closely related to the growth rate of the cells with the fastest growing cell requiring less

gemcitabine to be effective[35, 36]. In the presence of SKI-II, the percent of dead cells increased up to approximately ten percent potentially due to increased cell death signaling capacity although the gemcitabine induced DNA damage was presumably less due to the slowed growth. This increase was modest but reproducible, and statistically significant ($p \leq 0.06$ in the students t-test (n=3)) across all cell lines (Figure 5). We interpreted these results to mean that there was a counterproductive relationship between the mechanisms of action for gemcitabine and SKI-II. SKI-II slows slowed the growth of the cells, which protected them from gemcitabine treatment.

We subsequently tested how SKI-II affected cellular response to a BH3 domain-only peptide activator of mitochondrial mediated apoptosis (BH3I-1). The BH3 domain is a direct inducer of apoptosis via activation of pro-death Bcl-2 family members and therefor doesn't rely on DNA damage checkpoint activation to kill the cell. Similar to the gemcitabine treatment, the sensitivity to the BH3I-1 alone, as measured by the EC50, did not directly correlate with SphK1 quantitation and activation. However, the combined effect of added SKI-II and BH3I-1 was more robust than that observed with Gemcitabine for every cell line ($p \leq 0.02$ in the student's t-test (n=3)) (Figure 5), and did correlate with total S1P/C16 ceramide quantitation with the greatest effect of inhibition observed in the cell lines with highest S1P expression.

Discussion:

Lipids serve multiple functions in the cell and are common cellular signals used to promote the cancer phenotype (Figure 1). There have been many advances in the analysis of biological lipids. It remains a complex problem because lipids with high structural similarity can have very different biological roles. For example, a cis versus trans desaturation in a fatty acid is very important biologically, but can be very difficult to distinguish analytically. The scientific community is just beginning to develop the techniques to monitor the complex array of

biological lipids (lipidome). For example, liquid chromatography is an effective method to separate complex mixtures, but in our hands it was difficult to use on complex lipid samples. These issues were overcome by using a direct-injection based intra-source separation. We separated lipids based on the ionization potential in the mass spectrometer; positive and negative modes, with and without adduct additions. This doesn't achieve the same level of separation as effective chromatography, but was relatively fast, allowed detection of low abundance species, and was (in our hands) more robust than chromatographic techniques for lipids.

The lipidomics assay tested activity of multiple enzyme pathways simultaneously, monitoring substrate and product concentrations. We identified altered regulation of SphK1 in the sphingomyelin metabolic pathway based on changes in relative lipid distributions. We found that multiple pancreatic cancer cell lines had achieved lower C16-ceramide and higher S1P concentrations, through a combination of greater Sphingosine kinase (SphK1) enzyme expression and/or phosphorylation.

Inactive SphK1 is generally found in the cytosol away from its lipid substrates. After activation through phosphorylation at Ser-225, the enzyme relocates to the plasma membrane where it localizes onto functional lipid-raft subdomains for its catalytic activity.[37] Activating levels of SphK1 were high in all cancer lines with the fastest growing pancreatic cancer cell lines, PSN1 and PANC1, 2.5 fold higher than control (Figure 4). Interestingly, CAPAN1 which had the highest levels of activation, had the lowest amount of enzyme (Figure 5). This suggests that multiple mechanisms were used in this small panel of cell lines to shift the balance in ceramide versus S1P. CAPAN1 demonstrated a spreading growth pattern and BxPC3 often grew in small colony clusters. This could in part be explained by a dependence of cell-to-cell proximity for improved SphK1 signaling efficiency in BxPC3 where both quantitation and

activation of SphK1 is less than in the cell lines with independently activated SphK1 either through expression, activation, or both.

Pancreatic cancer has historically been very difficult to treat [38, 39]. Traditional chemotherapeutics have only offered limited success due to the resistant nature of the cancer and the treatment-refractory environment that the tumors establish[40, 41]. Here we show similar to previous studies[42, 43] that pancreatic cancer cells are resistant to apoptosis and chemotherapeutics. Our data suggest that depleted levels of the signaling lipid C16 ceramide prevent successful self-elimination. Even worse the cancer cells are actively producing and excreting pro-growth, pro-survival signals, S1P, due to the unregulated increase in sphingosine kinase activity.

Sphingosine kinase enzymes do not share homology with other lipid kinases[44]. Interestingly they do not show any homology with other lipid-binding proteins or contain previously known lipid binding domains.[45] Sphingosine Kinase 1 is a highly conserved kinase that can act independently to induce tumor growth by phosphorylating sphingosine to form sphingosine-1-phosphate. Overexpression of human SphK1 in NIH3T3 fibroblasts has demonstrated its ability to independently affect morphological changes and severely alter growth patterns. Transformed NIH3T3 cells with high SphK1 expression grown in serum exhibited enhanced growth patterns when compared to the empty vector control cells. Even when the transformed cells were cultured in nutrient deprived conditions they continued to exhibit elevated growth. The SphK1 cells continued to grow beyond saturation density thereby gaining the ability to escape the effects of contact inhibition. SphK1 transformed cells also acquired the ability to form anchorage-independent colonies in growth media.[46] Sarkar et al. were able to show that activation of SphK1 is required for migration, proliferation, and survival of MCF-7 human breast cancer cells.[47] SphK1 was cemented as a critical component of EGFR signaling. SphK1 was

shown to be activated through EGF and PDGR stimulation. This induced its translocation to the plasma membrane where it can act on its substrate, sphingosine. Down-regulation of SphK1 expression almost completely blocked cell migration and metastasis[47].

Interestingly, in the presence of SKI-II, there was a very modest increase in cell death for gemcitabine. We hypothesize that reduction of S1P has an anti-proliferative effect, and slower cell growth reduced the efficacy of the Gemcitabine. In order for a nucleoside analogue like gemcitabine to have maximal effect cells should be proliferating rapidly[34]. Based on these results, we chose to shift focus to a class of emerging chemotherapeutics, BH3 mimetics, that target the mitochondrial apoptotic machinery directly. The BH3 mimetic, BH3I-1, was a more effective companion to SK1-II than gemcitabine. This result may be explained by the role of S1P in increasing the ratio of anti-apoptotic to pro-apoptotic Bcl-2 family proteins at the mitochondria[48, 49]. Thus, a reduction in S1P would reverse the ratio and effectively pave the way for BH3 mimetic-induced mitochondrial outer membrane permeabilization.

The efficacy of reducing S1P levels to increase apoptosis may also be explained by the paracrine signaling roles of S1P. Olivera et al. showed that the proliferative response to exogenously added S1P is partially sensitive to pertussis toxin[50]. Pertussis toxin prevents G-proteins from interacting with their respective receptors thereby interrupting intracellular communication. This suggests the likely involvement of G-protein coupled cell surface receptors in the mechanism of S1P.

Several G-protein coupled receptors (GPCRs) respond to S1P: EDG-1, -3, -5, -6, and -8. Most GPCRs specific to S1Ps have nanomolar binding affinities. Although it requires micromolar concentrations of S1P to have any observable effects on most cancerous tumor types[46], there are a few cancer cell lines such as T lymphoblastoma and HTC4 hepatoma cells

that can respond to nanomolar concentrations of S1P. These cells are protected from apoptosis and even continue to proliferate in nutrient deprived conditions. Indeed, the addition of nanomolar concentrations of exogenous S1P was sufficient to activate ERK, induce c-Jun, and inhibit caspase-3 activity[22].

Additional research has shown that sphingosine kinase is activated and acts in an anti-apoptotic role when in hypoxic conditions that induce expression of hypoxia-inducible factor-1 (HIF-1).[51] Tumors that are nutrient poor and in hypoxic conditions have always led to a poor prognosis. High expression levels of sphingosine kinase have been found in A549 cancerous lung cells in hypoxic conditions with high levels of chemoresistance. When short interfering RNA against sphingosine kinase are introduced the cells lose their chemoresistance and become sensitive to cell death. Introducing lipid extracts from cells that were cultured in nutrient poor hypoxic conditions to non-chemoresistant cells was sufficient to protect cells from etoposide induced apoptosis.

Stopping the signaling cascade that promotes the cancer phenotype may be simplest by inhibiting production of the initial signal like S1P. Additional promising lipid targets in pancreatic cancer were also observed in this study. We observed a significant increase of lysophosphatidic acids (LPAs) in cancer cells, which are also important signaling lipids involved in oncogene regulation. There was also a reduction in acidic membrane anchoring lipids involved in regulating oncogenes such as the farnsyl-tail containing K-Ras4B.

We propose that lipidomics assays similar to this one can be used to identify modified enzymatic pathway activities, which drive the cancerous phenotype. This may lead to the use of combination therapies where inhibiting the pro-survival signals while promoting an apoptotic signal would represent a supremely effective technique for cancer treatment. Importantly, this

methodology could be used to test tumor biopsies in order to personalize treatment options and test efficacy.

Author Contributions:

Conception and Design: A. Swensen, J. Andersen, J. Prince, and J. Price.

Development of Methodology: A. Swensen, J. Prince, and J. Price.

Acquisition of data: A. Swensen, T. Chan

Analysis and Interpretation of data: A. Swensen, J. Andersen, J. Prince, and J. Price.

Writing of manuscript: A. Swensen, and J. Price.

Acknowledgements: We thank Dr. David Bearss for the generous gift of the pancreatic cancer lines, and Dr. Bearss and Dr. Daniel D. Von Hoff for helpful conversations. We also thank the BYU RIC facility for assistance in the cell death assay. We thank BYU and the Simmons Center for Cancer Research for financial support.

Works Cited:

1. Baenke, F.; Peck, B.; Miess, H.; Schulze, A., Hooked on fat: the role of lipid synthesis in cancer metabolism and tumour development. *Disease models & mechanisms* **2013,** *6* (6), 1353-63.
2. Beloribi-Djefaflia, S.; Vasseur, S.; Guillaumond, F., Lipid metabolic reprogramming in cancer cells. *Oncogenesis* **2016,** *5*, e189.
3. Furuya, H.; Shimizu, Y.; Kawamori, T., Sphingolipids in cancer. *Cancer metastasis reviews* **2011,** *30* (3-4), 567-76.

4. Wymann, M. P.; Schneiter, R., Lipid signalling in disease. *Nature reviews. Molecular cell biology* **2008,** *9* (2), 162-76.

5. Gabitova, L.; Gorin, A.; Astsaturov, I., Molecular pathways: sterols and receptor signaling in cancer. *Clinical cancer research : an official journal of the American Association for Cancer Research* **2014,** *20* (1), 28-34.

6. Jiao, J.; Ishikawa, T. O.; Dumlao, D. S.; Norris, P. C.; Magyar, C. E.; Mikulec, C.; Catapang, A.; Dennis, E. A.; Fischer, S. M.; Herschman, H. R., Targeted deletion and lipidomic analysis identify epithelial cell COX-2 as a major driver of chemically induced skin cancer. *Molecular cancer research : MCR* **2014,** *12* (11), 1677-88.

7. Schiffmann, S.; Ziebell, S.; Sandner, J.; Birod, K.; Deckmann, K.; Hartmann, D.; Rode, S.; Schmidt, H.; Angioni, C.; Geisslinger, G.; Grosch, S., Activation of ceramide synthase 6 by celecoxib leads to a selective induction of C16:0-ceramide. *Biochemical pharmacology* **2010,** *80* (11), 1632-40.

8. Jaffres, P. A.; Gajate, C.; Bouchet, A. M.; Couthon-Gourves, H.; Chantome, A.; Potier-Cartereau, M.; Besson, P.; Bougnoux, P.; Mollinedo, F.; Vandier, C., Alkyl ether lipids, ion channels and lipid raft reorganization in cancer therapy. *Pharmacology & therapeutics* **2016,** *165*, 114-31.

9. Reis, A.; Rudnitskaya, A.; Blackburn, G. J.; Mohd Fauzi, N.; Pitt, A. R.; Spickett, C. M., A comparison of five lipid extraction solvent systems for lipidomic studies of human LDL. *Journal of lipid research* **2013,** *54* (7), 1812-24.

10. Hannun, Y. A.; Obeid, L. M., Principles of bioactive lipid signalling: lessons from sphingolipids. *Nature reviews. Molecular cell biology* **2008,** *9* (2), 139-50.

11. Gault, C. R.; Obeid, L. M.; Hannun, Y. A., An overview of sphingolipid metabolism: from synthesis to breakdown. *Advances in experimental medicine and biology* **2010,** *688*, 1-23.

12. Morales, A.; Lee, H.; Goni, F. M.; Kolesnick, R.; Fernandez-Checa, J. C., Sphingolipids and cell death. *Apoptosis : an international journal on programmed cell death* **2007,** *12* (5), 923-39.

13. Smyth, M. J.; Obeid, L. M.; Hannun, Y. A., Ceramide: a novel lipid mediator of apoptosis. *Advances in pharmacology* **1997,** *41*, 133-54.

14. Olivera, A.; Spiegel, S., Sphingosine kinase: a mediator of vital cellular functions. *Prostaglandins & other lipid mediators* **2001,** *64* (1-4), 123-34.

15. Pettus, B. J.; Chalfant, C. E.; Hannun, Y. A., Ceramide in apoptosis: an overview and current perspectives. *Biochimica et biophysica acta* **2002,** *1585* (2-3), 114-25.

16. Kolesnick, R. N.; Haimovitz-Friedman, A.; Fuks, Z., The sphingomyelin signal transduction pathway mediates apoptosis for tumor necrosis factor, Fas, and ionizing radiation. *Biochemistry and cell biology = Biochimie et biologie cellulaire* **1994,** *72* (11-12), 471-4.

17. Schwandner, R.; Wiegmann, K.; Bernardo, K.; Kreder, D.; Kronke, M., TNF receptor death domain-associated proteins TRADD and FADD signal activation of acid sphingomyelinase. *The Journal of biological chemistry* **1998,** *273* (10), 5916-22.

18. Lin, T.; Genestier, L.; Pinkoski, M. J.; Castro, A.; Nicholas, S.; Mogil, R.; Paris, F.; Fuks, Z.; Schuchman, E. H.; Kolesnick, R. N.; Green, D. R., Role of acidic sphingomyelinase in Fas/CD95-mediated cell death. *The Journal of biological chemistry* **2000,** *275* (12), 8657-63.

19. Garcia-Ruiz, C.; Colell, A.; Mari, M.; Morales, A.; Calvo, M.; Enrich, C.; Fernandez-Checa, J. C., Defective TNF-alpha-mediated hepatocellular apoptosis and liver damage in acidic sphingomyelinase knockout mice. *The Journal of clinical investigation* **2003,** *111* (2), 197-208.

20. Siskind, L. J.; Kolesnick, R. N.; Colombini, M., Ceramide channels increase the permeability of the mitochondrial outer membrane to small proteins. *The Journal of biological chemistry* **2002,** *277* (30), 26796-803.

21. Bose, R.; Verheij, M.; Haimovitz-Friedman, A.; Scotto, K.; Fuks, Z.; Kolesnick, R., Ceramide synthase mediates daunorubicin-induced apoptosis: an alternative mechanism for generating death signals. *Cell* **1995,** *82* (3), 405-14.

22. Xia, P.; Wang, L.; Gamble, J. R.; Vadas, M. A., Activation of sphingosine kinase by tumor necrosis factor-alpha inhibits apoptosis in human endothelial cells. *The Journal of biological chemistry* **1999,** *274* (48), 34499-505.

23. Gault, C. R.; Eblen, S. T.; Neumann, C. A.; Hannun, Y. A.; Obeid, L. M., Oncogenic K-Ras regulates bioactive sphingolipids in a sphingosine kinase 1-dependent manner. *The Journal of biological chemistry* **2012,** *287* (38), 31794-803.

24. Hait, N. C.; Oskeritzian, C. A.; Paugh, S. W.; Milstien, S.; Spiegel, S., Sphingosine kinases, sphingosine 1-phosphate, apoptosis and diseases. *Biochimica et biophysica acta* **2006,** *1758* (12), 2016-26.

25. Bligh, E. G.; Dyer, W. J., A rapid method of total lipid extraction and purification. *Canadian journal of biochemistry and physiology* **1959,** *37* (8), 911-7.

26. Fahy, E.; Subramaniam, S.; Brown, H. A.; Glass, C. K.; Merrill, A. H., Jr.; Murphy, R. C.; Raetz, C. R.; Russell, D. W.; Seyama, Y.; Shaw, W.; Shimizu, T.; Spener, F.; van

Meer, G.; VanNieuwenhze, M. S.; White, S. H.; Witztum, J. L.; Dennis, E. A., A comprehensive classification system for lipids. *Journal of lipid research* **2005,** *46* (5), 839-61.

27. Fahy, E.; Subramaniam, S.; Murphy, R. C.; Nishijima, M.; Raetz, C. R.; Shimizu, T.; Spener, F.; van Meer, G.; Wakelam, M. J.; Dennis, E. A., Update of the LIPID MAPS comprehensive classification system for lipids. *Journal of lipid research* **2009,** *50 Suppl*, S9-14.

28. Prince, J. T.; Marcotte, E. M., mspire: mass spectrometry proteomics in Ruby. *Bioinformatics* **2008,** *24* (23), 2796-7.

29. Sud, M.; Fahy, E.; Cotter, D.; Dennis, E. A.; Subramaniam, S., LIPID MAPS-Nature Lipidomics Gateway: An Online Resource for Students and Educators Interested in Lipids. *Journal of chemical education* **2012,** *89* (2), 291-292.

30. Fahy, E.; Sud, M.; Cotter, D.; Subramaniam, S., LIPID MAPS online tools for lipid research. *Nucleic acids research* **2007,** *35* (Web Server issue), W606-12.

31. Tyanova, S.; Temu, T.; Sinitcyn, P.; Carlson, A.; Hein, M. Y.; Geiger, T.; Mann, M.; Cox, J., The Perseus computational platform for comprehensive analysis of (prote)omics data. *Nature methods* **2016,** *13* (9), 731-40.

32. Sud, M.; Fahy, E.; Cotter, D.; Brown, A.; Dennis, E. A.; Glass, C. K.; Merrill, A. H., Jr.; Murphy, R. C.; Raetz, C. R.; Russell, D. W.; Subramaniam, S., LMSD: LIPID MAPS structure database. *Nucleic acids research* **2007,** *35* (Database issue), D527-32.

33. Kind, T.; Liu, K. H.; Lee, D. Y.; DeFelice, B.; Meissen, J. K.; Fiehn, O., LipidBlast in silico tandem mass spectrometry database for lipid identification. *Nature methods* **2013,** *10* (8), 755-8.

34. de Sousa Cavalcante, L.; Monteiro, G., Gemcitabine: metabolism and molecular mechanisms of action, sensitivity and chemoresistance in pancreatic cancer. *European journal of pharmacology* **2014,** *741*, 8-16.

35. Hertel, L. W.; Boder, G. B.; Kroin, J. S.; Rinzel, S. M.; Poore, G. A.; Todd, G. C.; Grindey, G. B., Evaluation of the antitumor activity of gemcitabine (2',2'-difluoro-2'-deoxycytidine). *Cancer research* **1990,** *50* (14), 4417-22.

36. Noble, S.; Goa, K. L., Gemcitabine. A review of its pharmacology and clinical potential in non-small cell lung cancer and pancreatic cancer. *Drugs* **1997,** *54* (3), 447-72.

37. Hengst, J. A.; Guilford, J. M.; Fox, T. E.; Wang, X.; Conroy, E. J.; Yun, J. K., Sphingosine kinase 1 localized to the plasma membrane lipid raft microdomain overcomes serum deprivation induced growth inhibition. *Archives of biochemistry and biophysics* **2009,** *492* (1-2), 62-73.

38. Lennon, A. M.; Wolfgang, C. L.; Canto, M. I.; Klein, A. P.; Herman, J. M.; Goggins, M.; Fishman, E. K.; Kamel, I.; Weiss, M. J.; Diaz, L. A.; Papadopoulos, N.; Kinzler, K. W.; Vogelstein, B.; Hruban, R. H., The early detection of pancreatic cancer: what will it take to diagnose and treat curable pancreatic neoplasia? *Cancer research* **2014,** *74* (13), 3381-9.

39. Siegel, R.; DeSantis, C.; Virgo, K.; Stein, K.; Mariotto, A.; Smith, T.; Cooper, D.; Gansler, T.; Lerro, C.; Fedewa, S.; Lin, C.; Leach, C.; Cannady, R. S.; Cho, H.; Scoppa, S.; Hachey, M.; Kirch, R.; Jemal, A.; Ward, E., Cancer treatment and survivorship statistics, 2012. *CA Cancer J Clin* **2012,** *62* (4), 220-41.

40. Ireland, L.; Santos, A.; Ahmed, M. S.; Rainer, C.; Nielsen, S. R.; Quaranta, V.; Weyer-Czernilofsky, U.; Engle, D. D.; Perez-Mancera, P.; Coupland, S. E.; Taktak, A. F.;

Bogenrieder, T.; Tuveson, D. A.; Campbell, F.; Schmid, M. C.; Mielgo, A., Chemoresistance in pancreatic cancer is driven by stroma-derived insulin-like growth factors. *Cancer research* **2016**.

41. Takeuchi, S.; Baghdadi, M.; Tsuchikawa, T.; Wada, H.; Nakamura, T.; Abe, H.; Nakanishi, S.; Usui, Y.; Higuchi, K.; Takahashi, M.; Inoko, K.; Sato, S.; Takano, H.; Shichinohe, T.; Seino, K.; Hirano, S., Chemotherapy-Derived Inflammatory Responses Accelerate the Formation of Immunosuppressive Myeloid Cells in the Tissue Microenvironment of Human Pancreatic Cancer. *Cancer research* **2015,** *75* (13), 2629-40.

42. Chand, S.; O'Hayer, K.; Blanco, F. F.; Winter, J. M.; Brody, J. R., The Landscape of Pancreatic Cancer Therapeutic Resistance Mechanisms. *International journal of biological sciences* **2016,** *12* (3), 273-82.

43. Tamburrino, A.; Piro, G.; Carbone, C.; Tortora, G.; Melisi, D., Mechanisms of resistance to chemotherapeutic and anti-angiogenic drugs as novel targets for pancreatic cancer therapy. *Frontiers in pharmacology* **2013,** *4*, 56.

44. French, K. J.; Upson, J. J.; Keller, S. N.; Zhuang, Y.; Yun, J. K.; Smith, C. D., Antitumor activity of sphingosine kinase inhibitors. *The Journal of pharmacology and experimental therapeutics* **2006,** *318* (2), 596-603.

45. Taha, T. A.; Hannun, Y. A.; Obeid, L. M., Sphingosine kinase: biochemical and cellular regulation and role in disease. *Journal of biochemistry and molecular biology* **2006,** *39* (2), 113-31.

46. Xia, P.; Gamble, J. R.; Wang, L.; Pitson, S. M.; Moretti, P. A.; Wattenberg, B. W.; D'Andrea, R. J.; Vadas, M. A., An oncogenic role of sphingosine kinase. *Current biology : CB* **2000,** *10* (23), 1527-30.

47. Sarkar, S.; Maceyka, M.; Hait, N. C.; Paugh, S. W.; Sankala, H.; Milstien, S.; Spiegel, S., Sphingosine kinase 1 is required for migration, proliferation and survival of MCF-7 human breast cancer cells. *FEBS letters* **2005,** *579* (24), 5313-7.

48. Bektas, M.; Jolly, P. S.; Muller, C.; Eberle, J.; Spiegel, S.; Geilen, C. C., Sphingosine kinase activity counteracts ceramide-mediated cell death in human melanoma cells: role of Bcl-2 expression. *Oncogene* **2005,** *24* (1), 178-87.

49. Colie, S.; Van Veldhoven, P. P.; Kedjouar, B.; Bedia, C.; Albinet, V.; Sorli, S. C.; Garcia, V.; Djavaheri-Mergny, M.; Bauvy, C.; Codogno, P.; Levade, T.; Andrieu-Abadie, N., Disruption of sphingosine 1-phosphate lyase confers resistance to chemotherapy and promotes oncogenesis through Bcl-2/Bcl-xL upregulation. *Cancer research* **2009,** *69* (24), 9346-53.

50. Olivera, A.; Kohama, T.; Edsall, L.; Nava, V.; Cuvillier, O.; Poulton, S.; Spiegel, S., Sphingosine kinase expression increases intracellular sphingosine-1-phosphate and promotes cell growth and survival. *The Journal of cell biology* **1999,** *147* (3), 545-58.

51. Schnitzer, S. E.; Weigert, A.; Zhou, J.; Brune, B., Hypoxia enhances sphingosine kinase 2 activity and provokes sphingosine-1-phosphate-mediated chemoresistance in A549 lung cancer cells. *Molecular cancer research : MCR* **2009,** *7* (3), 393-401.

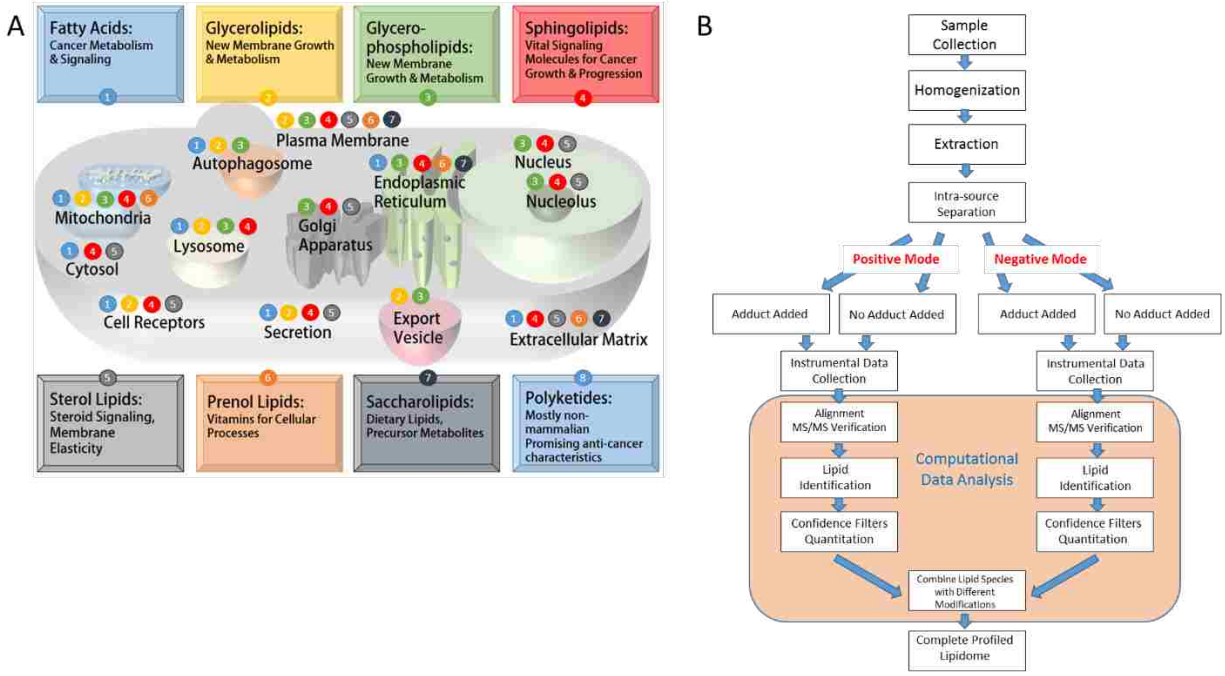

Figure 1: Lipids in Cancer and Our Global Lipidomics Workflow. A) General localization of lipid classes in the cell and roles promoting cancer. B) Lipidomics workflow used in this study

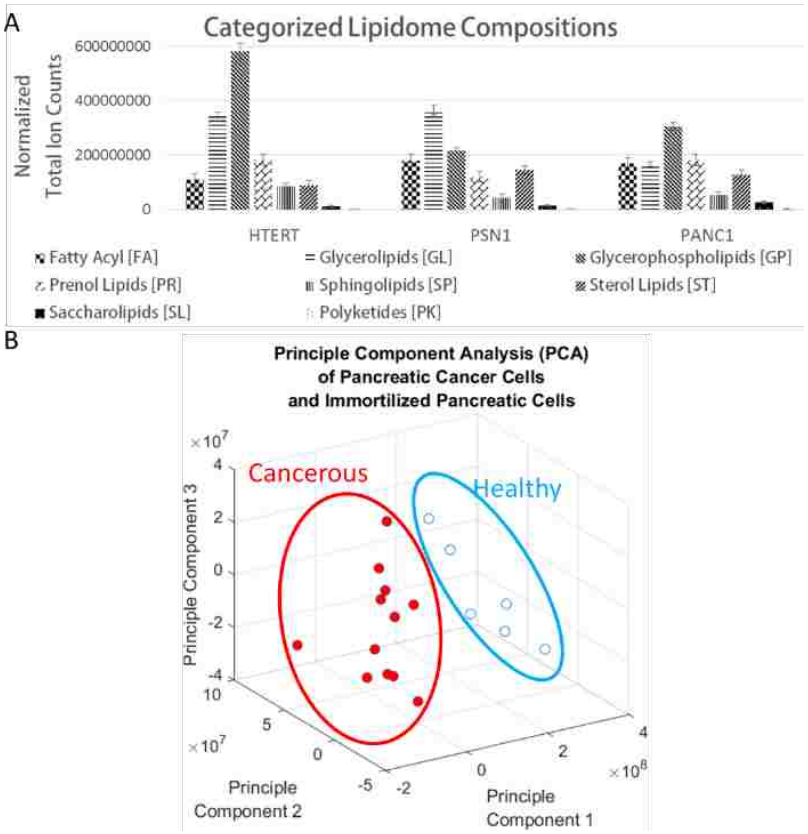

Figure 2: Categorical Composition Results from Global Lipidomics. A) Global lipidomic identification study involving two primary ductal adenocarcinoma cell lines, PSN1 and PANC1, and an immortalized pancreatic cell line, hTert-HPNE was conducted. Many differences were observed between all cell lines but with observable correlation of lipid identifications between cancer cell lines and fewer identification matches to the immortalized cell line. B) PCA analysis of pancreatic cancer cell culture lipidomes compared to the immortalized healthy (oncogene negative) pancreatic cell cultures. Using a three-dimensional PCA gave clear lipidome fingerprinting separation between healthy and cancerous cell types.

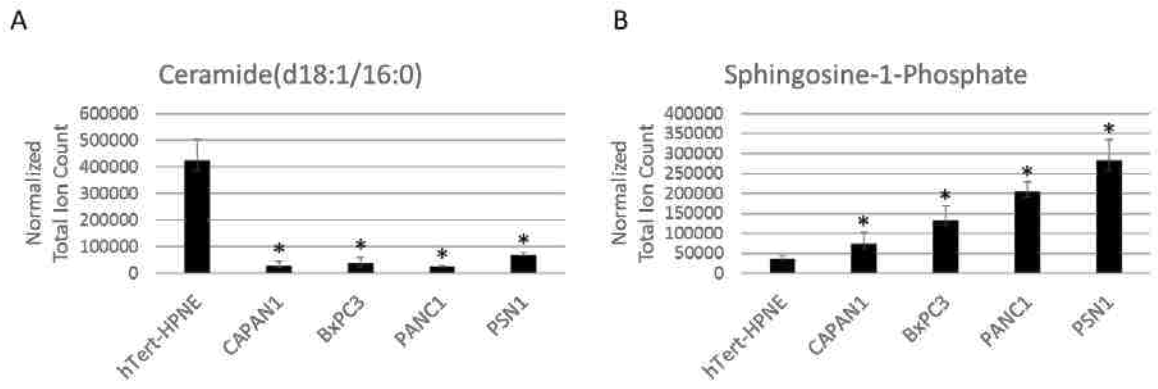

Figure 3: C16 Ceramide and Sphingosine-1-Phosphate Quantification in Pancreatic Cancer Cell Lines. A) All tested pancreatic cancer cell lines displayed severely depleted C16 ceramide concentrations in comparison to the immortalized healthy (oncogene negative) pancreatic cell line. B) Conversely all tested pancreatic cancer cell lines had elevated concentrations of sphingosine-1-phosphate when compared to the immortalized pancreatic cancer cell line. ($p \leq 0.05$ students t-test compared to hTert-HPNE)

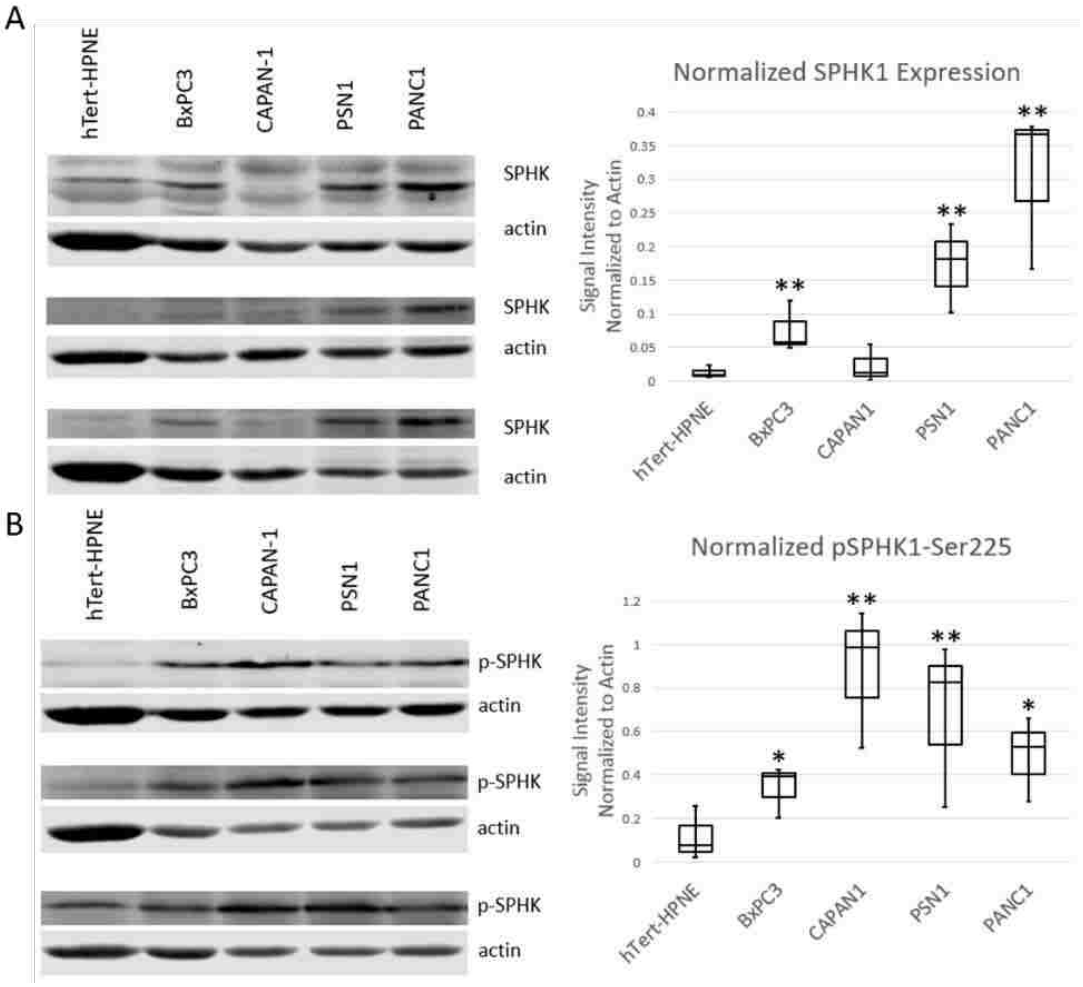

Figure 4: Western blot analysis of SphK1 expression and phosphor-activation in pancreatic cancer. Quantitative analysis of SphK1 was completed using lysates from pancreatic cell culture. A) Expression of SphK1 was elevated in each of the cell pancreatic cancer cell lines when compared to the immortalized pancreatic cell line. B) Activation of SphK1 through phosphorylation of residue Ser-225 was also observed to be elevated in comparison to the immortalized pancreatic cell line. * Represents where $p \leq 0.05$ in t test comparison to control (hTert-HPNE). ** Represents where $p \leq 0.05$ in Dunnett's test for comprehensive comparison.

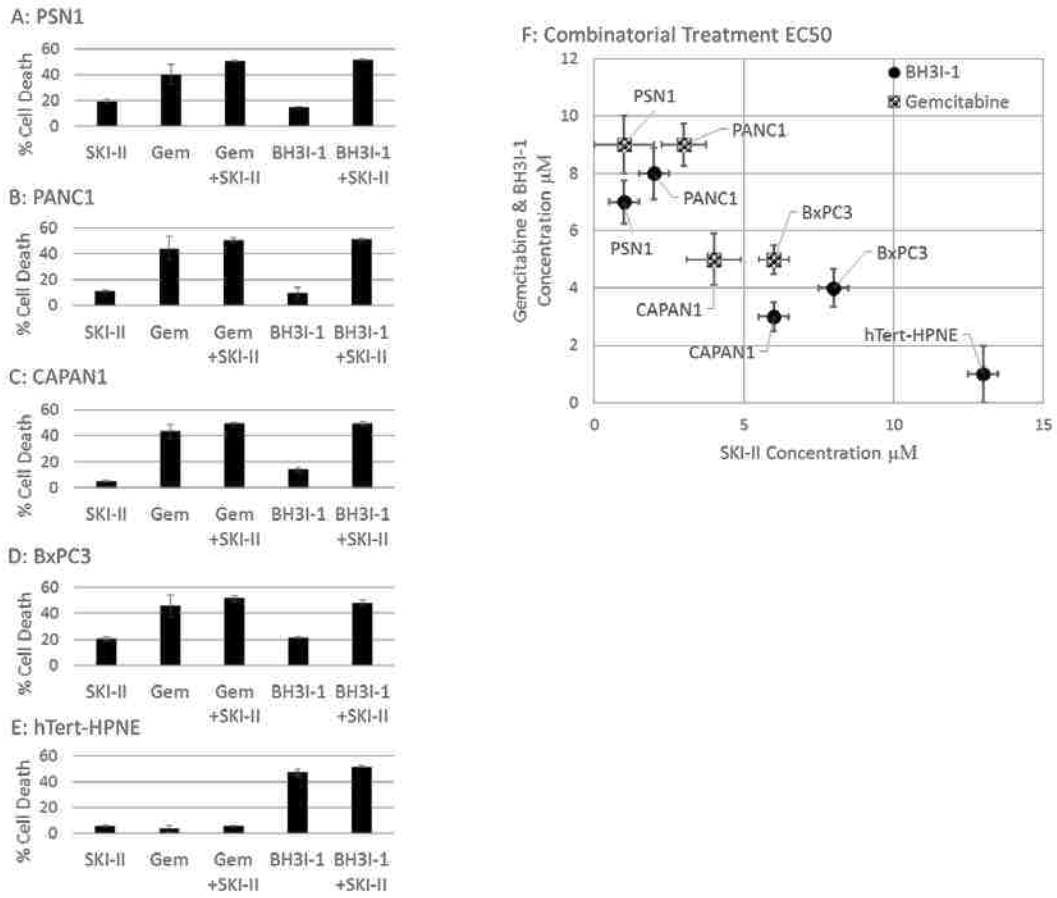

Figure 5: Sensitivity to Drug Treatment Increases with Sphingosine Kinase 1 Inhibition. Tissue cultures of PSN1, PANC1, CAPAN1, BxPC3, and hTert-HPNE were treated for 12 hours with apoptosis inducers alone or with a combination of apoptosis inducer and sphingosine kinase inhibitor. Dead cells were then stained with propidium iodide and run through a flow cytometer. Sensitivity to chemotherapeutic treatment was increased in the culture treated with the inhibitor. Significantly greater changes were observed with BH3I-1 as this targets mitochondrial mediated apoptosis directly and doesn't require fast cell growth as does gemcitabine. Treatment with sphingosine kinase inhibitor significantly slows cell growth rates. Samples were measured in biological triplicate (n=3) and normalized to vehicle controls. A) Treatment of PSN1 cell line with the following concentrations: SKI-II Only (1 µM); Gemcitabine Only (9 µM); BH3I-1 Only

(7 μM); Gemcitabine (9 μM) & SKI-II (1 μM) Combination; BH3I-1 (7 μM) & SKI-II (1 μM) Combination. B) Treatment of PANC1 cell line with the following concentrations: SKI-II Only (2 μM); Gemcitabine Only (9 μM); BH3I-1 Only (8 μM); Gemcitabine (9 μM) & SKI-II (3 μM) Combination; BH3I-1 (8 μM) & SKI-II (2 μM) Combination. C) Treatment of CAPAN1 cell line with the following concentrations: SKI-II Only (4 μM); Gemcitabine Only (5 μM); BH3I-1 Only (3 μM); Gemcitabine (5 μM) & SKI-II (4 μM) Combination; BH3I-1 (3 μM) & SKI-II (6 μM) Combination. D) Treatment of BxPC3 cell line with the following concentrations: SKI-II Only (8 μM); Gemcitabine Only (5 μM); BH3I-1 Only (4 μM); Gemcitabine (5 μM) & SKI-II (6 μM) Combination; BH3I-1 (4 μM) & SKI-II (8 μM) Combination. E) Treatment of hTert-HPNE with the following concentrations: SKI-II Only (13 μM); Gemcitabine Only (10 μM); BH3I-1 Only (1 μM); Gemcitabine (10 μM) & SKI-II (13 μM) Combination; BH3I-1 (1 μM) & SKI-II (13 μM) Combination. (Note: gemcitabine treatment of the slow growing hTert-HPNE line was ineffective. F) Dot plot of drug concentrations to achieve EC50 in each cell line with the exception of hTert-HPNE gemcitabine combination treatment was ineffective.

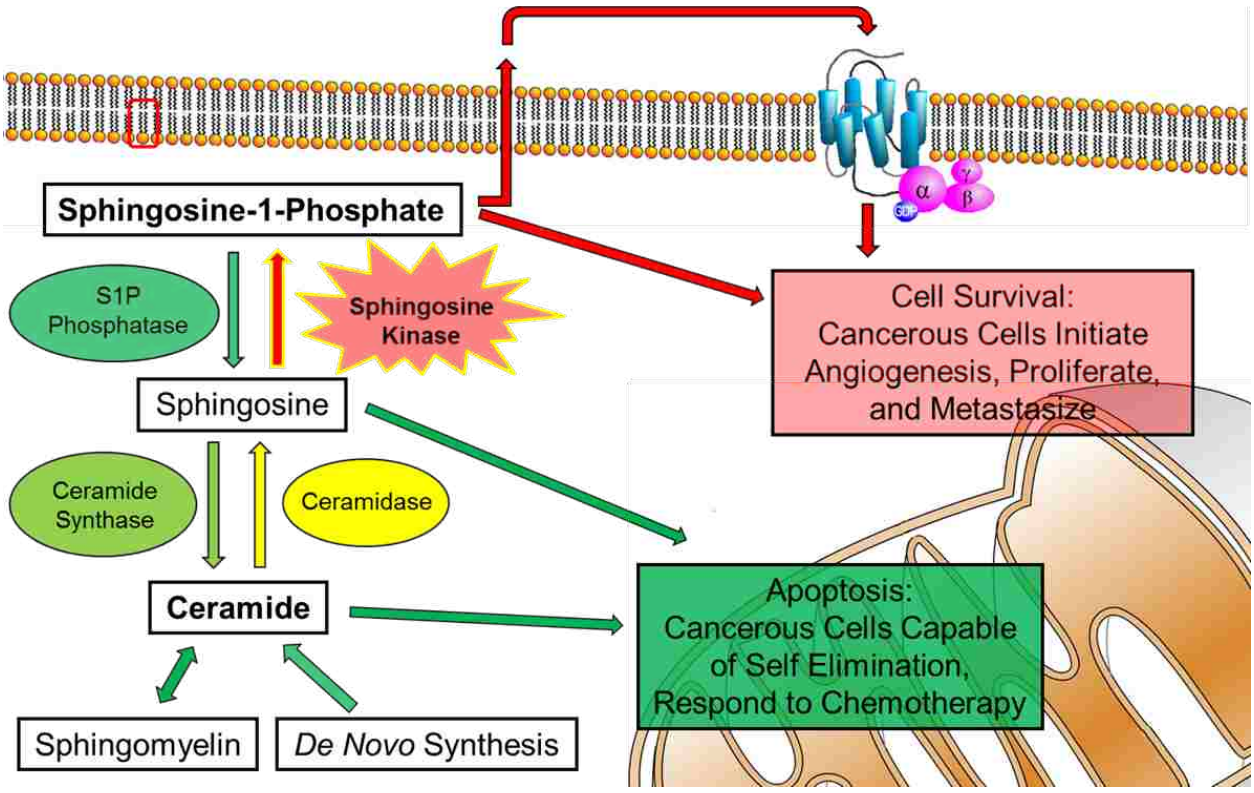

Figure 6: Signaling Lipids in Pancreatic Cancer. Signaling lipids play a major role in the development and regulation of cancer. Without C16 Ceramide the cells ability to apoptose becomes severely handicapped. Up-regulated signaling by S1P can impart many of the resistant and aggressive characteristics of pancreatic cancer.

Lipidomic profiling identifies modified sphingosine kinase 1 regulation and cell-fate signaling in pancreatic cancer: Supplemental Information

Lipid standards: As described in the methods, this standard mix was added to the diluent immediately preceding sample injection. N-heptadecanoyl-D-erythro-sphingosine (C17 ceramide) 30 µL from 5 mg/500 µL stock solution. 1,2-Di-O-Phytanyl-sn-Glycerol 20 µL from 5 mg/500 µL stock solution. 1-dodecanoyl-2-tridecanoyl-sn-glycero-3-phosphoethanolamine 30 µL from 5 mg/1 mL stock solution. Cholest-5-en-3beta-ol (d7) 30 µL from 0.5 mg/100 µL. 1-heptadecanoyl-2-tetradecanoyl-sn-glycero-3-phosphoserine 30 µL from 2 mg/200 µL stock solution. Retinoic acid 30 µL from 5 mg/500 µL stock solution. Di[3-deoxy-D-manno-octulosonyl]-lipid A (Kdo2-Lipid A) 20 µL from 5 mg/500 µL stock solution. Arachidonic acid 20 µL from 10 mg/1 mL stock solution. All stock solution bases were 2:1 chloroform:methanol (v/v) Folch reagent with trace toluene. Standards were purchased from Avanti Polar Lipids or Sigma Aldrich.

Mspire-Lipidomics Command Workflow:

Several Ruby scripts were used iteratively to generate lipid identification assignments. All scripts can be executed through command-line interface using Ruby-1.9.3 (or similar) with mspire (https://github.com/princelab/mspire) and mspire-lipid (https://github.com/princelab/mspire-lipid) gem packages and their corresponding dependencies. Each script will generate a usage/help screen when run without any options selected.

The first step is to execute the "*quant_compare_direct_injections.rb*" script. In order to function, the raw data files must first be converted to .mzML format with centroided peaks and only inclusive of high-mass-accuracy MS1 (survey scan) peaks. This will combine each of intensity values for each bin across the entire data collection run for each file into one tab separated file (.tsv) with rows corresponding to each m/z bin value. A simple baseline mass correction can be completed at this step to correct for mass deviations that are a result of current instrumental calibration deviation. The best base line correction requires that internal standards were added to the sample prior to data collection as described in *col_to_file.rb* step below.

quant_compare_direct_injections.rb uses the following options. (Example: "quant_compare_direct_injections.rb -o quant_compare_first_iteration.tsv -b 3 -m mzs -p -3 -v *.mzML")

--outfile, -o <s>: write results to this file (default: quant_compare.tsv)

--bin-width, -b <f>: width of the bins for merging (default: 5.0)

--bin-unit, -i <s>: units for binning (ppm or amu) (default: ppm)

--split, -s <s>: share|greedy_y|zero method used to distinguish peaks (default: share)

--sample-ids, -a <s>: a yml file pointing basename to id

--mz-prefix, -m <s>: use this prefix for mz values (default: mz)

--round-mz, -r <i>: round the final m/z values to this place (default: 6)

--round-intensity, -u <i>: round the final int values to this place (default: 6)

--simple-calibrate, -p <f>: adjust the m/z values by that amount (default: 0.0)

--verbose, -v: talk about it

--help, -h: Show this message

The next step uses the Ruby script "*col_to_file.rb*". This script requires the .tsv file created in the earlier step. This will extract only the binned masses from the .tsv in preparation for lipid identification into a new text (.txt) file. This script also allows for more advanced mass baseline correction which will be used later for lipid standard alignment in the high-mass-accuracy lipid identification assignment.

col_to_file.rb uses the following options. (Example: "col_to_file.rb quant_compare_first_iteration.tsv mzs -p 3.246")

--ppm-recal, -p <f>: vals deviate this amount (default: 0.0)

--linear-interp, -l <s>: begin,end,m,b[:...]

--interp-bins, -i <s>: x,y:x,y...

--help, -h: Show this message

The next step uses the Ruby script "*find_nearest_lipid.rb*". This script requires the .txt file created in the previous step and also the .tsv database file from LIPIDMAPS with high-mass-accuracy m/z's, LIPIDMAPS IDs, class, common name, and systematic name. This database file is available from LIPIDMAPS http://www.lipidmaps.org/resources/downloads/index.html. (Modification of this file using Notepad++ or similar program to eliminate lipid IDs not native to the organism of study can be completed to increases assignments based on the organism type. I.E. limited or no polyketides in mammalian samples.) During this step the allowable chemical and ion modifications can be added in as options. For example, water loss, protonation or adduct

addition can be included in this step. The number of top hits with the closest mass hit can also be selected in this step. Results can then either be shown on screen or pushed into a new .tsv or .csv file (via > command).

find_nearest_lipid.rb uses the following options. (Example: "find_nearest_lipid_massshift.rb LMSD_20120412_All.tsv -e quant_compare_first_iteration.3.246ppm.ONLY_MZS.txt -t 5 -s 1 -a 1 -p 2 > Lipid_IDs_First_Try.tsv")

--top-n, -t <i>: how many closest ions to print (default: 3)

modifications: (at least 1 charged mod is required)

--lithium, -l <i>: search for i down to 1 lithium adducts (default: 0)

--sodium, -s <i>: search for i down to 1 sodium adducts (default: 0)

--ammonium, -a <i>: search for i down to 1 ammonium adducts (default: 0)

--ammonia-loss, -m <i>: search for i down to 1 ammonia losses (default: 0)

--carbon-dioxide-loss, -c <i>: search for i down to 1 CO2 losses (default: 0)

--proton-gain, -p <i>: search for i down to 1 proton additions (default: 0)

--proton-loss, -r <i>: search for i down to 1 proton losses (default: 0)

--water-loss, -w <i>: if used, *all* mods are also considered with i down to 0 water losses (default: 0)

other:

--textfile, -e <s>: a text file with m/z values, one per line

--lower-bound, -o: use lower bound searching (requires m/z's to be in sorted order)

--sort: sorts the m/z's

--help, -h: Show this message

The next step involves a spreadsheet viewer of choice which supports .tsv file formats (We used Microsoft Excel). The original .tsv file created during the *quant_compare_direct_injections.rb* step must be opened and the final .tsv (or .csv) file created after the *find_nearest_lipid.rb* step must be opened. The quantitation numbers for each m/z bin can then be copied over to the corresponding m/z bin with the top matches. At this point of the workflow the new spreadsheet is searched for the lipid standards that were spiked into the sample prior to data collection. If the standards are found at the correct masses with low m/z deviation and the standard shows up with similar intensities across all samples in which it was spiked then we can check the raw spectra for fragmentation at that mass. If fragments match the suspected ID we can assign the lipid standard with confidence. Usually there will be some amount of mass deviation in the spectra when searching for the lipid standards. If this is the case, the expected mass is evaluated and the quantitation is compared for this m/z bin. The amount of deviation is calculated and the process reverts back to the *col_to_file.rb* step where mass deviation corrections can be made. This process is repeated until all lipid standards are being identified when *find_nearest_lipid.rb* is completed. Some analyses will work with only simple mass shifts and others require more complex linear deviations dependent on m/z or mass window used in during data acquisition. Normalization for each category of lipid is also completed by comparing the detected intensities for lipids in a specific category to the lipid standard belonging

to the same category that was spiked into the original samples. The detected lipid IDs can then be combined for each modified state in which they were observed and they can be evaluated across replicate runs for consistency for inclusion. Confidence filters can also be applied to the data in the spreadsheet where lipids with mass deviations greater than the desired amount can be eliminated from further analysis. Also during this step the lipid IDs can be filtered for impossible modifications (i.e. fatty acid IDs with ammonia loss as their possible modified state, etc…)

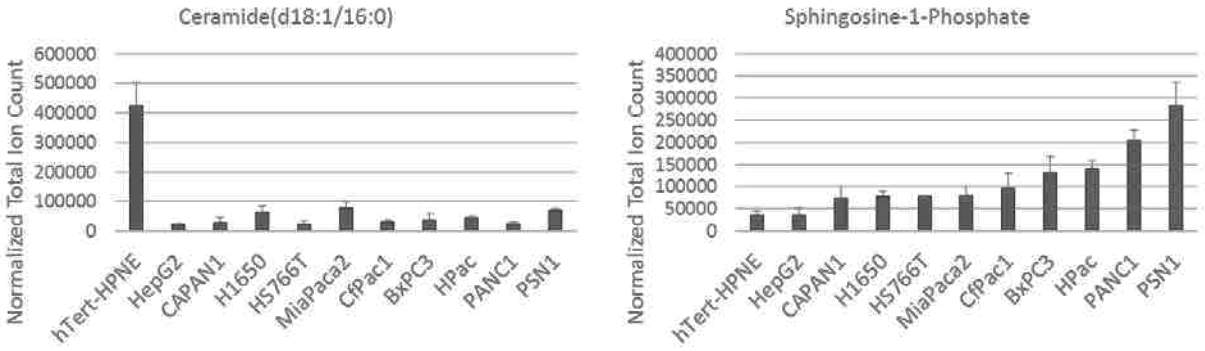

Supplemental Figure S1: Ceramide(d18:1/16:0) and Sphingosine-1-Phosphate Quantitation from immortalized pancreatic cell line compared to many cancerous cell types from pancreas (CAPAN1, HS766T, MiaPACA2, CfPac1, BxPC3, Hpac, PANC1, PSN1), Lung (H1650), and Liver (HepG2).

Method Name	Extraction Mixture	Categorical Unique IDs		Total IDs	
Folch[1]	Chloroform/ Methanol	Fatty Acyl [FA]	484	Positive	2209
		Glycerolipids [GL]	644		
		Glycerophospholipids [GP]	685	Negative	1953
		Sphingolipids [SP]	608		
		Prenol Lipids [PL]	375		
		Saccarolipids [SL]	164	Total Unique	3202
		Sterol Lipids [ST]	243		
Bligh and Dyer[2-4]	Chloroform/ Methanol/Water	Fatty Acyl [FA]	267	Positive	1659
		Glycerolipids [GL]	617		
		Glycerophospholipids [GP]	512	Negative	1521
		Sphingolipids [SP]	354		
		Prenol Lipids [PL]	285		
		Saccarolipids [SL]	114	Total Unique	2305
		Sterol Lipids [ST]	155		
Two Step Bligh and Dyer[5, 6]	Chloroform/ Methanol/Water	Fatty Acyl [FA]	406	Positive	2262
		Glycerolipids [GL]	688		
		Glycerophospholipids [GP]	752	Negative	2230
		Sphingolipids [SP]	528		
		Prenol Lipids [PL]	416		
		Saccarolipids [SL]	222	Total Unique	3232
		Sterol Lipids [ST]	220		
MTBE[7, 8]	MTBE/Methanol/ Water	Fatty Acyl [FA]	184	Positive	1540
		Glycerolipids [GL]	640		
		Glycerophospholipids [GP]	812	Negative	1472
		Sphingolipids [SP]	162		
		Prenol Lipids [PL]	144		
		Saccarolipids [SL]	205	Total Unique	2264
		Sterol Lipids [ST]	118		
Modified Bligh and Dyer Extraction	Chloroform/ Methanol/ Isopropanol/Water	Fatty Acyl [FA]	414	Positive	2476
		Glycerolipids [GL]	595		
		Glycerophospholipids [GP]	892	Negative	2311
		Sphingolipids [SP]	615		
		Prenol Lipids [PL]	369		
		Saccarolipids [SL]	176	Total Unique	3301
		Sterol Lipids [ST]	240		

Supplemental Table 1: Comparison of Common Lipid Extraction Protocols.

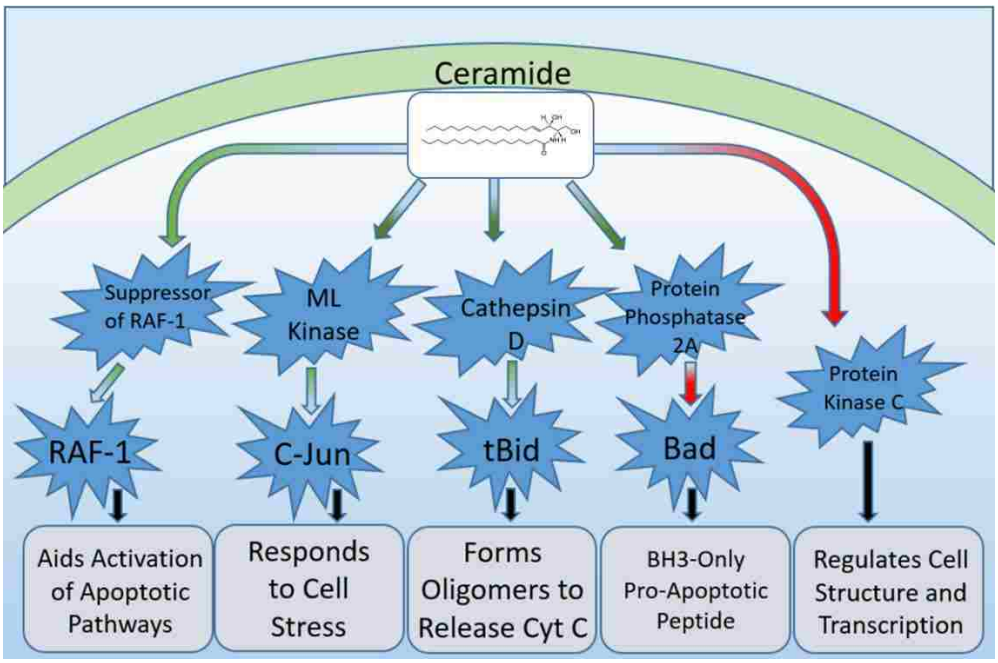

Supplemental Figure S2: Role of Ceramide in Cell Signaling Pathways.

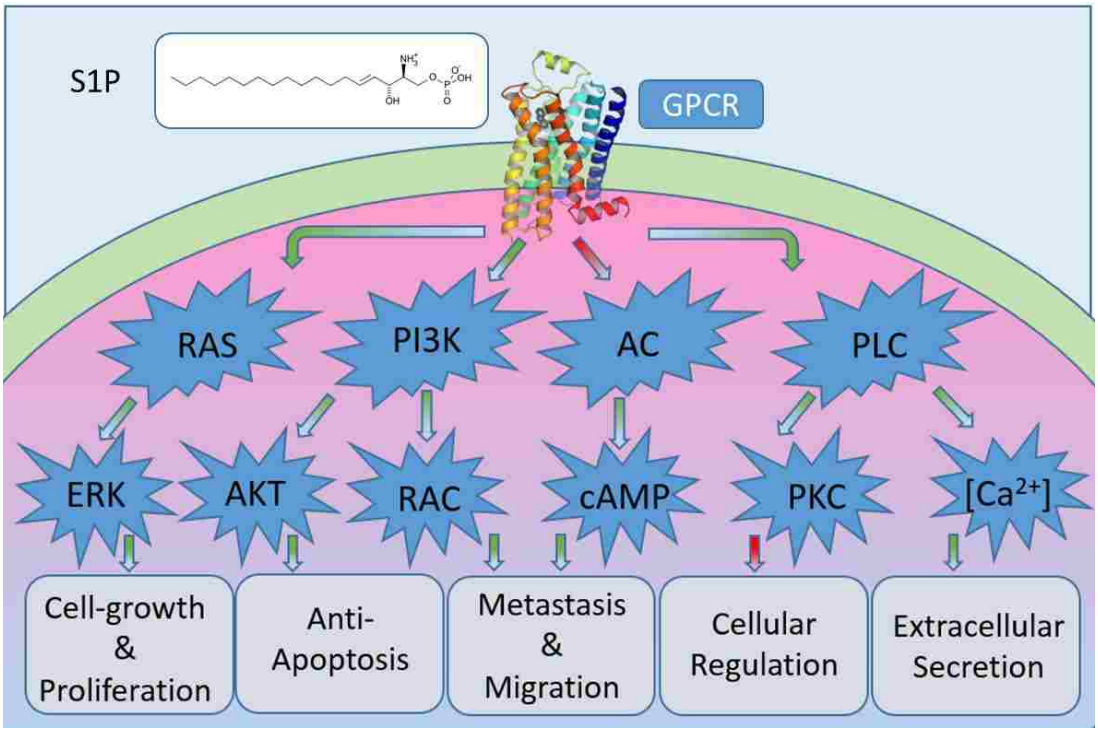

Supplemental Figure S3: Role of Spingosine-1-Phosphate in Cell Signaling Pathways.

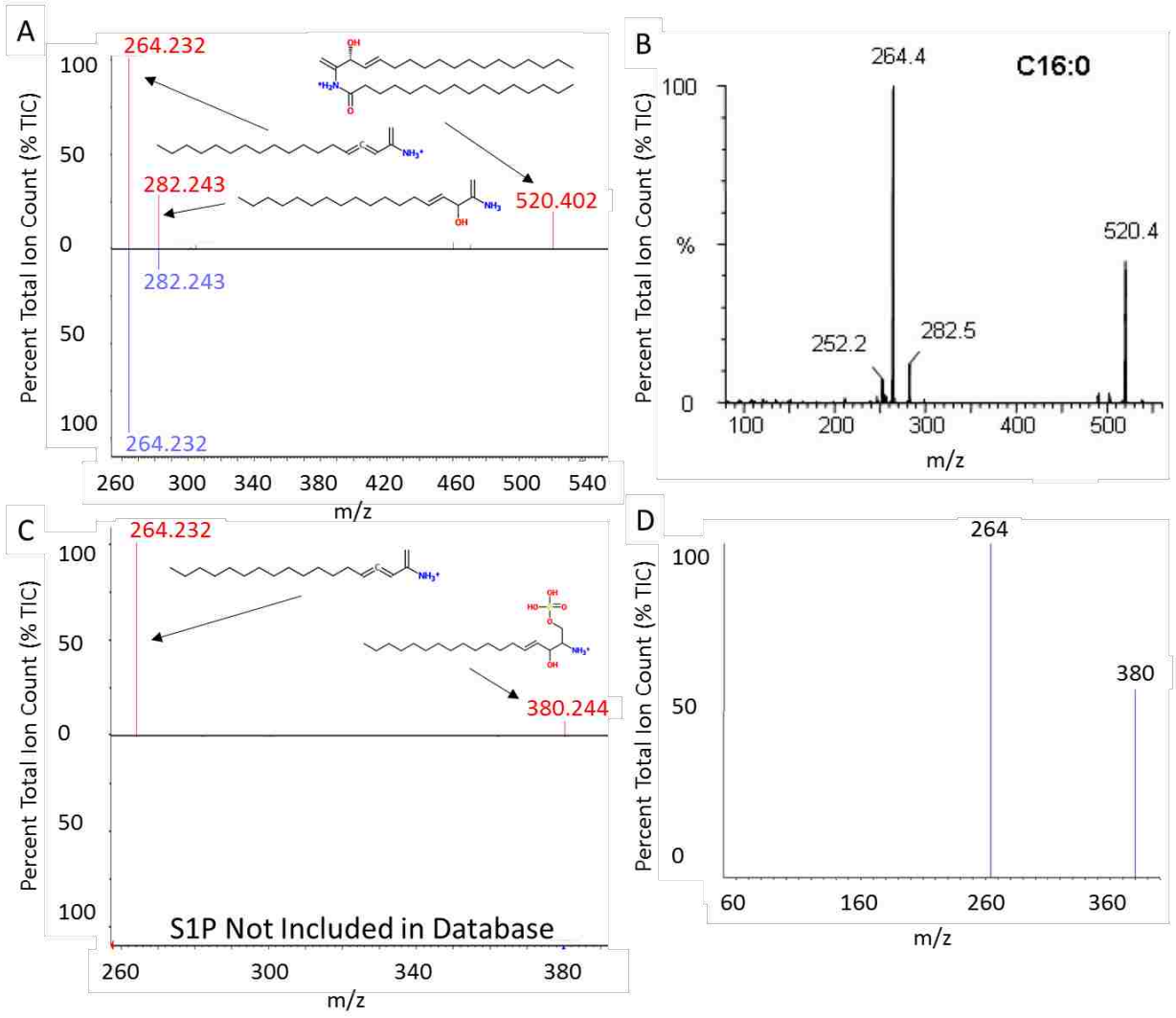

Supplemental Figure S4: Lipid Fragment Identifications for C16 Ceramide and Sphingosine-1-Phosphate. Experimental fragmentation shown for Cerimide (A) and S1P (C) shown in red. For the important signaling lipids specifically quantified in this study additional fragmentation was completed to increase confidence in assigned lipid identifications. Using our searching algorithm both C16 ceramide and S1P were the top ranked matches with the highest mass accuracy for the given peak mass. A) Additional verification was completed using LipidBlast for C16-ceramide with matches for all theoretical peaks and a score of 293. B) Comparisons for C16-ceramide were evaluated to known lipid fragmentation from Kasumov *et*

al. (figure adapted from Kasumov *et al*[1].) and Gu *et al*[2]. where we had matches for all major fragmentation peaks. C) At the time of this analysis LipidBlast did not have S1P in its database and could not therefore be scored in this manner. D) Comparisons for S1P were evaluated to known purified lipid standard fragmentation from LIPIDMAPS where we had matches for all major fragmentation peaks.

Figure S5

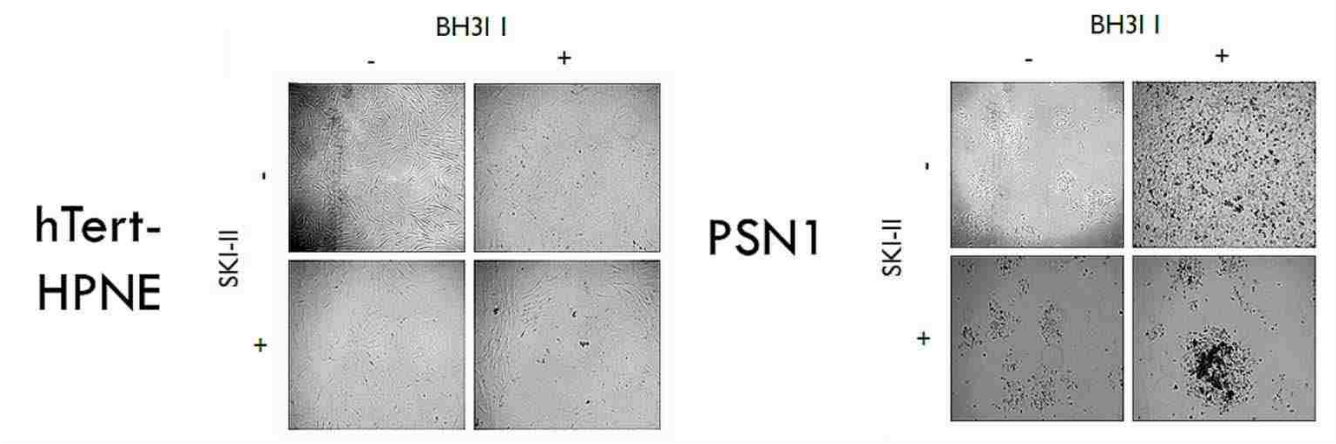

Supplemental Figure S5: Cell Death and Cellular Morphology changes due to Combinatorial Drug Treatment. Cells treated with SKI-II and BH3I-1 were imaged under a microscope and found to have an observable morphological changes in the PSN1 cell line where sphingosine kinase activity is elevated. Cells with high sphingosine kinase activity form less adhered clusters when treated with SKI-II.

Works Cited:

1. Kasumov, T.; Huang, H.; Chung, Y. M.; Zhang, R.; McCullough, A. J.; Kirwan, J. P., Quantification of ceramide species in biological samples by liquid chromatography electrospray ionization tandem mass spectrometry. *Anal Biochem* **2010,** *401* (1), 154-61.
2. Gu, M.; Kerwin, J. L.; Watts, J. D.; Aebersold, R., Ceramide profiling of complex lipid mixtures by electrospray ionization mass spectrometry. *Anal Biochem* **1997,** *244* (2), 347-56.

CHAPTER 4:

Development of a Liquid Chromatography Mass Spectrometry (LC/MS) Based Hepcidin-25 Quantitation Assay

Introduction:

The use of mass spectrometry for clinical applications is definitely on the rise. The advantages of mass spectrometry use for clinical analysis include: 1. One and only one mass spectrometer can be used to complete hundreds of complex analyses. Using traditional biochemical techniques requires that you keep expensive specialized reagents for each type of test you desire to complete. 2. Mass spectrometry based assays don't expire. Unlike the traditional ELISA assay, or other chemical based assays that have a limited shelf life, a mass spectrometer can sit for extended periods and then be used at a moment's notice without and loss of fidelity or accuracy. 3. Mass spectrometry based assays are adaptable. If some sampling condition changes or there is some sort of sample degradation, then this can be detected with the mass spectrometer. Traditional assays can't show a degradation pattern like a mass spectrometer can. If a sample sat too long or became oxidized the methods can be modified to adapt and record these changes that might not otherwise be detected with other assays. 4. Mass spectrometry based assays are cheaper. Eliminating the need for specific reagents can make mass spectrometry based assays cheaper because they use the same, or similar, reagents for sample preparation. 5. Mass spectrometry based assays can be more sensitive. Many mass spectrometry based assays have lower limits of detection than traditional assays and can give more information to a clinician. 6. Data can be researched after experimentation. With traditional chemical based

assays, you have one shot to collect the information you need and only that information. With a mass spectrometer you can collect as much or as little information as you desire and this can then be evaluated for new information that was not in the original search parameters. In this way new discoveries can be made without needed to go back and collect new samples to re-run specific experiments.

For the reasons listed above and due to the lack of widely available protocols we set out to develop a liquid chromatography mass spectrometry based assay for the detection and quantification of bioactive hepcidin-25 from complex matrices. This allows for us to search for not only human, but also rat, and mouse isoforms of the peptide hormone for use in evaluated efficacy of treatment in our studies. While the development of the assay continued longer than was really necessary the results we obtained we promising for this new assay.

Whole Blood and Urine Bioactive Hepcidin-25 Determination using Liquid Chromatography Mass Spectrometry

Summarizing my Contribution: Working in collaboration with the Dr. Richard Watt lab we determined a need to develop a simple mass spectrometry based measurement technique for a small signaling peptide known as hepcidin-25. The Watt lab created an animal model for anemia of chronic inflammation and needed to know the quantitation of this signaling hormone in order to determine the effectiveness of treatment. An ELISA kit exists for this signaling peptide but the LLOD and sensitivity of the assay weren't sufficient for us to determine accurate quantitation data. In order to address this need, I set out to develop a highly sensitive method of measurement using an LC-MS/MS based method that could be easily completed using widely available research equipment. Initially we thought that the method development would be simple but due to the complex nature of small peptide purification and the poor ionization character of cysteine-rich peptides, this method became a much more significant project than was anticipated. I was the primary driver of this project and determined the technique and direction this experiment should take.

Adam C. Swensen[1], Jordan Finnell[1], Catalina Matias Orozco[1], Andrew J. Gross[1,2], John T. Prince[1], Richard K. Watt[1], John C. Price[1]*

[1]Department of Chemistry and Biochemistry, Brigham Young University, Provo Utah 84602

[2]Roseman University of Health Sciences, South Jordan Utah 84095

* Correspondence should be addressed via email to JCPrice@chem.byu.edu

Analytical Biochemistry. Volume 517, 15 January 2017, Pages 23–30

http://dx.doi.org/10.1016/j.ab.2016.10.023

Abstract

Hepcidin is a small cysteine-rich signaling peptide that regulates blood serum iron concentrations[1-4]. Patients with chronic inflammation are known to have elevated levels of hepcidin in their blood and urine and often suffer from anemia as a result[5-10]. Measuring and quantifying the amount of active hepcidin in blood and urine can help to determine the cause and severity of the anemia thereby helping physicians determine the correct course of treatment[11-16]. We have developed a simple technique to isolate, chemically modify, and concentrate hepcidin from blood and urine coupled to high-pressure liquid chromatography mass spectrometry that can accurately and reproducibly measure and quantify the active hormone.

Introduction

Hepcidin is a peptide hormone that is activated under conditions of inflammation and reduces iron release into the blood. The inactive precursor peptides prohepcidin and preprohepcidin, which are also found in blood serum, are activated by the proteolytic enzyme furin[17]. When cleaved to the 25 amino-acid (aa) length active form, hepcidin binds to ferroportin thereby causing it to be endocytosed and degraded in the cell[18]. This prevents further iron release from the iron-rich cells, and can cause iron deficiency anemia in individuals with high hepcidin-25 serum concentrations[1, 19, 20].

The need to develop a simple, sensitive, and accurate method to measure hepcidin-25 concentrations from body fluids has been discussed previously[21, 22]. Several methods for detecting and quantifying hepcidin have been described in recent years. The first approaches

involved immuno-chemical techniques such as ELISA assays and Western blot methods[23]. While these techniques make it possible to quantify hepcidin from patients, basal hepcidin concentrations are often below the limit of sensitivity of current antibody based assays (typically 5 ng/mL $\approx 1.8\ nM$)[23]. More sensitive methods have been developed using matrix assisted laser desorption ionization mass spectrometry (MALDI-MS)[24, 25] and liquid chromatography mass spectrometry (LC-MS) based techniques[24, 26, 27]. The use of liquid chromatography is advantageous because it increases the specificity and sensitivity, but faces the problem of poor ionization of cysteine-rich peptides using electrospray ionization (ESI).

We have addressed the issue of poor electrospray response due to the cysteine residues by reducing the cysteine residues and covalently modifying the cysteines. Electrospray response and efficiency is determined by the ability to confer charge to the molecules of interest and the ability of the molecules to desorb from the liquid matrix that carries the spray. This can be accomplished by either adding easily ionizable functional groups to the molecule to add charge and/or adding non-polar functional groups to aid in desorption from the liquid solvent. We investigated several chemical covalent modifiers that take advantage of these electrospray-improving characteristics. Electrospray response improved for all chemical covalent modifiers of the peptide and allowed for greater sensitivity and a lower limit of detection for blood and urine hepcidin.

Our sample preparation technique uses widely available laboratory equipment to isolate and concentrate hepcidin from blood and urine and reduces sample-to-sample variation. Using this technique, we have shown that it is possible to isolate hepcidin from complex sample matrices including blood, and urine. The lower limits of detection in this method allowed us to

confidently measure hepcidin in just 250 □L of sample. This allowed us to compare hepcidin concentrations between healthy subjects in both urine and blood samples.

Materials and Methods

Supplies and instrumentation

Synthetic, purified, human hepcidin-25 standards were purchased to test concentration responses and for standard curve calculations (China Peptides). For electrospray ionization response optimization, commercially available iodoacetamide derivative chemical modifiers (Thermo, Sigma Aldrich) were purchased (Figure 2). Isotopically labeled iodoacetamide (CDN Isotopes) was also used for testing and quantification. Reduction of cysteine disulphide linkages was completed using tris(2-carboxyethyl)phosphine (TCEP) (Thermo). 30 kilo-Dalton and 3 kilo-Dalton cut-off (0.5 mL) centrifuge spin-filters were obtained for peptide isolation and concentration (Millipore Amicon). Mass spectrometry grade formic acid (FA) (Promega) was used as an ionization aid prior to injection into the mass spectrometer. ELISA Assay measurements of hepcidin-25 were completed using a commercially available kit from (DRG Diagnostics). An Agilent 1260 Infinity liquid chromatography system with an Agilent ChipCube C18 reverse phase column coupled to an Agilent 6530 Q-TOF tandem mass spectrometer was used for data collection and quantification of human blood and urine samples. A micro BCA protein assay kit (Thermo Fisher) was used to quantify total protein from urine using the included tube protocol.

Study participants

The Brigham Young University Internal Review Board (IRB) approved all aspects of the participant recruiting and sample collection. Blood and urine samples were collected from

healthy individuals for analysis of healthy basal hepcidin concentration measurements and to provide complex media for standard curve creation using synthetic hepcidin.

Measurement of urine total protein and creatinine concentrations

Total protein and creatinine measurements were conducted on urine samples to test for dilution effects and whether or not normalization of hepcidin-25 concentrations would be required (Supplemental Figure 1). Total protein was measured according to the manufacturer's protocol for tube measurement of total protein using the micro BCA protein assay kit. A 1:100 dilution of the urine was required to allow for measurement within the calibration curve. Total creatinine was measured by centrifuging urine at 18,000 g for 15 minutes and then drawing off 200 µL of supernatant. Supernatant was acidified to 0.5% FA (v/v) and then run on an Agilent 6530 QToF coupled to an Agilent 1260 Infinity with 10 cm C18 column using a 25 minute gradient. Gradient profiles started at 95% water 5% acetonitrile ramped up to 40% water 60% acetonitrile over 20 minutes and then ramped up to 5% water 95% acetonitrile over the final 5 minutes. Quantitation was calculated according to the extracted ion chromatogram peak volumes for creatinine (m/z= 114.3) with fragmentation verification of the creatinine peak (m/z=86.3 & 44.3).

Sample preparation

Collected blood and urine samples were immediately placed in refrigeration at 4 ºC and were centrifuged to complete the first-step filtration within 24 hours. Whole blood, serum, urine, cell culture media, and purified hepcidin were all analyzed using 250 µL of starting sample. A finger-prick for blood or small tube for urine provide adequate volumes for hepcidin analyses. The sample was placed on a 30 kilo Dalton spin filter (Fig 1). The filter separates away the large

highly abundant proteins while allowing the smaller proteins and peptides to pass through. Approximately 95% of the peptide was recovered in the flow through when analyzing a purified synthetic stock solution (data not shown). The large molecular weight retentate proteins were washed with 100 µL 8 M urea in 0.1 M Tris-HCl at pH 8.5 (urea buffer) to break any protein-protein interactions and allow any peptides to pass through the filter membrane. Although this step lysed the cells in whole blood we found that the filter efficiently retained all the protein components of the lysed cells. The filters were spun 45 minutes at 18,800 g, for each step.

The flow through (solution which passed through the 30kD filter) was treated with TCEP, 50 □L of 50mM stock in urea buffer) for 20 minutes to reduce the disulphide bonds and oxidized cysteine residues in the flow-through fractions. After completion of the reduction step 100 µL of 0.2 M iodoacetamide or one of its derivatives in urea buffer is added to the mixture and allowed to react for 30 minutes in the dark.

The reduced and alkylated sample was then transferred to a 3 kilo-Dalton cut-off spin filter and centrifuged at 18,800 g for about 1 hour (more time may be necessary if large sample volumes are used). The filter was then washed with 50 µL 50 mM ammonium bicarbonate and spun for 30 minutes at 18,800 g once. This step removes the urea, salts, and lipids from the sample while retaining the hepcidin above the filter. The spin filter retained 15 µL of the solution and this concentrates the hepcidin in preparation for mass spectrometry without the need for speed-vac concentrating of the sample. To recover the remaining concentrated peptides the spin filter was inverted in a clean collection tube and centrifuged at 2,500 g for 15 minutes (Figure 1). Completed samples were stored at -20 ^{o}C until ready for mass spectrometry at which point the samples were thawed and formic acid was added to 1% (v/v) prior to sample analysis via LCMS.

Samples are run on a C18 reverse phase column and eluted using acetonitrile. The HPLC method was modified based on the column and the derivative used (Figure 2). The amount of time required to elute the peptide mixture and varied between 10 and 20 minutes. Although the data presented here was collected using a QToF, individual samples were run on an Orbitrap mass spectrometer with similar results.

Consistent sample volumes of 0.5-1 µLs were injected into the column and eluted using a 27-minute acetonitrile gradient at a flow rate of 325 nL/min. A target peak list for selected reaction monitoring (SRM) was included in the method to selectively fragment (MS/MS) peaks of interest for peptide sequencing/fingerprinting to confirm hepcidin identification in each sample. For the iodoacetamide derivative (Fig 2A), peaks corresponding to the $[M+2H^+]^{2+}$ at 1397.53 m/z, $[M+3H^+]^{3+}$ at 932.02 m/z, $[M+4H^+]^{4+}$ at 699.27 m/z, and $[M+5H^+]^{5+}$ at 559.62 m/z were selected for fragmentation (Figure 3 A). A target peak list for selected reaction monitoring (SRM) was included in the method to selectively fragment (MS/MS) peaks of interest for peptide sequencing/fingerprinting to confirm hepcidin identification in each sample.

Addition of internal standards

Our assay allows for simple sample to sample comparison of relative hepcidin concentrations without needing to add a synthetic internal standard. However, to obtain actual peptide concentration values a synthetic hepcidin-25 internal standard must be used. Several methods were employed for the addition of the internal standard. For spiked response increase quantitation a 200 mM stock solution of synthetic hepcidin-25 in water (pH 7.5) was used to increase the sample hepcidin concentration in a split-reference sample by 5 nM prior to the initial sample filtration step. When heavy label iodoacetamide modifiers or multiplexed modifiers were

used in the same sample, the TCEP reduction and cysteine capping reactions were carried out prior to addition to the sample containing the biological hepcidin-25 to be quantified.

Data analysis

Electrospray ionization usually results in the production of multiple charge states (m/z). This means that hepcidin was often observed in the +6, +5 (dominant), +4(dominant), +3(dominant), and +2 charge states (Figure 3 A). For quantitation, we extracted ion chromatogram intensities for each of the charge states and summed the peak volumes found during the sample runs. Targeted fragmentation (MS/MS) was collected where possible and was verified through *de novo* sequencing and with the use of SearchGUI[28]/PeptideShaker[29] (Figure 3 B). Quantification was completed with the use of in-house developed quantification software and MassHunter (Agilent). We performed statistical analyses with Microsoft Excel software. Pearson correlation was used for comparison studies. P values <0.05 were considered significant.

Results and Discussion:

Cysteine rich peptides like hepcidin-25 often have poor ionization in electrospray. Our method, allows fast, reproducible sample preparation and improved ionizability for hepcidin-25. We also show that this method is relatively unaffected by sample matrix effects between blood and urine samples. Our method should also be compatible with commutable secondary reference materials, such as cyrolyoprotectant treated lyophilized plasma depleted of hepcidin-25 as demonstrated by harmonization attempts of hepcidin-25 quantification methods[30].

Covalent modification of the cysteine residues improves ionization

We tested efficiency of hepcidin ionization using several commercially available iodoacetamide derivatives to covalently modify the eight cysteine residues found within the

peptide (Figure 2). We tested the following covalent modifiers: iodoacetamide, D4-iodoacetamide, dimethylphenyl iodoacetamide, fluorescein iodoacetamide and pyrene iodoacetamide. Hepcidin with covalent modifications was quantified in a range of concentrations from 0.5 nM to 20 nM with linear response curves that had least squares linear fits of $R^2 \geq 0.95$ across all conditions. We found that each modifier improved ionization relative to the unmodified peptide. Due to the similar experimental performance, we chose to use standard iodoacetamide for the subsequent assays due to the wide availability and lower cost. Although we didn't test this experimentally, the similar performance also raises the possibility of multiplexing multiple differentially modified patient samples to determine comparative hepcidin-25 concentrations for multiple subjects simultaneously. This would increase throughput and reduce instrumental run-to-run variation. Therefore multiplexing samples could allow single run comparisons of multiple individuals. This would be most useful in non-clinical research applications where absolute concentrations are not as important as the comparative concentrations.

Summed chromatographic intensity allows accurate quantification

We found that the assay had a linear range of quantitation of more than 500 fold (0.1-50 nM) in buffer (Figure 4 A). We used a chromatographic quantification by monitoring masses which corresponded to the +5, +4, +3, +2, and +1 charge states of hepcidin-25 (Figure 3A). A least squares fit linear regression was used for the calibration curve and the coefficients of determination (R^2) were greater than 0.95 in either blood or urine. The lower limit of quantification (LLOQ) was determined as the lowest regularly detected concentrated calibration standard, 0.1 nM, with a signal/noise ratio against the background greater than five. Only one charge state of the modified peptide was typically observed at this low concentration. Our limit

of detection and the limit of quantification are below the reported values of basal hepcidin in healthy controls[11, 31, 32].

In order to examine matrix effects on the hepcidin measurement, we created standard curves in blood and urine (Figure 4 B-C). We found that the use of synthesized hepcidin as an internal standard allowed efficient and accurate quantification from basal concentrations up to 50 nM. We tested two different methods for the assay. First, we split each sample in half, adding a known reference amount of synthetic hepcidin in one half of the sample. We calculated the basal concentration as the difference between samples (Figure 5 B,D). Second, prior to adding the synthetic hepcidin reference, we alkylated it with heavy isotope labeled iodoacetamide (Figure 2B), which we spiked into the sample prior to the filtration steps. Subsequent alkylation of sample did not affect the previously modified hepcidin. We then compared the signal of the light and heavy hepcidin (+ 32 Daltons) through summation of total chromatographic peak volumes within the same sample. Concentration was calculated as the ratio of heavy to light hepcidin multiplied by the known concentration of the heavy standard (Figure 5 A,C)**.** Simultaneous elution of the heavy labeled standard was another metric to increase the specificity of the method. Both methods allow for accurate quantification and when compared against each other, had statistically insignificant differences in total quantification (Figure 5 E-F).

We determined that absolute quantitation could be determined through either three measurements (basal and two spiked concentrations) or a single measurement with spiked heavy-labeled hepcidin, with a maximum variance between methods of only 0.036. For absolute quantification, the method only requires the addition of synthetic human hepcidin-25. The advantage of the heavy isotope labeled standard is that it reduces the number of mass spectrometry samples.

Detection of hepcidin-25 in blood

A benefit to our method is that whole blood can be used without the need to separate plasma or sera from the blood first. The ultra-filters are capable of simultaneously segregating the very abundant protein components whole blood (hemoglobin, serum albumin, etc.) from the hepcidin. Previous precipitation methods have been known to cause co-precipitation of hepcidin along with the abundant proteins in blood thereby biasing the total amount of hepcidin-25 that is recovered for quantification. Centrifuge times are lengthened due to the high protein content in whole blood relative to serum, but the sensitivity of the LCMS method allowed us to use small volumes of whole blood which reduced the required centrifugation time. Also in whole blood, the complexity of the final sample increased with more compounds co-isolated with hepcidin, but the chromatographic and mass separation were sufficient to allow specific and sensitive detection of hepcidin. The increased sample complexity did required a higher amount TCEP (0.2 M) to reduce fully all of the cysteines of the hepcidin peptide due to the overall higher cysteine concentrations in blood.

Spiking in covalently modified hepcidin-25 into whole human blood and then extracting the peptide using our method resulted in linear correlations with $R^2 > 0.99$ in all samples tested (Figures 4 C, 5 A-B). Detection of the peptide in blood after preparation of the sample gave similar instrumental responses as other tested complex matrices. In all patient samples tested basal hepcidin concentrations were above the LLOQ for our assay. Additionally we were able to detect concentration increase differences accurately with only 0.5 nM incremental spiked additions of modified peptide with coefficients of variance less than or equal to 0.076 for all concentrations when samples were run contiguously. (Figure 4 B-C).

Detection of hepcidin-25 in urine

Urine does not contain as many complex abundant proteins as blood and is processed rapidly using the same method as the blood. In our assay, urine hepcidin-25 concentrations correlate to blood hepcidin concentrations and can potentially be used for clinical diagnostic purposes if required. According to our measurements, the excreted concentrations of hepcidin-25 are generally less than that found in blood. Among the nine volunteers that were able to donate time, matched blood and urine samples the mean urine hepcidin concentration was 1.3 ± 0.1 nM compared to a mean hepcidin concentration of 5.9 ± 0.5 nM in blood. Spiking in covalently modified hepcidin-25 into human urine and then extracting the peptide using our method resulted in linear correlations with $R^2 > 0.99$ in all samples tested (Figures 4 B-C). Additionally we were able to detect concentration increase differences accurately with only 0.5 nM incremental spiked additions of modified peptide with coefficients of variance less than or equal to 0.045 for all concentrations when samples were run contiguously. (Figure 4 B-C).

LC/MS assay has a linear correlation with ELISA, but increases range and sensitivity

Using donated blood samples collected through finger prick (minimum sample volume of 400 μL) and time matched urine samples we analyzed 11 blood and 9 urine samples using a commercially available hepcidin-25 ELISA (DRG Diagnostics EIA-5258) and our LC/MS assay. The lowest detected concentration of hepcidin in blood was 1.51 nM and 0.349 nM in urine. Interestingly, all samples contained concentrations of hepcidin-25 that were detected in both the LC/MS method and in the ELISA. All concentrations were within the known LLOQ for the MS assay. However, while the ELISA assay was able to detect and quantify lower concentration levels of hepcidin-25, it was at or near the quantitation limit for the assay. This resulted in a lower correlation between assays at concentrations near or below 1 nM where spectrophotometric variations in the ELISA measurements were greatest. Additionally this could

potentially be due to detection of truncated isoforms of hepcidin in the ELISA with proportionally higher concentrations of truncated peptide when active isoform concentrations are low. Overall, similar concentrations were detected in each method with a standard deviation of 1.39 nM at high concentrations in blood and 0.228 nM at high concentrations in urine when assays were compared side by side using the same samples (Figure 6 A-B).

Biological observations of hepcidin-25 in human body fluids

Comparison of blood and urine hepcidin concentrations from the same individual suggests that the urine hepcidin concentration is about 25% of the blood concentration (Figure 6 C). Many factors could affect the correlation of hepcidin-25 that is measured in the blood compared to measurements in urine. Temporal spikes due to transient furin activation in the blood can occur which rapidly increase concentrations. Removal of the peptide from the blood into urine may represent the average over a longer time interval when compared to shorter interval spikes in blood peptide concentration changes.

We tested to see if urine dilution between subjects could explain the variation in our measurements. Hepcidin-25 concentrations appear to change independent of total protein detected (Supplemental Figure 1 A). Creatinine concentration which is also used as a normalizing factor in urine samples[33], did not increase the correlation between blood and urine (Supplemental Figure 1 B). Of note for application of this assay, recent research indicates that normalization to creatinine concentrations in urine under conditions of prolonged inflammation may be inappropriate.[34]

Interestingly, all of our human sample donors (n=11) had detectable levels of hepcidin-25 in both blood (>1.51 nM) and urine (>0.349 nM). This was surprising as we expected the

possibility of donors with no detectable hepcidin present. No significant difference was observed between male (n=6) and female donors (n=5) from our sample set.

Conclusion

This method detects and quantifies hepcidin in complex samples using a simple isolation, modification, and quantification technique that can be used effectively on widely available LC-MS/MS instruments. Our assay also showed a linear correlation with ELISA results and is very robust to sample matrix effects. Human blood and urine samples evaluated with our method produced reproducible linear standard curves for all modified compounds tested and are capable of differentiating sub-nano molar concentration changes of hepcidin-25 in complex matrices. Three orthogonal methods were used for confident identification of hepcidin-25: accurate mass detection of multiple hepcidin charge states, simultaneous chromatographic elution profiles for the different hepcidin charge states, and fragmentation sequencing through MS/MS based on the amino acid structure of the peptide. This method can be used for small single sample analysis or for high throughput multi-sample analysis. These techniques may also be applicable to other small cysteine rich peptides that have traditionally been hard to detect because of their low concentrations and poor ionizability.

Acknowledgements

We thank the members of the Prince, the Price, and Watt research groups for helpful discussions. This research was supported by Start-up funding to JTP and JCP from BYU.

Works Cited:

1. Ganz, T., Hepcidin, a key regulator of iron metabolism and mediator of anemia of inflammation. *Blood* **2003,** *102* (3), 783-8.
2. Ganz, T., Hepcidin in iron metabolism. *Current opinion in hematology* **2004,** *11* (4), 251-4.
3. Ganz, T., Hepcidin and its role in regulating systemic iron metabolism. *Hematology / the Education Program of the American Society of Hematology. American Society of Hematology. Education Program* **2006**, 29-35, 507.
4. Park, C. H.; Valore, E. V.; Waring, A. J.; Ganz, T., Hepcidin, a urinary antimicrobial peptide synthesized in the liver. *The Journal of biological chemistry* **2001,** *276* (11), 7806-10.
5. Peters, H. P.; Laarakkers, C. M.; Swinkels, D. W.; Wetzels, J. F., Serum hepcidin-25 levels in patients with chronic kidney disease are independent of glomerular filtration rate. *Nephrology, dialysis, transplantation : official publication of the European Dialysis and Transplant Association - European Renal Association* **2010,** *25* (3), 848-53.
6. Niihata, K.; Tomosugi, N.; Uehata, T.; Shoji, T.; Mitsumoto, K.; Shimizu, M.; Kawabata, H.; Sakaguchi, Y.; Suzuki, A.; Hayashi, T.; Okada, N.; Isaka, Y.; Rakugi, H.; Tsubakihara, Y., Serum hepcidin-25 levels predict the progression of renal anemia in patients with non-dialysis chronic kidney disease. *Nephrology, dialysis, transplantation : official publication of the European Dialysis and Transplant Association - European Renal Association* **2012,** *27* (12), 4378-85; discussion 4384-5.

7. Shu, T.; Jing, C.; Lv, Z.; Xie, Y.; Xu, J.; Wu, J., Hepcidin in tumor-related iron deficiency anemia and tumor-related anemia of chronic disease: pathogenic mechanisms and diagnosis. *European journal of haematology* **2015,** *94* (1), 67-73.

8. Divakaran, V.; Mehta, S.; Yao, D.; Hassan, S.; Simpson, S.; Wiegerinck, E.; Swinkels, D. W.; Mann, D. L.; Afshar-Kharghan, V., Hepcidin in anemia of chronic heart failure. *American journal of hematology* **2011,** *86* (1), 107-9.

9. Uehata, T.; Tomosugi, N.; Shoji, T.; Sakaguchi, Y.; Suzuki, A.; Kaneko, T.; Okada, N.; Yamamoto, R.; Nagasawa, Y.; Kato, K.; Isaka, Y.; Rakugi, H.; Tsubakihara, Y., Serum hepcidin-25 levels and anemia in non-dialysis chronic kidney disease patients: a cross-sectional study. *Nephrology, dialysis, transplantation : official publication of the European Dialysis and Transplant Association - European Renal Association* **2012,** *27* (3), 1076-83.

10. Theurl, I.; Schroll, A.; Sonnweber, T.; Nairz, M.; Theurl, M.; Willenbacher, W.; Eller, K.; Wolf, D.; Seifert, M.; Sun, C. C.; Babitt, J. L.; Hong, C. C.; Menhall, T.; Gearing, P.; Lin, H. Y.; Weiss, G., Pharmacologic inhibition of hepcidin expression reverses anemia of chronic inflammation in rats. *Blood* **2011,** *118* (18), 4977-84.

11. Roe, M. A.; Collings, R.; Dainty, J. R.; Swinkels, D. W.; Fairweather-Tait, S. J., Plasma hepcidin concentrations significantly predict interindividual variation in iron absorption in healthy men. *The American journal of clinical nutrition* **2009,** *89* (4), 1088-91.

12. D'Angelo, G., Role of hepcidin in the pathophysiology and diagnosis of anemia. *Blood research* **2013,** *48* (1), 10-5.

13. Girelli, D.; Nemeth, E.; Swinkels, D. W., Hepcidin in the diagnosis of iron disorders. *Blood* **2016,** *127* (23), 2809-13.

14. Konz, T.; Montes-Bayon, M.; Vaulont, S., Hepcidin quantification: methods and utility in diagnosis. *Metallomics : integrated biometal science* **2014,** *6* (9), 1583-90.

15. Kemna, E. H.; Tjalsma, H.; Willems, H. L.; Swinkels, D. W., Hepcidin: from discovery to differential diagnosis. *Haematologica* **2008,** *93* (1), 90-7.

16. Kroot, J. J.; Tjalsma, H.; Fleming, R. E.; Swinkels, D. W., Hepcidin in human iron disorders: diagnostic implications. *Clinical chemistry* **2011,** *57* (12), 1650-69.

17. Valore, E. V.; Ganz, T., Posttranslational processing of hepcidin in human hepatocytes is mediated by the prohormone convertase furin. *Blood cells, molecules & diseases* **2008,** *40* (1), 132-8.

18. Nemeth, E.; Tuttle, M. S.; Powelson, J.; Vaughn, M. B.; Donovan, A.; Ward, D. M.; Ganz, T.; Kaplan, J., Hepcidin regulates cellular iron efflux by binding to ferroportin and inducing its internalization. *Science* **2004,** *306* (5704), 2090-3.

19. Weinstein, D. A.; Roy, C. N.; Fleming, M. D.; Loda, M. F.; Wolfsdorf, J. I.; Andrews, N. C., Inappropriate expression of hepcidin is associated with iron refractory anemia: implications for the anemia of chronic disease. *Blood* **2002,** *100* (10), 3776-81.

20. Nicolas, G.; Bennoun, M.; Porteu, A.; Mativet, S.; Beaumont, C.; Grandchamp, B.; Sirito, M.; Sawadogo, M.; Kahn, A.; Vaulont, S., Severe iron deficiency anemia in transgenic mice expressing liver hepcidin. *Proceedings of the National Academy of Sciences of the United States of America* **2002,** *99* (7), 4596-601.

21. Lefebvre, T.; Dessendier, N.; Houamel, D.; Ialy-Radio, N.; Kannengiesser, C.; Manceau, H.; Beaumont, C.; Nicolas, G.; Gouya, L.; Puy, H.; Karim, Z., LC-MS/MS method for hepcidin-25 measurement in human and mouse serum: clinical and research implications in iron disorders. *Clinical chemistry and laboratory medicine* **2015,** *53* (10), 1557-67.

22. Delaby, C.; Beaumont, C., [Serum hepcidin assay in 2011: where do we stand?]. *Annales de biologie clinique* **2012,** *70* (4), 377-86.

23. Ganz, T.; Olbina, G.; Girelli, D.; Nemeth, E.; Westerman, M., Immunoassay for human serum hepcidin. *Blood* **2008,** *112* (10), 4292-7.

24. Bansal, S. S.; Abbate, V.; Bomford, A.; Halket, J. M.; Macdougall, I. C.; Thein, S. L.; Hider, R. C., Quantitation of hepcidin in serum using ultra-high-pressure liquid chromatography and a linear ion trap mass spectrometer. *Rapid communications in mass spectrometry : RCM* **2010,** *24* (9), 1251-9.

25. Laarakkers, C. M.; Wiegerinck, E. T.; Klaver, S.; Kolodziejczyk, M.; Gille, H.; Hohlbaum, A. M.; Tjalsma, H.; Swinkels, D. W., Improved mass spectrometry assay for plasma hepcidin: detection and characterization of a novel hepcidin isoform. *PloS one* **2013,** *8* (10), e75518.

26. Wolff, F.; Deleers, M.; Melot, C.; Gulbis, B.; Cotton, F., Hepcidin-25: Measurement by LC-MS/MS in serum and urine, reference ranges and urinary fractional excretion. *Clinica chimica acta; international journal of clinical chemistry* **2013,** *423*, 99-104.

27. Macdougall, I. C.; Malyszko, J.; Hider, R. C.; Bansal, S. S., Current status of the measurement of blood hepcidin levels in chronic kidney disease. *Clinical journal of the American Society of Nephrology : CJASN* **2010,** *5* (9), 1681-9.

28. Vaudel, M.; Barsnes, H.; Berven, F. S.; Sickmann, A.; Martens, L., SearchGUI: An open-source graphical user interface for simultaneous OMSSA and X!Tandem searches. *Proteomics* **2011,** *11* (5), 996-9.

29. Vaudel, M.; Burkhart, J. M.; Zahedi, R. P.; Oveland, E.; Berven, F. S.; Sickmann, A.; Martens, L.; Barsnes, H., PeptideShaker enables reanalysis of MS-derived proteomics data sets. *Nature biotechnology* **2015,** *33* (1), 22-4.

30. Troutt, J. S.; Butterfield, A. M.; Konrad, R. J., Hepcidin-25 concentrations are markedly increased in patients with chronic kidney disease and are inversely correlated with estimated glomerular filtration rates. *Journal of clinical laboratory analysis* **2013,** *27* (6), 504-10.

31. Troutt, J. S.; Rudling, M.; Persson, L.; Stahle, L.; Angelin, B.; Butterfield, A. M.; Schade, A. E.; Cao, G.; Konrad, R. J., Circulating human hepcidin-25 concentrations display a diurnal rhythm, increase with prolonged fasting, and are reduced by growth hormone administration. *Clinical chemistry* **2012,** *58* (8), 1225-32.

32. Koliaraki, V.; Marinou, M.; Vassilakopoulos, T. P.; Vavourakis, E.; Tsochatzis, E.; Pangalis, G. A.; Papatheodoridis, G.; Stamoulakatou, A.; Swinkels, D. W.; Papanikolaou, G.; Mamalaki, A., A novel immunological assay for hepcidin quantification in human serum. *PloS one* **2009,** *4* (2), e4581.

33. Stimpson, S. A.; Leonard, M. S.; Clifton, L. G.; Poole, J. C.; Turner, S. M.; Shearer, T. W.; Remlinger, K. S.; Clark, R. V.; Hellerstein, M. K.; Evans, W. J., Longitudinal changes in total body creatine pool size and skeletal muscle mass using the D3-creatine dilution method. *Journal of cachexia, sarcopenia and muscle* **2013**.

34. Tang, K. W.; Toh, Q. C.; Teo, B. W., Normalisation of urinary biomarkers to creatinine for clinical practice and research--when and why. *Singapore medical journal* **2015,** *56* (1), 7-10.

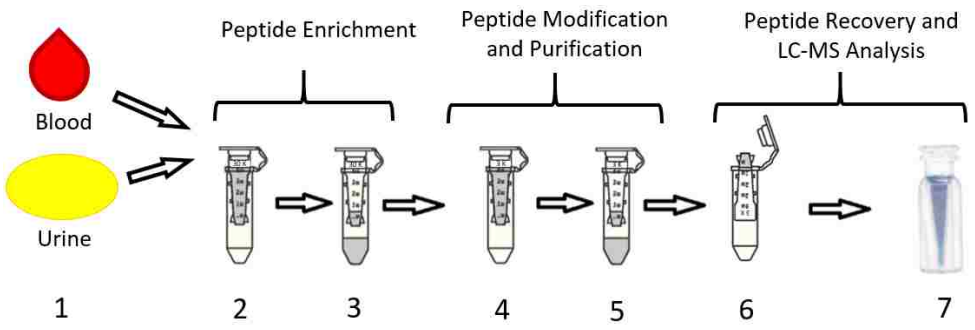

Figure 1: Sample Preparation Protocol. 1. Sample collection from blood, or urine. 2. Ultrafiltration with 30 kDa cut-off filter to remove abundant large proteins. Washed with urea to break protein-protein interactions. 3. Filtrate contains small proteins and peptides without the use of precipitation. 4. Filtrate transferred to 3 kDa cut-off filter and then treated with TCEP and iodoacetamide covalent modifier. 5. Ultrafiltration with 3 kDa cut-off filter retains modified hepcidin-25 peptide. Washed with ammonium bicarbonate (ABC)/methanol to remove salts and lipids. 6. Filter recovery of modified hepcidin-25 peptide using inverted filter collection. 7. Sample transferred to mass spectrometry vial and acidified to 1% (v/v) formic acid prior to LC-MS analysis.

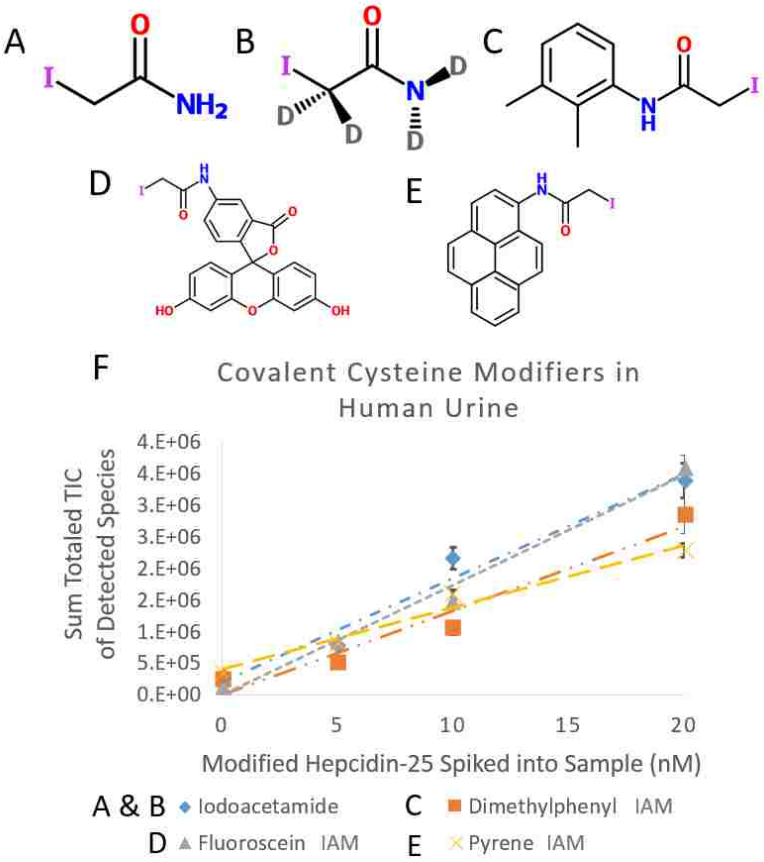

Figure 2: Iodoacetamide Based Chemical Covalent Modifiers. Chemical compounds used to modify the eight cysteine residues in hepcidin-25 in order to aid in electrospray response. (A) Standard iodoacetamide (IAM) (B) Heavy label iodoacetamide (IAM-D4) (C) Dimethylphenyl IAM (D) Fluorescein IAM (E) Pyrene IAM (F) Comparison of Chemical Covalent Modifiers used to aid Electrospray Response. All of the tested chemical modifiers improved the ionizability of hepcidin-25. Unmodified and unreduced hepcidin-25 remained undetected.

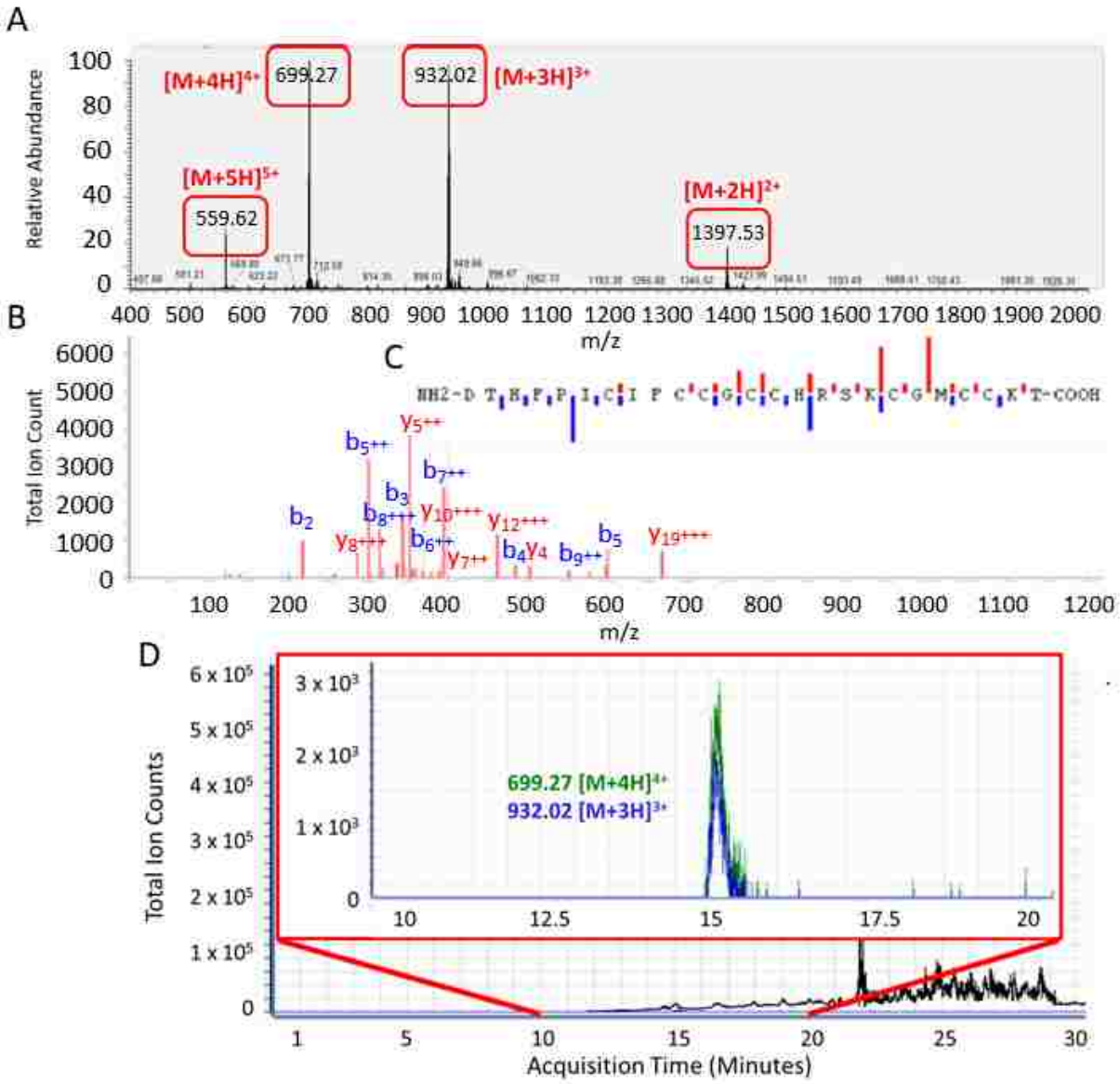

Figure 3: Detection of Hepcidin-25 by Mass Spectrometry and Confirmation through MS/MS Sequencing and Chromatographic Profiling. Three orthogonal methods for confident identification of hepcidin-25: mass fingerprinting of multiple charge states, MS/MS fragmentation sequencing, and chromatographic separation profile. (A) Multiple charge states used for quantification of hepcidin-25 modified with iodoacetamide. (B) Fragmentation sequencing through collision-induced dissociation (CID) MS/MS used to verify the identity of

hepcidin-25. Spectra generated using PeptideShaker with a 0.5 Da 90% confidence interval. (C) B and Y ion series fragments of the peptide detected from fragmentation. (D) Extracted ion chromatograms for 2 detected charge states, 699.27 m/z [M+4H]4+ and 932.02 m/z [M+3H]3+, at basal detection level in healthy human blood (see Figure 4 C).

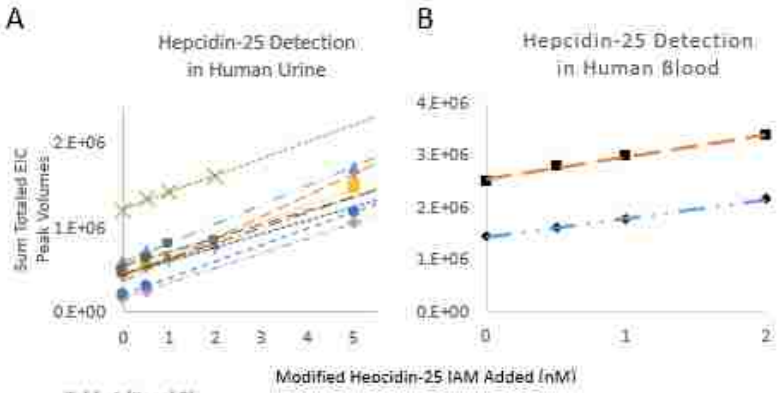

Table 1 (Panel B)

Calculated Basal Concentration		Amount Spiked	Calculated Concentration	Coefficient of Variance (CV)
Subject 1	2.4 ± 0.2 nM			
		0.5 nM	2.8 ± 0.1 nM	0.028
		5 nM	7.4 ± 0.6 nM	0.032
Subject 2	1.8 ± 0.2 nM			
		0.5 nM	2.6 ± 0.1 nM	0.030
		5 nM	7.4 ± 0.6 nM	0.032
Subject 3	0.7 ± 0.1 nM			
		0.5 nM	1.1 ± 0.1 nM	0.076
		5 nM	4.4 ± 0.6 nM	0.053
Subject 4	1.9 ± 0.2 nM			
		0.5 nM	2.2 ± 0.1 nM	0.035
		5 nM	5.9 ± 0.6 nM	0.040
Subject 5	0.8 ± 0.1 nM			
		0.5 nM	1.3 ± 0.1 nM	0.064
		5 nM	4.8 ± 0.6 nM	0.048
Subject 6	5.9 ± 0.6 nM			
		0.5 nM	6.6 ± 0.1 nM	0.012
		1 nM	7.0 ± 0.1 nM	0.024
		2 nM	7.9 ± 0.2 nM	0.007
Subject 7	2.1 ± 0.2 nM			
		0.5 nM	2.6 ± 0.1 nM	0.031
		1 nM	3.0 ± 0.1 nM	0.056
		2 nM	3.7 ± 0.2 nM	0.015
Subject 8	2.1 ± 0.2 nM			
		0.5 nM	2.8 ± 0.1 nM	0.028
		1 nM	3.1 ± 0.1 nM	0.054
		2 nM	4.0 ± 0.2 nM	0.014
Subject 9	2.4 ± 0.2 nM			
		0.5 nM	3.1 ± 0.1 nM	0.025
		1 nM	3.9 ± 0.1 nM	0.043
		2 nM	4.1 ± 0.2 nM	0.014

Table 2 (Panel C)

Calculated Basal Concentration		Amount Spiked	Calculated Concentration	Coefficient of Variance (CV)
Subject 1	3.0 ± 0.2 nM			
		0.5 nM	3.4 ± 0.1 nM	0.024
		1 nM	3.8 ± 0.1 nM	0.045
		2 nM	4.6 ± 0.2 nM	0.012
Subject 2	5.3 ± 0.4 nM			
		0.5 nM	5.9 ± 0.1 nM	0.014
		1 nM	6.3 ± 0.1 nM	0.027
		2 nM	7.1 ± 0.2 nM	0.008

Figure 4: Lower Limit of Detection and Low Level Concentration Determination from Complex Matrices. (A) Calibration curves detecting hepcidin-25 at low concentrations in human urine. Linear differentiation of hepcidin-25 concentrations was achieved with as low as 0.5 ± 0.1 nM concentration increase increments in urine. (B) Synthetic hepcidin-25 was spiked

into human whole blood and collected using our protocol. Response across all samples was linear with predictable ion intensity increases for each spiked amount. Linear differentiation of hepcidin-25 concentrations was achieved with as low as 0.5 ± 0.1 nM concentration increase increments in whole blood.

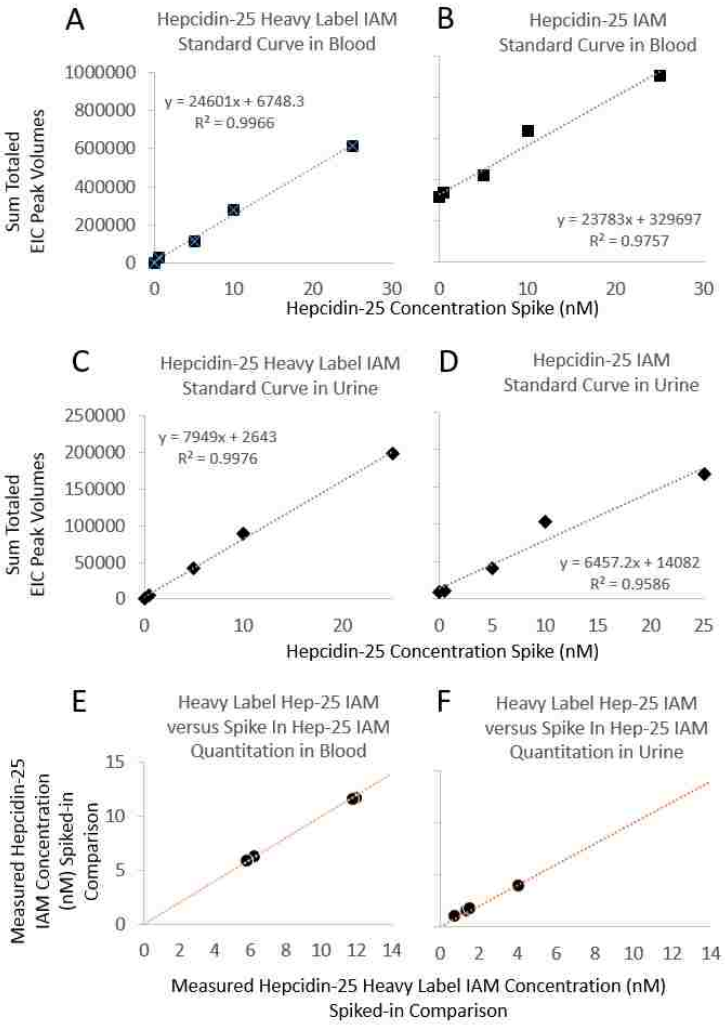

Figure 5: Comparison of Spiked Standard Ion Intensity EIC Peak Volume Quantitation versus Isotopically Heavy Labeled Internal Standard Quantitation. Blood and urine samples from 4 patients were analyzed for quantitation using two methods. The first method involved splitting one sample and spiking in a known concentration of synthetic hepcidin-25 (5 nM concentration spike)(China Peptides). These two samples were run in tandem and the EIC peak volume difference was determined for the increased spiked sample. This was then used to determine the EIC peak volume signal increase per nM increase of hepcidin-25. The second method involved spiking in known concentrations of isotopically heavy labeled IAM modified hepcidin-25 in order to generate a standard curve by which the natural isotopically light

hepcidin-25 EIC peak volume can be used to calculate a concentration. (A) Standard curve generated from heavy isotope modified Hep-25 IAM in blood. (B) Standard curve generated from spiked in unmodified Hep-25 IAM in blood. (C) Standard curve generated from heavy isotope modified Hep-25 IAM in urine. (D) Standard curve generated from spiked in unmodified Hep-25 IAM in urine. (E) Comparison of measured hepcidin-25 concentrations from heavy label standard vs comparative spiked standard in human blood. (F) Comparison of measured hepcidin-25 concentrations from heavy label standard vs comparative spiked standard in human urine.

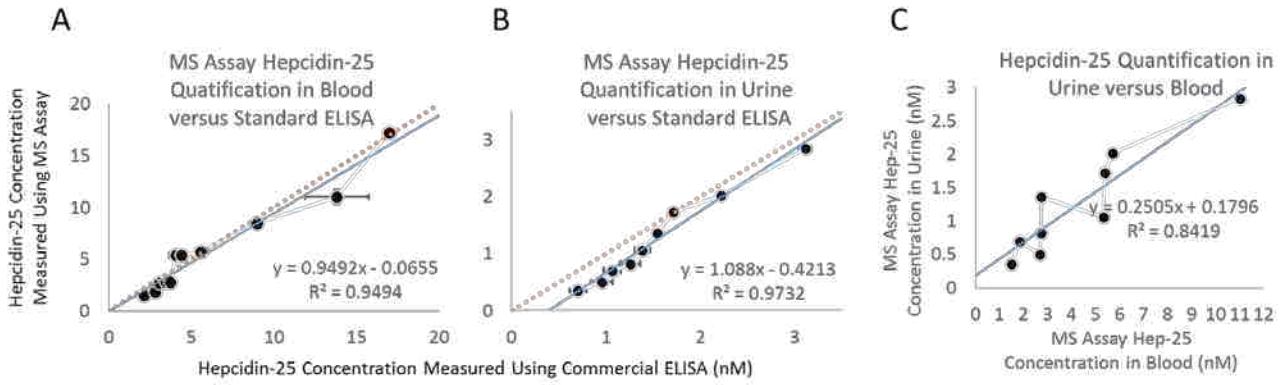

Figure 6: Comparison of MS Detection Protocol versus Standard Hepcidin-25 ELISA. (A) Comparison of measured hepcidin-25 concentrations from ELISA and LC-MS/MS Assays in human blood and (B) in human urine (analyzed with biological duplicates). Volunteers gave blood and urine samples that were prepared in parallel for ELISA and for the MS Assay. Quantitation was determined for the ELISA by generating a standard curve with purified synthetic hepcidin-25. Quantitation for the MS assay was completed by aliquoting one of the samples and spiking in a known concentration of hepcidin-25 for comparative ion-count-per-concentration quantitation. Samples were run in duplicate. (C) A correlation can be made between time-matched blood and urine samples. The concentration of hepcidin-25 in urine is approximately 4-fold less than in blood. All concentrations were within the known LLOQ for the MS assay. However, while the ELISA assay was able to detect and quantify lower concentration levels of hepcidin-25, it was near the quantitation limit for the assay. This resulted in a lower correlation between assays at concentrations near or below 1 nM where spectrophotometric variations in the ELISA measurements were greatest. Additionally this could potentially be due to detection of truncated isoforms of hepcidin in the ELISA with proportionally higher concentrations of truncated peptide when active isoform concentrations are low.

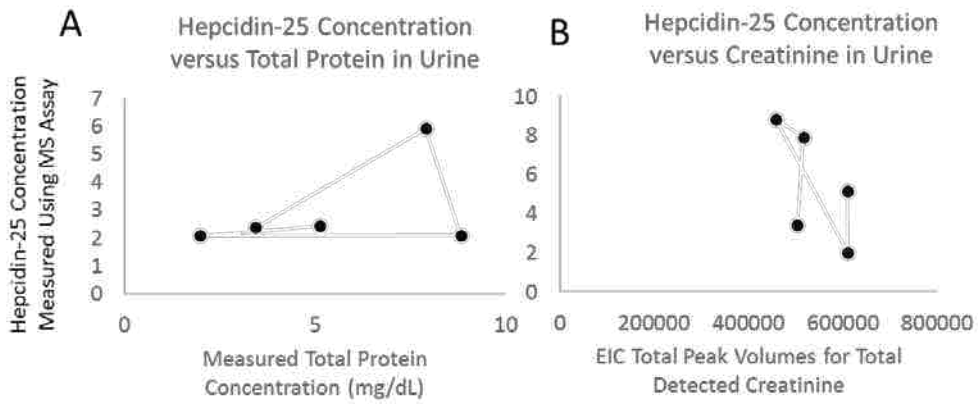

Supplemental Figure 1: Total protein and creatinine normalization evaluation. (A) Total protein concentration measured in urine did not show a statistically significant correlation to detected hepcidin-25 concentrations. (B) Normalization of detected hepcidin-25 concentrations can also be determined by measuring creatinine concentrations using established methods described previously although may not be necessary or appropriate.

CHAPTER 5:

Development of an Ultra-High Pressure Liquid Chromatography (UPLC) System for High Performance Separations

Introduction:

In order to maximize the number of identifications of peptides and proteins in a complex sample you must separate them into simpler mixtures. There are several methods by which this can be accomplished but the most common by far for proteomics is liquid chromatography. Using the inherent chemical properties of the peptides in a complex sample they can be attached to a surface through non-covalent interactions. These interactions will change based on the ionizability of the peptide, its size, its hydrophobicity, and by its charge. Once a peptide is attached then additional small molecules can be used to compete away these interactions to make it so that only a small portion of the peptide will detach from the surface based on the concentration of the small molecule that is competing the peptide away. By using a gradient this concentration can change gradually and result in the release of peptides in a controlled manner and in a way so that only a few similar proteins will be observed in the mass spectrometer at any given time instead of all of them at once.

The performance of the liquid chromatography system can also be improved by changing a few parameters as well. Greater separation of peptides can occur if the there is more surface area for peptide binding and less room for the peptide to get through a matrix without contacting a binding surface. This is usually accomplished by using very small beads with high surface area packed into a small diameter column. As the bead size decreases and the surface area increases

the amount of pressure required to push the peptides and solvent through the column also increases. Sometimes these pressures are so great they require special instrumentation to give it enough push to actual get the solvent and peptides into and ultimately through the column.

This is where the next project came in. I helped develop a system that can not only provide enough pressure to push peptides into a small efficient column but is also small enough to be easily portable. Many of the previous pump systems available were much to large to be easily transported and also lacked the performance that the pump system we developed can achieve. We tested the instrument with great success with purified peptide mixtures and tryptic digests using very small sample volumes. This was able to show the utility of the system in providing portable high performance in the field of proteomics.

Compact Ultra-high Pressure Nano-flow Capillary Liquid Chromatograph Coupled to an Orbitrap Mass Spectrometer for Proteomics

Summarizing my contribution: This project initially began to restore functionality to the LTQ Velos Pro Orbitrap Elite because of the failure in our Eksigent HPLC system we had been using. As it turned out the new experimental portable HPLC system mentioned in this publication was still in development and still required many additional modifications and revisions. I was involved in the final set-up, rotor modification, method development and performance analysis of the pumping system. I directed and collected all of the relevant mass spectrometry data using a compound mixture that I designed as well as a method that I proposed, developed, and executed. I assisted in the writing, editing, and layout of the final paper.

Xiaofeng Zhao,[†a] Xiaofeng Xie,[†a] Sonika Sharma,[†] Luke T. Tolley,[‡] Alex Plistil,[§] Hal E. Barnett,[§] Martin Brisbin,[§] Adam C. Swensen,[†] John C. Price,[†] Paul B. Farnsworth,[†] H. Dennis Tolley,[‖] Stanley D. Stearns,[§] and Milton L. Lee[*, †]

†Department of Chemistry and Biochemistry, Brigham Young University, Provo, UT 84602, USA

[‡]Department of Chemistry and Biochemistry, Southern Illinois University, Carbondale, IL 62901, USA

[§]VICI, Valco Instruments, Houston, Texas 77055, USA

[‖]Department of Statistics, Brigham Young University, Provo, UT 84602, USA

[†a]These two authors contributed equally to this work.

[*]Corresponding author: Milton_lee@byu.edu

Abstract:

A compact ultra-high pressure nano-flow liquid chromatograph (LC) was developed specifically for coupling to mass spectrometry (MS) for proteomics studies. The system utilized innovative nano-flow pumps, integrated with very low volume stop-flow injector and mixing tee. The system weighed only 5.9 kg (13 lbs) and could hold up to 1100 bar (16,000 psi) pressure. The total volume pump capacity was 60 µL. In this study, the sample injection volume was determined by either a 60 nL internal sample loop machined in a high pressure valve rotor or by a 1 µL external sample loop, although other sample loops could be selected. The gradient dwell volume was approximately 640 nL, which allowed significant reduction in sample analysis time. Gradient performance was evaluated by determining the gradient step accuracy. A low RSD (0.6%, n = 4) was obtained for day-to-day experiments. Linear gradient reproducibility was evaluated by separating a three-component polycyclic aromatic hydrocarbon mixture on a commercial 150 µm inner diameter capillary column packed with 1.7 µm particles. Good retention time reproducibility (RSD < 0.17%) demonstrated that the pumping system could successfully generate ultra-high pressures for use in capillary LC. The system was successfully coupled to an Orbitrap MS in a simple and efficient way; LC-MS of a trypsin-digested bovine serum albumin (BSA) sample provided narrow peaks, short dwell time and good peptide coverage.

Introduction

Ultra-high pressure liquid chromatography (UHPLC) has been around for almost two decades, introduced to overcome the pressure limitations of conventional pumping systems and to allow the use of very small particles as stationary phases.[1-3] Due to its excellent separation efficiency, short analysis time, low solvent consumption and easy coupling to mass spectrometry (MS), UHPLC has become a very popular and green analytical tool, and is becoming widely used for environmental, biochemical and pharmaceutical analysis.[4-10]

Very small particles (sub-2 μm) can result in improved performance in LC, as well as high speed separations.[1,11-14] However, without shortening the column length, the use of small particles requires high pressures. Operating at high pressures can create frictional heating, which can impact the retention of solutes and, in some cases, cause decomposition,[1,14] eventually destroying the column efficiency.[15,16] Heat dissipation can be facilitated by reducing the column diameter.[1,12,17] Small diameter packed fused silica columns allow fast heat dissipation, low organic solvent usage and minimal waste generation.

The first UHPLC system for capillary columns packed with 1.5 μm nonporous silica particles was a home-built system reported by Jorgenson's group.[1] The same group also constructed a gradient UHPLC system and separated a tryptic protein digest using 1.0 μm particles at 9000 bar.[2] However, the system was very large, inconvenient, and not amenable to routine use. A subsequent UHPLC system was constructed by modifying a Waters Model 6000 pump, which was coupled to a tandem MS using a capillary packed with 1.5 μm nonporous particles.[18] This system demonstrated a high duty cycle, good signal-to-noise and full automation. This work led to the introduction of commercial UHPLC instrumentation in 2004.[19] Currently, more than 20 different UHPLC systems are commercially available, with upper

pressure limits between 600-1500 bar.[4,20,21] However, these commercial instruments are still primarily constructed by modifying conventional HPLC instrumentation, and they remain somewhat bulky. They are limited to laboratory operation, and cannot be easily used for field applications. Additionally, when coupled to MS in the laboratory, long connecting tubing is needed, which greatly reduces the performance of the UHPLC system.

Compared to standard columns, e.g., 4.6-1.0 mm i.d., extra-column band broadening becomes much more critical when using smaller internal diameter columns.[21] Fekete et al. compared the extra-column peak variance contributions of several commercially available LC systems, and concluded that losses in efficiency can reach 30–55% with these UHPLC systems, even when optimized.[22] Further improvements in instrumental design could be achieved by using smaller volume capillary fitting, smaller and shorter connecting capillary tubing and smaller volume detector cell to reduce detrimental extra-column dead-volume.[22-26] Furthermore, small dwell volume is also highly desirable for UHPLC.[21]

The injection system for UHPLC should hold extremely high pressure, deliver a reproducible small volume, eliminate all carryover and minimize brand spreading.[27] Static-split injection technology was reported by Jorgenson's group, which withstood high pressures.[1,2,28] Wu et al. used a pressure-balanced injection method to introduce sample, and found it to be effective and reproducible.[3] A commercial system (Waters ACQUITY UPLC) uses a flow-through-needle injector.[29] The gradient passes through the needle during injection, ensuring complete sample transfer. In addition to the above-mentioned concerns, the detector data-acquisition rate is also very important. Narrow peaks (as small as 1 s in some cases) require at least 10-15 data points per peak to accurately specify resolution.[21]

Significant effort has been made in the past to miniaturize LC.[30-34] However, little effort has been made to miniature UHPLC. Recently, we reported a compact gradient LC system with an LED UV-absorption detector (260 nm).[31] This system meets many of the requirements for a field-portable LC, i.e., light-weight (9 lbs), low mobile phase consumption and waste generation, and battery operation. The pressure generated by this pump could reach up to 8,000 psi. Although nano-flow UHPLC systems are commercially available, they are not portable.

One of the most popular applications for UHPLC is mass spectrometry-based proteomics.[35] Due to the complex nature of protein/peptide samples, integrated UHPLC-MS is commonly used to analysis these samples. UHPLC is used prior to MS to separate complex peptides or proteins for accurate identification and quantitation. High separation power, fast analysis, small sample volume and easy coupling to MS are some of the key requirements for an UHPLC system used for proteomics. A simplified portable UHPLC system would reduce the footprint of the system, increase the duty cycle, simplify maintenance, reduce costs and even improve the separation power.

In this work, a small, portable gradient ultra-high pressure nano-flow pumping system was developed and evaluated using an on-column LED-based UV-absorption detector reported earlier, [36] as well as with an Orbitrap MS. The system was designed specifically for capillary columns. Gradient performance and separation were evaluated using this new integrated UHPLC-UV system. Efficient coupling of the nano-flow UHPLC to an Orbitrap MS for analyzing trypsin-digested BSA for proteomics was demonstrated.

Experimental section

Chemicals and reagents

Water, methanol, propyl paraben, and three polycyclic aromatic hydrocarbon (PAH) standards (fluorene, anthracene, and benzo[*a*]pyrene) were purchased from Sigma-Aldrich (St. Louis, MO, USA). Acetonitrile (ACN) was purchased from Fisher Scientific (Pittsburgh, PA, USA). All solvents and chemicals were HPLC or analytical grade. Chromatographically purified bovine serum albumin (Sigma-Aldrich) ≥ 95% was prepared for bottom-up mass spectrometry analysis using a filter aided sample preparation (FASP) technique.[37] Approximately 500 µg of protein were loaded onto a 30 kDa cut-off ultra-filtration spin filter (Vivicon) for the FASP protocol. Due to the high concentration of the final BSA peptide mixture, it was diluted 100 or 1000 fold and cleaned once more with a C-18 solid phase extraction cartridge (Sigma-Aldrich) prior to injection into the LC.

Instrumentation

The pumping system for the new gradient nano-flow UHPLC instrument (Figure 1) was engineered at VICI Valco Instruments (Houston, TX, USA). Compared to our previous gradient pumping system, several important modifications were made as follows: (1) the "Y" design (i.e., two pumps and one valve) was changed to two individual pumps (each with stepper motor and high-pressure valve), which were connected to a separate injection valve (Figure 1);[38] (2) a new sealing material was used to seal around the piston; and (3) smaller i.d. tubing was used to reduce the dwell volume.

Overall, the pumping system included two pumps, each with separate high pressure valve and stepper motor, a three-way static mixing tee connected to a serpentine tube for solvent mixing, and another high pressure valve (18,000 psi) with a stop-flow injector. The pumping system weighed 5.9 kg (13 lbs) and could hold up to 1100 bar (16,000 psi) pressure. Each pump volume capacity was 30 µL. The stop-flow injector contained a sample groove in the rotor,with

sample volume of 60 nL or a 1 µL external sample loop; however, the groove or external sample loop could be engineered to deliver sample volumes anywhere between 5 nL and the low µL range. Zero dead-volume (360 µm) fittings especially designed for capillary columns were used for all connections, and no splitting was employed. This system provided accurate non-split flow in the low nanoliter to microliter per minute range, and was fully software-controlled. An on-column deep UV LED (260 nm) absorption detector described earlier,[36] or an orbitrap MS (described later in this section) was used for detection.

System evaluation

The methods used to determine the dwell volume and gradient step accuracy were reported earlier.[31] In brief, methanol and propyl paraben in methanol were used as mobile phases A and B, respectively. A linear gradient was programmed through a hollow capillary (150 µm i.d.) from 0 to 100% B in 10 min with an isocratic hold at 100% B for several min. An injection of uracil was used to determine the capillary dead volume. The dwell volume of the system was calculated by subtracting the capillary dead volume from the gradient delay volume.

For evaluating step accuracy, the system was programmed from 0% B to 100% B 10% intervals. The gradient was stopped every 10% step for several minutes to record the UV-absorption signal. The absorbance record by the detector increased as the proportion of B in the mobile phase increased, and reached a maximum at 100% B. Every measurement was repeated at least four times to determine the precision of the results. The recorded absorbance value at each step was divided by the absorbance recorded at 100% B, which served as a reference.

Injection carry-over was studied by recording the signal obtained by first injecting uracil (0.33 mg/mL in an ACN/water mixture, 70:30 v/v). Then, the injector was thoroughly cleaned by

purging with mobile phase, and a blank injection (mobile phase) was made. Isocratic elution was used (ACN/H_2O, 70:30 v/v), and the flow rate was 2 µL/min. These experiments were repeated three times, and the detector signals were recorded. For each experiment, the peak area in the blank divided by the peak area of an analyte signal, multiplied by 100%, was reported as the percent carry-over.

Chromatographic performance was evaluated using a packed capillary column (ACQUITY BEH130 C18, 1.7 µm, 100 mm × 150 µm i.d., Waters, Milford, MA) to separate a PAH mixture under gradient programming conditions. The post-column capillary was removed and replaced by a UV-transparent fused silica capillary (150 µm i.d.), which was used as a detection window. Gradient elution was programmed from 50% A to 100% B in 11.6 min. Solvent A was water and solvent B was ACN. The flow rate was 2 µL/min. The retention time reproducibilities (n = 4) of components were calculated.

Coupling to Orbitrap MS

Polyimide coated fused silica tubing (75 µm i.d. × 365 µm o.d.) was used to prepare a column for coupling to the MS. Before packing, one end of the capillary was melted using a small butane micro torch, and pulled into a narrow tip (approximate 25 µm i.d.) to be used for electrospray ionization (ESI). Then, the capillary was packed with 1.7 µm BEH C18 particles (Waters, Milford, MA) by slurry packing. After the desired length was packed, the column was flushed with ACN before being used for MS analysis.

A hollow capillary (25 µm i.d. × 365 µm o.d., 15 cm total) was used for the transfer line between the column with integrated ESI tip and injection valve. A VICI zero dead volume union was used to connect the transfer line and the column as well as to apply the high voltage for

electrospray (photographs of the all connections and column with integrated electrospray tip ware shown in the Supplemental Information, Figures S1-S2). MS detection was carried out after ESI in the positive-ion full-scan mode. An LTQ Veles Pro Orbitrap Elite tandem MS from Thermal Fisher (Waltham, MA USA) was used, and the settings of the MS were as follows: spray voltage, 2.5 kV; capillary temperature, 325°C; and scan range, 150-2000 m/z. Nitrogen was used as sheath gas (3 arb. units). Data acquisition and analysis were performed using Thermo Xcalibur software Version 2.2.

Results and Discussion

Pump operation

The UHPLC system contained a four-port injection valve to switch between sample loading and injection (Figure 2). Each port served a specific purpose as described in the following: S is the sample injection port, W is the waste port, C is the column port, and M is the port through which the mixed mobile phase flowed to the internal sample loop and then to the column and detector. SG represents the sample groove in the rotor for loading the sample.

Software controls the pump to switch automatically between the "load" and "inject" positions. In the load position, the pumps were automatically refilled with their respective mobile phases A and B at the preset rate of 20 µL/min through a 200 µm i.d. tube. At the same time, the sample was introduced manually into the 60 nL sample loop. After the valve was switched to the inject position (i.e., the rotor rotated by 90°), solvents from the pumps were mixed at the tee to form a gradient flow. Then this gradient flow was used to carry the sample in the sample loop through the analytical column to the detector for analysis.

Dwell volume

The dwell volume is defined as the volume from the solvent mixing point to the head of the analytical column.[39] The sample experiences undesirable isocratic broadening in the dwell volume. When performing fast separations in LC, there are two main concerns related to large system dwell volume: (1) unreliable gradient method transfer between columns of different geometries, and (2) greater than expected separation time.[21] Small dwell volume is highly recommended for fast analysis, especially when small i.d. columns are used, such as capillary columns. Knowing the dwell volume of a new system is also very critical for transferring methods from conventional LC to UHPLC.

The dead volume was calculated by subtracting the capillary dead volume from the gradient delay volume. The dead volume was 1.91 μL (1.91 min × 1.0 μL/min), so the dwell volume of this system was calculated to be 0.64 ± 0.008 μL. This value is less than half of the dwell volume measured for our previous nano-flow gradient system (1.3 μL),[31] and less than the delay volume of a Waters NanoACQUITY UPLC system (< 1 μL).

Gradient profile

Good gradient accuracy and precision is a prerequisite for achieving reproducible separations. To test the accuracy of the gradient, experimental step errors were plotted against their corresponding theoretical step percentage values as illustrated in Figure 3A. Deviations from predicted values were less than 0.8%. A gradient step accuracy of ± 1% is considered to be acceptable for an LC system.[31] In order to evaluate the precision of the gradient, experimental RSD values were calculated for a series of step percentages and plotted against their respective theoretical step percentages. As shown in Figure 3B, the RSD values (n = 4) were less than 0.6%, which is comparable to commercial instruments. Therefore, the gradient performance of this system was found to be excellent in terms of step accuracy and precision.

Low carry-over is important for quantitative analysis in LC. Uracil was chosen as test analyte because a non-retained marker is commonly used to evaluate the injector performance. Data from this work showed that the nano-flow pump injector had low carry-over (0.20 ± 0.1%). This indicated that the flow-through injector is very reliable for quantitative work.

Reproducible retention time is a fundamental requirement for chromatographic separations. Under gradient conditions, high reproducibility comes from high gradient accuracy. As shown in Figure 4, highly reproducible retention times of PAHs were obtained by using the UHPLC system. The RSD values were calculated to be less than 0.12%, which is better than the value (1.42%) obtained from our previous "Y" design gradient pumping system.[31] Day-to-day reproducibility was also measured from experiments conducted over three days with three injections per day. The RSD was less than 0.17% for these PAH compounds. It should be noted that there was still some dead-volume between the column and UV detector, so separation performance could be further improved if this dead-volume was removed.

Performance under high pressure and coupling with MS

Another nano-flow UHPLC system with 1.0 μL sample loop was coupled to an Orbitrap MS for proteomic analysis. Due to the small particle size (1.7 μm) used in the analysis, higher backpressure (>10,000 psi) was required. Under high pressure, solvents compress to a certain extent, which leads to inaccurate flow rate and distorted gradient. Most commercial pumping systems use reciprocating designs, while some use flow and feedback control to solve this problem.

In our system, for simplicity, no flow and pressure sensors were employed. In order to obtain a good gradient, we evaluated two different ways to solve this issue. In the first approach,

at the beginning, both pumps were moved at the same speed until pressure was built up, and then the pump for solvent A (water) was programmed to pump at full speed while the other pump was temporarily stopped to wash all of solvent B (acetonitrile) out of the line. Sample was then injected into the flow stream and a normal linear gradient was started. For the second approach, a serials of gradient steps were generated at the first of the run to compensate for the solvent compressibility. As shown in Figure 5A, without an initial compensation procedure, the gradient was not linear, but jumped rapidly from 0 to 40% solvent B (uracil was added to solvent B for easy detection) with a steep slope at the beginning. By adding two gradient steps (gradient solvent B at 25% for 10 min and then 5% for 10 min), a near linear gradient from 5% to 40% was obtained as shown in Figure 5A. Both of these approaches were used to separate a trypsin-digested bovine serum albumin (BSA) sample. Using the method of delay injection, a 25 min gradient from 5% to 45% acetonitrile was used, for the chromatogram shown in Figure 5B. The FWHM peak width was approximately 10 s, the dwell volume was less than 2 μL, and an identified peptide coverage of over 90% was obtained using Mascot.[40] Similar results were obtained using the stepwise gradient compensation as shown in Figure 5C, with a gradient from 5% to 30% in 30 min and FWHM of approximately 15 s. These results were comparable to previously reported LC results. Further work is currently being done to implement an initial solvent compression routine into the operating software.

Conclusions

Ultra-high operating pressures for capillary LC were made possible using a newly developed LC pumping system. This new nano-flow gradient system showed excellent gradient performance, and gave highly reproducible retention times of PAH compounds on a capillary column packed with sub-2 μm particles. Efficient gradient separation of peptides was also

demonstrated when coupled to an Orbitrap MS. The advantages demonstrated in this study include: (1) fast analysis with minimum solvent consumption, (2) easy positioning of the small pumping system and analytical column close to the electrospray source, which greatly reduced band broadening and analysis time, and improved detection limits, and (3) simple and powerful separation systems for MS-based proteomics analysis.

Works Cited:

1. MacNair, J. E.; Lewis, K. C.; Jorgenson, J. W. *Anal. Chem.* **1997**, *69*, 983-989.

2. MacNair, J. E.; Patel, K. D.; Jorgenson, J. W. *Anal. Chem.* **1999**, *71*, 700-708.

3. Wu, N.; Lippert, J. A.; Lee, M. L. *J. Chromatogr. A* **2001**, *911*, 1-12.

4. De Vos, J.; Broeckhoven, K.; Eeltink, S. *Anal. Chem.* **2016**, *88*, 262-278.

5. Bouvier, E. S. P.; Koza, S. M. *TrAC, Trends Anal. Chem.* **2014**, *63*, 85-94.

6. Gumustas, M.; Kurbanoglu, S.; Uslu, B.; Ozkan, S. A. *Chromatographia* **2013**, *76*, 1365-1427.

7. Denoroy, L.; Zimmer, L.; Renaud, B.; Parrot, S. *J. Chromatogr. B* **2013**, *927*, 37-53.

8. Purcaro, G.; Moret, S.; Bučar-Miklavčič, M.; Conte, L. S. *J. Sep. Sci.* **2012**, *35*, 922-928.

9. Kumar, A.; Saini, G.; Nair, A.; Sharma, R. *Acta Pol. Pharm.* **2012**, *69*, 371-380.

10. Howard, J. W.; Kay, R. G.; Pleasance, S.; Creaser, C. S. *Bioanalysis* **2012**, *4*, 2971-2988.

11. Broeckhoven, K.; Desmet, G. *TrAC, Trends Anal. Chem.* **2014**, *63*, 65-75.

12. Jorgenson, J. W. *Annu. Rev. Anal. Chem.* **2010**, *3*, 129-150.

13. Anspach, J. A.; Maloney, T. D.; Colón, L. A. *J. Sep. Sci.* **2007**, *30*, 1207-1213.

14. Nováková, L.; Matysová, L.; Solich, P. *Talanta* **2006**, *68*, 908-918.

15. Gritti, F.; Martin, M.; Guiochon, G. *Anal. Chem.* **2009**, *81*, 3365-3384.

16. Gritti, F.; Guiochon, G. *J. Chromatogr. A* **2007**, *1138*, 141-157.

17. Colón, L. A.; Cintrón, J. M.; Anspach, J. A.; Fermier, A. M.; Swinney, K. A. *Analyst* **2004**, *129*, 503-504.

18. Tolley, L.; Jorgenson, J. W.; Moseley, M. A. *Anal. Chem.* **2001**, *73*, 2985-2991.

19. Mazzeo, J. R.; D.Neue, U.; Kele, M.; Plumb, R. S. *Anal. Chem.* **2005**, *77*, 460 A-467 A.

20. Fekete, S.; Schappler, J.; Veuthey, J. L.; Guillarme, D. *TrAC, Trends Anal. Chem.* **2014**, *63*, 2-13.

21. Fekete, S.; Kohler, I.; Rudaz, S.; Guillarme, D. *J. Pharm. Biomed. Anal.* **2014**, *87*, 105-119.

22. Fekete, S.; Fekete, J. *J. Chromatogr. A* **2011**, *1218*, 5286-5291.

23. Wu, N.; Bradley, A. C.; Welch, C. J.; Zhang, L. *J. Sep. Sci.* **2012**, *35*, 2018-2025.

24. Omamogho, J. O.; Hanrahan, J. P.; Tobin, J.; Glennon, J. D. *J. Chromatogr. A* **2011**, *1218*, 1942-1953.

25. Alexander, A. J.; Waeghe, T. J.; Himes, K. W.; Tomasella, F. P.; Hooker, T. F. *J. Chromatogr. A* **2011**, *1218*, 5456-5469.

26. Gritti, F.; Sanchez, C. A.; Farkas, T.; Guiochon, G. *J. Chromatogr. A* **2010**, *1217*, 3000-3012.

27. Swartz, M. E. *J. Liq. Chrom. Relat. Tech.* **2005**, *28*, 1253-1263.

28. Jorgenson, J. W.; Guthrie, E. J. *J. Chromatogr. A* **1983**, *255*, 335-348.

29. Waters.

30. Baram, G. I. *J. Chromatogr. A* **1996**, *728*, 387-399.

31. Sharma, S.; Plistil, A.; Barnett, H. E.; Tolley, H. D.; Farnsworth, P. B.; Stearns, S. D.; Lee, M. L. *Anal. Chem.* **2015**, *87*, 10457-10461.

32. Sharma, S.; Plistil, A.; Simpson, R. S.; Liu, K.; Farnsworth, P. B.; Stearns, S. D.; Lee, M. L. *J. Chromatogr. A* **2014**, *1327*, 80-89.

33. Sharma, S.; Tolley, L. T.; Tolley, H. D.; Plistil, A.; Stearns, S. D.; Lee, M. L. *J. Chromatogr. A* **2015**, *1421*, 38-47.

34. Zhou, L.; Lu, J. J.; Gu, C.; Liu, S. *Anal. Chem.* **2014**, *86*, 12214-12219.

35. Aebersold, R.; Mann, M. *Nature* **2003,** *422* (6928), 198-207.

36. Sharma, S.; Tolley, H. D.; Farnsworth, P. B.; Lee, M. L. *Anal. Chem.* **2015**, *87*, 1381-1386.

37. Wisniewski, J. R.; Zougman, A.; Nagaraj, N.; Mann, M., *Nature methods* **2009,** *6* (5), 359-62

38. The "Y" design used a size 11 actuator, which could only hold up to 8,000 psi (550 bar) pressure, while the new design uses a size 17 actuator, which is more accurate and can hold up to 16,000 psi (1,100 bar) pressure.

39. Li, Y.; Tolley, H. D.; Lee, M. L. *J. Chromatogr. A* **2011**, 1218,1399 − 1408.

40. Perkins, D. N.; Pappin, D. J. C.; Creasy, D. M.; Cottrell, J. S. *Electrophoresis* **1999,** *20*, 3551-3567.

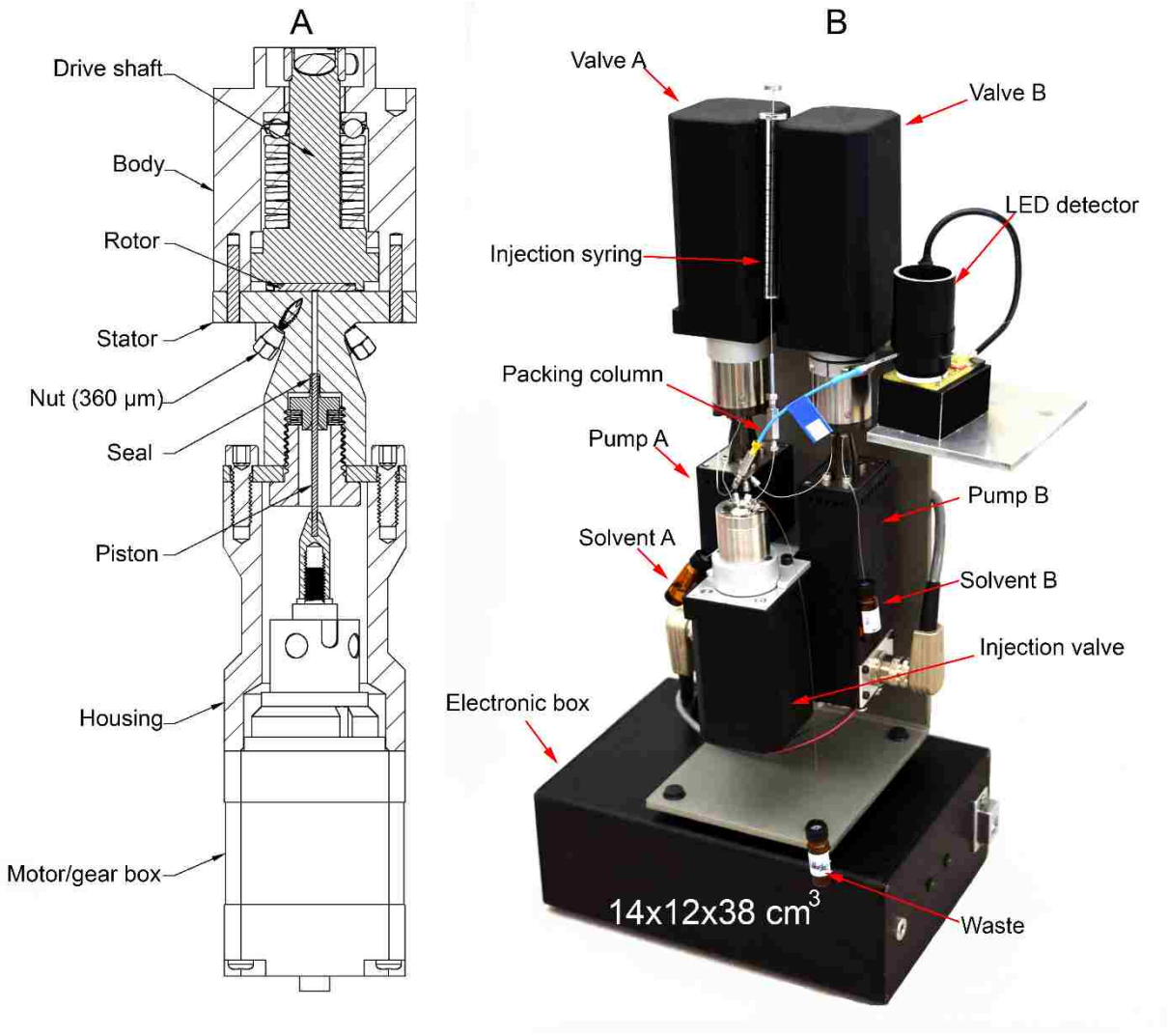

Figure 1: UHPLC system. (A) Cut-away drawing of a single nano-flow pump; (B) photograph of the nano-flow UHPLC with LED detector.

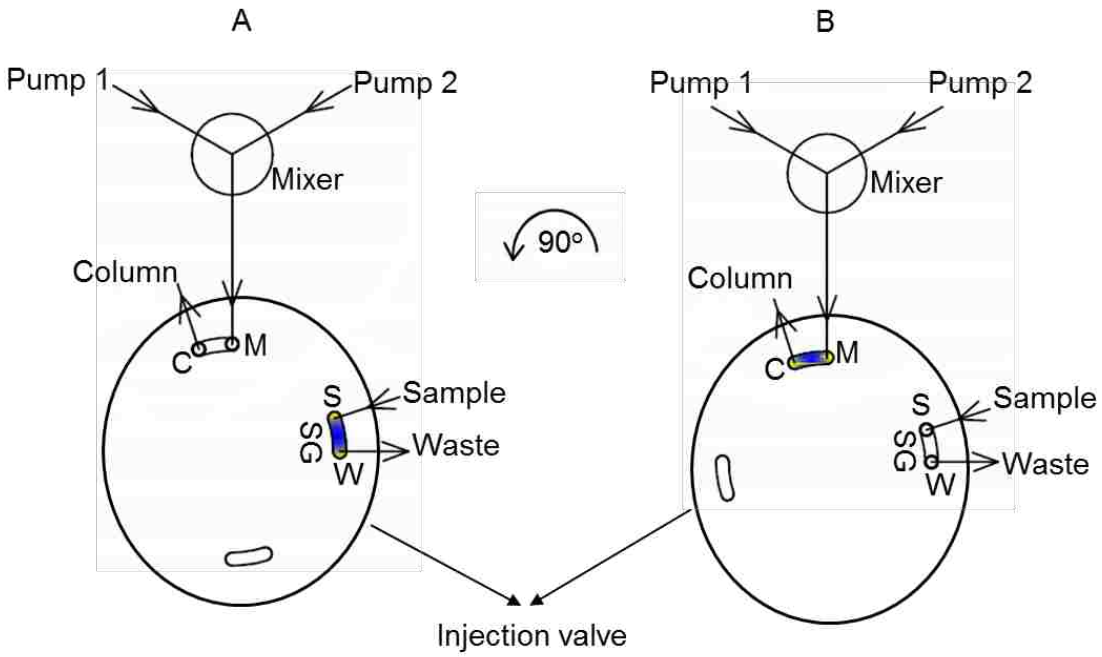

Figure 2: UHPLC valve operation. Operating schematics of the nano-flow UHPLC injection valve. (A) load position, (B) inject position.

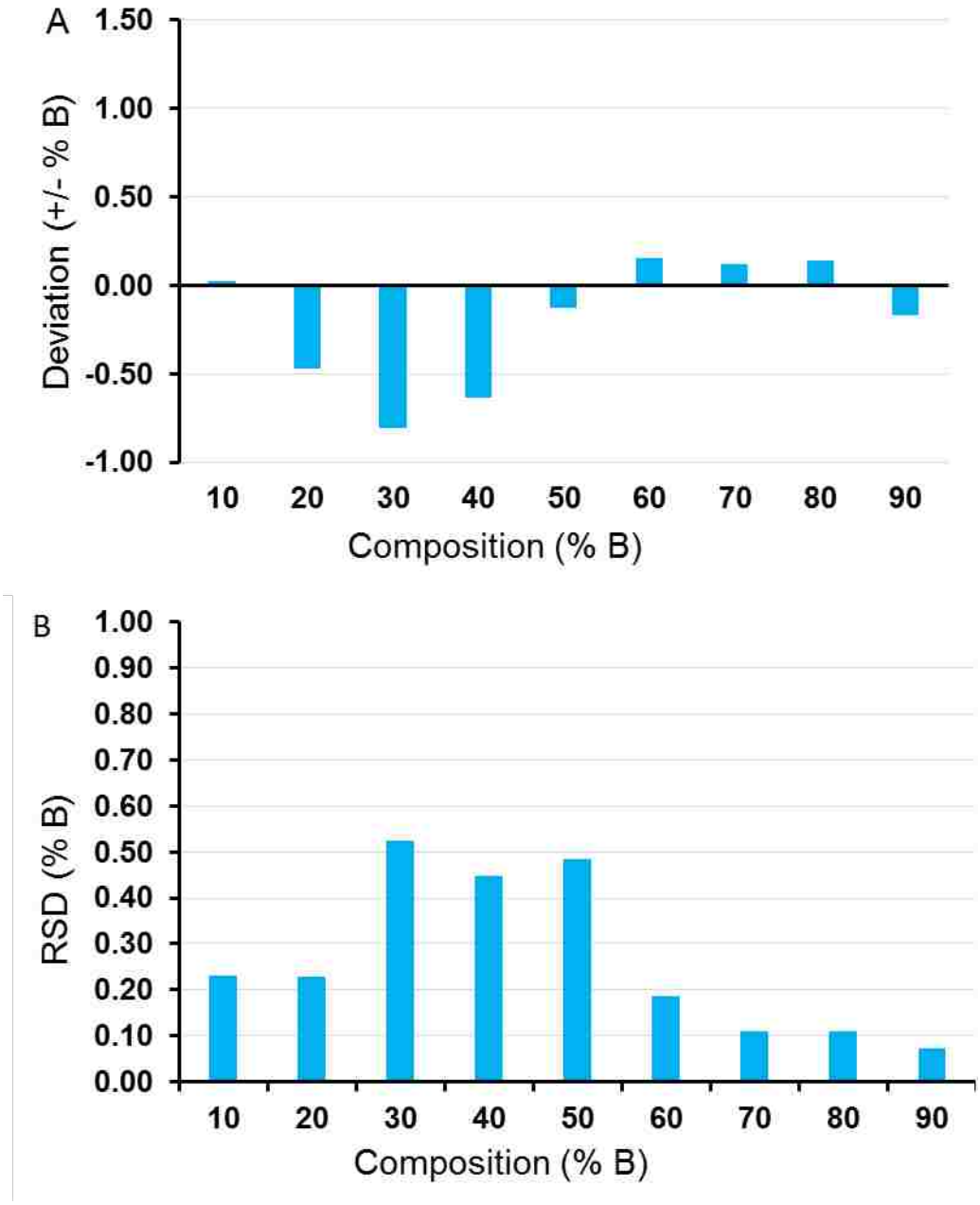

Figure 3: Gradient accuracy. (A) Gradient step accuracy (±% B) and (B) precision in gradient step accuracy.

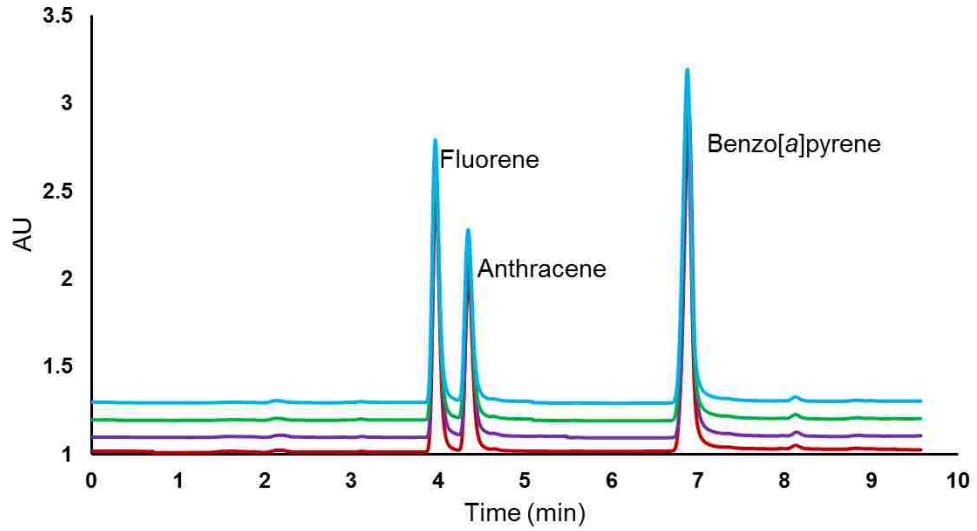

Figure 4: Reproducibility in retention time of a mixture of PAHs.

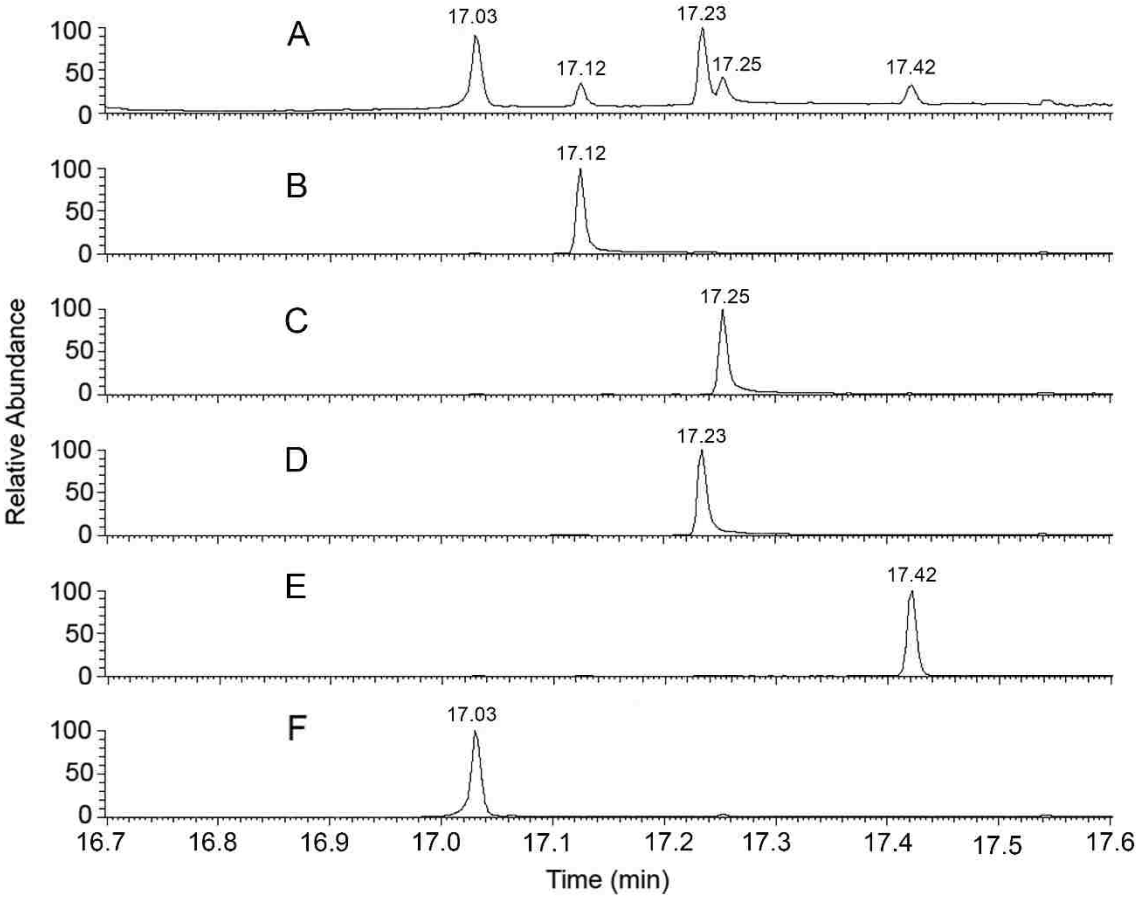

Figure 5: Chromatograms of a peptide mixture by UHPLC-Orbitrap MS: (A) total ion chromatogram of five target peptides, (B) extracted ion chromatogram of [Asn^1, Val^5]-angiotensin II ([M + 3H]$^{3+}$, 345 m/z), (C) extracted ion chromatogram of angiotensin I ([M + 3H]$^{3+}$, 432 m/z), (D) extracted ion chromatogram of angiotensin II ([M + 3H]$^{3+}$, 349 m/z); (E) extracted ion chromatogram of leu-enkephalin ([M + 3H]$^{+}$, 556 m/z), and (F) extracted ion chromatogram of Angiotensin fragment 1-7 ([M + 3H]$^{2+}$, 450 m/z). Experimental conditions: column with integrated ESI tip, 12 cm (75 µm i.d. × 365 µm o.d.); mobile phase A, 0.1% formic acid in water-ACN (95/5, V/V); mobile phase B, 0.1% formic acid in ACN; gradient program, 100% A for 5 min, then ramp to 100% B in 20 min with a flow rate at 500 nL/min; injection volume, 60 nL.

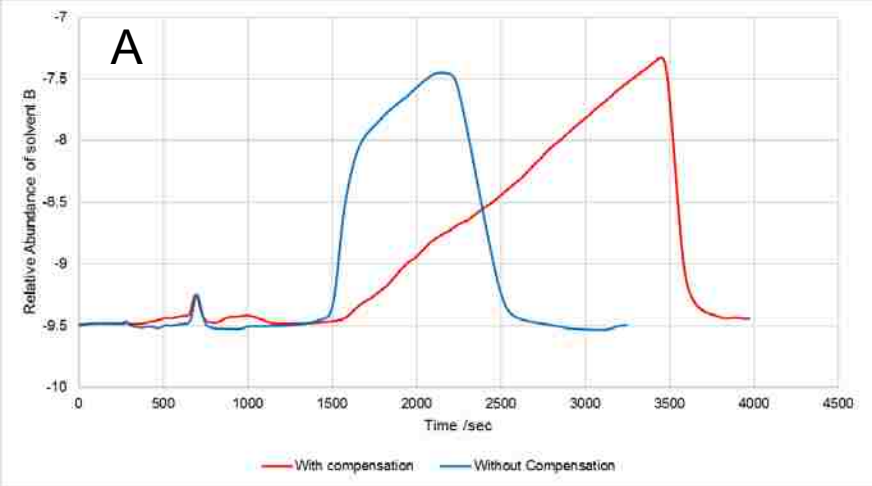
A
Relative Abundance of solvent B
-7
-7.5
-8
-8.5
-9
-9.5
-10
0
500
1000
1500
2000
2500
3000
3500
4000
4500
Time /sec
With compensation
Without Compensation

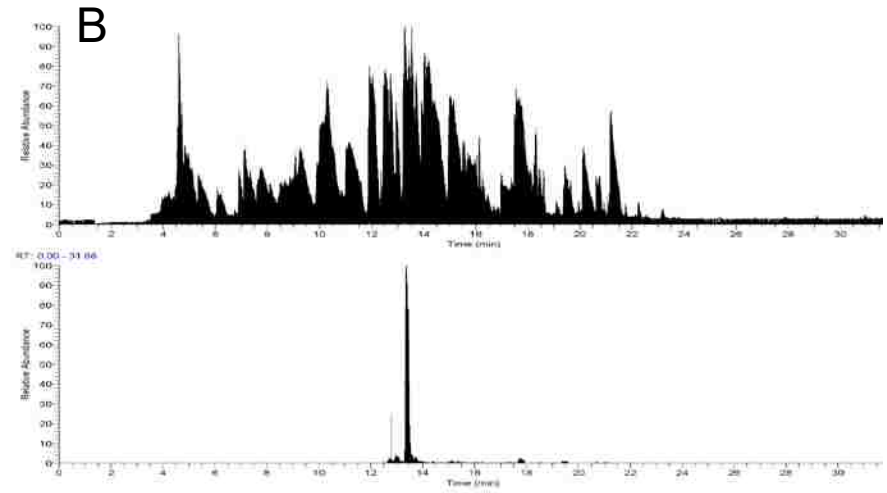
B
Relative Abundance
Time (min)
RT: 0.00 - 31.66
Relative Abundance
Time (min)

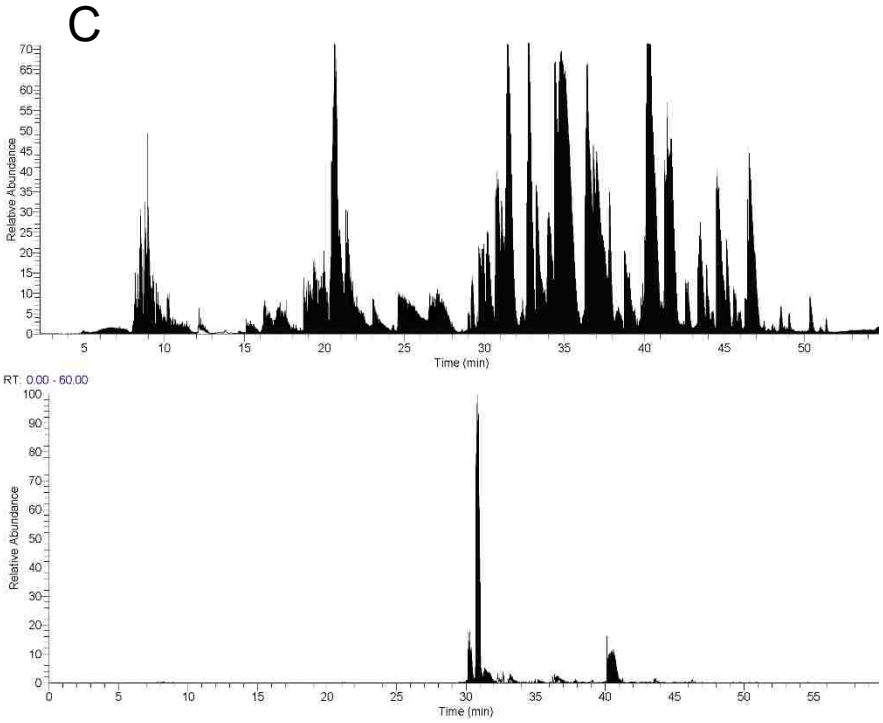
C
Relative Abundance
Time (min)
RT: 0.00 - 60.00
Relative Abundance
Time (min)

Figure 6: Comparison of gradient profiles and tryptic BSA base-peak resolved chromatography. (A) Comparison of gradient profiles (uracil was added to monitor the concentration of solvent B, acetonitrile); blue: no compensation step from 0% to 40% B; red: two step compensation, 10 min at 25% B and then 10 min at 5% B. (B and C) Chromatograms of a trypsin-digested BSA sample using coupled UHPLC-Orbitrap MS: (B) sample injected 20 min after 10 min 50:50 (A/B, water/ACN) and 10 min 95:5 wash (total-ion and extracted-ion chromatograms, m/z = 632). (C) Sample injected at 0 min, compensation steps of 75:25 (water/ACN) for 10 min and 95:5 for 10 min before linear gradient of 5% to 30% (total-ion and extracted-ion chromatograms, m/z = 654). Experimental conditions: column with integrated ESI tip, 12 cm (75 µm i.d. × 365 µm o.d.); mobile phase A, 0.1% formic acid in water/ACN (95:5 v/v); mobile phase B, 0.1% formic acid in ACN; flow rate, 500 nL/min; injection volume, 1.0 µL.

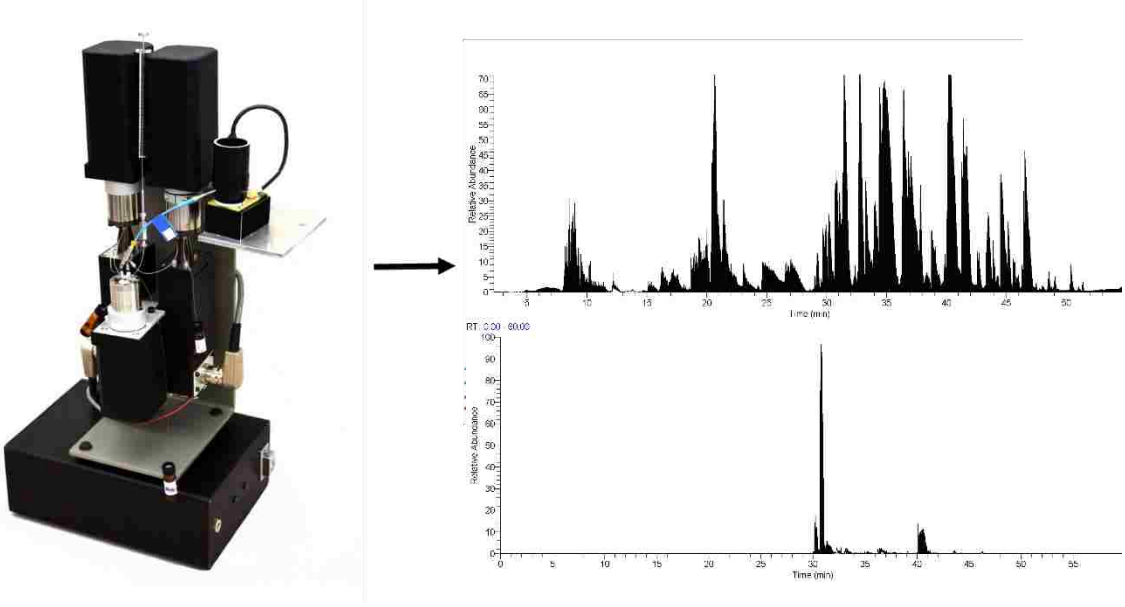

Figure 7: Abstract graphic UHPLC performance.

Supplemental Information

A

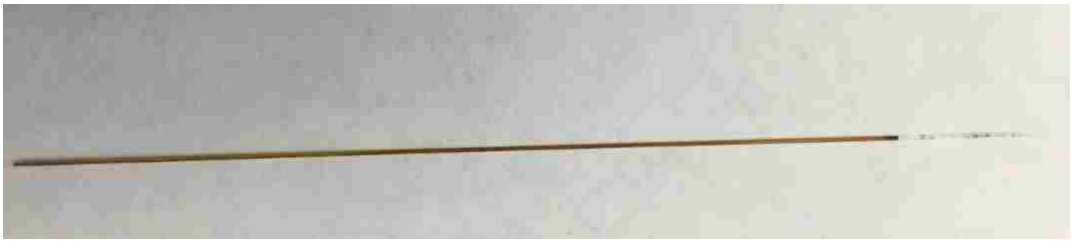

B

Supplemental Figure S1. Column with integrated electrospray tip. (A) Column packed with 1.7 µm C18 and (B) pulled electrospray tip.

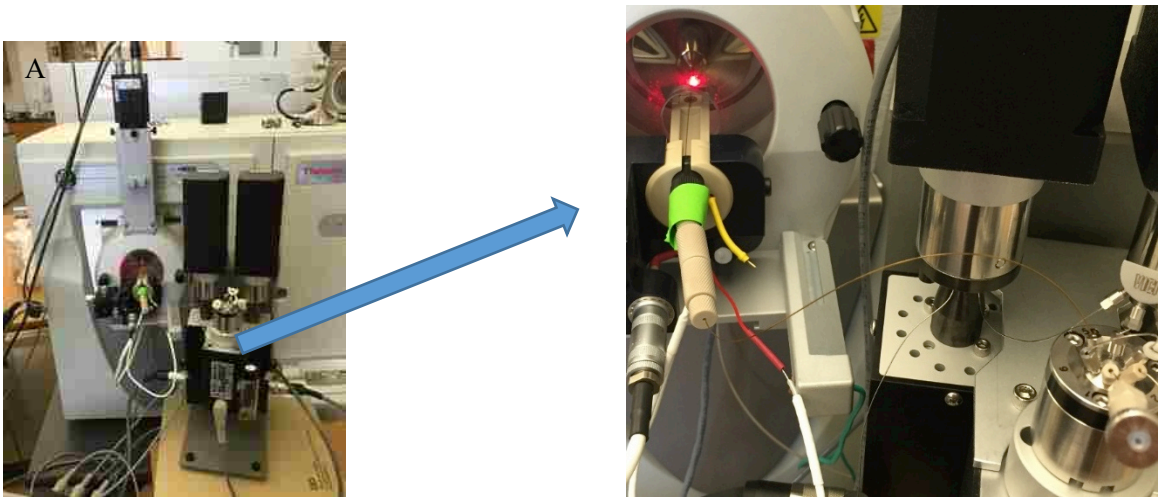

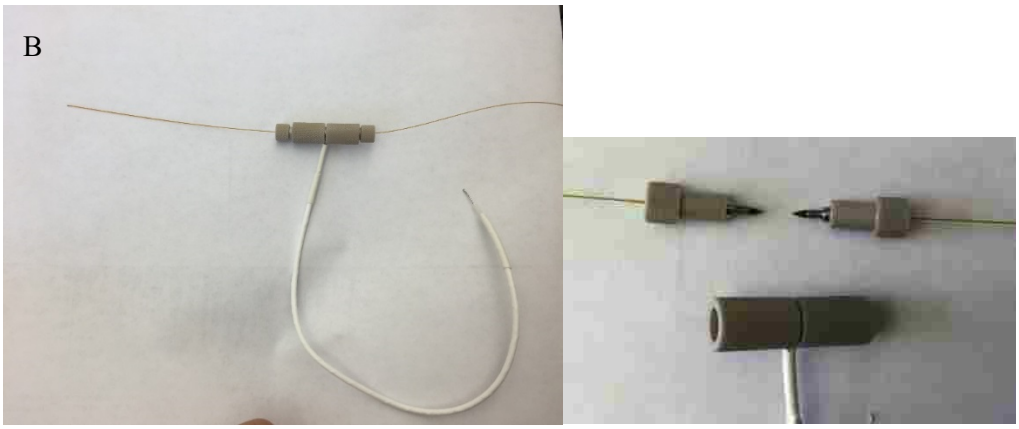

Supplemental Figure S2. Interface between the nano-flow UHPLC system and Orbitrap MS. (A) Connection between the injection valve and electrospray source and (B) zero-dead volume union used for connecting the column and transfer line from the pump.

CONCLUSION:

I have shown that in biological systems, small changes can have significant impacts. Through the process of my doctoral research I was able to demonstrate that very simple small molecules can make tremendous changes to an organism. Whether these changes are the result of inflammation signaling and the proteolytic activation of bioactive hepcidin-25 in iron transport control or changes in ceramide concentrations resulting in mitochondrial function impairment or insulin signaling impairment or cell-fate signaling due to lipids in cancer the outcome is significant. The new techniques and new pathways I helped elucidate help to further our understanding of disease and the way in which we can measure and diagnose them.

Mass spectrometry has proven to be a very useful tool in elucidating biological changes even at a very small scale. My proteomics based techniques have been critical in identifying and quantifying proteins and peptides in complex systems and have allowed us the ability to track the efficacy of treatment in pharmacological studies. This work resulted in the development of a scalable method to detect and quantify the small iron-regulatory hormone known as hepcidin from a variety of samples such as blood, urine, and cell-culture media. I showed that our improved high-resolution mass spectrometry based lipidomics techniques are capable of identifying small changes in diseased states that are associated with inflammation, mitochondrial shape and function, and cancer. Without this knowledge there were few ways to confidently and quantitatively know whether or not our hypotheses regarding the biological systems were actually true. I was also able to show the discovery of a new oncogenic pathway in pancreatic cancer that had never been observed before. The new knowledge about this pathway and the lipidomics technique I helped develop may allow for new treatment options that can be explored and the assay I developed can also be used as a companion diagnostic to track disease

progression and treatment efficacy. Our techniques we have been able to extract, identify, and quantify several thousand unique lipid species from complex samples with confidence.

I was also instrumental in evaluating and revising a new ultra-high pressure liquid chromatography (UHPLC) system that allows for better separation of analytes from complex mixtures for identification and quantification. Development of these technologies will help to dispense the availability of powerful instrumentation for use in more areas where this would have otherwise been impossible.

Through these advances we hope to aid researchers and clinicians to enable them to further our knowledge about the small but significant changes that regulate complex biological systems through the use of direct injection and liquid chromatography mass spectrometry.